AN INVESTIGATION INTO

THE DESIGN FOR VIBRATION

DAMPING OF EXTENDED LENGTH TOOL HOLDERS

by

Ayoub Shirvani

A thesis submitted for The Degree Of Doctor Of Philosophy

Department Of Engineering

University Of Warwick

COVENTYRY CV4 7AL

COPYRIGHT

FEBRUARY 1995

ACKNOWLEDGEMENT

The author wishes to express his sincere gratitude to Professor D.J. Whitehouse for his invaluable supervision, guidance, encouragement and proof reading of the final manuscript.

The author is also grateful to all technical staff and the department of engineering at Warwick University for providing the experimental facilities to carry out this research.

Last but not the least the author is deeply indebted to his parents and family for their continuous support throughout the course of his study.

DEDICATION

I WOULD LIKE TO DEDICATE THIS DISSERTATION TO MY FATHER WHO ALWAYS CHERISH OF HIS SON ACHIEVEMENT.

AND

TO MY MOTHER FOR HER LOVE AND SUPPORT THROUGHOUT MY LIFE

TABLE OF CONTENTS

CHAPTER 3 FUNDAMENTALS OF CUTTING TOOL VIBRATION

CHAPTER 4 VIBRATION CONTROL BY MATERIAL SELECTION

CHAPTER 5 EXPERIMENTAL PROCEDURE AND RESULTS

CHAPTER 6 FINITE ELEMENT MODELLING

PART I : FINITE ELEMENT BACKGROUND AND THEORY

DECLARATION

I hereby declare that this thesis is composed by me and I have carried out all the work recorded in this thesis for the purpose of fulfilment of the requirement for the award of the Degree Of Doctor Of Philosophy in Manufacturing Systems Engineering.

AYOUB SHIRVANI

ABSTRACT

This thesis presents a theoretical and experimental investigation into the design of extended length tool holders, with specific emphasis on vibration damping and the attenuation of chatter in boring bars.

The theoretical strategy was to evaluate the general mechanics of vibration characteristics, as applied to metal cutting operations. This was used to provide an insight into possible control parameters, and demonstrate a practical approach to the design and optimization of the boring bar structure.

Consideration of vibration control parameters and its interaction with functional specifications of the tool resulted in a modified design of the tool holder. The design aspects were confined to passive damping, to enable its application for practical use in industry. Passive damping can be separated into two areas: Material specification and system configuration. Both have been exploited here through the development of a new material.

The theoretical design approaches were further examined through metallurgical consideration. From this the practical aspects of material development were confined to improving equivalent stiffness through alloying elements and processing techniques. Research into developing a Titanium Carbide (TiC) composite is detailed, involving powder metallurgy under controlled processing conditions.

The experimented results indicate a 47.39% reduction in density, combined with 27.14% improvement on its modulus of elasticity leading to an increase in equivalent stiffness up to 84.59% compared to steel.

Although the results demonstrated considerable improvements of mechanical properties and substantiate the suitability of such material as a candidate for the bar material, even better properties were obtained through Hot Isostatic Pressing (HIPing) process. A further 13.48% increase in elastic modulus lead to an improvement of 109.58 % on the value of equivalent stiffness.

Experimental examination of tools, was confined to simple internal turning operations (boring). This required the design of fixtures for setting up the test rig. The experimental verification of the combination boring bars was undertaken through comparative stability performance, assessed from the attained machining quality under varying machining conditions.

A computational verification of the combination boring bars was performed using Finite Element Method. The dynamic compliance of the tool was evaluated in the frequency range relevant to machine tool and cutting processes for the fundamental mode with appropriate boundary conditions. The computational and practical analyses, support the conclusions implicit in the theoretical model, that the combination approach to the design through material development and system configuration offers high performance, practical devices.

CHAPTER 1

1.0 INTRODUCTION

The importance of the dynamic performance of machining processes is increasing with the proliferation of flexible manufacturing systems.

In metal cutting operations involving the use of a boring bar, problems arise due to the vibration phenomenon known as chatter. This occurs particularly in boring out deep, small bore holes with a long slender bar. In such cases the vibration of the bar caused by harmonic forces set up during a cutting operation can lead to an unstable process with the cutting tool leaving characteristic chatter marks on the workpiece. Moreover, the undesirable and often violent vibration causes poor surface roughness, loss of machining accuracy and reduction of tool life.

The study of the elimination of cutting process vibration is of considerable importance with regard to the productive capacity of the machine tools. There are three types of machining vibrations that may attribute to the quality of surface roughness.

a) Forced vibrations, which are periodic forces present in the machine which may be transmitted to the tool structure and work piece via connecting elements.

b) Free vibrations which are generated as a result of impulses of foreign origin transmitted through the machine foundation.

C) Self induced vibrations, which are as a result of the interaction of the cutting process and the structural dynamics of the boring bar.

Substantial research efforts have been aimed at the resolution of

this problem. Most of the proposed improvements involve the enhancement of the structural stiffness or the implementation of damping devices.

The first method may only be possible with additional supports or by improving the material for greater stiffness. The effectiveness of the second approach is limited because often it is difficult to attach dampers to a vibrating structure like a rotating workpiece or to slender tools.

1.1 CHATTER VIBRATION IN MACHINE TOOLS

A machine tool can be idealised as a construction of localised masses and massless springs, each of which contain moving parts. Various parts of machine tool structures are all subjected to loading in different ways. Changes in the cutting process parameters result in a vibratory system having a very complex dynamic behaviour. These vibrations are detrimental to the cutting tool, product quality and affects the economy of production.

In the design of the boring tool, the main concerns are with the vibrations that affect the metal cutting process, ie, self induced vibration and special cases of forced vibration.

There are many factors involved in setting up the conditions to produce chatter. In fact, almost all of the components of the machine tool and machining conditions may be involved. Some of the defined parameters under consideration are listed below.

The design of machine tool, the type of work piece material, the type of cutting operation, the type and design of tooling and fixture system, the geometry of the cutting tools, the selection of feeds, speeds and the depth of cut, all play their role in chatter proneness of a process.

An important criterion for the control of chatter proneness is the rigidity of the machine tool and the cutting system.

When designing a special tooling system, the rigidity of the

machine cannot easily be changed, but improvement in the cutting tool and work holding devices may be possible through improved equivalent stiffness and the damping of the tool holder.

1.2 FORCED CHATTER

In forced vibrations the frequency of the vibrating force corresponds to the frequency of the vibrating agent. This may be quite different from the natural frequency of the vibrating members.

The frequency of the disturbing forces is proportional to the ratio of the speed of the cutter or workpiece to the distance of successively produced chatter marks (1.2).

Thus;

$$\text{Frequency} = \frac{\text{Cutting Speed}}{\text{Measured Distance Between Chatter Marks}} \quad \text{(Hz)} \qquad (1.1)$$

If this frequency corresponds to the sum of the number of teeth on a gear and its rotational speed, the vibration is forced and caused by the contacts between the gear teeth. If it corresponds to the rotational speed of bearing, pulley or spindle, imbalance of the rotating members may be responsible (1.2).

When force conditions acting upon a cutting tool cause it to vibrate at a frequency near the natural frequency of the machine, a resonant condition is set up in which even a low excitation can produce maximum amplitude. The cutting tool will vibrate at the same frequency as the natural vibration within the machine, but due to the lack of equivalent stiffness of the tool holder the amplitude will jump to extremely high levels.

The boring bar may also be excited by a forced vibration within the cutting process. For example, the formation of metal chips where the reoccurring fracture of metal at the shear plane produces rhythmic vibrations in force, which may cause the cutting tool to vibrate. This

is a forced vibration in which the tool is made to deflect and misalign the centre line of the tool rhythmically.

There are four methods of tackling machine tool forced vibration (1.2):

1. by eliminating the exciting force at source,
2. by vibration isolation,
3. by an undamped dynamic vibration absorber,
4. or by a Lanchester vibration absorber.

In all machining operations the most significant vibration problem is due to self excited regenerative type chatter mechanism.

1.3 REGENERATIVE CHATTER

Self-excited vibrations are spontaneous. They are not induced by external periodic forces, but by the forces generated in the vibratory processes themselves. For the machine tool, the self-excited vibration is the result of interaction between the cutting force dynamics and the machine tool structure dynamics. It draws the energy for its maintenance from the tool or workpiece drive.

Because of overlapping cuts, vibrations resulting from machining of the wavy surface left from the previous revolution of the workpiece can amplify the superseding vibration. This type of vibration is called regenerative chatter. These disturbances are further magnified if the structure lacks sufficient positive damping as it progresses along the work piece.

The fluctuations in the cutting forces are subjecting the tool to vibration while further cutting subjects the process to further energy magnification. In practical machining operations, the so called regenerative chatter is more liable to occur than other types of vibration (1.5).

1.4 MODE COUPLING CHATTER

This type of chatter has been described in terms of a simple linear vibration theory. That is when forces acting in one direction on a machine tool structure cause movement in another and vice versa.

The principle of mode coupling can be explained by considering the effect of an oscillating force acting on the system. The motion of the vibrating body (boring bar) will not be solely confined to one mode, but follows an elliptical path, which is made up of motions in two principle planes. This elliptical motion will be superimposed on the cutting path and will have the effect of transferring energy to the system; energy which could under certain conditions overcome the system damping (1.6). The effect of modal shape of tool holders is further analyzed in chapter eight.

1.5 DESIGN CRITERION FOR CHATTER SUPPRESSION

Fundamentally, chatter is caused by lack of adequate dynamic stiffness in the machine and tooling structure. This difficulty is attributable to low natural frequency and inadequate damping inherent in the structure materials used for boring bars, limits the degree of energy dissipation desired for reducing the response levels.

A necessary prerequisite to the control of the vibration of a cutting process is an examination of the dynamic behaviour of the system under excitation by measuring the forces at various points. Many approaches towards this task exist, including direct measurement of the required information. These attempts have resulted in various design improvements of the dynamic stability in machine tools.

The design approach in this investigation is generated by analytical recognition of the boundary conditions and variables

involved to enable practical stability characteristics to be isolated. The theoretical strategy was to classify the applied mechanics of vibration characteristics in metal cutting operations. The design aspects have been confined to passive damping, to enable its application for practical use in industry. The science of passive damping is separated into two areas; material specification and system configuration, both of these have been enhanced using advances in material development and structural configuration.

Analytical consideration of vibration control parameters and their interaction with the functional specification of the tool has resulted in a modified design of the tool holder.

1.5.1 ACTIVE CONTROL

Active control is where chatter suppression is achieved by controlling the machining parameters which sustain the variation in the cutting forces.

The basic approach of active control has been to minimise the relative motion between the cutting tool and the workpiece.

Identifying the dynamic characteristic of the cutting process under actual cutting conditions requires rather expensive sensors, control systems and software.

In present research this method was considered to be expensive and less practical in an industrial workshop environment.

1.5.2 PASSIVE CONTROL

Passive control of chatter is a process by which the system instability could be sustained in the tooling structure by improving the static and dynamic stiffness. This in turn leads to an enhanced

resonant frequency and reduced amplitude response in the tool structure.

1.6 DETERMINATION OF PARAMETERS FOR IMPROVED DESIGN

The level of structural vibration due to a given source is controlled by the physical characteristics of mass, stiffness and damping. The design of a cantilever cutting tool must take account of the structural response with respect to these three properties. Therefore, for any successful design the correct correlation of mass, stiffness and damping is required. Improving one at the expense of the others (such as when using tungsten carbide boring bars) may not be advantageous under all circumstances.

The present study demonstrates an approach in design of boring bars based on the concept of the correct correlation of the physical parameters. From these considerations an analytical approach is developed and presented in chapter three. The design of the boring system was based on the development of a new material (chapter four) and on structural optimisation (chapters three, seven and eight). The fabricated boring bars are tested for comparative stability performance (chapter five) and to verify the dynamic rigidity as a measure of attained machining quality.

The following methods of vibration control have been considered in the design.

-Structural design.

-Material selection and development.

-Artificial damping.

-Localised additives.

CHAPTER 2

THEORETICAL REVIEW ON METAL CUTTING

2.0 INTRODUCTION

In this chapter the review of literature with respect to essential theoretical consideration of the cutting process based on contribution of previous research is presented.

2.1 HISTORICAL BACKGROUND

The history of problems in machining quality dates back to the history of metal cutting, not fully appreciated until the late 19th century.

The first real step in metal cutting was taken in the latter part of the eighteenth century. In 1775 Wilkinson invented his boring machine which enabled Watt to carry out the development of the steam engine.

Following this achievement Maudslay developed his practical screw cutting lathe in 1800. The first drill with automatic power feed was developed in 1840 (2.1).

At the turn of the nineteenth century, metal cutting tools were made from high carbon steel used in the manufacture of files and wood cutting tools. In the early 1900's, Fredric Taylor and associated metallurgists developed high speed steel (HSS) and nearly revolutionised the metal-cutting industry (2.1). By this time the problems associated with vibration had become apparent as a result of the high speed machining capability of HSS.

The next significant development in metal cutting came in the 1920's with the introduction of sintered carbides as a cutting tool

material. Because of this cutting speeds were doubled.

The search for a better tool material resulted in the significant development in the 1940's where oxide (ceramic) was used as cutting tool inserts. The carbide cutting speeds were also substantially increased.

Advances in cutting tool materials as well as in work materials such as metal matrix composites, and super alloys necessitated the redesigning and development of more productive machines and tools.

Other benefits of tool-material and cutting tool development are; improved impact and shock resistance, improved stability performance with greater metal removal rate.

2.2 METAL CUTTING AND RELATED TERMINOLOGY

Metal cutting process of single point cutting could be idealised as a system containing three basic elements; machine tool , workpiece and cutting tool.

A lathe, as an example of a machine tool, has the work piece held firmly in the chuck which rotates at a predetermined speed with respect to the cutting edge of the tool. This is referred to as the cutting speed (m/min). The tool is held rigidly in a tool-post of the machine tool, which could also travel at a predetermined rate, with respect to the rotating work piece, producing a velocity component known as feed rate (mm/rev).

A cutting tool generally consists of a cutting part (tool tip), and a shank which supports the cutting part.

The tool tip consist of a special geometric feature which aides the cutting process to take place. The components of the cutting tool are illustrated in Figure 2.1.

The thickness of the unwanted material " Depth of cut (mm) " is removed from the work piece by setting the cutting tool in a

predetermined position. When fed towards the rotating workpiece it cuts through the material at an effective rate set by the combination of the speed, feed and depth of cut.

Metal removal rate is a parameter used to determine the efficiency of the cutting operation; it is the product of the cutting speed, feed rate and depth of cut.

The rake face is the tool surface over which the chip flows during the machining process.

The flank face is the surface of the tool over which the freshly cut surface of the workpiece passes.

The primary cutting edge is the intersection of the flank with the rake face and forms the cutting edge.

The secondary cutting edge is the remainder of the cutting edge which may not actually be engaged in the cutting process.

The cutting nose is the intersection of the primary and secondary cutting edges. In order to achieve higher strength at the cutting edge a radius is provided.

The shear zones: there are two major zones of shear when a chip forms. One is the primary shear zone which is the boundary between the un-sheared work material and the chip, the other is the secondary shear zone, also known as flow zone, which is the interface between the tool and the chip on the rake face.

Orthogonal cutting, is the process where the major cutting edge is used and the rake face of the tool is positioned perpendicular to the direction of the relative tool-work motion with zero approach angle.

2.2.1 CUTTING PROCESS

In metal cutting deformation of the work material takes place in a localised area due to the pressure applied by the cutting tool as a result of relative motion between the work piece and the tool.

Figure 2.2, illustrates the localised area which centres on an intensive plastic deformation zone surrounded by an elastic - plastic zone (2.2).

The idealised diagram, Figure. 2.2 a, shows the workpiece material being cut by progressive slip relating to the tool point, at an angle that corresponds to the shear angle. The theoretical model assumes that the tool's tip (ie: where the clearance and the rake face converge) is sharp. In reality there is always some modification of the point after the tool enters the work piece. The exaggerated form of this is illustrated in Figure 2.2 b, where the tip geometry is represented as an arc of a circle.

In fact, the rake angle becomes progressively more negative as it approaches the clearance face. There is a critical point on the tool above which the material is cut and forms the chip. The minimum un-deformed chips thickness is above this critical point and below this chips are not formed. When the tool' s edge is sharp, it follows that the minimum un-deformed chip thickness is small, therefore very high pressure must be involved in that region, and material is extruded from the interface between the tool and work piece. (2.2).

2.3 CUTTING TOOL FAILURE AND ITS MONITORING

Machining instability may be due to process instability produced as a result of the combination of cutting parameters, insufficient rigidity and damping as well as many kinds of tool failure. The most common causes of tool failure are ;

1. Temperature failure, where the tool temperature becomes high enough to cause plastic deformation at the cutting edge.
2. Fracturing, either a complete tool failure or small chipping of the cutting edge, caused by fatigue or excessive forces.
3. Gradual wear, including both crater wear and flank wear.
4. Tool vibration and Chatter.

Figure 2.3 a and b, illustrates the effect of both crater wear and flank wear.

The review of research with regard to monitoring the cutting tool in turning, established that basically three types of methods are used (2.3, 2.4, 2.5, 2.6).

1) Direct methods, involving the measurement of the actual tool wear and fracture of a cutting tool (such as optical techniques).
2) Indirect methods, involving measurement of parameters associated with the cutting processes (such as cutting forces and vibration)
3) Surface analysis, based on the assumption that the surface texture of a machined workpiece is the fingerprint of a cutting process.

Although numerous methods have been proposed, surface analysis is considered to be the most practical and probably the most economical method used in research for the quality of stability performance.

2.3.1 MONITORING TOOL FAILURE USING CUTTING FORCE DATA

One of the parameters that can be used to characterise tool wear is the cutting force. This has the advantage that it is relatively easy to measure. It can be used to monitor the cutting processes since cutting forces vary as the tool wears. It usually gets greater because of the increase in the coefficient of friction between tool and workpiece. Some theoretical models based on force measurements for on-

line tool wear and breakage sensing have been presented and verified (2.7, 2.8).

A method of wear estimation for carbide tools, using a function of the cutting forces, has also been considered (2.9). A wear index was proposed to categorize the state of wear on a tool as a percentage value. For perfect tools the value was defined as 0% while extremely badly damaged tools were given a value of 100% .

The cutting force method could be regarded as an effective technique for detection of tool failure. However, it cannot be generalised because tool wear and failure have a complex relationship with the cutting force. The results can be different for sensing tool wear in similar studies.

2.3.2 MONITORING TOOL FAILURE USING VIBRATION DATA

According to recent investigations (2.10), the vertical tool vibrations in the course of stable machining are almost sinusoidal, with a frequency equal to the natural frequency of the tool.

In further experiments (2.10), the power of the acceleration signal obtained by spectral analysis was found to be a linear function of the cutting speed and of the tool wear, and varied with the ratio of 1:10 between a new tool and a worn tool.

The Data Dependent System (DDS) (2.11), measures tool wear by using the signal from an accelerometer mounted on the tool holder at a safe distance away from the cutting process. The DDS picks the mode of vibration most sensitive to tool wear and gives its power contribution. The trend remains unchanged under different cutting conditions.

Since vibration signals vary with tool failure, this technique may be regarded as a practical method in tool condition monitoring. However, due to the sophistication of transducers and instrumentation needed for the measurement this technique may not be cost-effective.

2.3.3 MONITORING TOOL FAILURE USING SURFACE DATA

The surface texture produced on the workpiece can be regarded as the *fingerprint* of the whole machining process. It contains much information about the process, particularly process *vibration* and tool wear. Therefore, by analysing the surface, in principle it is possible to estimate the severity of vibration.

Whitehouse (2.12), showed that the surface and its measurement can provide a link between the manufacturing workpiece and its function.

There are two approaches to this : one is based on probability and stochastic theory, the other is deterministic.

The surface data in this investigation is used to predict the stability boundary of the dynamic cutting process on the assumption that surface undulations are a faithful replica of the process.

2.4 OBSERVATION OF CHIPS IN METAL CUTTING

Chips in the metal cutting processes are produced as a result of metal shear facilitated by deformations lying ahead of the cutting edge of the tool.

Observations on chip formation (2.13) under different cutting conditions with different materials confirm four different types of chip. The significant deviations from the ideal models described in theories are often due to vibrations.

The chip segmentation or serrated chip arises as a result of instabilities in the cutting process (2.14). This can further be increased by the dynamic response of parts of the machine tool structure. Four types of serrated chips have been reported, with different explanations for their mechanism of formation.

1- The wavy chip , forms as a result of cyclic variation in the undeformed chip thickness, rake angle and clearance angle are due to regenerative chatter under self excited vibrations. The mechanism of formation of this chip has been studied by several researchers beginning with the work of Arnold (2.13). It is considered that limited rigidity and the low damping of the tool are responsible for this.

2- Catastrophic shear chip; caused by the material characteristic of certain materials such as titanium alloys which have poor thermal properties. Their ability to deform plastically varies with temperature due to possible phase transformation and consequent change in crystal structure (2.14).

3- Segmental chips, are considered to be continuous chips with periodic variation in thickness. They have been reported to occur only in certain speed ranges and cutting conditions. Chip segmentation also depends on the composition and microstructure of the work material, with the vibratory behaviour of the test bar playing a secondary role (2.14).

4- Discontinuous chip, is a special case of the catastrophic shear chip, where complete separation between chip segments occur as a result of periodic rupture of the shear failed surface. But unlike catastrophic shear chip there will be no rewelding of individual segments (2.14). This type of chip is most likely to occur when machining brittle materials and also at low speeds with all other materials.

From the review of literature there appears to be some significant differences in the assumptions made by various researchers regarding the nature of chip segmentation. Some have considered it to

be a case of self excited vibration, others a case of forced vibration and a few have not given any consideration to the important role of the dynamic response of the machine tool.

2.5 FORCES IN METAL CUTTING

Forces in machining are an important parameter. Knowledge of their behaviour is useful in the design and manufacture of machine tools to provide sufficient rigidity and eliminate vibrations. Accurate measurement of the forces present in metal cutting will also help in the design of tool geometries.

Figure 2.4 a and b, illustrates a simple model of the orthogonal metal cutting process and the corresponding force system, first considered by Ernst and Merchant (2.16, 2.17). The forces present during cutting can be resolved into three components.

The first component is the cutting force F_c' which is usually the largest force acting on the rake face in the direction of the cutting velocity. The second force, (Feed force) F_t' acting parallel to the direction of the tool feed. The third force component is the redial force F_r' which tends to push the tool away in a radial direction. In orthogonal cutting, where the approach angle is zero there is no force due to this direction hence not represented in Figure 2.4 a.

The contact length between the tool and the chip plays an important role in metal cutting, it is directly related to the cutting forces. The maximum compressive stress acts on the edge and reduces to zero as at the end of the contact zone.

Cases which produce discontinuous chips tends to produce lower forces due to the shorter contact length. Increase in the feed rate will increase the contact length between the chip and the tool, resulting in higher forces.

Another factor which influences the cutting forces is the rake

angle. Selection of the tool with a large rake angle will require lower forces but the increase in the rake angle will have the tendency to weaken the cutting edge thereby creating conditions for tool failure.

Cutting speed also influences the cutting forces. As the cutting speed increases the forces acting on the tool generally decrease due to the excessive heat generated in the cutting zone. This tends to soften the work material. The variation of flank clearance with respect to velocity of vibration also produces a damping component. The influence of the process damping and excessive heat, results in the reduction of the cutting force. The mechanics of process damping with respect to the effect of cutting speed are detailed in section 2.10.

2.6 STEADY-STATE METAL CUTTING.

The steady state metal cutting models, proposed by various researchers, only represents the simple theoretical basis to the complex and variable conditions of practical situations. However, these analyses have been further enhanced by modified models that may be in closer agreement with the practical mechanics of machining.

Ernst and Merchant (2.16), by applying the minimum energy principle for a shearing process within a shear zone, proposed the following shear angle relationship.

$$\Phi = \frac{\Pi}{4} - \frac{\beta}{2} + \frac{\alpha}{2} \qquad (2.1)$$

Where:

β = Friction angle at the rake face of the tool

α = Rake angle of the tool.

About 10 years later Lee and Shaffer (2.18) proposed another relationship based on slip-line plasticity theory. They assumed that the shear plane to be a plane of maximum shear stress, the flow stress

to be constant and the stress on the tool face considered to be uniformly distributed.

$$\Phi = \frac{\Pi}{4} - \beta + \alpha \qquad (2.2)$$

Neither of these prediction are in good agreement with the experimental results as reported by Kobayashi et. al (2.19). These assumptions are true to a limited degree. They considered the coefficient of friction of tool-surface to be independent of shear angle.

Zorev (2.20) and Shaw (2.21) indicated that the friction associated with metal cutting is of a different nature than the friction associated with sliding.

Zorev (2.20) observed that shear stress and normal stress act along the chip tool contacting length and further showed that shear process on the tool face and the shear plane interact strongly.

Kobayashi (2.19, 2.22, 2.23) and Egglestone (2.24) concluded from experimental results that the shearing force on the idealised shear plane is proportional to the shear plane area. Further Wallace and Boothroyd (2.25) found that for aluminium, the tool nose force is independent of the depth of cut, the chip contact-length and the chip thickness.

Shaw (2.26) reported that forces on the clearance face should have no effect on the chip formation process since forces arise after the chip is formed.

The universal machinability index ' D' as the ratio of the cutting stresses to the shearing stress was published by Das and Tobias (2.27). They analyzed the previously published data and observed that the component of the cutting force in the direction of cutting is proportional to the shear plane area, under a wide range of cutting conditions. Using the constancy of the shearing stress on the shear plane, the machinability chart was plotted as shown in Figure 2.5.

2.7 DYNAMIC METAL CUTTING

A great deal of attention has been focused on the problems associated with the dynamics of the cutting process with the underlining problem of self-induced chatter vibration arising in machine tools. This is closely related to the dynamic behaviour of the cutting forces and machine structure. Cutting forces are affected by cutting conditions, tool angles, shear angles and the frictional conditions between chip and tool surfaces. Among these the dynamic cutting forces induced by the variation of chip thickness and the periodic variation of shear angle is the main reason for the chatter occurring (2.28, 2.29) .

Under steady state cutting, where no relative vibrations exist between the tool and workpiece, the cutting force is assumed to be constant. However, when an assumed steady state cutting is disturbed, for example by a hard spot in the cut metal or by undulations in the surface conditions, the tool will be forced into an oscillating motion and as a result components of the cutting force will follow a similar pattern.

This dynamic force is usually out of phase with the tool oscillations. If the cutting force leads the tool oscillations, a positive damping is generated by the cutting process and the tool oscillations die out (2.30). However, if the dynamic cutting force lags, the tool's oscillation energy is fed into the vibrating system and the cutting process is considered to generate a negative damping.

When this negative damping exceeds the positive damping of the machine tool structure it leads to dynamic instability i.e; chatter. If the nature of the cutting force variation is such that the maximum cutting force occurs sometime after the maximum chip thickness variation, then some energy is available to maintain the vibrations between the tool and the work piece. This type of vibration system has been known as regenerative chatter. Figure 2.6, illustrates the

graphical representation of the force displacement loop (2.30).

Chisholm (2.30) considered that chatter is self excited vibrations caused by the falling characteristic of the cutting force with increase in cutting speed.

Hahn (2.31) disputed this hypothesis and showed that chatter could also occur with materials which do not show a fall in the cutting force with cutting speed. He also suggested that the main cause of chatter is the feed-back due to the overlap of successive cuts i.e: regenerative effect.

Tobias (2.32) and Smith (2.33), carried out dynamic cutting tests with an oscillating tool, with a range of frequencies up to 400 Hz at cutting speed of 400 M/Sec. They tested for both wave removal and wave generation, on mild steel. They concluded that at low frequencies the cutting forces lag behind the chip thickness variation, in agreement with the result of (2.34). However, this lag changes sign and becomes a lead as the frequency of tool oscillation increases.

Shamsheruddin (2.35) examined the dynamic cutting performance for both wave removal and wave generation and suggested that the dynamic cutting forces depended on the variation in the rate of change of chip thickness as well as the cutting speed and penetration rate as suggested by Tobias and Fishwick (2.32). He also concluded that ;

1) The torsional oscillation of the system could cause the cutting force to lag behind the tool displacement.
2) The normal and tangential components of the cutting forces are leading the chip thickness variation for all the cutting speeds investigated.
3) Determination of the value of chip thickness coefficient from the dynamic cutting tests has a smaller value than that found under steady-state cutting conditions.

The effect of tool vibrations on the cutting forces was also analyzed by Wallace and Andrew (2.36, 2.37). They assumed that there are two components of the oscillating thrust forces,

I) The component which is proportional and in phase with the oscillation in un-deformed chip thickness.

II) A component caused by the contact between the small area of the tool flank and the freshly cut surface, which leads the oscillations in un-deformed chip thickness by 90° degree.

In the second assumption, the instantaneous flank force varies linearly with the clearance angle.

Wallace et all (2.36) and (2.37), developed a theoretical model for the case of removing a wavy surface. They assumed that the shear angle variation to be in phase and proportional to the surface slope, and the curvature of the chip varies with un-deformed chip thickness. They derived expressions for the instantaneous shearing force on the shear plane and the instantaneous friction forces on the rake face. To verify the method, wave removing tests were carried out. They measured the amplitude and the phase of the thrust force and of the tangential cutting force relative to the chip thickness variation and compared the results with the theoretical values. They concluded that the dynamic cutting forces could be predicted from the theoretical approach.

Although their approach carried some degree of accuracy different assumptions were made for the two cases of (I) tool vibration and (II) wave removal.

The condition for a successful and realistic dynamic cutting model to be related to the steady-state cutting data must be based on the fundamentals of metal cutting process.

Das and Tabias (2.38) considered the dynamic variation of the cutting direction and the shear plane length, and found the dynamic force components dF_c and dF_t along and normal to the mean cutting direction.

Although the correlation between their theoretical predictions and experimental dynamic cutting tests were reported to be satisfactory (2.38), their assumptions could be criticised, since the presence of a stationary shear plane contradicts the theoretical and experimental

work of many researchers.

Kainth (2.39) showed that Das and Tobias (2.38) made contradictory mathematical assumptions by employing a dynamic angle which is not in complete agreement with their proposed equation during their analysis.

The improved version of the instantaneous shear angle was assumed by Kainth (2.39) to be represented by:

$$\Phi = \Phi + d_{\Phi} \tag{2.4}$$

Where the dynamic variation of the effective shear angle d_{ϕ} is given by:

$$d_{\Phi} = n_1 \, d_s + n_2 \, d_{\alpha} \tag{2.5}$$

where ; ϕ = Shear angle, s = Chip thickness, α = Rake angle.

In equation 2.5, n_1 and n_2 can be obtained from steady-state cutting data from the slopes of (ϕ - s) and (ϕ - α) respectively, represented by:

$$n_1 = \frac{\partial \Phi}{\partial s} \qquad n_2 = \frac{\partial \Phi}{\partial \alpha} \tag{2.6}$$

The modified theory of Kainth (2.39) led to the prediction of unconditional threshold of stability level, which was above that measured experimentally. Knight (2.40) with the aid of high speed photography showed that equation (2.6) is not adequate for representing the shear plane oscillation under regenerative cutting. Knight (2.41) also found that the shear plane responds to the dynamic changes in the cutting conditions. Therefore it can be concluded that the cutting geometry under dynamic conditions could be assumed to be the same as it is under steady state conditions. The contribution of both researchers (2.40, 2.41) indicate that the analysis of the dynamic cutting process still requires further examination of the influential parameters specially with respect to the shear plane response to the dynamic variation in the cutting conditions.

2.8 MECHANISM OF THE REGENERATIVE TYPE CHATTER.

For the machine tool, the self-excited vibration is the result of interaction between the cutting force dynamics and the machine tool structure dynamics. It draws the energy for its maintenance from the tool or workpiece drive.

Because of overlapping cuts, vibrations resulting from the machining of the wavy surface from the previous stroke or revolution of the workpiece or tool, can amplify the subsequent vibration.

These vibrations have an harmonic shape (their frequency is around the natural frequency of the structure) with exponential growth. The block diagram of a simple orthogonal turning operation may be represented as in Figure 2.7. The stability of the demonstrated system depends on the depth of cut, b, and the dynamic characteristics of the cutting operation and machine tool structure . The critical depth of cut (b_{lim}) at the threshold of instability is given (2.42) by:

$$b_{lim} = \frac{1}{2K_c\, Re(G_s)_{min}} \qquad (2.7)$$

where K_c is the cutting coefficient (assumed to be the same for inner and outer modulations, and constant at all the frequencies), and $Re(G_s)_{min}$ represents the minimum value of the real part of the complex structural dynamic frequency response curve.

For unstable cutting conditions, the output of the system in Figure 2.7 b, has a dominant frequency also the vibration of the system increases continuously. The initiation of chatter vibrations in response to a small disturbance is compared with the response of a stable cutting operation in Figure 2.8, (2.43).

Tansel (2.45) has simulated a three-dimensional cutting operation by considering tool geometry, and experimentally obtained the transfer functions of cutting and structural dynamics. The block diagram of

three-dimensional turning operations representing the process under dynamic conditions is illustrated in Figure 2.9. The simulations showed that the workpiece vibrations of the system (uncut chip area variation is non-linear) have an harmonic wave form and their amplitude increase after the initiation of chatter. The growth of workpiece vibrations for different depths of cut from the results of (2.43) are shown in Figure 2.10.

2.9 DYNAMIC BORING BAR FORCE MODEL

There is no satisfactory steady state cutting force model available which can predict the cutting forces under the varying cutting conditions. However, the cutting force under steady state conditions may reasonably be taken to be directly proportional to the uncut chip cross-sectional area.

The dynamic cutting force element produced in a boring bar machining system acts on the machine tool and forces the tool structure into vibration. This causes a change in the relative position of the cutting edge from its equilibrium (steady state) position (see Figure 2.11). The disturbance forces the tool to vibrate in one of its natural modes of vibration. The natural mode of vibration determines the relative motion of the cutting edge with reference to the work and is therefore partly responsible for deciding the form and characteristics of the dynamic force element.

If the natural mode of vibration is in the direction perpendicular to the cutting speed, the speed of the rotation of the work remains constant, no variation in the cutting speed can take place. The only component of the dynamic cutting force to exert any influence on the cutting process is the one in line with the motion. Therefore chip thickness variation results in chatter.

If the vibration direction is parallel to the cutting speed this

will give constant chip thickness but a variable degree of penetration. Hence the cutting speed is also varied.

The quantity of the dynamic cutting forces therefore depends on the relative motion between the cutting edge and on the angle between the constant cutting force and the direction of the principle vibration.

Due to the slenderness of the boring bar, the vibration amplitude at the tool tip is large. This results in a significant variation in the chip thickness and chip width. Hence, the boring force model to be used for the analysis of the boring bar performance should take this into account.

Rao (2.46) proposed an analytical model of a boring bar system working on the assumptions that;

1) The instantaneous boring force is proportional to the instantaneous uncut chip area of the cross-section, under dynamic boring conditions.

2) The effect of radius of curvature of the work on the chip geometry is negligible.

3) The geometrical orientation of the resultant cutting force under dynamic cutting conditions is the same as that in the steady state conditions.

4) The change in the uncut chip cross-sectional area by the nose radius is negligible.

The geometry of the dynamic boring case as considered by (2.46), is shown in Figure 2.11 :

Where R is the resultant force with the components tangential force P_T, and the radial force P_r.

The boring bar undergoes a deflection W_i at the tool tip in the same direction as that of the force R, (W_i being a function of time).

Accounting for this deflection, the instantaneous depth of cut, d_i is given by;

Where d_o is the originally set depth of cut.

$$d_1 = d_o - W_1 \cos \beta \qquad (2.8)$$

To visualise the modification that is taking place in the uncut chip thickness, reference is made to Figure 2.12, where the cutting zone is shown in a plane through the axis of the workpiece.

This figure illustrates the effect of the dynamic boring bar force model by considering the change in the chip cross sectional area under dynamic conditions.

Position 2, in the Figure 2.11, represents the tool location, as if there was no forces acting on the tool.

Position 3, in the same figure, represents the tool location after one revolution of the workpiece from position 1. Therefore the component of the dynamic cutting force which is in line with the motion causing the variation in chip thickness causes chatter.

2.10 EFFECT OF CUTTING SPEED ON DAMPING

At low cutting speeds, stability of the cutting process is high. This has been reported to be associated with an increased damping in the cutting process (2.47). It is found that at low cutting speeds the relationship between chip thickness variation and cutting force variation is such that there is a phase shift between them (2.48). The generally accepted physical explanation of this damping component of the cutting force is based on Figure 2.13 (2.47).

In diagram (a) (position **E**) a tool is shown cutting a chip by moving from left to right while vibrating and producing an undulated surface. **A** small wear flat is shown on the flank of the tool. During the downward motion, from **A** to **C** the clearance between the tool flank and the machined surface is diminished and an interface occurs, as shown in **B** by the shaded area.

Conversely, during the upward motion, from **C** to **E** a positive clearance occurs on the flank. The cutting force consists

correspondingly of a steady component F_{av} and a periodic component shown in (b) which is proportional to chip thickness variation and is in phase with the tool vibration. There is an additional component, shown in (c) which occurs mainly in the F_N component of the force, and which is due to the vibrations of the flank clearance. It is a maximum at B when the down-velocity is a maximum and it is a minimum at D when the up-velocity is a maximum. It is, hence, in phase with the velocity of the vibration and as such it represents a damping force.

From the above discussion it is obvious that this damping will be larger with shorter waves when the slopes are steeper. It will also increase with flank wear of the tool due to an increased interference at B. It should be realised that the wavelength *(w)* is proportional to the cutting speed and inversely proportional to the frequency *(f)* of the vibration.

2.11 CHARACTERISTIC,S OF CHATTER DEPENDENT VARIABLES

The machining stability boundary, if predictable , usually sets a limit for the production rate and workpiece finish. In-process chatter suppression may be possible under some conditions whereby reduction of the cutting speed could improve the dynamic stiffness of the process.

Of the variables affecting the machining stability, tool geometry and machining conditions are the most available and most cost effective control parameters for use by the operator.

The characteristics of chatter may also be considered with respect to the structural response, cutting process or interaction of cutter with the workpiece. Figure 2.14 shows the cutting process parameters that could affect boring bar instability.

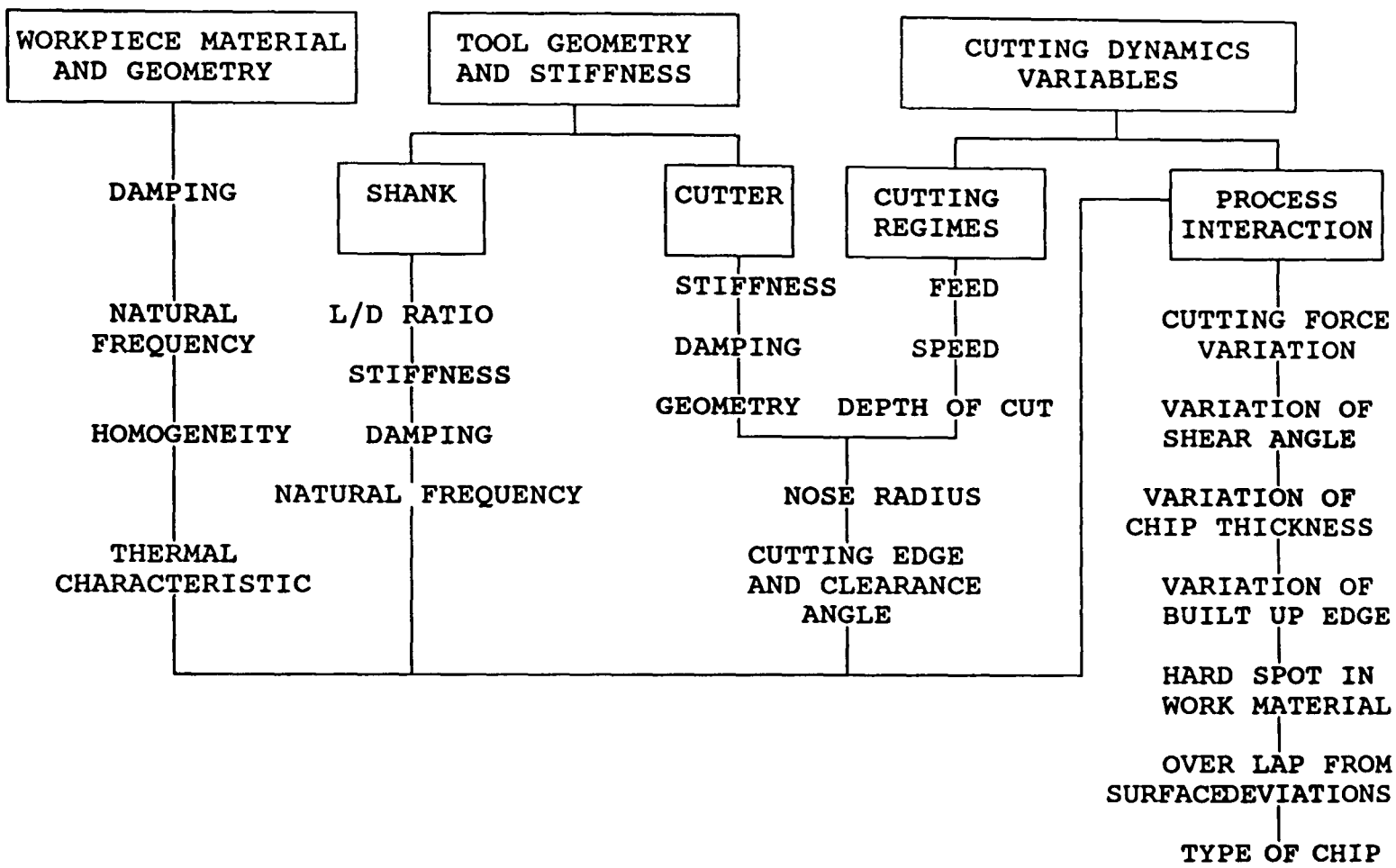

Figure 2.14 : Characteristics of chatter dependent variables with respect to cutting process parameters.

Of the numerous dependent variables involved, the rational approach in design would be to improve the control of the motion of the cutting edge through improved dynamic rigidity of the shank.

2.12 SUMMARY ON THE CAUSES OF CHATTER

The rotating work piece or tool is subjected to forced and free vibrations which may be controlled until the cutting begins. The workpiece and the tool are further disturbed when contact is made by the tool tip which is generally supported by a cantilever structure, such as a boring bar. The impact of the tool and the work piece produces a sudden shock to both the tool and the work and deflects them due to the force encountered by removing material in the form of the

chip.

Provided that the stiffness of the tooling and the work are sufficiently high , the vibrations caused at impact could die out through the natural damping of the system and the damping of the process and allow the operation to continue with acceptable vibration levels.

However, under special circumstances where the damping of the machine elements is not sufficient to sustain the disturbances, the cutting process will produce a dynamic cutting force element which is both velocity and time dependent in nature. This acts on the machine tool and forces the structure into vibration.

This vibration causes a change in the relative position of the cutting edge, which inturn leads to a change in the dynamic cutting force. The disturbance forces the tool to vibrate in one of its natural modes of vibration. The natural mode of vibration determines the relative motion of the cutting edge with reference to the work and is therefore partly responsible for deciding the form and characteristic of the dynamic force element.

If the natural mode of vibration is in the direction perpendicular to the cutting speed, (Direction of the principle vibration) the speed of the rotation of the work remains constant, no variation in the cutting speed can take place . The only component of the dynamic cutting force to exert any influence on the cutting process is the one in line with the motion. Therefore chip thickness variation results in chatter.

If the vibration direction is in parallel to the cutting speed this will give constant chip thickness but variable degree of penetration, and hence the cutting speed is also varied.

The quantity of the dynamic cutting forces therefore depends on the relative motion between the cutting edge and the angle between the constant cutting force and the direction of the principle vibration.

The source of disturbance in self induced vibration is the

interaction of the cutting process with the structure. Cutting speed is responsible for generation of forces that are velocity dependent and can be regarded as damping forces consequently they may either add or subtract from the damping forces contained in the system. If the damping introduced by the dynamic cutting force is positive (ie, absorbs energy) it will increase the structural damping, with the result that the disturbance will rapidly decay. If the damping force brought about by the disturbance is negative (ie, energy is introduced into the system) it will reduce the damping of the system. If this negative damping exceeds the positive damping of the machine tool structure it leads to dynamic instability, i.e, Chatter. Figure 2.15, illustrates a boring bar machining system. It consists of a machine tool transfer function, cutting process sub system, a boring bar structure and a feed back mechanism which forms the link between cutting process subsystem and the boring bar structure.

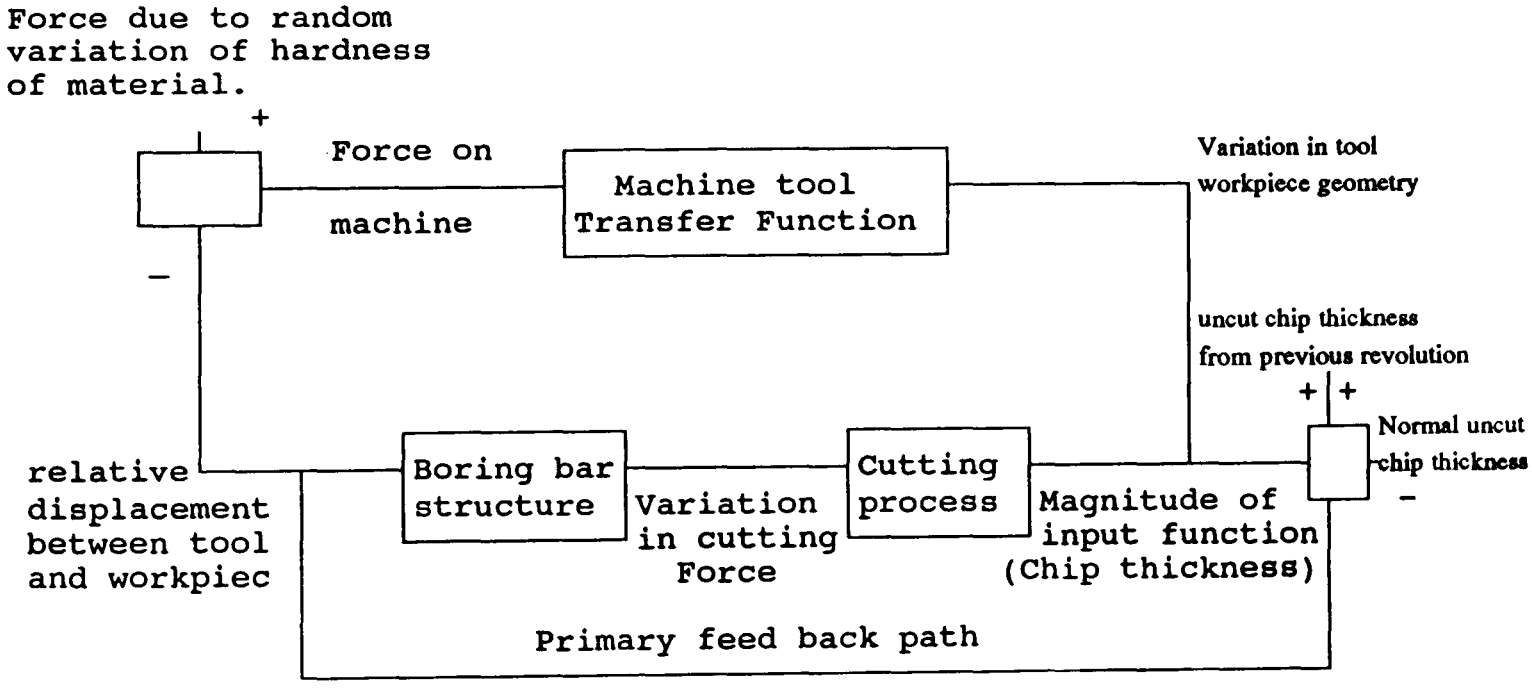

Figure 2.15: Closed loop boring machining system.

The output and the input pair of the boring bar machining system is defined as a pair of displacement of the tool motion in the direction normal to the machine surface and the chip thickness to be cut.

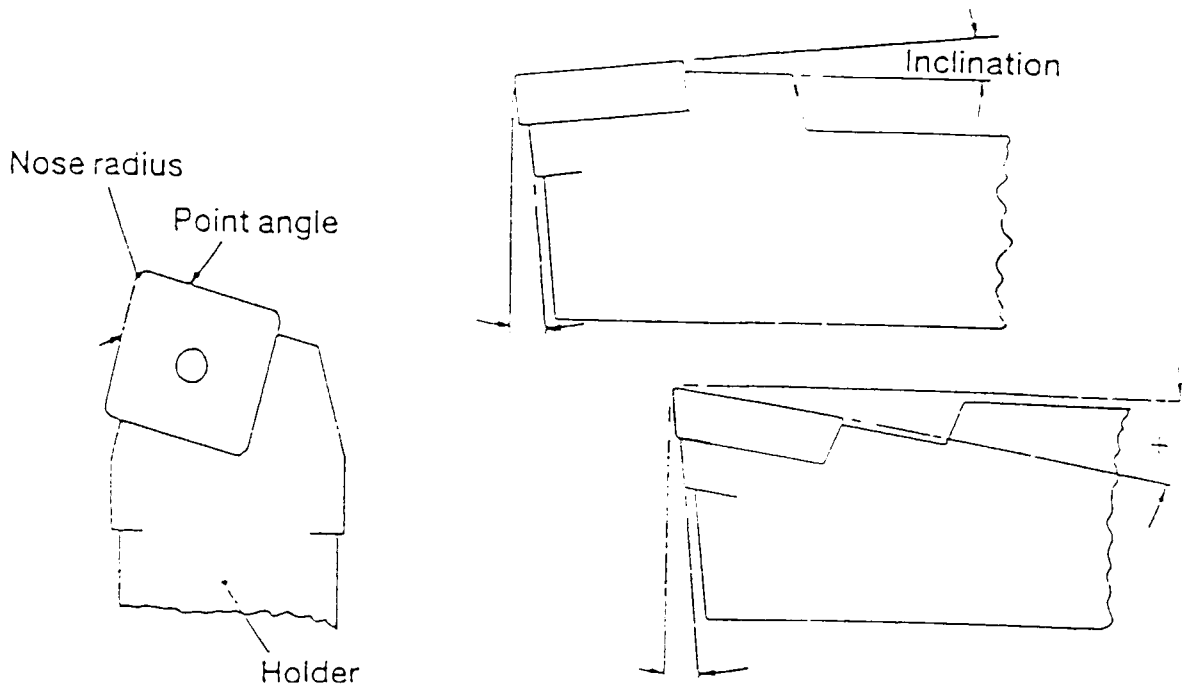

Insert shape and orientation when located in the holder

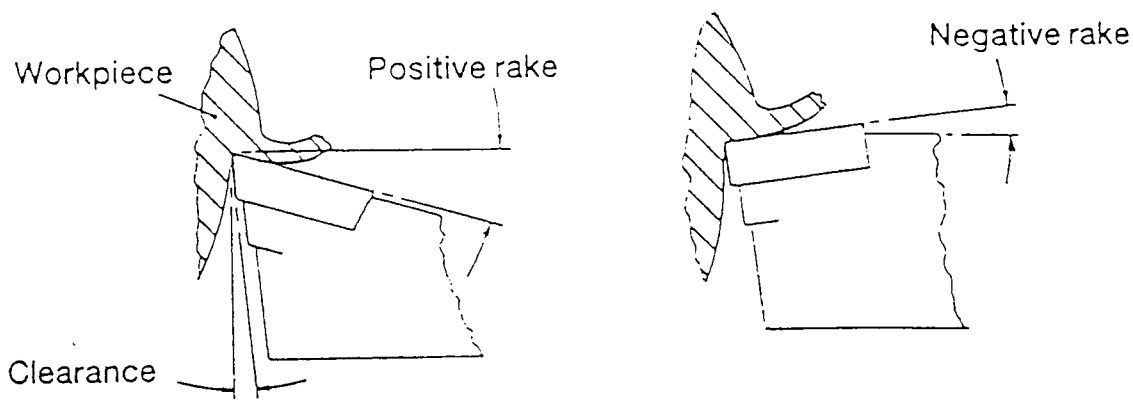

Insert orientation to the workpiece

Figure 2.1 : Turning insert orientation and geometry.

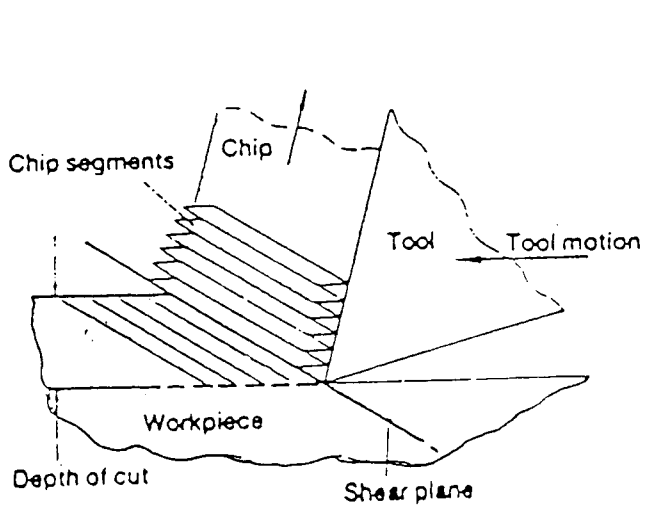

Figure 2.2 a Idealised formation of continuous chip

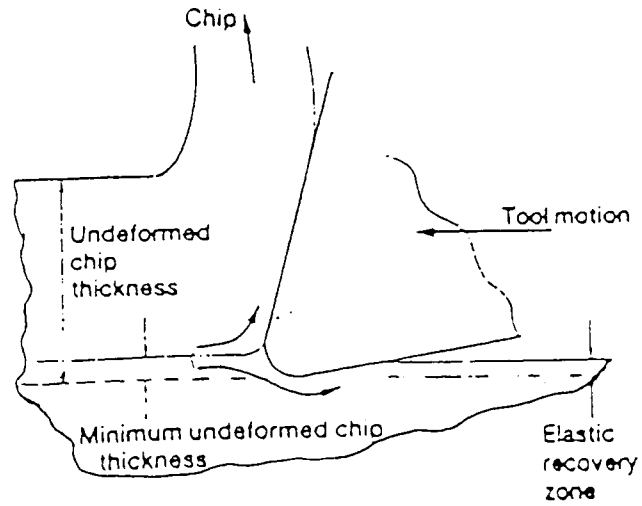

Figure 2.2 b A tool's cutting edge showing the large radius and minimum undeformed chip thickness.

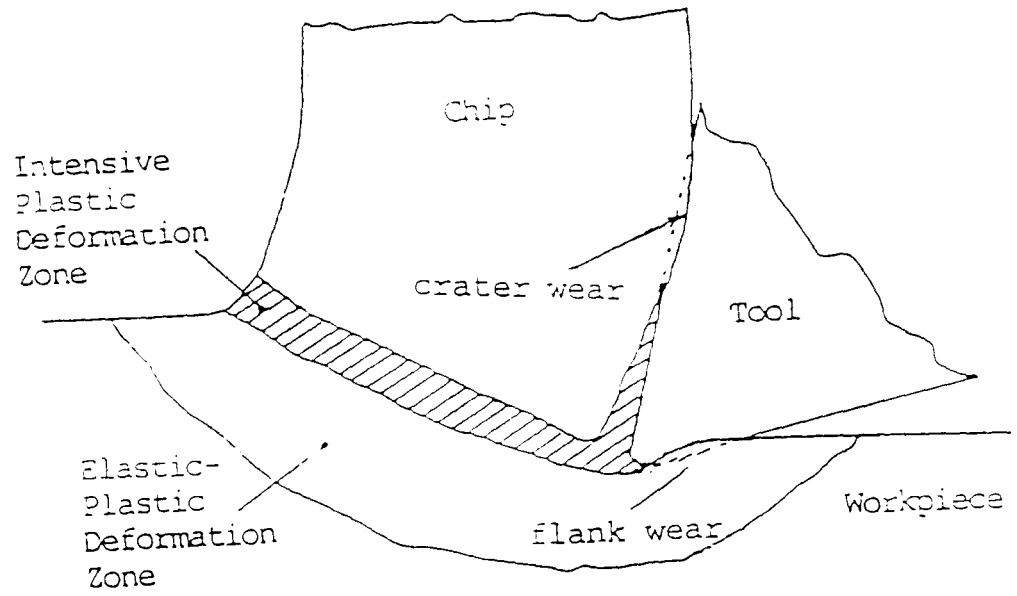

Figure 2.3a: Region of tool wear and deformation zone

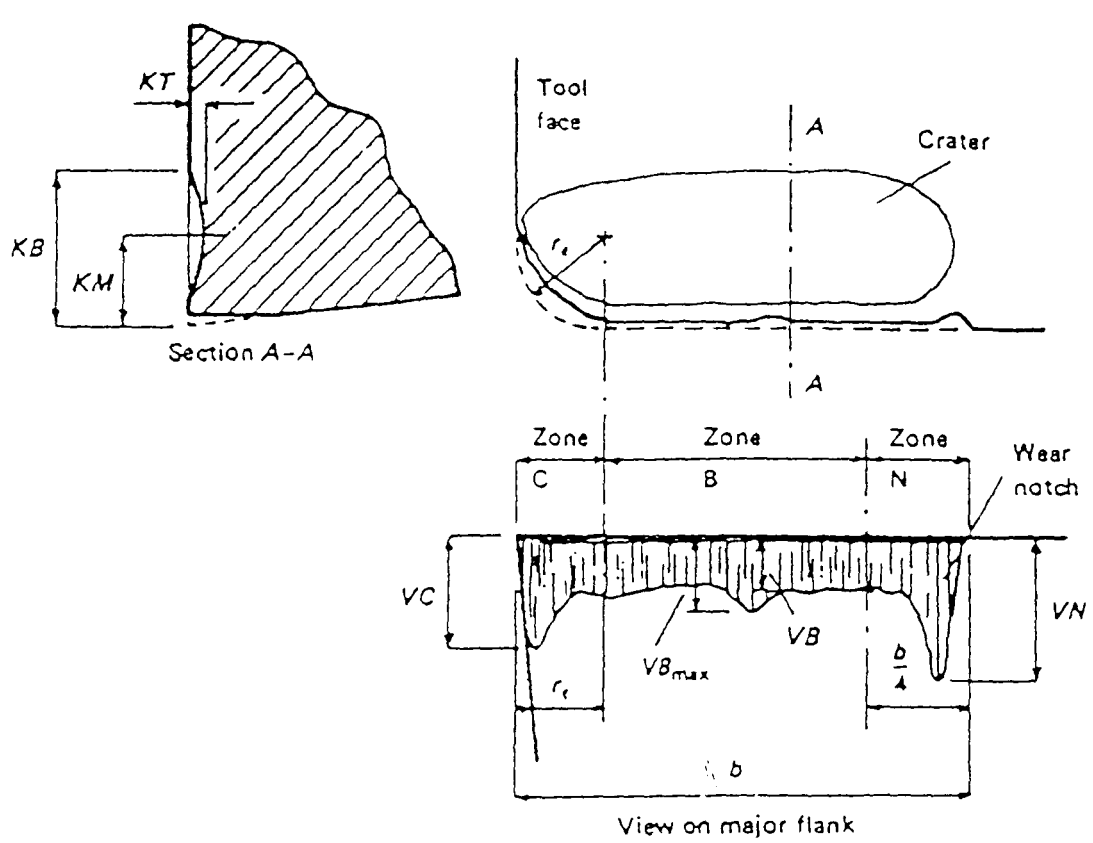

Figure 2.3b: Features of single-point-tool wear (from Boothroyd 1975, p 112). KT is the crater depth measured at the deepest point of the crate, VB is the average wear land width in the central portion of the active cutting edge, VC is the width of the flank wear land at the tool corner, VN is the width of the wear land at the wear notch.

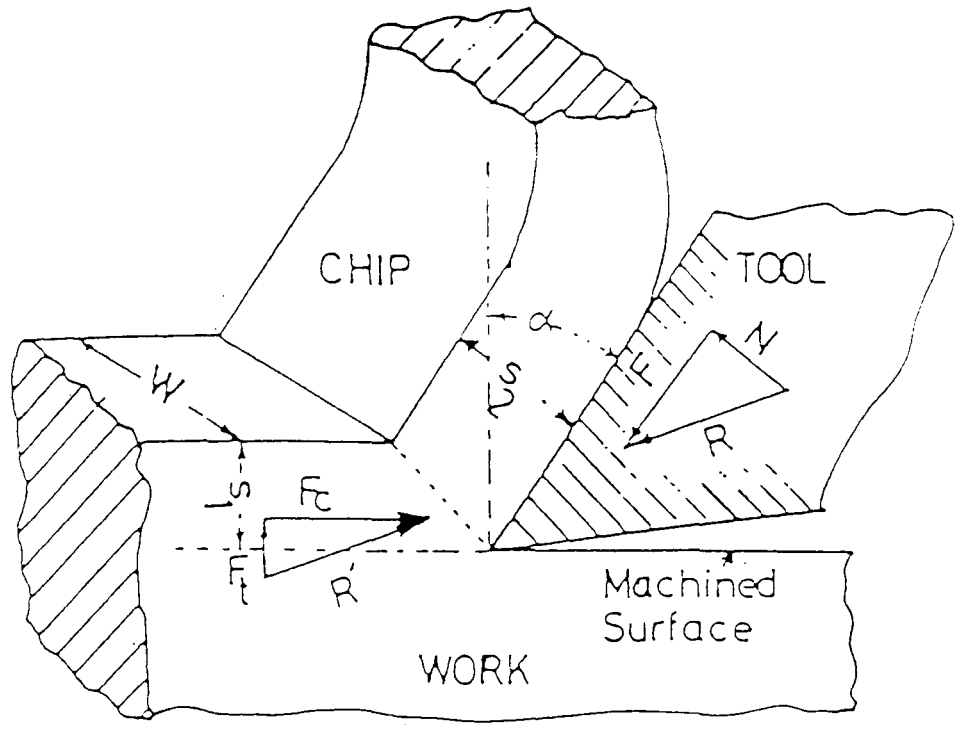

FIGURE 2.4a: MODEL OF ORTHOGONAL METAL CUTTING.

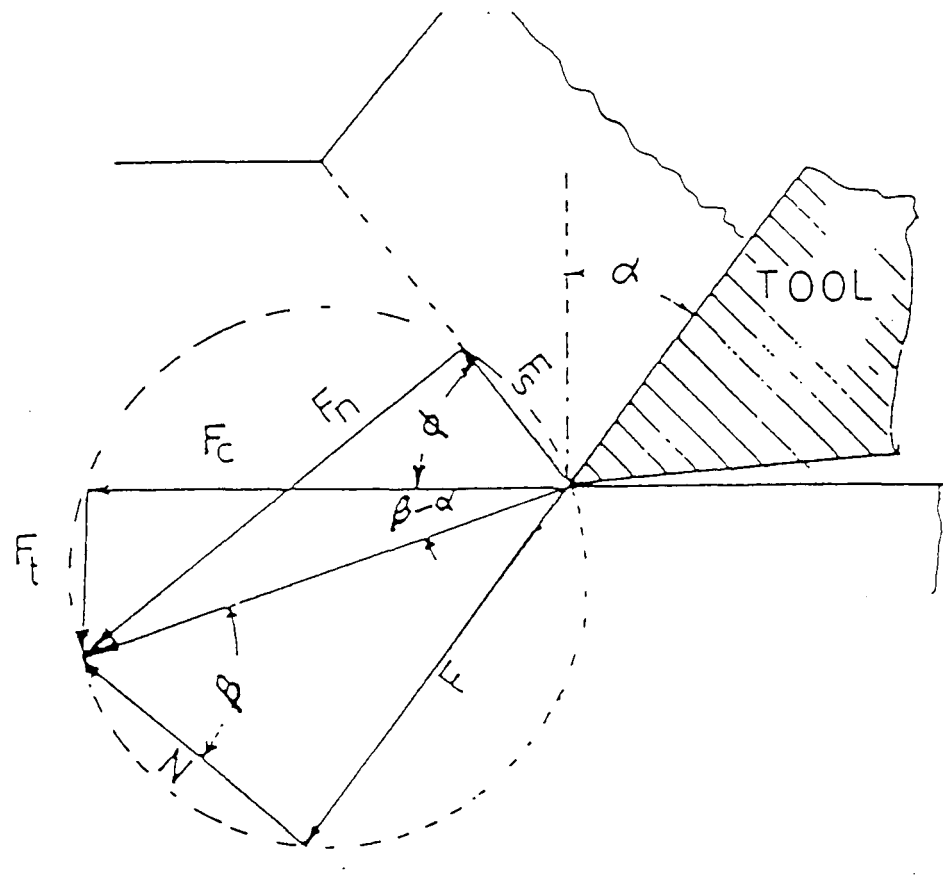

FIGURE 2.4b: FORCE SYSTEM OF ORTHOGONAL CUTTING.

(Ernst and Merchant (2.16))

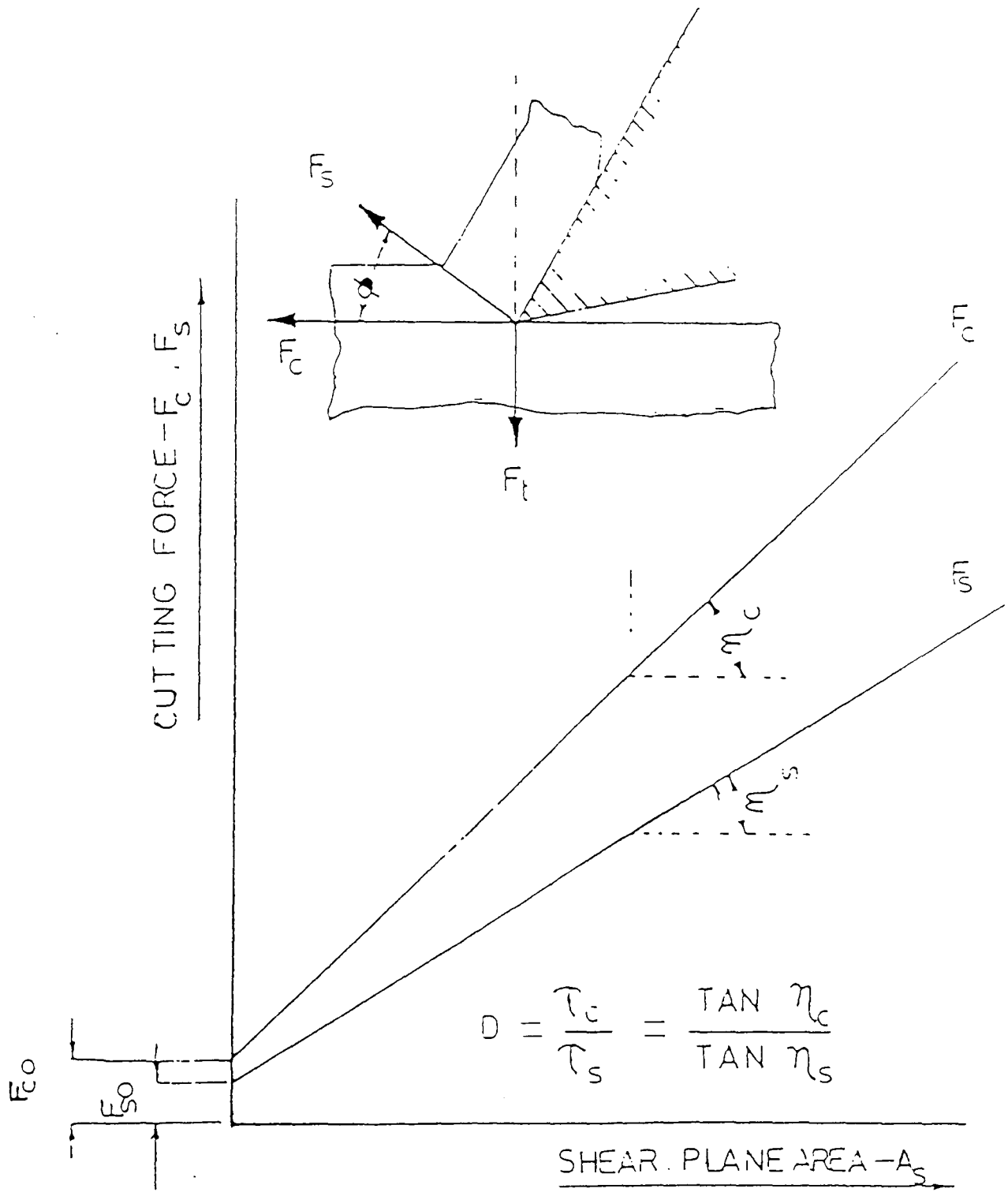

Figure 2.5: UNIVERSAL MACHINABILITY CHART (Das and Tobias (2.27))

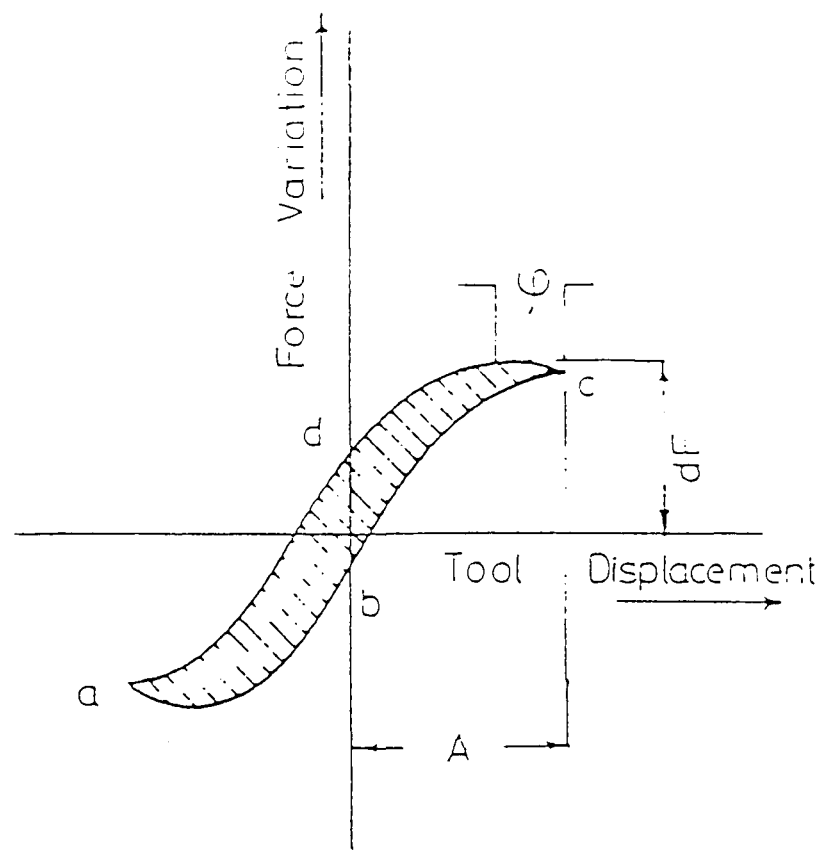

A = Amplitude of vibration
dF = " " Force Variation
φ = Phase Lag or Lead
abcd Lagging Force path.
cdcb Leading " "

Figure 2.6: FORCE DISPLACEMENT LOOP. (Chisholm (2.30))

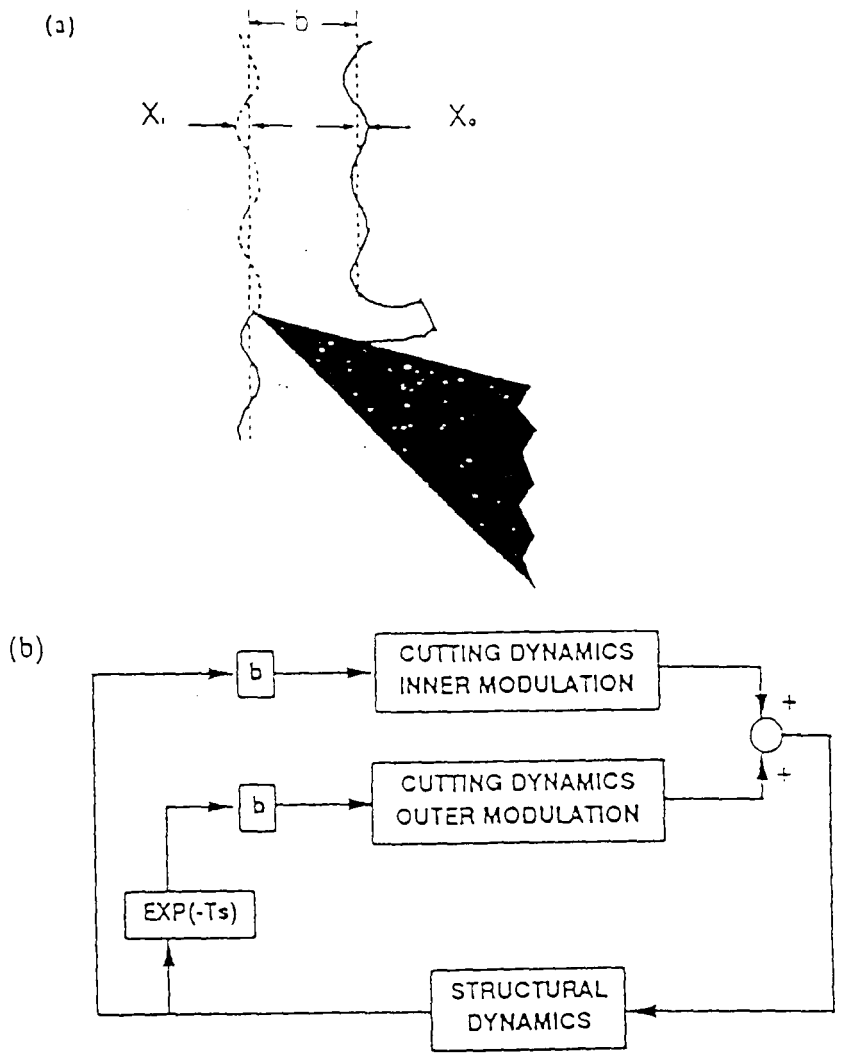

Figure 2.7: Simplified turning operation and an assumed block diagram representing the process under dynamic condition

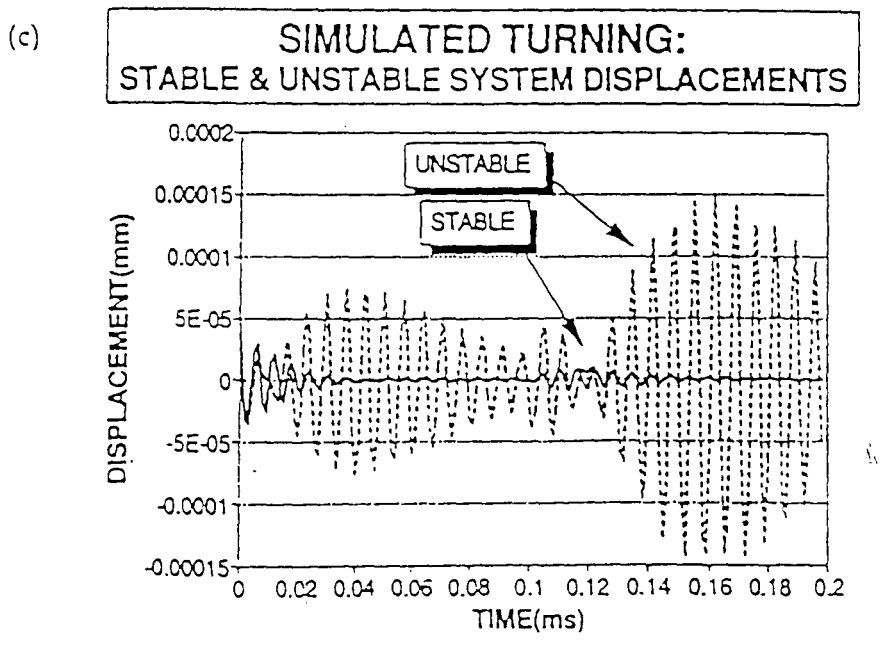

Figure 2.8: Simulated vibration signals of turning operation

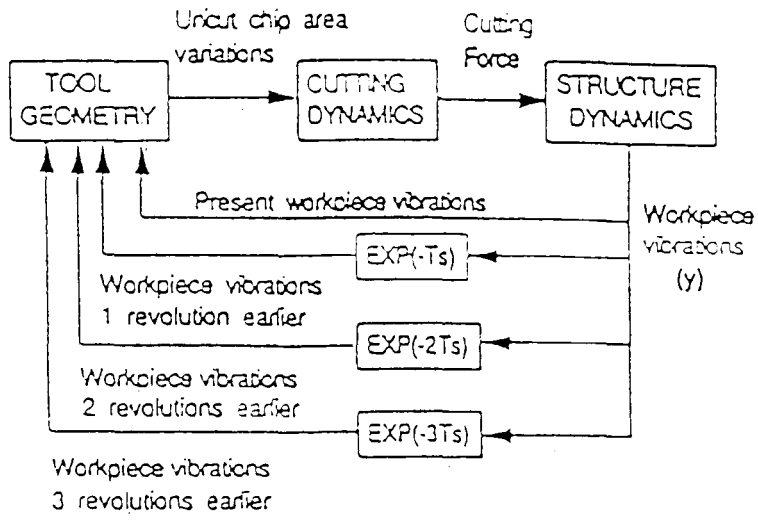

Figure 2.9: Block diagram of three-dimensional turning operation representing the process under dynamic condition

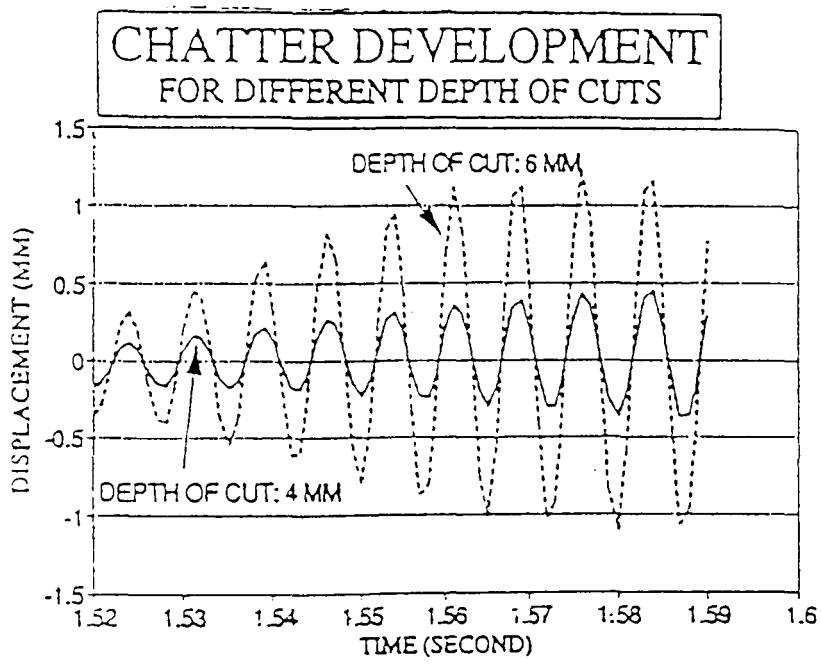

Figure 2.10: Growth of workpiece vibration after chatter starts

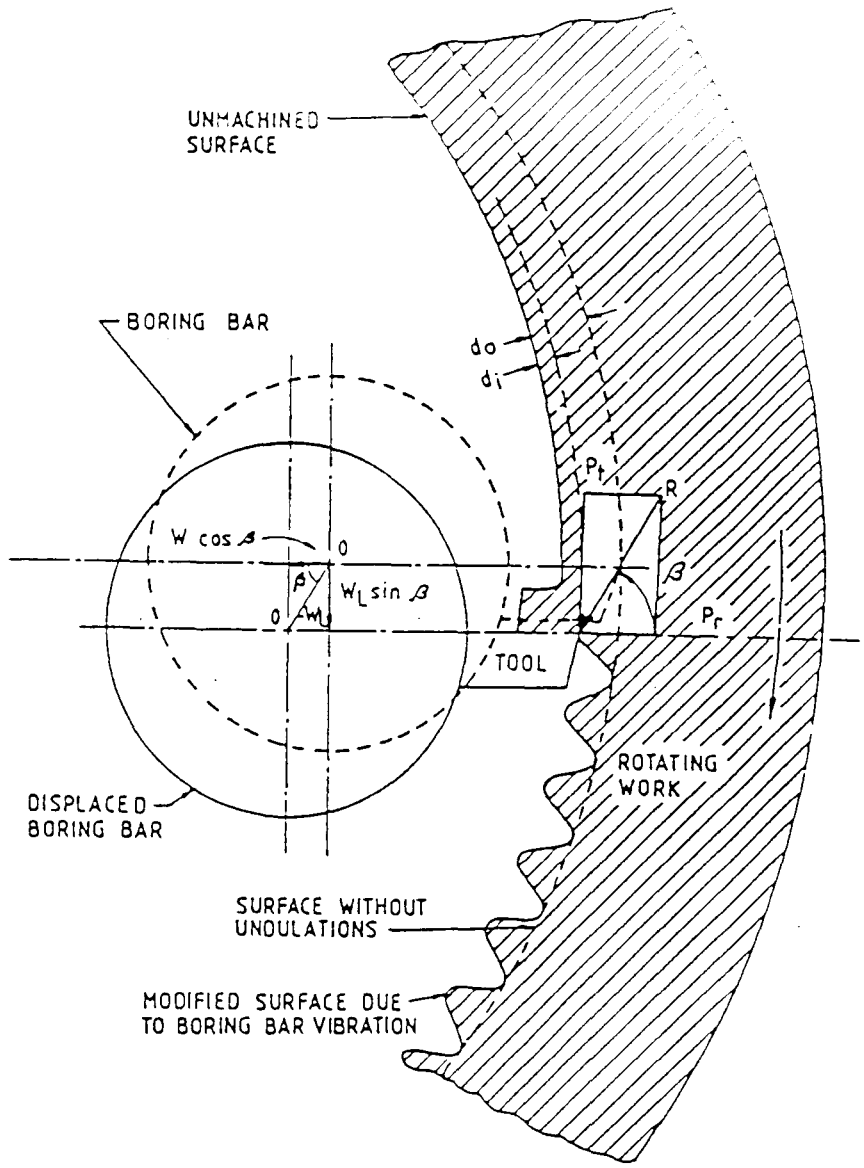

Figure 2.11: End view of boring operation

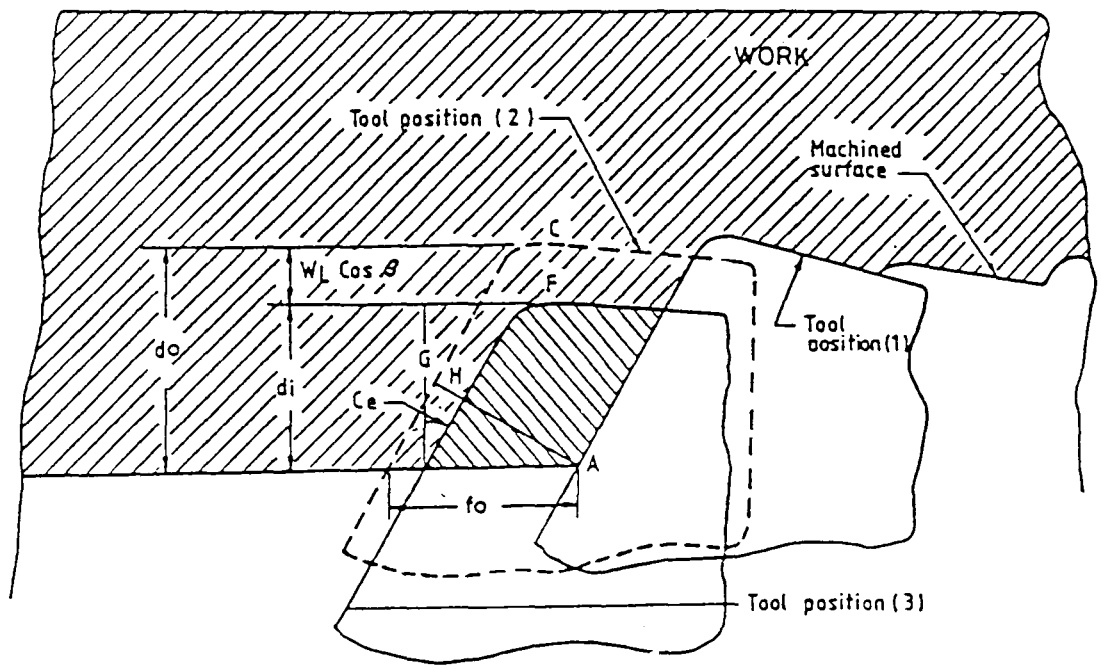

Figure 2.12: Cutting zone in the plane parallel to the axis of the work.

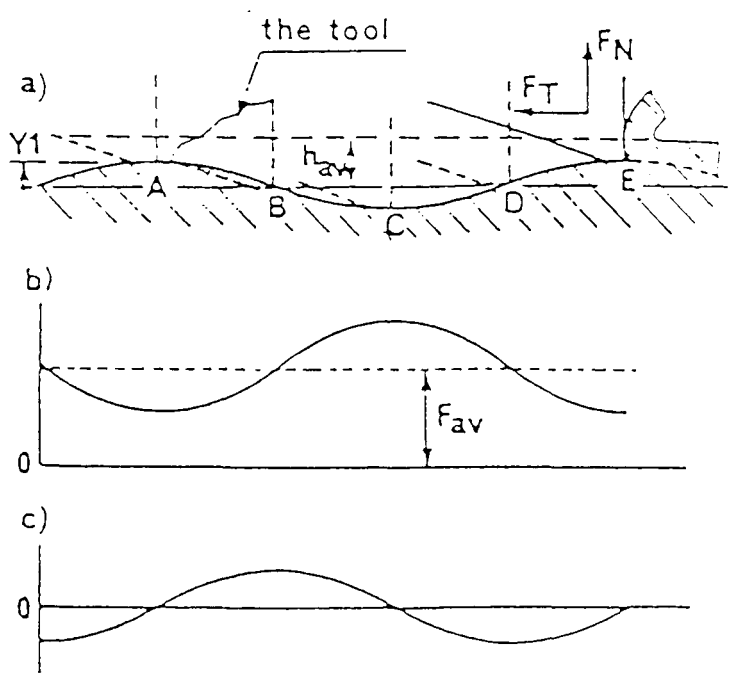

Figure 2.13: Physical causes of process damping.

CHAPTER 3

3.0 FUNDAMENTALS OF CUTTING TOOL VIBRATION

This chapter outlines the general mechanics of vibration characteristics, as applied to cutting tools. It also provides an insight into possible control parameters that can be employed to limit the unwanted oscillations of the boring bar structure.

The general review of the research on the subject of boring bar design for the prevention of chatter are further analyzed.

Finally: from the analytical consideration of the vibration control parameters and functional specification of extended length tool holders a feasible approach is adapted for the design.

3.1 INTRODUCTION

The response of most real-world engineering systems to applied action is usually difficult if not impossible to determine by a closed form mathematical solution. However, there are some approximate numerical methods outlined in this chapter that offer a convenient way of obtaining practical design solutions.

The complex mechanics of machine tool vibrations comprises of the static and dynamic characteristics of the cutting tool, workpiece, machine tool and most importantly the interaction of different elements of the cutting process. In order to propose an optimised solution for reducing the dynamic force response in the tool, analytical consideration of the related mechanics of vibration control are required.

3.2 SYSTEM EQUATION OF MOTION (ONE DEGREE OF FREEDOM).

An idealized one-degree of freedom vibratory system Figure 3.1, is the simplest system, consisting of a spring 'K', a mass 'm' and a dashpot 'C, (3.1).

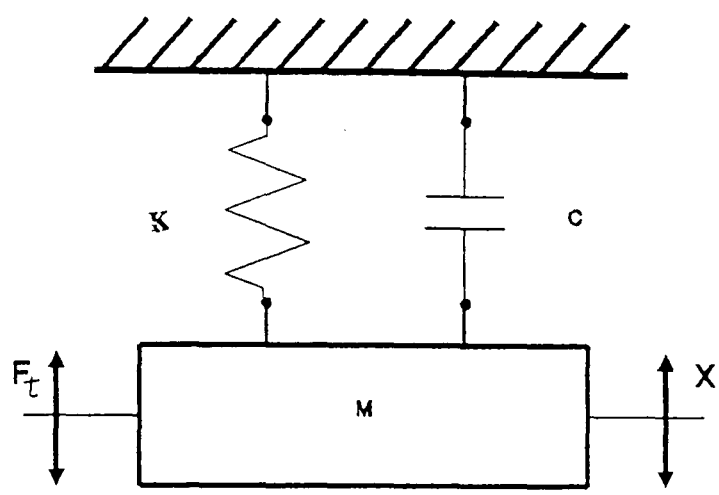

Figure 3.1: Single degree of freedom system

If the mass "m" is displaced from its position of rest, it will be acted upon by the following forces: the weight of mass "m", the restoring force of the spring Stiffness "K", the damping force of the dashpot "C" and the external exciting force F(t). From Newton's second law of motion,

$$m\ddot{x} = F(t) - Kx - C\dot{x} \qquad (3.1)$$

where x is the displacement from the rest position (therefore the weight of the mass is balanced by the initial movement of the spring). Rewriting,

$$m\ddot{x} + C\dot{x} + Kx = F(t) \qquad (3.2)$$

The basic equation for a system with One degree of freedom.

Let ;

$$\delta = \frac{C}{2m} \qquad (I)$$

$$\omega_0^2 = \frac{K}{m} \qquad (II)$$

$$D = \frac{\delta}{\omega_0} \qquad (III)$$

Then Equation 3.2 can be written as ;

$$\ddot{x} + 2\delta\dot{x} + \omega_0^2 x = \frac{F(t)}{m} \qquad (3.3)$$

$$\ddot{x} + 2D\omega_0\dot{x} + \omega_0^2 x = \frac{F(t)}{m} \qquad (3.4)$$

If F(t) = 0, The system would only be subjected to Free Vibration.

If F(t) ≠ 0, The system would be subjected to Forced Vibration.

3.2.1 STATIC STABILITY

In order to operate properly, a machine-tool has to be stable. A system is said to be statically stable only if it returns to its original equilibrium state after the removal of the static disturbance. This means that the restoring force "K" tends to restore the system to its equilibrium condition.

Therefore, a one degree of freedom is stable if the restoring force K > 0, Otherwise it is not.

3.2.2 DYNAMIC STABILITY

After an impact or other disturbances, a system in a steady-state condition of uniform motion may vibrate. If the vibration dies away and the uniform motion is restored it is said to be dynamically stable. However, it can also happen that the vibration will increase

continuously. This type of system is termed dynamically unstable.

For a one degree of freedom vibratory system with K > 0 this system is dynamically stable only if the damping force C > 0,

3.3 VIBRATION CONTROL.

The control and reduction of unwanted vibration levels demands the study of the source of vibration with the objective of minimizing the magnitude of the source levels. This involves consideration of balancing of machine elements and tuning the interaction of cutting process with the supporting structure. However, there is always a limit to the amount of reduction which is possible, so the boring bar structure which is made to vibrate, must be designed to respond to the minimum extent.

There are several different methods of vibration control. Each has its optimum sphere of application.

The vibration control parameters may be summarized as:

ACTIVE CONTROL OF THE DYNAMIC SYSTEM :

Cutting process parameters and tool geometry control.

PASSIVE CONTROL OF THE DYNAMIC SYSTEM :

Structural design, Material selection, Localized additions and Artificial damping.

The level of structural vibration due to a given source is controlled by the threefold characteristics of mass, stiffness, and damping.

The mass and stiffness determine the natural frequency of the structure, whilst stiffness and damping relate to the magnitude of the level at which the structure will experience oscillating deformation at

resonance.

It can be shown that the amplitude responses at low frequencies are controlled by stiffness "K", at high frequencies by mass "m", and at natural frequency by damping "C" (3.2). The vibrations experienced by extended length tool structures may generally be regarded as low frequency under forced conditions and resonant condition under self excited chatter.

3.4 AVOIDING RESONANCE

If a system does not have much damping, then it is necessary to try to avoid resonance if large amplitudes of vibration are to be prevented. In a single degree of freedom system it is possible to avoid resonance provided that the exciting forces occur only at a limited number of distinct frequencies.

The natural frequency analyzed by (3.3) for a uniform cantilever bar is given by;

$$\omega_n = 2\,\pi\, f_0$$

$$f_0 = \frac{1}{2\pi}\sqrt{\frac{K}{m}} \qquad (3.5)$$

$$\textit{Where the stiffness } K = \frac{3E\,I}{L^3}$$

If the natural frequency of the boring bar is close to the forcing frequency of the cutting process increasing "K" or reducing the effective mass "m" of the tool holder moves the operating point on the response curves of Figure 3.2 from near the peak over to the left hand region. In a typical system with little damping, this would greatly reduce the vibration amplitude.

The alternative is to decrease the stiffness or increase the mass. This moves the operating point to the right hand side of Figure 3.2,. The amplitude of vibration is likewise reduced, but there are obvious disadvantages. Decreasing the stiffness of the boring bar may

mean that it is insufficiently rigid to fulfil its function property of dimensional fidelity resulting in excessive deflections or even plastic deformation which consequently results in misalignment of the centre line of the tip relative to the workpiece.

Often the frequency of an exciting force is linked to the speed of rotation of the tool or workpiece as discussed in chapter two. During starting and stopping, the force frequency changes between zero and its normal operating value. If the natural frequency of the tool is less than the forcing frequency during normal cutting, so as to operate on the right hand side of Figure 3.2, then the system has to pass through resonance during starting and stopping. This requires either a lot of damping so that the peak amplitude is not too great, or the ability to speed up is sufficiently rapidly to prevent the peak amplitudes building up. The bar may also be externally excited above its fundamental natural frequency to operate above resonance peak.

In a system with many degrees of freedom such as the cantilever boring bar, there will be many natural frequencies, (see chapter eight) each of which will have a resonance peak associated with it. Therefore it may be difficult to avoid resonance, particularly if the exciting force has components at a number of different frequencies.

For example, the exciting force may change due to varying machining conditions, variation of surface quality of previously cut surface, existence and disappearance of built up edge, metallurgical homogeneity or hard spots as well as behavioural properties inherent in the cutting of different materials.

Ideally the lowest natural frequency must be higher than the highest exciting frequency, thereby ensuring that resonance does not occur. In circumstances where this may not be possible the damping treatments considered in the next section may be required for more satisfactory control of vibration amplitude.

3.5 DAMPING

Simply stated, damping is the dissipation of energy in the vibrating systems that results in either the control of the amplitude of oscillations or their eventual decay (3.5). In mechanical systems, damping can be classified as passive or active.

Active damping uses externally applied feedback control forces to limit the deformation.

Passive damping makes use of properties that can be incorporated as an inherent feature of the system. Energy dissipation takes place within stressed elements of the vibrating system or as energy being imparted to the surroundings.

3.5.1 INTERNAL DAMPING IN STRUCTURE AND MATERIALS

When a material is deformed, part of the energy put into the material is stored as elastic strain energy which can be recovered when the deforming forces are removed. The remainder is dissipated as heat (3.5) and to some extent as sound.

Except for special alloys, such as manganese copper, the damping that can be obtained from structural metals is too small to prevent high resonance peaks. Nevertheless, since the height of peaks is inversely proportional to the damping, it may occasionally be worth considering the damping capacity in design, when selecting materials. Thus cast iron may be preferable to steel because it has about four times the damping capacity.

However, more damping will probably come from sources other than from the materials themselves. Material modification may be more significant in improving the static and dynamic stiffness of the boring bar.

Initial structural damping originates in :

a) Hysteresis of the structural material,

b) Friction at structural joints,

c) Friction with attached non-structural items,

d) Viscous damping at lubricated sliding surfaces.

It is convenient to quantify the damping in terms of the dimensionless loss factor, η_m, corresponding to the given mode of vibration (3.2). Then;

$$\eta_m = \frac{1}{2\pi} \frac{\sum \textit{Energy dissipated per cycle by each source}}{\textit{Maximum energy stored In the structure per cycle}} \quad (3.6)$$

Friction at structural joints is often the major contributor to structural damping. Analysis of the energy dissipated in structural joints are detailed by reference (3.6). Figure 3.3 illustrates the effect of damping on free response (3.4).

3.6 ARTIFICIAL DAMPING THROUGH ADDED DAMPING LAYERS

The structural composite damping was reported (3.19 - 3.21) to be strongly dependent on structural configuration and deformation state. In order to realise significant structural benefits from the damping of composite materials, integrated damping mechanics are required (3.5).

The theory suggests that if a beam vibrates in flexure, it can be damped by the addition of a layer of damping material. As the whole system vibrates the layer undergoes cyclic strain and thereby dissipates energy (3.2). The damping material is usually a syntactic rubber (PVA/PVC) or a bitumen-based compound (3.2).

These materials have high capacity for dissipating energy, and this is quantified by the material loss factor. The complex cyclic stress and strain are related through the complex moduli, thus if ϵ and γ are direct and shear strains respectively. η_d and β_d (the loss factors

in direct and shear strain respectively) are usually assumed equal (3.2).

$$\textit{Direct stress} \qquad \sigma = E' (1 + i\eta_d)\, \epsilon \qquad (3.7.a)$$

$$\textit{Shear stress} \qquad \tau = G' (1 + i\beta_d)\gamma \qquad (3.7.b)$$

E´ and G´ are the 'storage moduli', and the maximum energy stored per unit volume in a strain cycle of amplitude ϵ or γ is

$U = E'\epsilon^2/2$ or $G'\gamma^2/2$.

The corresponding energy dissipated per cycle is;

$$\Delta W = \pi E' \eta_d \epsilon^2 \qquad (3.8)$$

$$\Delta W = \pi G' \beta_d \gamma^2 \qquad (3.9)$$

For a given strain amplitude, the energy dissipated per cycle is proportional to the *product* $E'\eta_d$ or $G'\beta_d$.

Consideration of the application of surface damping treatment as a design option for boring bar vibration control is useful since any material disturbance would carry its maximum strain energy on the surface of the body. The analyses of the results from the finite element model in chapter seven and modes of vibration for a given tool, chapter eight, can be used to determine the position of the most effective part (ie, position of maximum strain energy concentration) of the boring bar where such treatments may be applied for maximum damping effects.

Discussion of vibration related problems in boring out deep holes with experienced engineers revealed the fact that the operator's remedy to this problem would be to hold the shank simply by hand or by wrapping elastic bands around the tool. Such treatments can easily be applied to existing structures that may provide good damping capability over narrow temperature and frequency ranges.

3.6.1 EXTENSIONAL DAMPING TREATMENT;

This method of damping treatment makes use of an unconstrained layer of damping material added to the surface of a beam with its outer surface perfectly free. As the beam bends, the layer is subjected to direct bending strains which are proportional to the local curvature shown in Figure 3.4.

The damping layer dissipates energy principally by virtue of bending strain cycles of the boring bar under dynamic loading of the cutting process. For maximum energy dissipation, the material must have high values of storage moduli E′ and loss factor η_d

The analyses widely accepted for such damping treatments are due to Ni and Adams (3.18) where they consider a layer of uniform thickness of damping material attached to a beam or plate of uniform cross section. The modal loss factor of flexure vibration for beams or plates is given by;

$$\eta_m = \eta_d \frac{E' I_d}{E_s I_s + E' I_d} \qquad (3.10)$$

Where;

I_d is the 2nd moment of damping material
I_s is the 2nd moment of structure

Damping material	H_2
Structure	H_1

When only one mode is to be damped greater efficiency of unconstrained layers are obtained by removing the damping material from regions of low bending curvature and adding it to regions of high curvature. This ensures that the damping material is subjected to the greatest direct strains, and so dissipates the most energy. It should be mentioned that the effectiveness of every damping device is subjected to certain boundary conditions, and for this type of damping

system the principle factors are:

a) TEMPERATURE EFFECTS;

Since the performance of Visco-elastic materials is directly governed by the working temperature of the material it is important to take the temperature element into consideration.

At low temperatures the material is in the glassy regime, therefore whenever the system is subjected to cyclic bending, small deformations occur and hence energy dissipation is small. Energy dissipation at high temperatures are also minimal since the material is in the rubbery and soft regime. Between these two extremes, the material possesses an optimum modulus value, so that the energy dissipation for the system goes through a maximum.

b) EFFECTS OF THICKNESS;

The next variable in the design for surface damping treatment is the thickness of the damping material relative to that of the structure.

Figure 3.5, illustrates the variation of composite loss factor with temperature for different thickness of damping material. From this diagram it can be seen that by increasing the thickness of the Visco-elastic layer higher damping can be achieved in the system. However, this increase in damping is not a linear function of thickness (3.4).

However, with practical designs there is a limit to the thickness of visco-elastic material that can be incorporated into the boring bar structure.

Further improvement in loss factor may be achieved through combining the material with a constraining element, so that more energy is dissipated by subjecting the damping layer to shear.

3.6.2 SHEAR DAMPING TREATMENT;

This treatment is similar to the unconstrained layer except that the Visco-elastic material is constrained by a metal layer. Therefore whenever the structure is subjected to cyclic bending the metal layer will constrain the Visco-elastic material and force it to deform in shear. The shear deformation is the mechanism by which the energy is dissipated. Figure 3.6, illustrates the basic concept of constrained layer damping. The shear type of treatment is more efficient than the unconstrained-layer damping (3.4). However, this efficiency is offset by being more difficult to apply.

In addition to the properties of the damping material, the maximum shear deformation in the middle layer is a function of:

a) The shear modulus and the thickness of the constraining layers,

b) The thickness of the damping layer,

c) The wavelength of vibration,

The term that contains these variables is the shear parameter "g" which is given by:

$$g = \frac{G_2}{E_3 H_3 H_2 P^2} \qquad (3.11)$$

Constraining layer	H_3
Damping material	H_2
Structure	H_1

Figure 3.6 : Constrained-layer treatment. (3.4)

Where;

E is Elastic Modulus, G is Shear Modulus, H is Thickness, P is the wave number ($P = \zeta_n/L$), ζ_n = nth Eigen value, Subscript 1 refers to base structure, Subscript 2 refers to damping layer, Subscript 3 refers to constraining layer,

The variation of loss factor with shear parameter "g" for different thickness ratios $h_2 = H_2/H_1$ and $h_3 = H_3/H_1$ is illustrated in

Figure 3.7 and Figure 3.8 (a) and (b).

It is evident from these plots that to fully utilize this type of treatment, the shear parameter must be selected so that the system loss factor is a maximum. Therefore, the flexibility in the design process of a vibratory system with fixed wavelength may be through variation of the damping and constraining layer thicknesses to achieve the desired level of damping.

The performance of the constrained layer damping also depends on the geometry and type of constraining layer. Usually it is desirable to have the constraining layer as stiff as possible to introduce maximum shear strains into the Visco-elastic layer.

3.7 VIBRATION CONTROL BY LOCALISED ADDITIONS

Damped vibration absorbers (DVA) are typical examples of localized additions that can be incorporated in cantilever structures for improving the dynamic compliance of such systems. They have been described as devices that can be added to a system to reduce vibration amplitude by the introduction of equal and opposite dynamic forces and/or by introducing damping to dissipate energy (3.7).

The principle of operation of a vibration absorber is to put a second spring and inertia mass system in series with the primary system. Theoretically, by correct phasing of the spring and mass dynamic system, the displacement of the primary system can be reduced to zero.

A common problem that may arise is that of tuning the absorber for optimum performance. When an absorber is designed, the spring constant and effective mass are determined. The goal is to tune the absorber so that the frequency ratio is unity.

The effectiveness of a DVA for a given mass depends on the vibration amplitude at its attachment point. Accordingly, absorbers are

usually installed in the farthest available positions along the cantilever. Another factor determining their effectiveness is the mass value of the inertia weight of the DVA.

To achieve a reasonable degree of DVA effectiveness materials with very high specific density must be used for inertia weights.

The theory of DVA, and its application in boring bars has been thoroughly analyzed and well documented, however, optimisation of such systems is required for effective design of such tools. In Appendix "B" precise analysis for optimisation of such absorbers has been made using finite element as the tool. The object of this exercise was to quantify values of the design parameters.

3.8 REVIEW OF THE PREVIOUS WORK ON BORING TOOL DESIGN

Several techniques are available for enhancing the chatter-resistance of cantilever tools. They may be classified as either passive or active approaches.

The application of passive devices is directed at reducing the dynamic compliance of the boring bar in the frequency range of the machine tool and the cutting process fundamental mode. The concept more generally refers to the correct correlation between the mass, the stiffness and the damping in design of the boring bars for an optimised dynamic system.

The up-to-date approaches in the design of boring bars are:

- Use of high Young's modulus and/or high damping materials;
- Use of passive Dynamic Vibration Absorbers, (DVA) .

In the late 1950,s due to a realization of the benefits of high modulus carbides, machineable sintered tungsten carbide with an elastic modulus equal to 3.5×10^3 GPa was introduced to industry as a solution to the problem of chatter.

The problem with these materials was their high cost both in material and the manufacturing process. Moreover, since they are nearly twice as heavy as steel with an elastic modulus value of about 1.6 times that of steel, therefore the compliant frequency response is infact 20 % lower than that of steel bars.

An alternative to the use of materials as a means for improved equivalent stiffness was proposed by Lee (3.9). The boring bar was fabricated with high moduli graphite epoxy composite material with both specific stiffness and damping higher than that of steel.

From the observations of the results the main drawback of this design was the limited length to diameter ratio achievable, this was a factor of 7-8, the other drawback is the relatively difficult method of manufacture.

The use of impact dampers for application of chatter control in machine tools was first introduced to industry by Kennametal in the late 60,s (3.8). These devices consisted of a wheel that rolls on the outside circumference of the workpiece. The wheel is supported by a hinge yoke and contacts the work just behind the cutting tool. The wheel is held on the workpiece by gravity. The wheel contains inertia disks which are free to float with in the wheel housing. When the rotating workpiece begins to vibrate the inertia disks make random impacts which are transmitted to the work through the contact wheel, and set up a counter force to resist the vibrating force. There are several drawbacks to this method,

a) There will always be a time delay between the dynamic force response of the process and the damper. Therefore a phase shift of the counter force on the work may not follow an effective damping.

b) The chips and debris on the workpiece could easily make unwanted impacts on the work subjecting the process to forced response.

c) The disturbing force and impact force may not be of the same magnitude.

In the late 60,s Austin tool company (3.8) developed a composite boring bar, where the root segment of the bar was made of tubular tungsten carbide, while the front section incorporated a damper. This damper makes use of Coulomb or friction damping. A large mass element as shown in Figure 3.9, was located in the working end of the tool. This was spring loaded against a suitable bearing surface and supported concentrically within a tapered cavity. The cavity in the large mass contains a small mass which is also spring loaded. The arrangement produces movements of both elements during severe vibration.

With this method of damping there must always be relative motion between damping mass elements and the bearing surface to generate Coulomb friction, which provides the resisting force to dissipate the vibration energy. This force though small, was reported to operate at such a high frequency that its damping effect was similar to that of laying a finger on a vibrating violin string.

Vernon Devices (3.8) have developed a boring tool that uses an entirely different principle to prevent vibration as shown in Figures 3.10 (a) and (b). This tool is designed to support a boring bar at the cutting edge and is reported to be six times as rigid as an unsupported boring bar of similar proportion. The tool consists of a trueing bit which starts the boring by correcting the initial misalignment and out-of-roundness of the pre-drilled hole. The nose cone which is used to support the bar inside the bore, contacts the perimeter of the hole; coolant flow begins when the nose cone engages the workpiece.

The boring bit engages the work piece as the nose cone receives pressure from the internal spring. The boring cutters now receive full support. The bore bit generates the desired hole in a single path. Although this is one of the most effective methods of generating good quality bores, it can also be regarded as one of the most expensive methods.

There may also be further drawbacks due to:

a) The bore size is limited to the range of the adjusting radius of the bore bit. Typically 45 - 60 mm.

b) The nose cone is in direct contact with the initial bore, causing wear on the part which would require frequent maintenance and increase cost of operation.

c) entrapped chips or debris on the nose cone could cause instability of the process.

R.S.Hahn (3.12) applied the Theory of Damped Vibration Absorbers (DVA) to a boring bar. The damper shown in Figure 3.11, consists of a piece of heavy-tungsten alloy that is placed unconstrained in a cavity located as near to the free end of the bar as possible. The cavity and the slug are accurately finished so that the slug will be supported by an air film. When under dynamic excitation, inertia of the slug damps out the vibration of the bar.

Although this design was revolutionary in its nature some basic problems associated with it eliminated the widespread use in industry and further research was necessary to alleviate the following problems.

a) There were no controlling parameters of the inertia force, so that if the inertia force was in phase with the vibratory frequency, it would result in feeding energy to the vibratory motion rather than damping.

b) The overall stiffness of the bar was not considered.

c) No consideration was given to impaired natural frequency of the bar due to inertia weight. This theory was further investigated by numerous researchers (3.13 - 3.17).

Rivin (3.13) in a US patent 3,820,422 (1974) improved the Hahn damper by making the root segment of the bar, which is responsible for maximum potential energy from a high modulus material to improve the stiffness and made the free end from steel which incorporates the damper.

This design suffered from lack of provision of controlling parameters. Also the use of tungsten at the root segment increases the mass of the bar which in turn reduces the natural frequency.

R.W.New et al. (3.17, 3.18) during continuous research from 1974 to 1983, had correlated the required parameters, and used them in designing the tool holder. The bar was basically of the same construction as in reference (3.12) with the difference that the brittle tungsten carbide was protected in a steel tube. The free end of the bar incorporated the DVA construction with the physical parameters correlated and optimised for improved effective damping. The tool was reported to operate at Length to Diameter ratios of 15 to 1.

The improved version of the Hahn (3.12) damper currently in use in industry is the Sandvic TNS Bars as shown in Figure 3.12. The design differs from the Hahn damper whereby a tuning mechanism of the inertia mass has been introduced to the boring bar. The dynamic compliance of the inertia mass which is suspended in the tool cavity by rubber bushes may be altered by a screw ram, so that for a particular vibratory motion the response of the inertia mass is tuned to the operating frequency.

The technical problems of Sandvic TNS Bars are as follows ;

a) Since the response of a process could change during cutting, in-process tuning may not be possible.

b) The root segment of the bar is made of standard tool steel and makes no contribution to the overall stiffness of the bar.

There are numerous other reported researches on the subject with claims of possible improvement on chatter suppression. The major part of these reports fall into the Active treatment category (which is in-process measurement and control of the cutting parameters). These methods could have some potential, although they are mainly laboratory techniques and require expensive sensory and measurement devices. The end result is usually a reduction of production rates.

3.9 DESIGN PRACTICE,

3.9.1 THE TOOL MOUNTING DESIGN

An important link in the prevention of vibrations during the machining process and performance of the complete system is the tool mounting. The tool holder should have the highest natural frequency possible. The greater the dynamic stiffness that characterises the holding device the higher the natural frequency of it. If the tool mounting does not have a high natural frequency, there may be a tendency for the bar and the tool mounting to oscillate at the same frequency, as one body.

It is also important that the clamping arrangement is designed such that maximum contact is provided for the tool. This relates to the correct choice of clamping length, accuracy, surface finish and hardness. The recommended values for tool mountings by tool manufacturers are;

Clamping Length: 3 - 4 x the bar diameter.

Hole tolerance: H8

Surface finish: $R_a = 1.8\ \mu m$

Hardness: 45 Rockwell 'C' or better.

For the benefit of experimental work in this thesis a tool mounting was designed which constituted part of the test rig. The designed fixture provides support in all directions whilst allowing good contact by having a honed surface finish. The corresponding value of the measured surface is given in Figure 3.13. Since at different overhang the static deflection of the bar varies it was important to design a mechanism that could cater for any centre line misalignment. A cam-shaped sleeve was fabricated to allow for the required adjustment. Figure 3.14, illustrates the constructed clamping arrangements.

3.9.2 BORING BAR AS A STATIONARY CANTILEVER STRUCTURE

The critical limiting factor in the application of cantilever structures is their sensitivity to both resonant (Forced) and especially self excited chatter vibrations. Both resonance frequencies and chatter resistance are correlated with the length (L) to radius (r) ratio of the cantilever holder .

The external diameter of a cantilever boring bar is limited by application constraints, therefore the only way for stiffness enhancement is to select a material with a higher Young's modulus.

In addition to material selection, shape optimization could also benefit from enhanced natural frequency or reduced deflection caused by inertial forces. An optimal shape would be a variable cross sectional bar whose cross section is gradually diminishing with position along the cantilever with greatest thickness near the clamped end. However, for a boring bar some minimum space is necessary to attach a cutting tool.

With conventional boring tools it is difficult to achieve stable cutting at overhang ratios exceeding length to diameter ratio L/D = 4. While this ratio is not high, it should be noted that to machine a hole the diameter "D" of the tool has to be smaller than the hole diameter to accommodate the cutting head, but the length "L" of the tool should be longer than the hole depth to eliminate danger of interference between the fixture holding the tool and the part being machined.

In the design of the tool physical laws concerning the relationship between length and cross sectional area are essential. For example:

a) Bending stiffness or flexural rigidity = EI , where $I = \pi d^4 /64$.

Therefore the stiffness of the bar is proportional to the 4th power of the diameter. Thus a 50 mm diameter bar of the same length is 16 times as stiff as a 25 mm bar.

b) The static stiffness of the boring bar is also proportional to

the 3rd power of the unsupported length, this is given by:

$$Deflection \qquad D = \frac{F L^3}{3 E I} \qquad (3.12)$$

Therefore, the force required to deflect the tool will decrease as a cube of its length, ie, if the overhang of a single point tool is increased three times from a 25 mm length, the amount it will deflect under a given load will increase 27 times. The formula also shows that a better grade of the same material does not improve the stiffness of the tool unless the elastic modulus is increased.

c) Improving the threshold of the natural frequency of the boring bar structure is also of considerable importance to increase the operating frequency spectrum. Since natural frequency is determined by the relationship $\omega = \sqrt{K/m}$, reducing the mass "m" without reduction in stiffness "K" could make this possible.

However, the only method to reduce the effective mass of the boring bar through the structural design, would be to increase the effective moment of inertia "I", by making the bar a hollow cross section.

Since, For the hollow bar, $I = \pi(D^4 - d^4) / 64$, Therefore, for a bar with OD = 50 mm and ID = 25 mm, would result to an increase of the bar's natural frequency by 16 %. This would result in a 25 % reduction in mass with minimum reduction in stiffness (only 6 %) .

3.9.3 DYNAMIC ANALYSIS

Various investigations of chatter during boring with a cantilever boring bar have shown that the chatter occurs most frequently at the fundamental bending mode of the cantilever bar. Accordingly, this mode is considered in this analysis. The dynamic model of a conventional

boring bar of uniform cross section is shown in Figure 3.15, where,

E = modulus of elasticity of the bar material;

I = cross sectional moment of inertia;

m_b = mass of the bar (assumed to be uniformly distributed);

m_t = mass of the tool head.

F_c = Cutting force applied at the tool head.

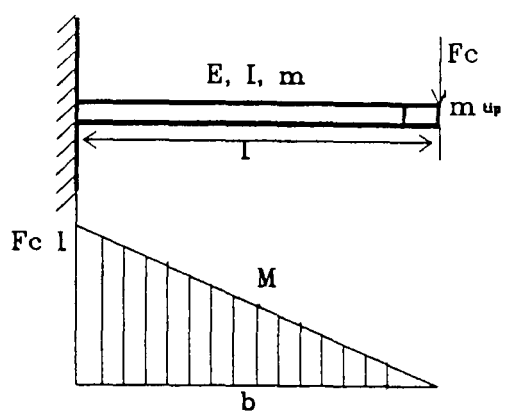

Bending moment diagram

Figure 3.15 **a** Dynamic model of cantilever solid bar.

The basic structural dynamic parameters of the system shown in Figure 3.15, which might influence its dynamic stability, are:

A) Stiffness relative to the force .

B) Effective mass of the bar in the fundamental vibratory mode.

C) Natural frequency of the fundamental mode.

3.9.4 STIFFNESS RELATIVE TO THE CUTTING FORCE F_c

From Figure 3.15, it can be seen that the bending moment increases linearly towards the built-in end.

Accordingly, the root portion of the bar has a dominating

influence on its deflection at the tool end. On the other hand, the influence on deflection of the portion of the bar which is close to the tool head is minimal.

Expressing the same conclusion analytically, the expression for potential energy (U_b)of the bar deflected in bending is given by;

$$U_b = \int_0^L \frac{M^2\, dx}{2\, E\, I} = \frac{M_{max}^2\, L}{6\, E\, I} \qquad (3.13\ a)$$

thus for a moment diagram shown in Figure 3.15,

For The bar segment

$$0 \le x \le \frac{l}{2} \ \ldots\ldots\ (I) \qquad (3.13\ b)$$

and

$$\frac{l}{2} \le x \le l \ \ldots\ldots\ (II) \qquad (3.13\ c)$$

The potential energy will be, respectively,

$$U_I = \frac{7}{8}\, U_b \quad , \quad U_{II} = \frac{1}{8}\, U_b \qquad (3.13\ d)$$

Since high structural rigidity is important for both accuracy and chatter resistance of the boring bar, the main concern in the structural design of the bar has to be with the rigidity (EI) of the root portion of the bar. The rigidity of the overhang portion is not very important.

3.9.5 EFFECTIVE MASS IN THE FUNDAMENTAL VIBRATORY MODE

During an oscillatory motion, the built-in end of the boring bar experiences no deflection and thus its velocity is assumed zero. The free end of the tool has a maximum deflection and, accordingly, maximum velocity because the kinetic energy of the uniform vibrating bar is given by;

$$K_e = \omega^2 \int_0^L \rho A y^2 \, dx \qquad (3.14)$$

where

y = Deflection, A = Cross sectional area,

ω = Fundamental frequency, ρ = Material density of the bar.

The dominating contribution to the kinetic energy of the vibrating bar is from the overhang section of the bar located close to the tool head. Thus;

In the root portion $K_I = 1/4\ K_e$,

and at the free end $K_{II} = 3/4\ K_e$

Accordingly, only the free segment (ie, $1/2 \leq x \geq 1$) of the bar determines the effective mass of the fundamental mode. This conclusion means that to reduce the effective mass, for improved dynamic stability, the mass of the overhang portion has to be reduced.

3.9.6 NATURAL FREQUENCY OF THE FUNDAMENTAL MODE

There are indications that increasing the natural frequency of the fundamental mode of the boring bar is beneficial for its chatter resistance. The natural frequency (f_o) of the fundamental mode of the model shown in Figure 3.15 is (3.3) ;

$$f_0 = \frac{1}{2\ \pi} \sqrt{\frac{3\ E\ I}{L^3 (m_t + 0.23\ m_b)}} \qquad (3.15)$$

For boring bars m_b is normally much larger than m_t. It follows from the above expression that to increase f_o for a given length L, and I, the modulus of elasticity E has to be increased and/or the density of the bar material reduced.

Although sintered carbides, which are used for critical applications, have an "E" value of about 1.6 times higher than steel (solid sintered tungsten carbide E = 3.5 x 10^5 MPa) their density is also about 2.3 times higher (Density of steel = 7.8 x 10^3 Kg/m^3 Density of tungsten carbide = 16.8 x 10^3 Kg/m^3) ; Thus the natural frequency of the carbide bar is in fact 20% lower than that of the steel bar and its amplitude response benefits due to its stiffness.

However, from the above it can be concluded that since the root portion of the bar dominates its potential energy and the overhang portion dominates its kinetic energy, a substantial increase in natural frequency may be achieved by utilising a combination bar structure.

Therefore, the root portion will be designed with high modulus material developed for this purpose. In such a structure, a high natural frequency would be accompanied with the high structural rigidity necessary for accurate machining.

3.9.7 VIBRATION CONTROL BY STRUCTURAL DESIGN;

The vibration control by structural design implies that the cutting tool structure is designed with the magnitudes and distribution of mass and stiffness which minimize the vibration generated by the machine tool.

In the simplest case, the structure is assumed to be subjected to a fixed-frequency sinusoidal force. The design would ensure that no resonant frequency coincided with excitation frequency, but that the excitation frequency lay behind or in front of the resonant frequency, in the response curve. This may be achieved by modelling the tool in such a way that the modal response and fundamental natural frequency of a given construction can be estimated. This technique is demonstrated by the finite element model examined in chapter eight section 8.2.

By measuring the frequency response of the cutting process it

would be possible to avoid resonance simply by selecting the minimum overhang ratio for which the fundamental frequency of the tool lay behind or in front of the chatter frequency, hence avoiding chatter.

The interaction of the cutting dynamics with the structure could alter the exciting frequencies. Therefore any practical structural design should aim to increase the natural dominant frequency of the structure over a broader frequency spectrum to eliminate chatter. In this theses the development of the composite material (detailed through chapter four) points towards this objective by means of high stiffness high damping characteristics.

3.9.8 INTEGRATED CONSTRUCTION OF COMPOSITE BORING BAR

Numerous designs have been considered and proposed during the course of this work. However, material development combined with a composite construction was considered to be the preferred option. All parameters sensitive to vibration control (Mass, Stiffness and Damping) could be utilised to some degree.

The use of vibration control by composite structural design for limiting the chatter sensitivity of boring bars aims at giving the maximum functional specification, using the design procedure presented earlier.

Another strategy is to restrict the design to its simplest form thereby enabling cheaper development cost as well as allowing the flexibility necessary to combine the design with other methods of vibration control mechanisms. The design of boring bar shown in Figure 3.15 is a constant diameter type, of 50 mm outer diameter, which corresponds to the conventional and Sandvic tuned bars tested for comparative verification.

The composite construction of the boring bar consists of a mild steel grade EN8 tube with a Titanium carbide composite insert at the

fixed end with a shrunk-on fit. The mechanical properties of composite inserted materials are presented in Table 4.7 (Chapter four).

The estimated length to diameter ratio for the tool of proposed design, with acceptable response levels, was set at eleven times the diameter. Utilising the analyses presented in section 3.9.4 and 3.9.5, the dimensions of the fabricated composite insert was estimated at 60% of the total overhang length. The final dimensions of the composite insert are 38 mm diameter and 380 mm in length.

For the boring bar to possess maximum stiffness, the compliance of the joint between the Titanium carbide composite insert and the steel tube had to be minimised. The contact stiffness characteristics of joints between two metal surfaces is highly nonlinear (stiffness increases progressively with increasing the pre-load pressure). In addition the stiffness can be enhanced by improving the flatness and surface finish of surfaces being joined. The experimental observation of (3.21) showed that the contact stiffness is saturated (reaches very high levels thus practically eliminating joining influence on the bars deflection) at contact pressure exceeding 60 to 70 Mpa . Such pressure may be obtained in the proposed design by means of friction fit (although in practise it was not found possible to measure this pressure). The analyses of the influence of interface pressure through Finite Element simulation of the design is detailed in chapter eight. This verifies that the effect has almost reached saturation .

3.9.9 FABRICATION PROCEDURE

The steel boring bar blank was deep hole drilled and honed to size (37.9 mm), to allow a 84μm interference fit between the Titanium composite (TiC) insert diameter and the hole diameter. The expansion rate for the interference to be a clearance when heated had to be calculated and allowed for. The steel bar was heated to 400° C and the insert placed into the hollow bar. Within a matter of seconds the bar cooled and shrunk over the TiC insert ensuring approximately even interference fit over its length.

The effects of interference pressure between the bar and the insert under dynamic loading are analyzed in chapter eight.

Figure 3.16, illustrates the fabricated boring bar which is designed to have modular construction. The modular construction of the front section benefits from a design variation made of aluminum and steel. The front of the tool which incorporates a Micro-bore adjusting mechanism is fixed to its rigid body through a threaded insert. The pitch of the thread is kept to a minimum (0.5 mm) so that a maximum number of turns are allowed for friction damping to take place.

In chapter 8, it is shown that a composite structure boring bar outperforms conventional tools due to its high specific stiffness and damping. Hence the option of passive structural damping is an added advantage to the designed structure. Consideration of the application of surface damping treatment as a design option for the boring bar vibration control is useful since any material disturbance would have its maximum strain energy on the surface of the body.

This design is further modified by including a "constrained layer damping" treatment on the tool structure, as detailed in section 3.6.

The analyses of the results from the finite element model in modes of vibration of a given tool (chapter eight section 8.2), were used to determine the position of high strain concentration.

Manufacturers of damping materials have optimised the material content to yield maximum values of equivalent damping over a broad frequency and temperature range. From a family of high energy dissipative polymers of 3M Industrial Products two types of constrained layer damping were selected for the design. The selection of the type of Visco-elastic material were based on damping performance and the practical temperature range given in the product specification.

The specified damping performance associated with 3M, ISD 112 was considered the best practical option. This was based on the chart produced by the manufacturer shown in Figures 3.17. The design for optimum performance of damping material was for the operating frequency and temperature range of 100 to 1000 Hz, and 20 to 40°c, respectively. The estimated natural frequency of combination boring bar was 150 Hz, at length to diameter ratio corresponding to eleven times the diameter. The average shear storage modules (G') and loss factor η, of ISD 112, were larger than other available materials in the family.

The constraining layers available in the range were aluminium and stainless steel, both of which carried some problems for the design. The aluminum constraining layer though it was easily applied suffers from lack of stiffness compared to the composite boring bar. The problem with stainless steel constraining layer was due to its attachment on the boring bar structure. Since it was not possible to provide the effective adhesion of the stainless steel constrained layer damping on the boring bar tests were only carried out with the aluminium constraining layer.

The specific configuration of the constraining material and damping material for both systems is listed below ;

Visco-elastic material type ISD 112, Thickness 0.254 mm,

Stainless steel constraining layer 0.127 mm

Aluminium constraining layer 0.254 mm

The method of application recommended by the manufacturer was followed. The compound boring bar is illustrated in Figure 3.18 & 3.19.

For the construction of these materials on the boring bar as mentioned previously the modal shape analyses were used so that the cyclic tension and compression of the constraint and damper would yield the maximum loss factor in the vibrating boring bar.

Practical studies and experimental verification illustrate the merits of such materials and provide valuable information for the design of composite laminated structures with moderate dynamic characteristics.

The integrated construction of the boring bar design benefits from the threefold characteristics of mass, stiffness and damping via the through optimisation of the structural design, material design, friction and Visco-elastic dampers.

Although the incorporation of vibration absorbers has been shown to be an effective means of chatter attenuation it has been excluded from the experimental design procedure. This is mainly due to availability of sufficient data and much research on the fine tuning of such systems for boring bar application.

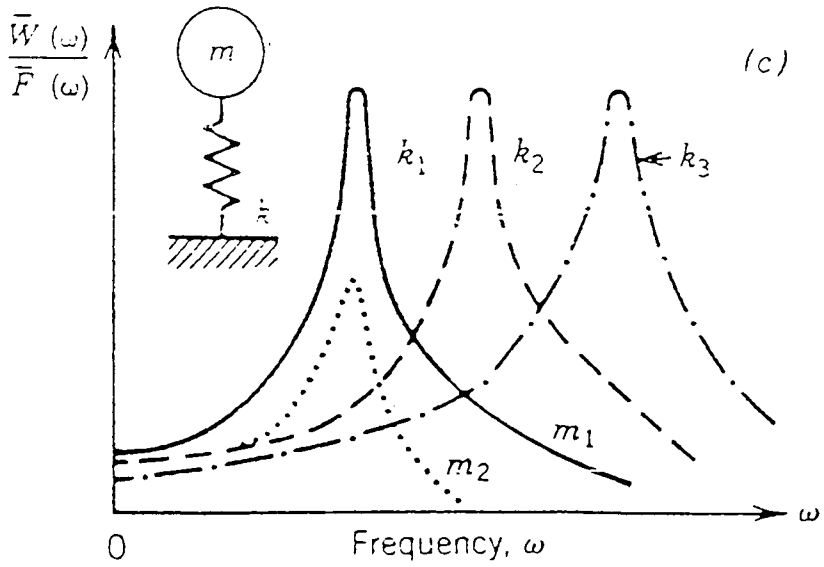

Figure 3.2 : Random responce behavior

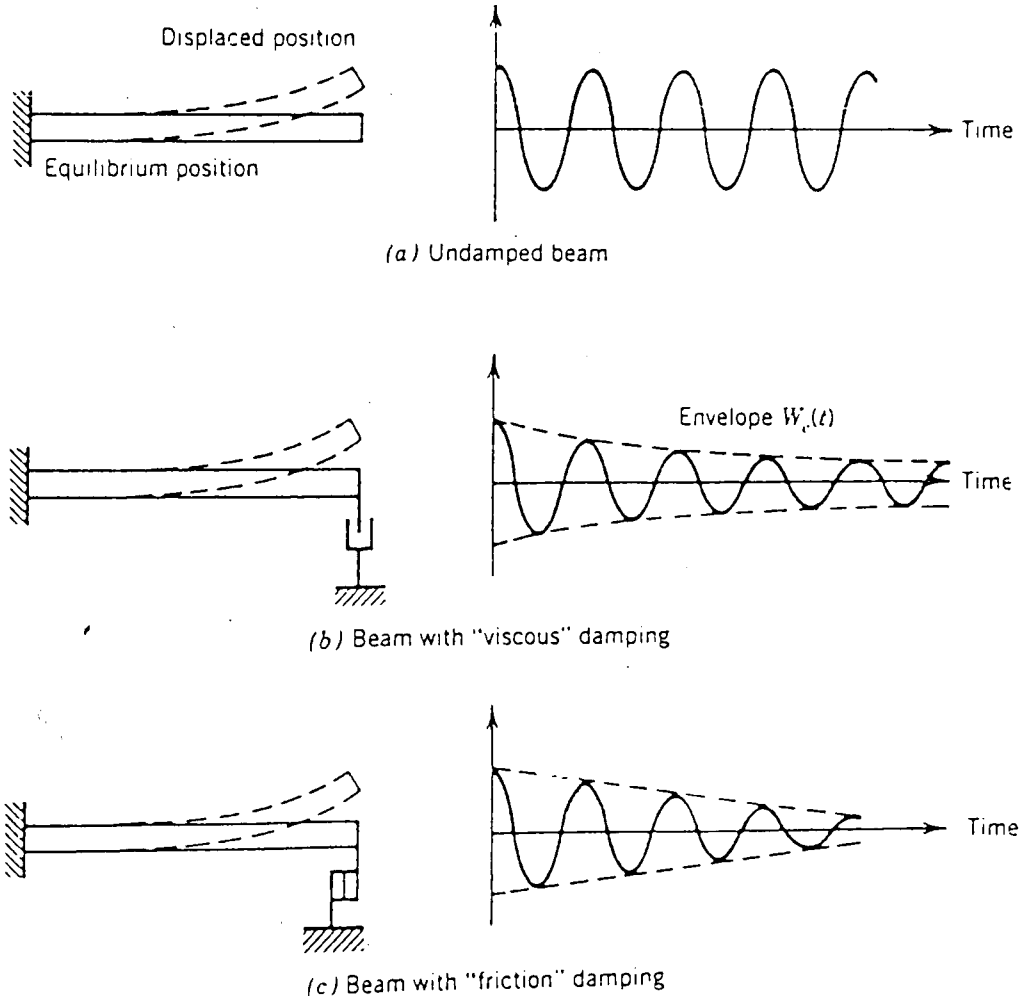

Figure 3.3 : Effect of damping on free response

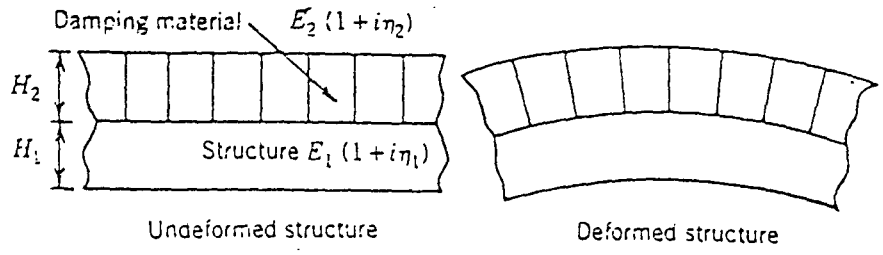

Figure 3.4 : Unconstrained damping treatment

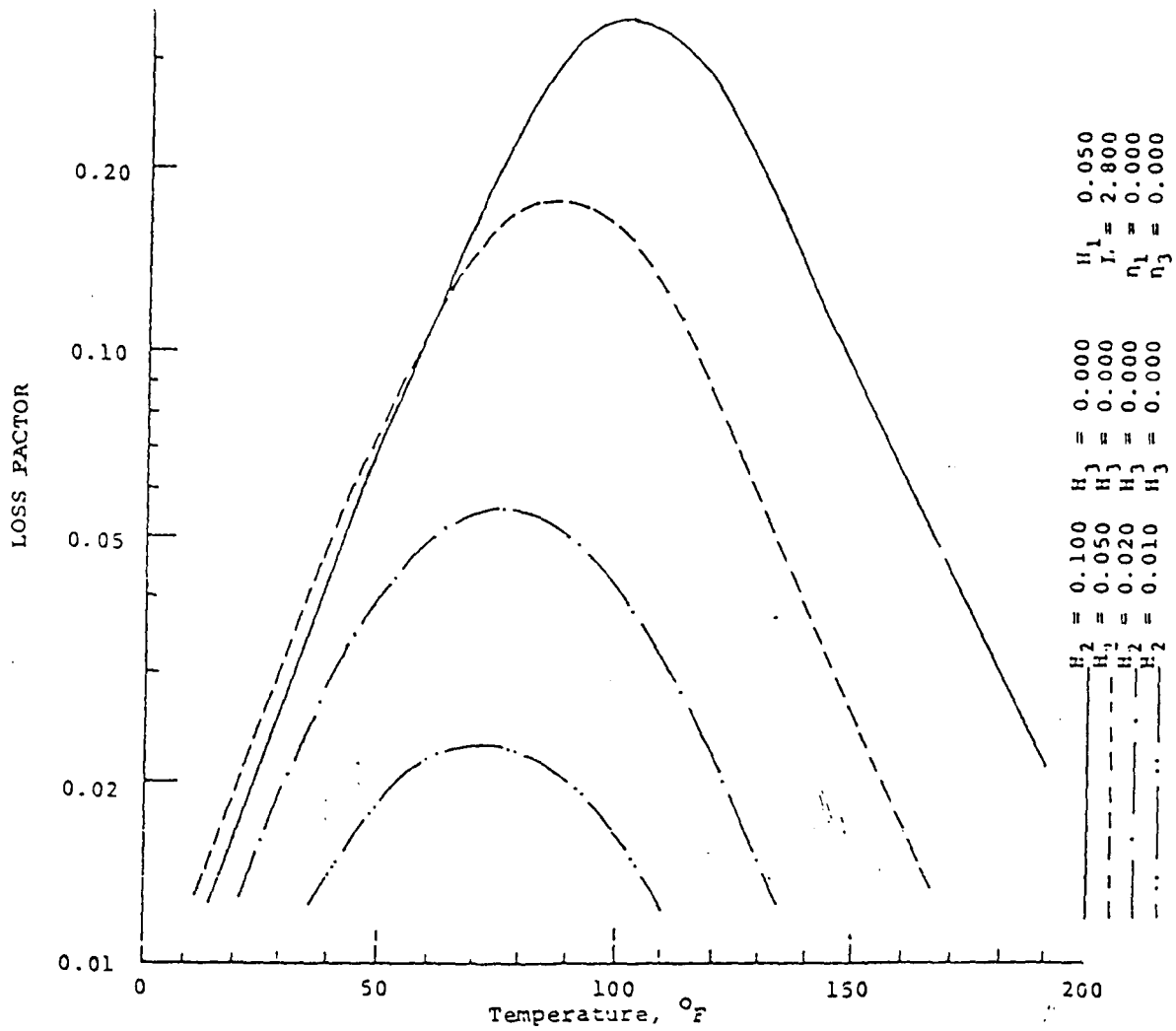

Figure 3.5 : Variation of the damping performance of an Unconstrained damping treatment with tempreture and thickness.

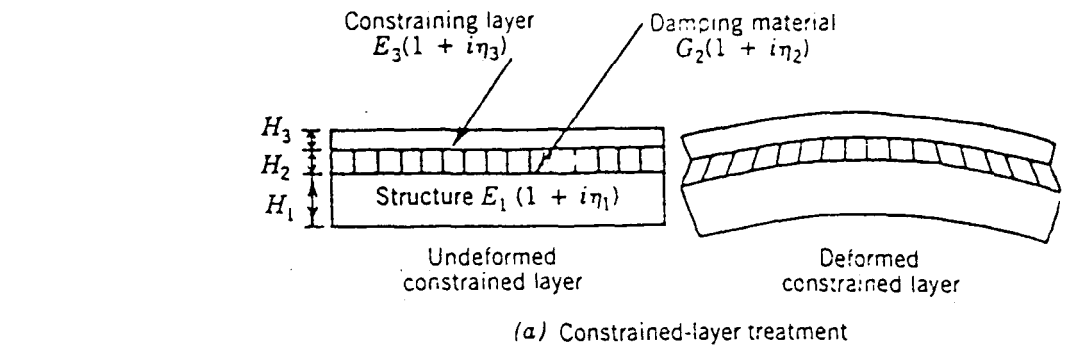

(a) Constrained-layer treatment

Figure 3.6 : Constrained damping treatment

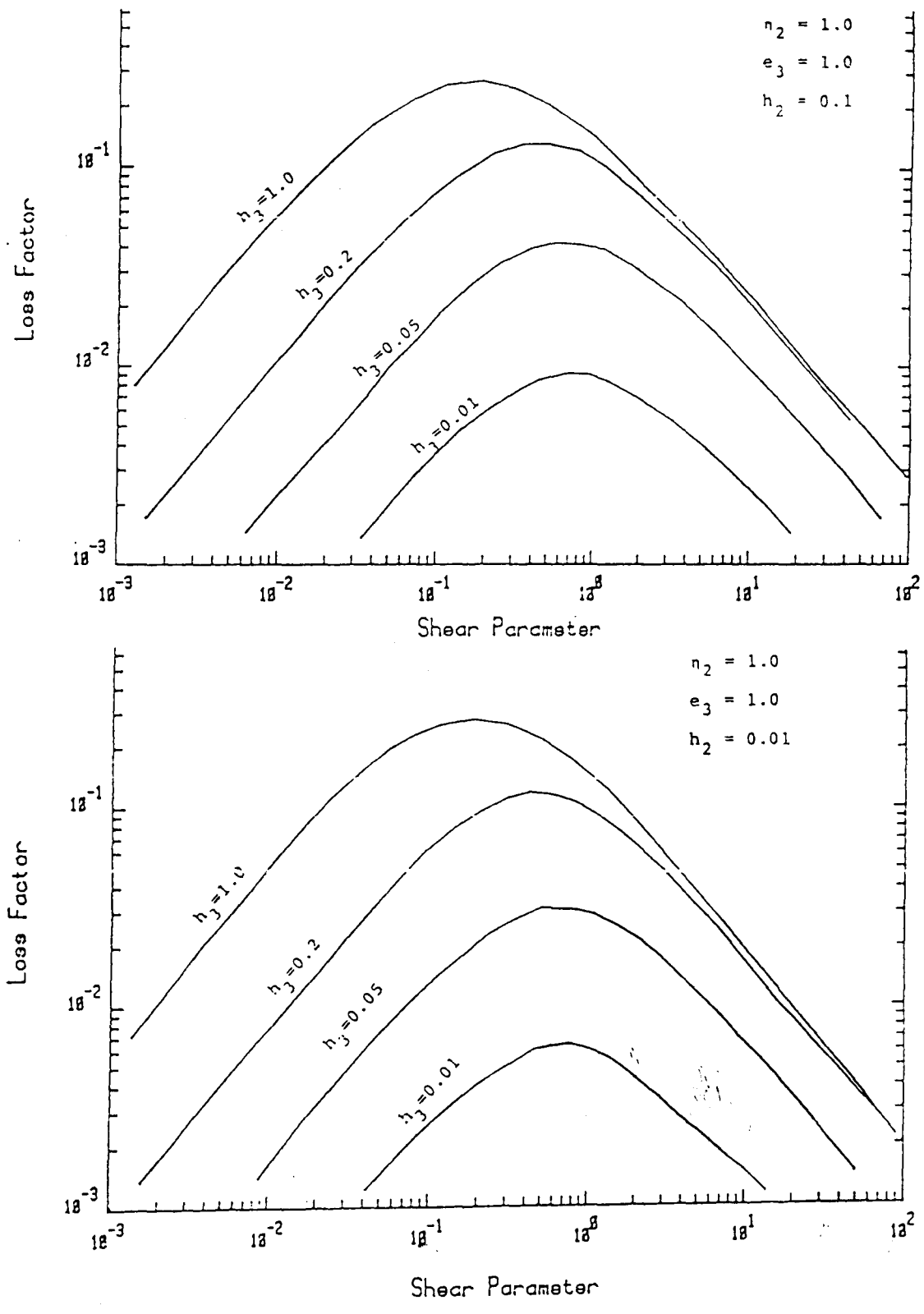

Figure 3.7 : Variation of modal loss factor with the shear parameter.

(a) $h_1 = 0.01$, (b) $h_1 = 0.1$.

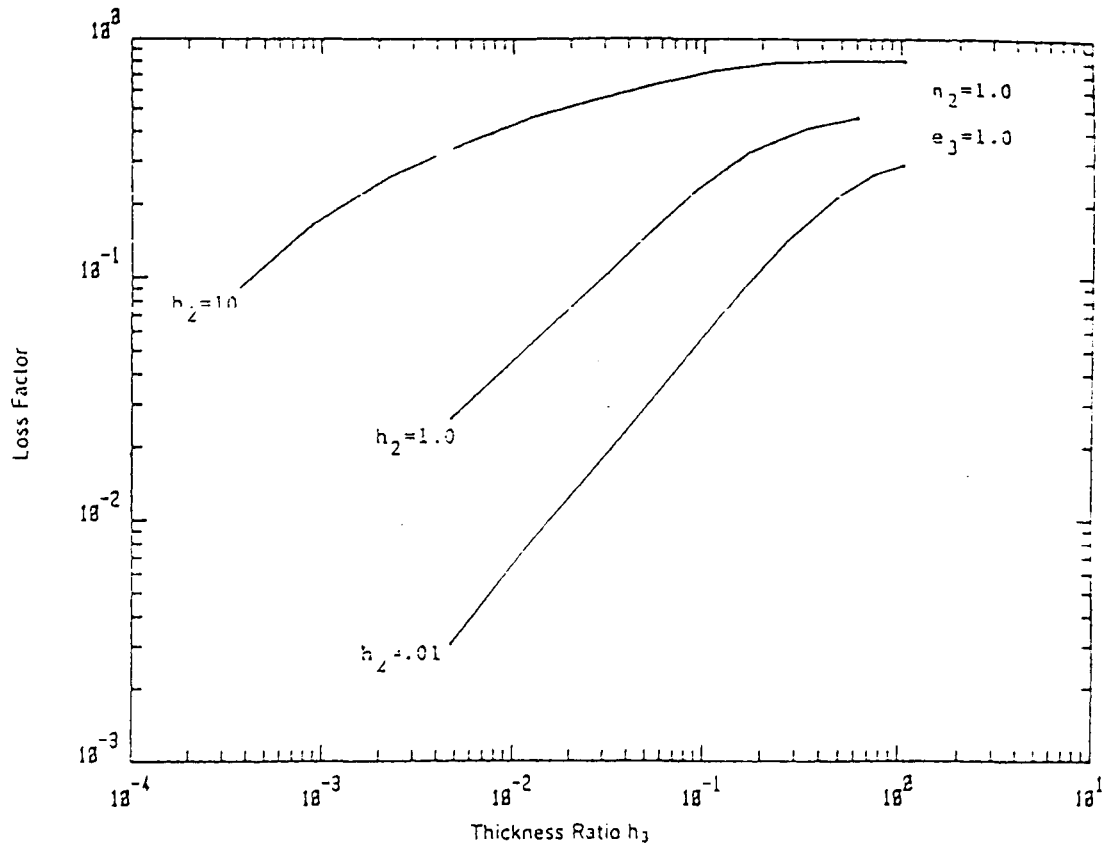

Figure 3.8 : Variation of maximum loss factor with thickness ratio

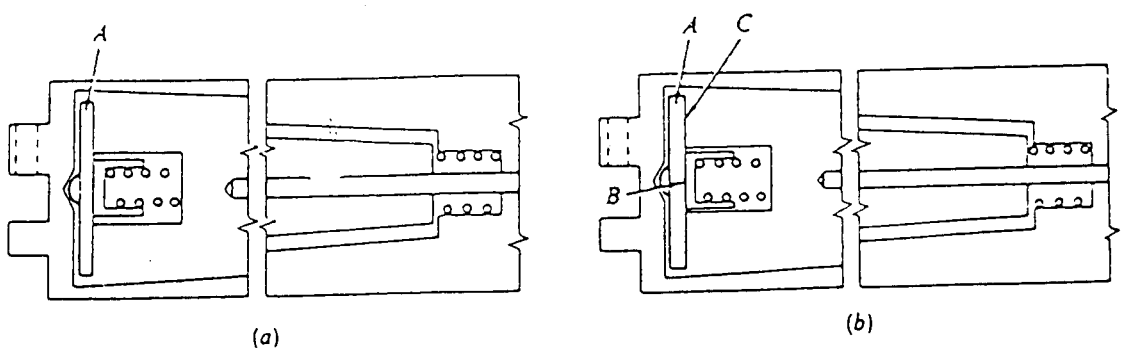

Figure 3.9 : Friction damping system for boring (Austin tool Co)

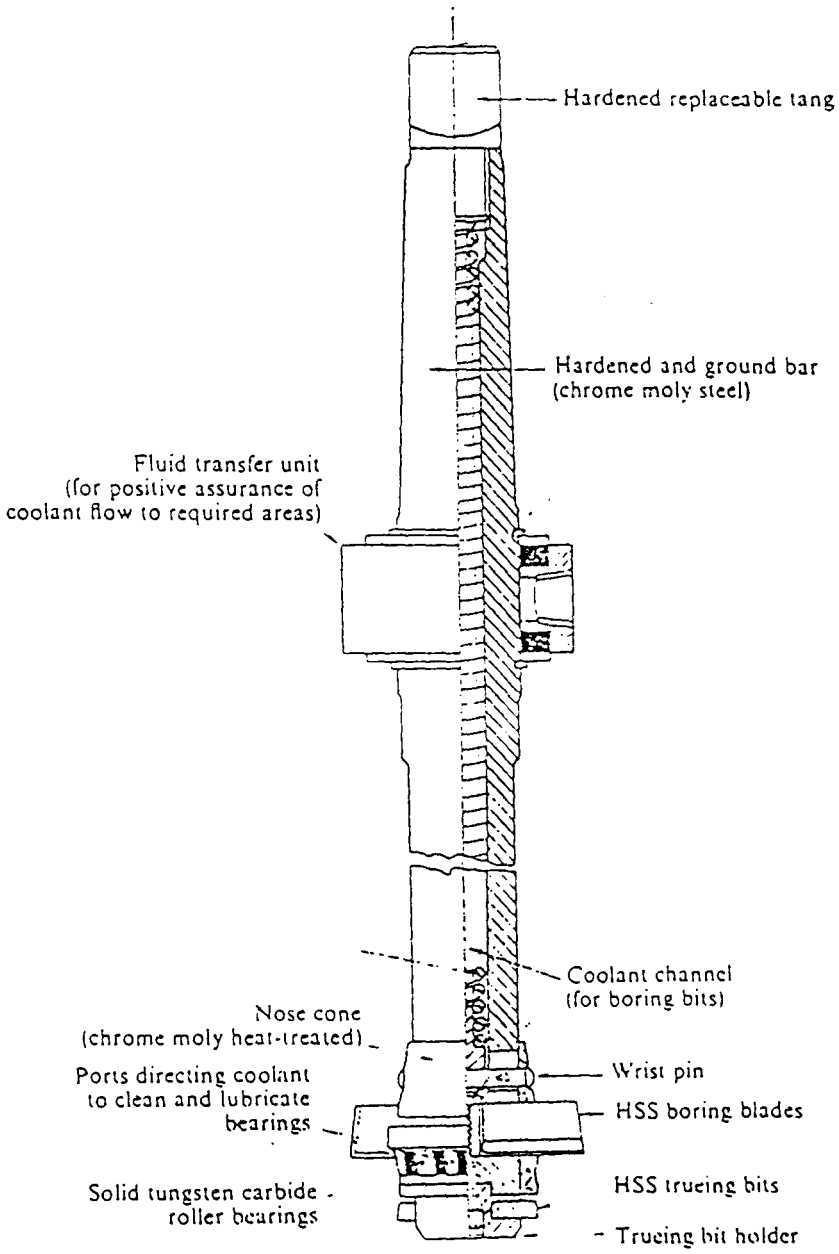

Figure 3.10 (a) : Construction of the Vernon Bore-Bit.

(Vernon devices Inc)

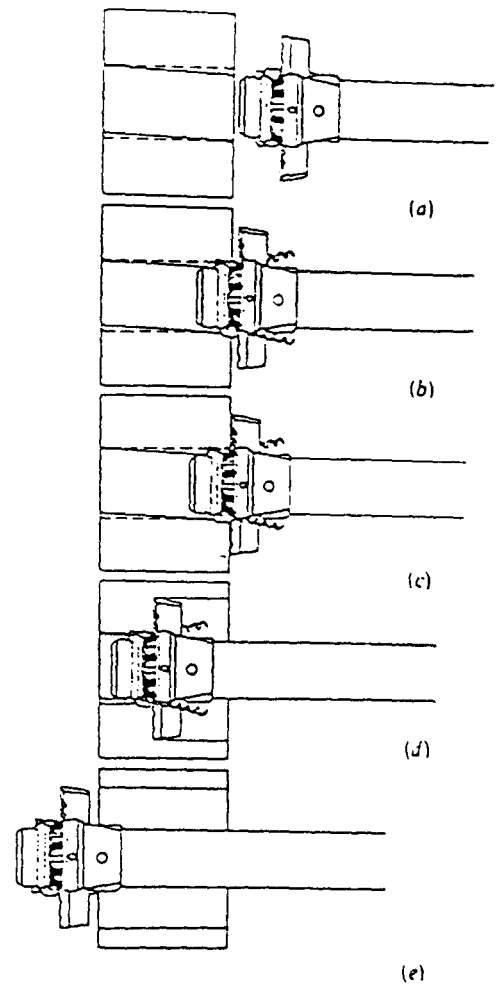

Figure 3.10 (b) : Cutting action of vernon Bore-Bit.

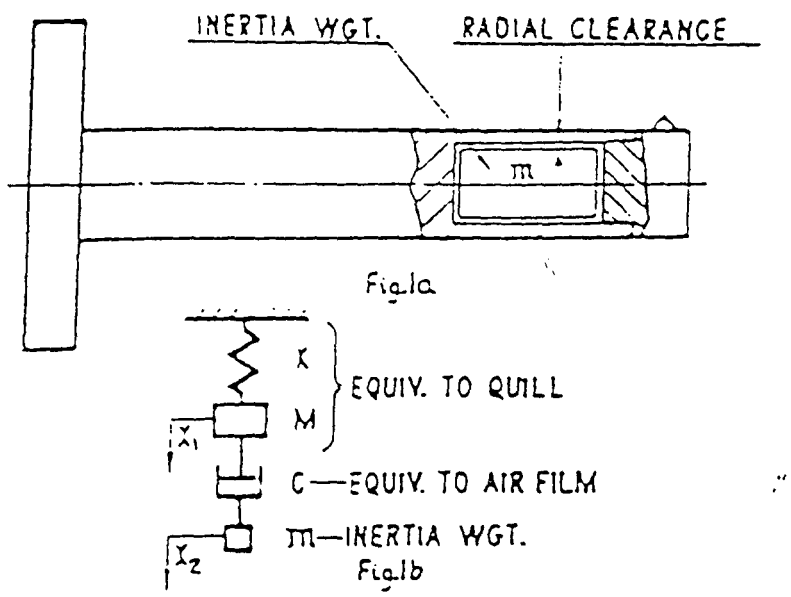

Figure 3.11 : Boring bar with lanchester damper (Hahn 1951)

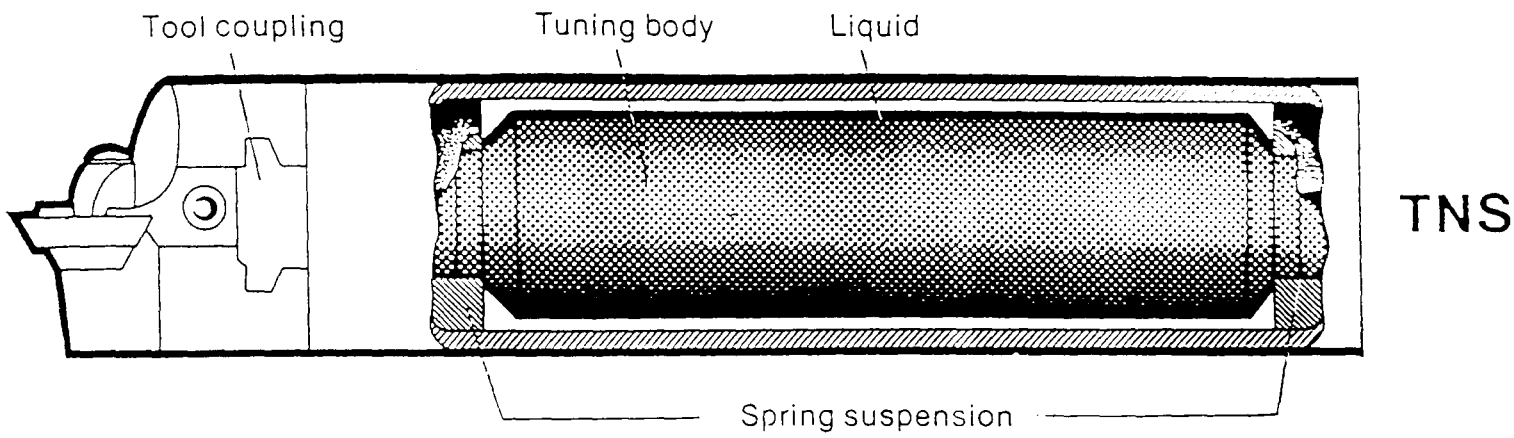

Figure 3.12 : SANDVIC TNS Boring bars

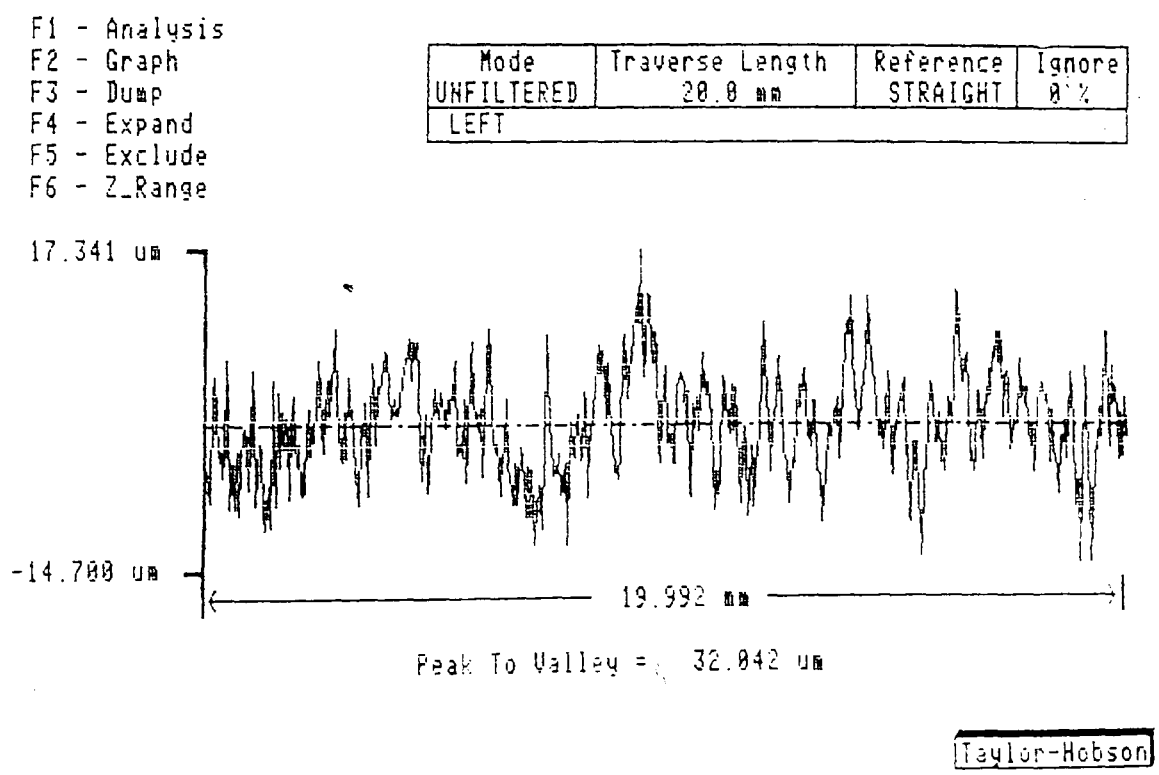

Figure 3.13 : Surface profile of the Boring bar clamping sleave.

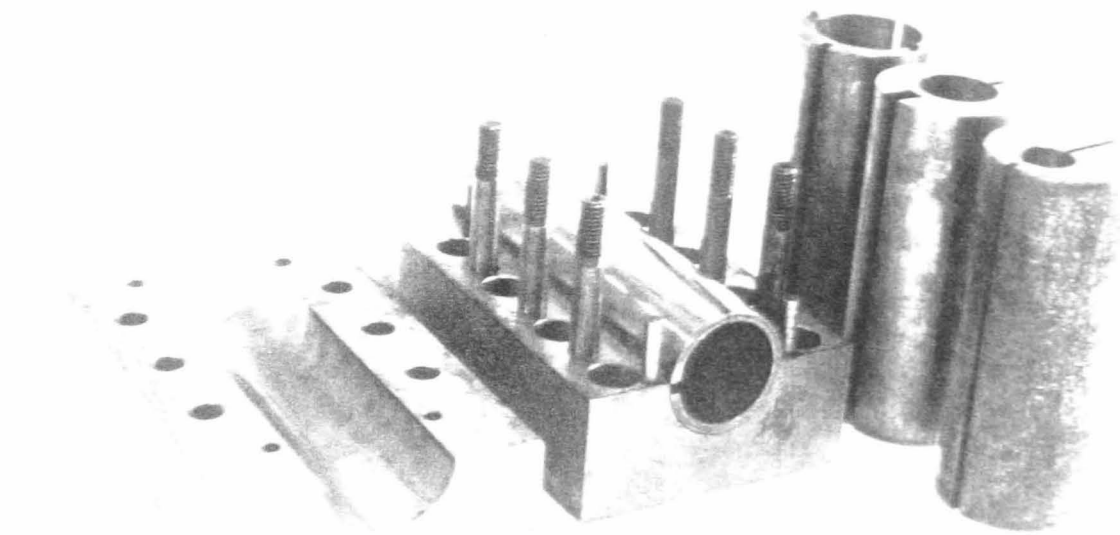

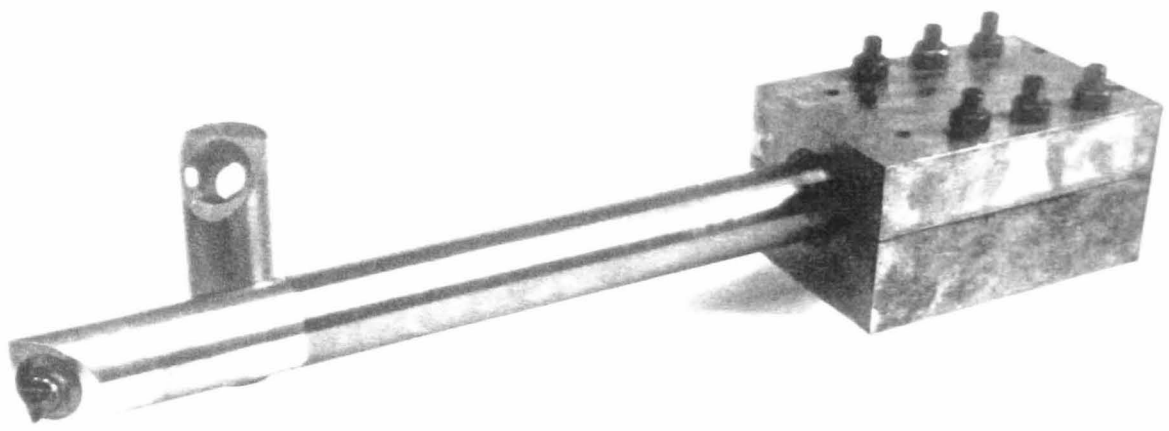

Figure 3.14 : Constructed clamping arrangement.

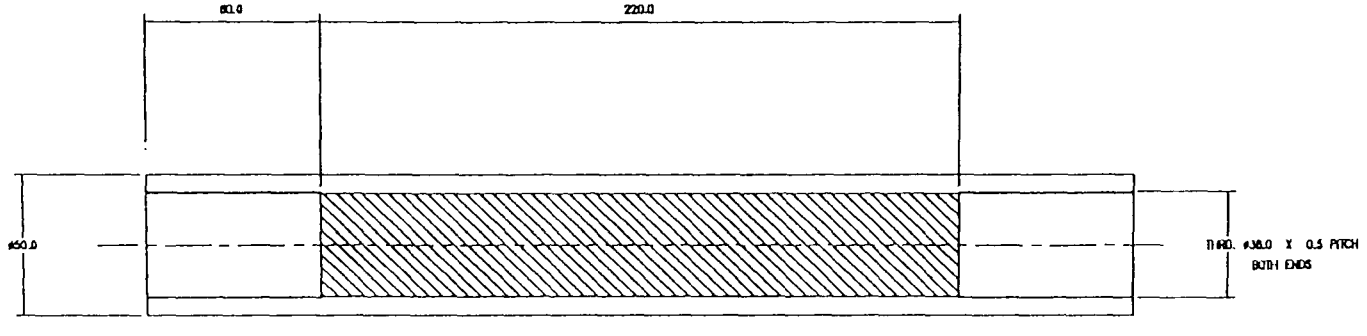

DET 1 STAGE 3 WITH COMPOSITE BAR FITTED SLEEVE IS MACHINED TO DIMENSIONS SHOWN

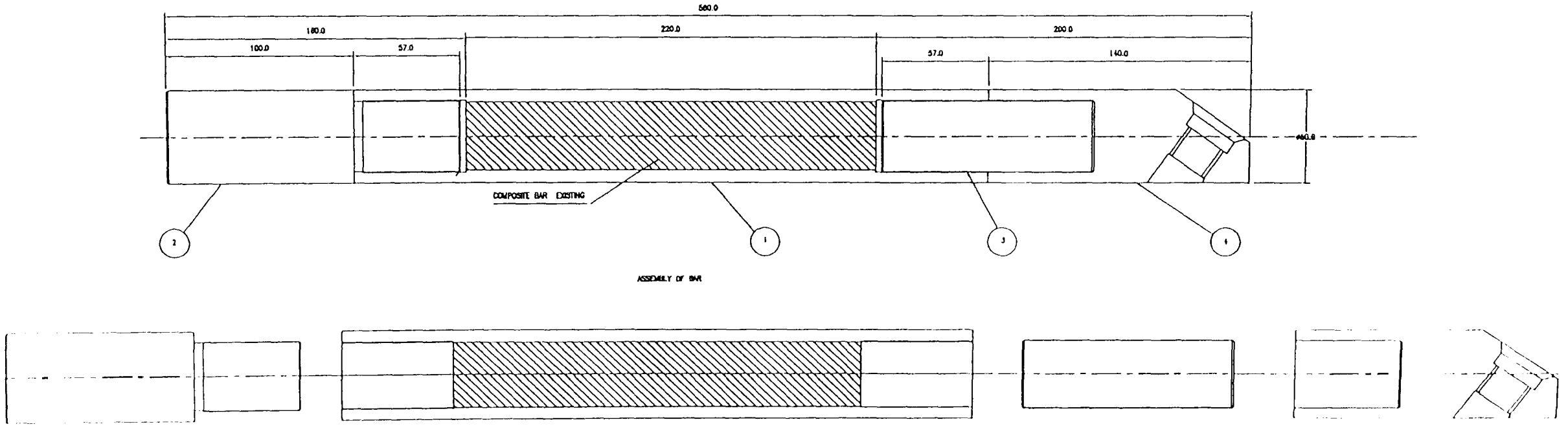

Figure 3.15 b : Composit structure boring bar design.

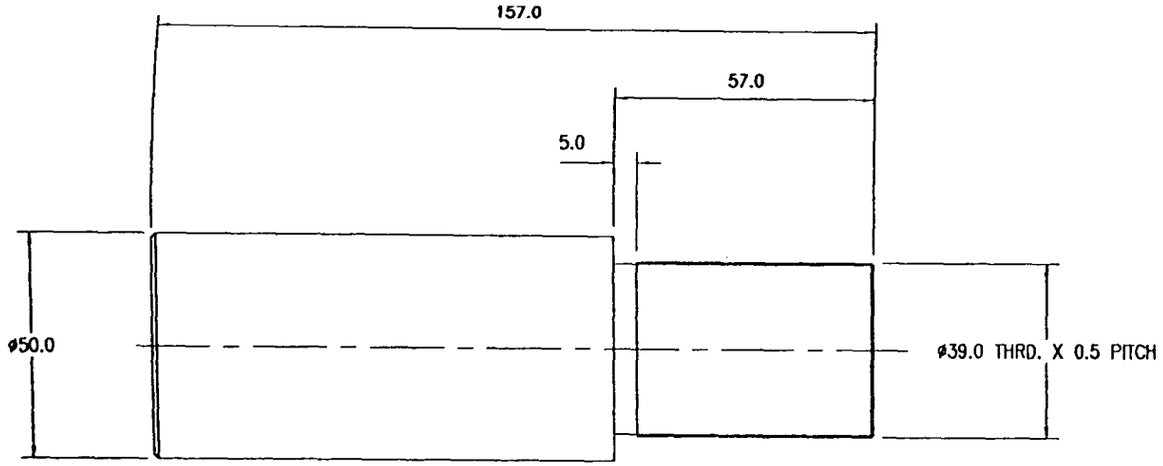

DET 2 ADAPTOR 1 OFF

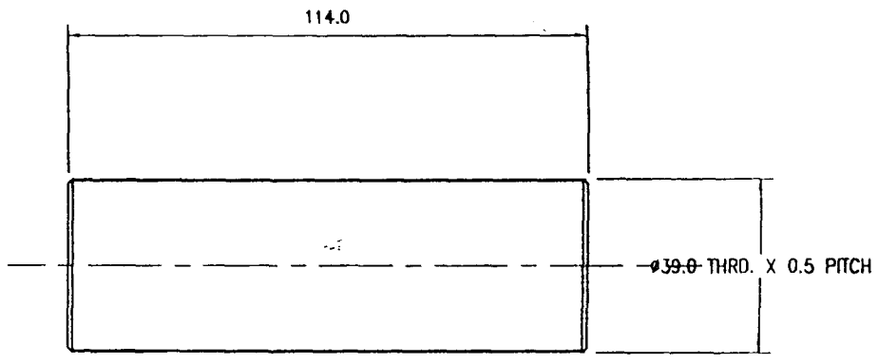

DET 3 THREADED ADAPTOR 1 OFF

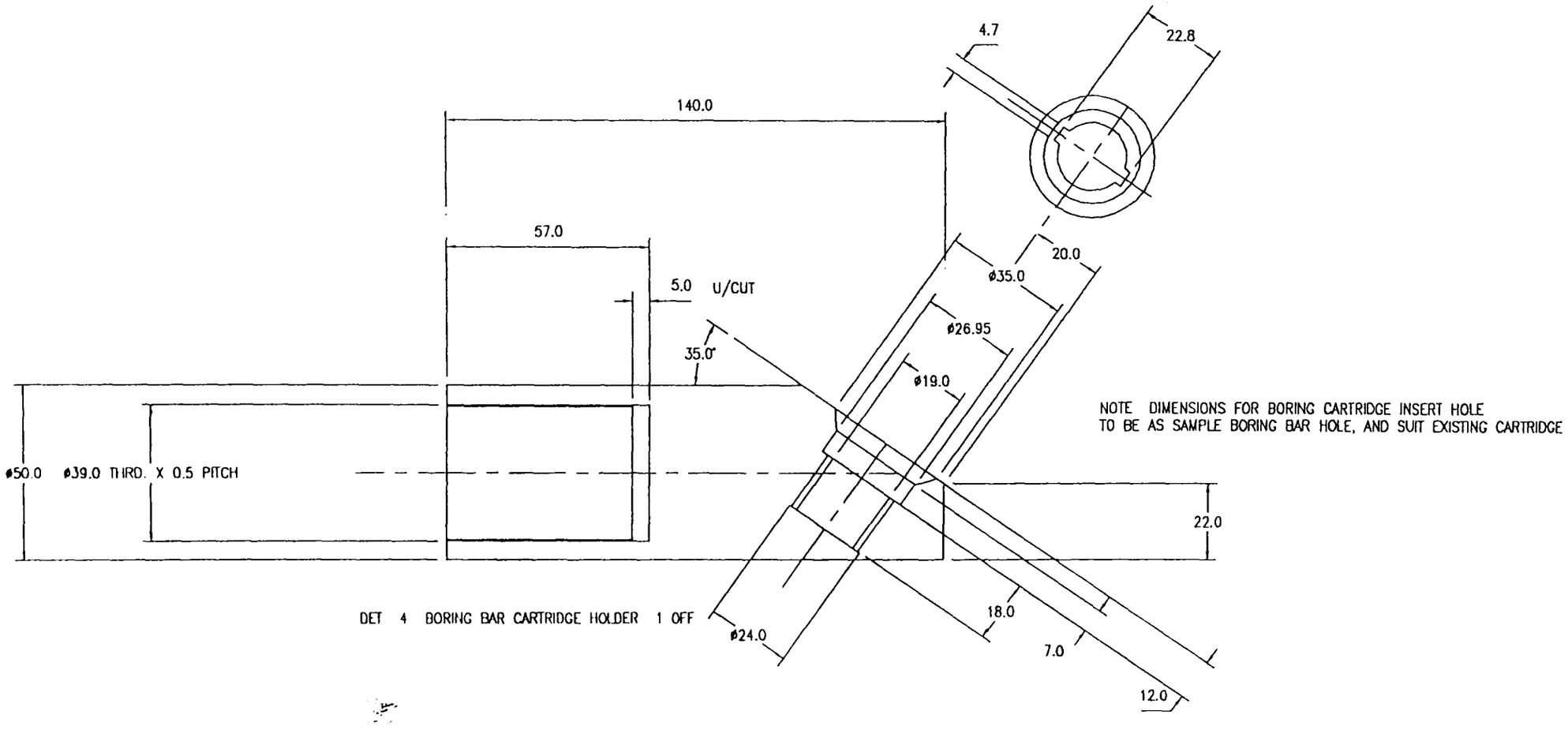

DET 4 BORING BAR CARTRIDGE HOLDER 1 OFF

NOTE DIMENSIONS FOR BORING CARTRIDGE INSERT HOLE
TO BE AS SAMPLE BORING BAR HOLE, AND SUIT EXISTING CARTRIDGE

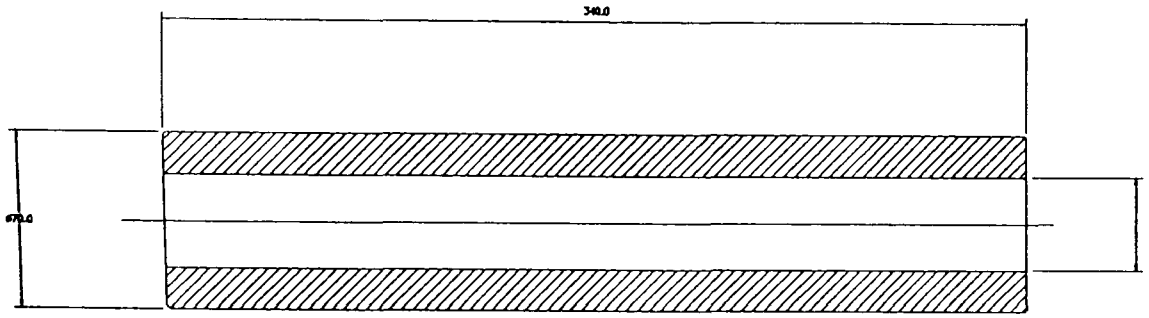

DET 1 SLEEVE 1 OFF
MTL.
STAGE 1 SLEEVE MACHINED TO DIMENSIONS SHOWN & BORE HONED TO BE HEAT SHRINK FIT ON COMPOSITE BAR (EXISTING)

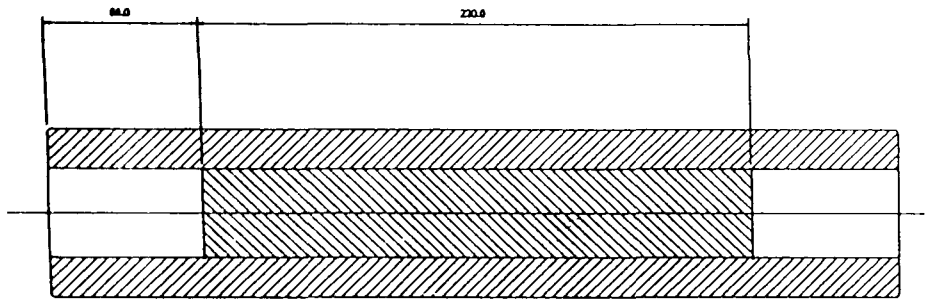

DET. 1 STAGE 2 COMPOSITE BAR IS FITTED WITH PRESSURE & HEAT IN POSITION SHOWN

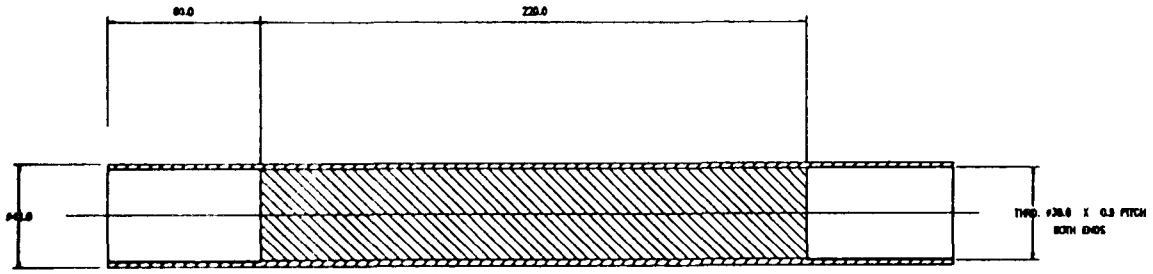

DET 1 STAGE 3 WITH COMPOSITE BAR FITTED SLEEVE IS MACHINED TO DIMENSIONS SHOWN

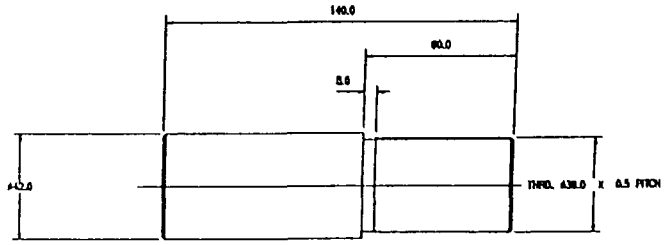

DET 2 ADAPTOR 1 OFF
MTL.

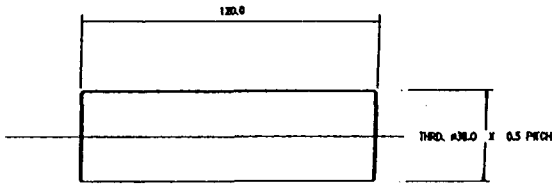

DET 3 THREADED ADAPTOR 1 OFF
MTL.

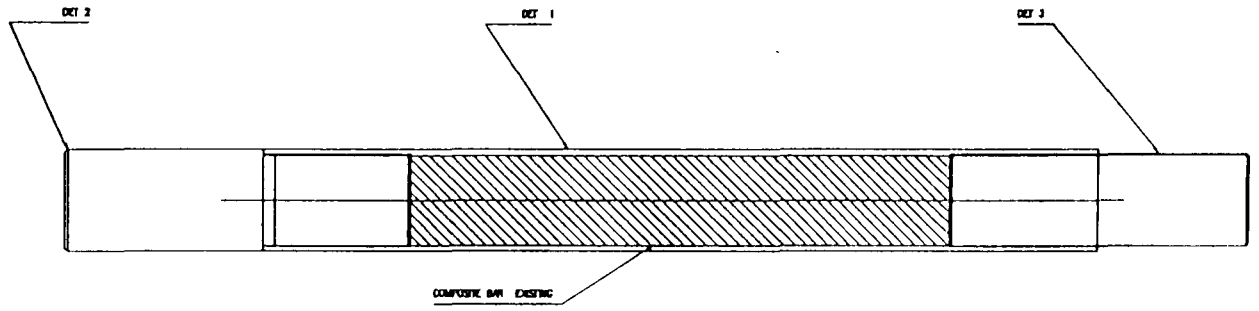

ASSEMBLY OF BAR

ITEM	QTY.	SHT.	DESCRIPTION	MTL.
			MANUFACTURED ITEMS	

UNIVERSITY OF WARWICK

DEPARTMENT OF ENGINEERING

TITLE OF PROJECT:- COMPOSITE SHAFT

DRAWN	A.E.R.	DRG. NO.	ES824
DATE	APR 94		
SCALE	1:1		
THIRD ANGLE		SHEET 1 OF 1 SHEETS	

MACHINE AT 'F'
GRIND AT 'G'
GENERAL TOL. ± 0.25
I.S.O. TOLERANCES

TITLE

COMPOSITE SHAFT

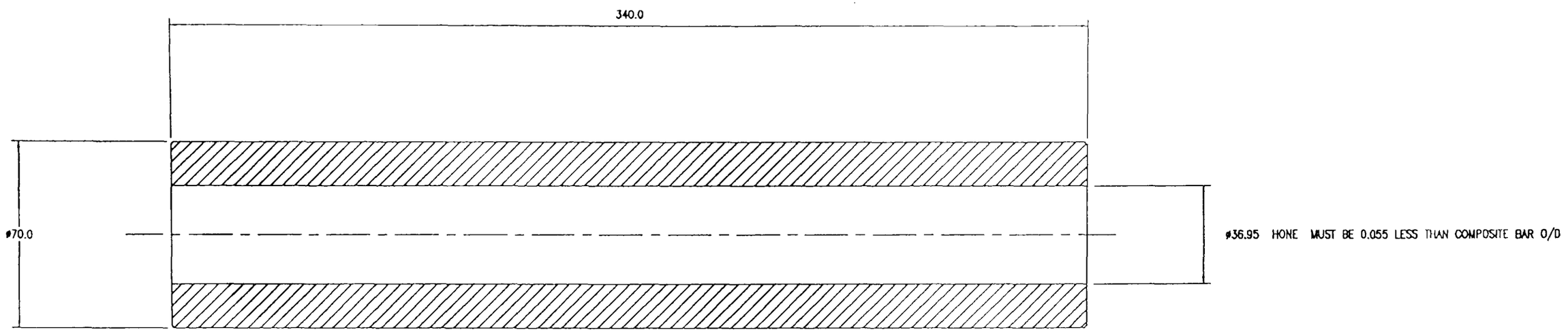

DET 1 SLEEVE 1 OFF
MTL.
STAGE 1 SLEEVE MACHINED TO DIMENSIONS SHOWN & BORE HONED TO BE HEAT SHRINK FIT ON COMPOSITE BAR (EXISTING)

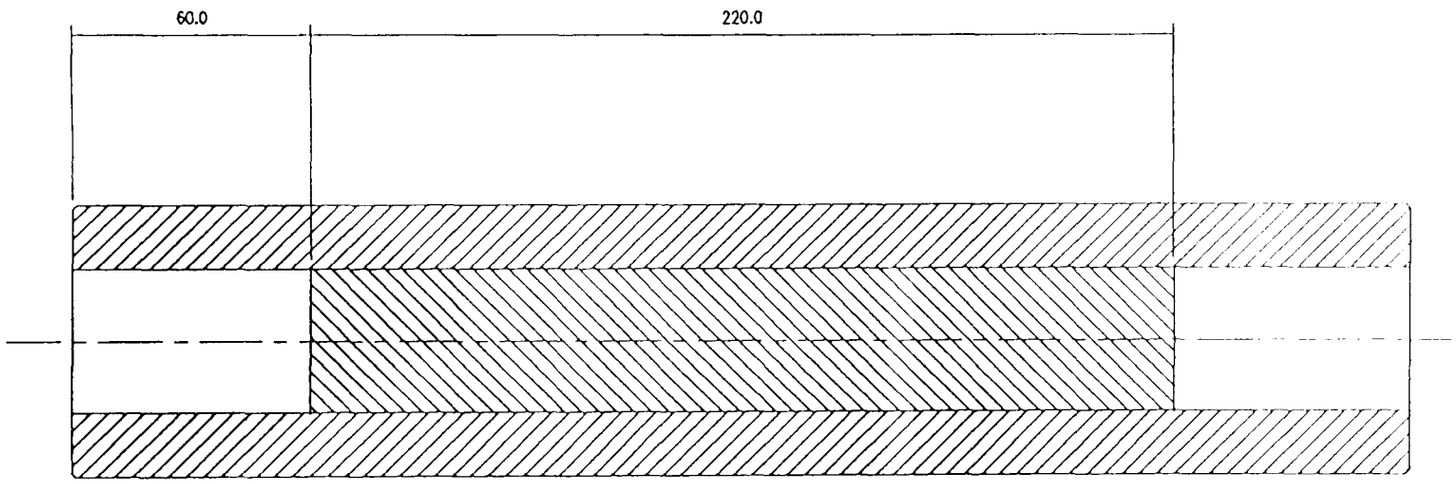

DET. 1 STAGE 2 COMPOSITE BAR IS FITTED WITH PRESSURE & HEAT IN POSITION SHOWN

Figure 3.16 : Modular construction of composite structure boring bar

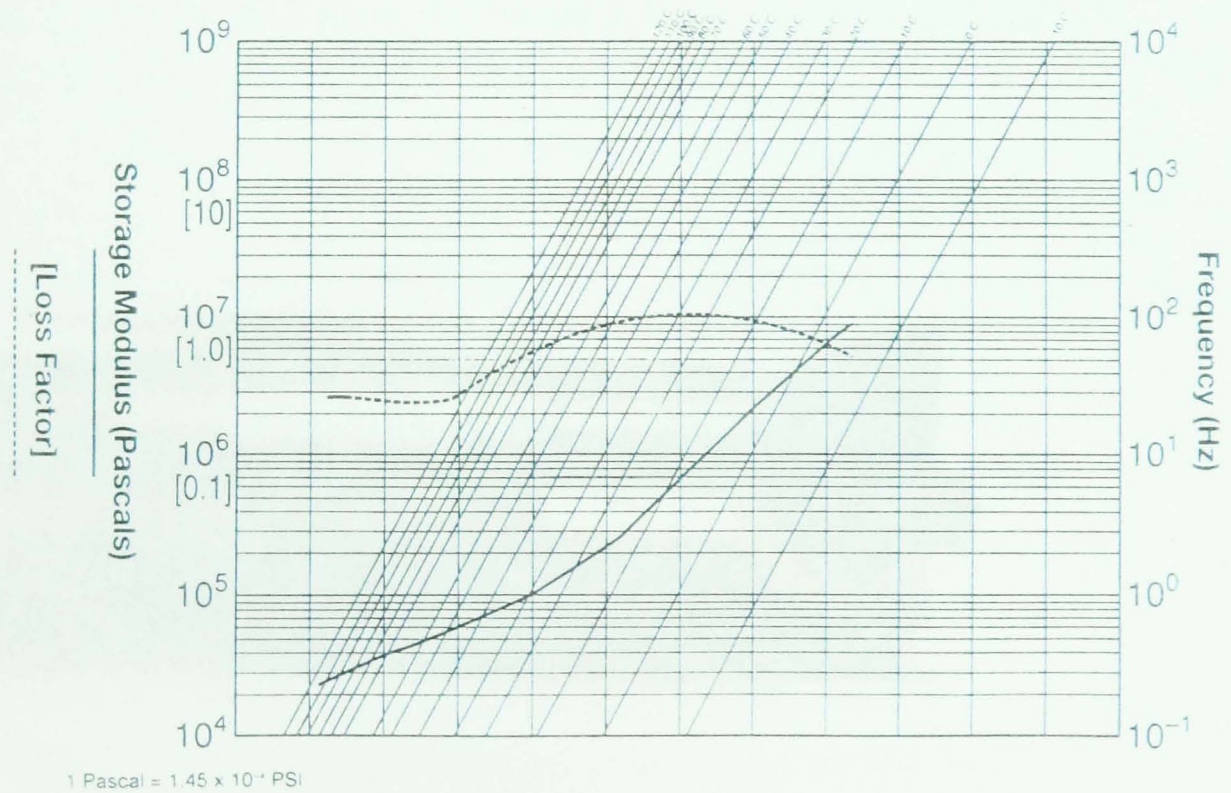

Figure 3.17 : The specific damping performance of 3M, ISD 112, provided by 3M company.

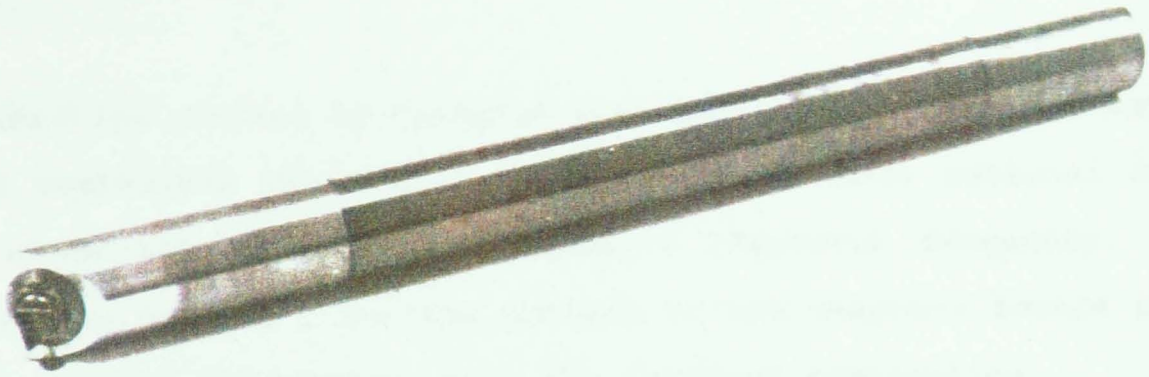

Figure 3.18 : Fabricated composite structure boring bar

Figure 3.19 : Combination Boring bar with constraint layer damping

CHAPTER 4

4.0 VIBRATION CONTROL BY MATERIAL SELECTION

4.1 INTRODUCTION

Vibration control by changing the chemistry of the structure for enhanced mechanical properties is probably the most rational design option since all the required criteria ("Natural frequency, Mass, Stiffness and Damping") for the control of the response levels in the structure may be tailored to suit the designed application.

If there is a choice of material from which the structure could be made the lowest vibration amplitude at resonance would be obtained with the material having the highest value of Young's modulus E and loss factor η, and minimum specific gravity.

The search for a material that could provide the required stability without impaired problems of fundamental natural frequency resulted in a qualified conclusion that;

High damping materials often lack in stiffness, and, High modulus materials such as sintered carbides, suffer from low damping and high mass which may not be suitable for cutting operations where the length to diameter ratio exceeds seven.

The emphasis in this part of the thesis is based on considering the various materials that may be suitable as a design option. As an objective for exposition of an original contribution the approach through material development is considered. The practical aspects of material development are confined to improved equivalent stiffness through alloying elements and processing techniques.

4.2 CONSIDERATION OF THE TYPES OF SUITABLE MATERIALS

According to the theory of machine tool dynamics (4.1), the maximum depth of cut that can be taken without expectation of chatter is approximately proportional to the static stiffness and damping of machine tool. Therefore, the material for the tool structure should have a high static stiffness and damping in its property to improve the dynamic performance.

Table 4.1 illustrates the typical required values of loss factor for machine-tools and their typical operating frequency range (4.2).

Table 4.1: TYPICAL LOSS FACTORS FOR MACHINE TOOLS

CLASSIFICATION	EXAMPLE	FREQUENCY RANGE (Hz) MIN	MAX	LOSS FACTOR (%) MIN	MAX	MODE SHAPES
MACHINE-TOOLS	LATHE	0	500	4	18	BENDING & TORSION
	MILLING MACHINE	0	250	4	12	BENDING & TORSION

The consideration of the type of materials that offer relatively high equivalent stiffness (E/ρ) immediately points towards ceramic materials. However these materials suffer from the lack of the toughness required for structural components both for static loading in tension or shear. Under dynamic loading they exhibit a relatively low damping characteristic. On the other hand materials that posses relatively high loss factor η, such as polymers, lack in stiffness. Therefore, for the specific requirements of boring bars, metals must be selected with a compromise between the two.

4.2.1 HIGH DAMPING METALS AND ALLOYS

Metallic materials in general do not exhibit an appreciable level of damping. Moreover, due to the damping mechanisms involved, the characterization of the damping properties of metals is not straightforward. The general damping mechanisms distinguishing composite metallic materials, in turn, implies a dependence upon the microstructure (4.2). Several commercially available high damping metals and alloys investigated by (4.2) are illustrated in Table 4.2.

A possible classification of these materials consists in the consideration of their loss factor with respect to their elastic modules. From Figure 4.1., and Table 4.2, it can be seen that the damping capabilities of " Proteus and Gentalloy " exceed significantly that of steel. However, the elastic modules of Gentalloy and Proteus exhibit relatively lower values than that of conventional steel tools.

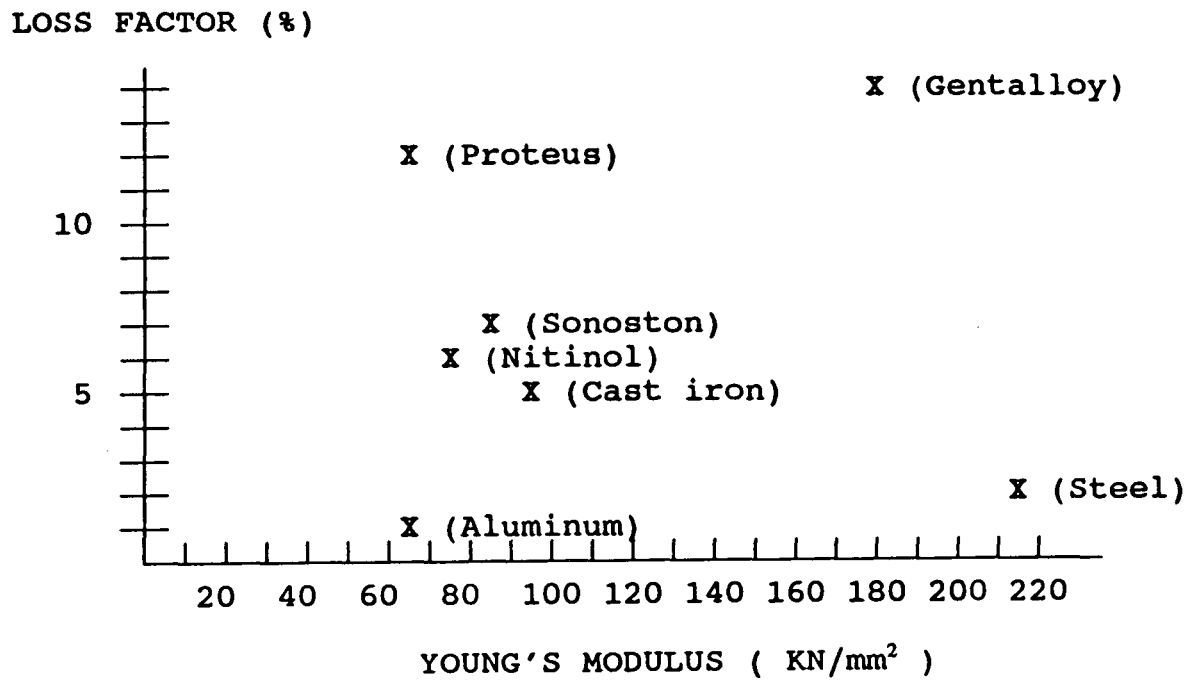

Figure 4.1 : Classification of high damping metals and alloys

Table 4.2: Properties of commercially available high damping metals

ALLOY NAME	DENSITY (Kg/m^3)	DAMPING MECHANISM	MODULUS, E (KN/MM^2)	LOSS FACTOR (%)
PROTEUS Cu,Zn,Al	7734	MARTENSITIC TRANSFORMATION	50 - 70	11 - 14
GENTALLOY Fe,Cr,Mo.	8679	FERROMAGNETIC ALLOY	180	14
SONOSTON Mn, Cu	5922	MOVABLE CRYSTAL AND PHASE BOUNDARY	80	7
NITINOL Ti, Ni	6526	MOVABLE CRYSTAL AND PHASE BOUNDARY	70	6
CAST IRON	7658	COMPOSITE MATERIAL	90 - 110	5
STEEL Fe-ALLOY	7834	MAGNETO-MECHANICAL	210	2

4.3 MATERIAL DEVELOPMENT

The initial consideration in design for a chatter resistant boring bar was to develop a material that could reduce the amplitude response level through improved equivalent stiffness. By scanning through the literature (U.S patent 2,752,666 (4.3) on the development of Titanium carbide (TiC) composite materials) it was observed that relatively high elastic modules were associated with these materials, whilst the density due to the large TiC content was relatively low.

Since these materials were not commercially available the approach to the problem of dynamic instability of extended length tooling was to develop such materials and further attempt to improve their mechanical properties through alloying and processing techniques.

Some of the properties associated with the reported materials

(4.2), are listed below;

Specific gravity 10^3 kg/m^3 = 6.0 - 6.4

Hardness, Vickers c Scale = 55 - 58

Elastic Modulus N/m^2 = 259 x 10^6

The constituting elements of these materials are essentially similar to Gentalloy with additional Titanium carbide TiC, 33% by weight dispersed through the steel matrix elements. The steel matrix contains by weight 3% Cr (Chromium), 3% Mo (Molybdenum), 0.6% C (Carbon), and the balance 60.4% Fe (Iron).

The metal matrix composite is produced using powder metallurgy as a cost effective measure and near net shape form. The process consists of mixing the powdered titanium carbide with the steel-forming ingredients. Compacts are then formed by pressing the mixture into a mould and subjecting it to liquid phase sintering under non-oxidizing conditions.

4.3.1 COMPOSITE ADDITIVES AND ALLOYING ELEMENTS

The uniformly dispersed particles of very hard titanium carbide (TiC Hardness = 2500 Knoop) are surrounded by softer, more ductile steel matrix particles (4.3). The particulate composite makes use of very small particles of TiC (0.1 to 7 μm) that could block the movement of dislocations, hence producing a pronounced strengthening effect

The composite was formed by a powder metallurgy process. The tool steel making particles of Fe, Cr, Mo, c, Ni and TiC powders are blended and compacted at high pressure. This is followed by sintering under a non oxidizing atmosphere.

The prerequisite in the design of a component of high natural frequency, was to limit its density without impairing its effects on

the stiffness. The "rule of mixture" was used to introduce higher quantity of particles with minimum density (table 4.3). The observation on the effect of alloying elements are detailed in the table of results.

4.3.2 POWDER METALLURGY

Powder methods were employed because the combination of properties required could not be readily achieved by other methods. Moreover, the powder route is more cost effective for the production of samples compared to other routes. The particulate elements are also highly reactive at elevated temperatures. Therefore, the powder route was considered to be the most suitable.

4.3.3 DENSIFICATION WITHOUT THE USE OF PRESSURE

There are various methods to enhance densification during sintering of powders without the use of external pressure. In the idealized case liquid-phase sintering, a low-melting-point constituent is present in sufficient quantities to wet all the powder particles. There is no reaction between the liquid and the particles, but the liquid allows particles to move relative to each other so as to pack more effectively. The stresses generated by capillary attraction at contact points between particles are sufficiently high to cause plastic deformation and hence aid densification.

4.3.4 APPLICATION OF PRESSURE WITHOUT HEAT

Densification can to a certain extent be achieved by the application of pressure alone. This is the process occurring in cold isostatic pressing (CIP). A slow compaction speed allows particle rearrangement to occur while approaching zero porosity or theoretical density.

The pressure causes particle rearrangement by slippage and restacking, elastic and plastic deformation at contact points, and cold working of ductile particles. Brittle particles may fracture under the imposed stress, leading to comminution (4.4).

At the contact points, the heat generated by friction may be sufficiently high for local melting to occur. On re-solidification the particles are welded together across the interface. High local stress can also lead to recrystallization across contact points, again effectively giving local welding.

4.4 EXPERIMENTAL PROCEDURE (MATERIAL DEVELOPMENT)

4.4.1 CHEMICAL COMPOSITION

Table 4.3, shows the chemical composition of the compound powder prepared for processing and development of test specimens. They are grouped into two categories.

Group I- (TC 1) Is comprised of the composition reported in U.S patent 2,752,666 (4.3)

Group II- (TC 2 through to 8) is comprised of varying the percent by weight of the primary alloying elements and addition of Nickel.

Table 4.3 : Chemical composition of the alloy and its components.

Matrix, % by weight	CHEMICAL COMPOSITION TiC	C	Cr	Mo	Ni	Fe
GROUP I-						
1.....	33	0.6	3	3	-	60.4
GROUP II-						
2.....	30	0.6	3	3	-	63.4
3.....	35	0.6	3	3	-	58.4
4.....	35	0.6	4	3	-	57.4
5.....	35	0.6	4	4	-	56.4
6.....	35	0.6	4	2	-	58.4
7.....	35	0.6	4	3	0.5	56.9
8.....	35	0.6	4	3	1	56.4

4.4.2 POWDER CHARACTERISTICS, (PARTICLE SIZE EFFECT)

Powder particles are not all of perfect geometry and uniform size. At the design stage the void space may be reduced by mixing small and large particles together so as to fill the gaps in between them. This is illustrated in Figure 4.2. However even if a variety of particle size are used the theoretical density can not be achieved. This is due to gaps and geometrical blockage, or inter-particle force and electrostatic attraction (4.4). Even if smaller particles gaps do exist porosity inevitably results.

Loosely contacting powders have negligible tensile strength for practical purposes. To develop strength, heat and pressure must be applied. Sintering occurs when heat is applied to a powder containing pores; the driving force for sintering is the reduction of the surface area associated with pores. The physical means available for

approaching the theoretical density of the material are;

a) Refined particles of varying size (particle size 5 to 50 μm) mixed thoroughly through the matrix with smaller particles constituting the major volume.

b) Slow application of isostatic or unidirectional compaction pressure for closure of gaps and parasites for maximum cold density.

c) Partial constituent additions that could provide a liquid phase under application of temperature, provided it would not impair the mechanical properties of the component.

In order to achieve relatively high pack density the particle size was selected so that approximately equal volume of cores and fine particles are mixed through the matrix. The titanium carbide particles were intended to take the form of the fine constituent component and the steel matrix the coarse particles. Since the Titanium Carbide content of 35% by weight is about 46% by volume the remainder of the matrix was selected so that approximately equal volume was achieved.

Table 4.4 illustrates the partial size distribution considered appropriate to achieve a relatively good packing density.

The powders were analyzed to assess the quality and distribution of particle size effect. The process was carried out using Coulter LS, partial size analyzer, by pouring a small quantity of the individual powders in to the inlet chamber. The results are given as a printed output as shown in Figure 4.3. The analyzed results of the supplied materials were in accordance with the required specification.

TABLE 4.4 : Designated particle size of the compound.

Element	Tic	Fe	C	Mo	Cr	Ni
particle size μm	2-4	20-25	> 1	2-4	20-25	2-4

4.5 PROCESSING OF THE COMPOUND POWDER

In producing a Titanium Carbide composite, the compositions of each group, presented in table 4.3 are mixed together and poured into the container of a hexane milling unit, which was half filled with stainless steel balls. The purpose of milling the composition was two fold: One to achieve uniform partial distribution throughout the mix and the other to crush large particles to size.

The maximum capacity of the container, for effective milling was approximately one kilogram of mix per cycle. Therefore, for the preparation of the test specimen several cycles were required to produce the required quantity. As recommended by the machine instruction, ten grams of paraffin were also used which acts as a lubricant and prevents excess heat production. Milling was carried out for twenty four hours to ensure uniform dispersion of the composition through out the matrix. After completion of milling, the mix was removed and oven dried at 60°C. Cylindrical compacts of 10 mm in diameter and 60 mm in height were then pressed into shape. An average 38% reduction in volume was observed.

4.5.1 SINTERING OF SAMPLES

Because titanium carbide is highly reactive at high temperature it was necessary to sinter the samples in a controlled atmosphere such as a vacuum furnace. The samples were placed on a ceramic (non reactive alumina) dish at a sintering temperature of 1450 °C (recommended by U.S patent 2,752,666 (4.3)) for one hour after which the samples were furnace cooled to room temperature.

The samples were then sectioned to the required dimension described in section 4.9, in preparation for testing the mechanical properties .

4.5.2 COMPACTION, ENCAPSULATION AND SINTERING OF FULL SIZE TEST SPECIMEN

Although it was relatively simple to sinter the samples of small dimension in a conventional research type vacuum furnace sintering of the full size test specimen due to their relatively large geometrical dimensions (50 mm in diameter and 400 mm in length) in such a furnace was not possible.

The principle problem associated in fabricating the large powder compact was due to the requirement of the green compact to be sintered in a controlled atmosphere to avoid contamination and oxidation.

For this purpose it was necessary to design a special vacuum chamber as shown in Figure 4.4, so that compaction and gas evacuation could be done in the same vessel. As the sintering temperature was lower than the melting temperature of mild steel, the compaction mould and vacuum chamber was constructed of this material.

The mixed compound was poured into the mould and pressed using a ram arrangement at 20 tonne per square inch. The container was then sealed on the top by welding the designed vacuum mechanism. A vacuum pump was used to evacuate entrapped gas in the chamber until a pressure of 10^{-2} torr was achieved. The vacuum mechanism was secured and tested for leaks. The complete unit was then placed in an ordinary furnace and heated to the required temperature.

The sintering cycle was the same as the previous case with the exception that the component was left to soak at a temperature of 1150 °C for three hours. Figures 4.5 and 4.6, illustrate the compact in the vacuum capsule before and after sintering respectively.

An important practical parameter overlooked at this stage was that the casing itself was subjected to oxidation. Therefore, the effect of encapsulation is thought to have been diminished leading to severe surface contamination and oxidation as shown in Figure 4.7. The sintering of the compact was therefore not fully effective and led to

the failure of the sintered component whilst machining.

Furthermore, with conventional uniaxial powder-pressing techniques almost invariably some residual porosity, distributed as fairly randomly sized voids, would be expected. Hot Isostatic pressing (HIPping) has been reported to remove the residual pores. This is normally carried out in the semi-solid pasty zone at temperatures of (1300-1390 °C) and pressure of 70-140 MPa.

4.6 ADAPTED PROCESSING TECHNIQUE (HOT ISOSTATIC PRESSING)

The Hot Isostatic Pressing (HIP) enables the simultaneous application of heat and pressure. It involves the application of a high-pressure gas at an elevated temperature in a specially constructed vessel. With this method the combination of pressure and temperature can be used to achieve a particular density at a lower temperature than would be required for sintering alone. Application of pressure reduces the melting point of the particles by increase of intermolecular friction. The effect of lower temperature is such that unacceptable grain growth can be avoided. The densification enhancement of powders through introduction of additives such as low-melting-point constituents which may have damaging effects on mechanical properties, may not be needed (4.4).

4.6.1 THEORETICAL REVIEW (HOT ISOSTATIC PRESSING)

In HIPing, the driving force for pore closure is due to relatively high external pressure. Under pressure the gas diffuses to the surface, rather than to another pore as in sintering. The pore then collapses. It is only when a pore reduces to a diameter of perhaps 40 nm that the driving force due to surface energy becomes comparable with

that due to the externally applied pressure (4.4).

Yield stresses decrease for most metals and ceramics with increasing temperature. HIPing conditions are generally chosen so that the gas pressure is greater than the reduced yield point of the material at that temperature. Plastic flow can then occur on a microscopic scale (4.4).

In cold pressing, densification is retarded by the effects of work hardening within particles. In hot pressing, though at temperatures above the recrystallization temperature, the dislocation tangles and pile-ups are constantly eliminated by recovery mechanisms so that particles can continue to deform.

During the final stages of HIPing densification, when only isolated pores are present, the surfaces of the pores are not simply pushed together to develop a planar crack; bonding occurs because atoms diffuse in both directions across the interface (4.4). At this stage pore dimensions are small (1 μm or less) and the sustain time of one hour is adequate to allow complete closure.

4.6.2 ENCAPSULATION

The powder for consolidation by HIPing treatment is encapsulated in a gas-tight envelope which readily deforms at the processing temperature, thus transmitting the gas pressure. The envelope is evacuated prior to sealing to prevent contamination of the encapsulated material and to remove internal gas which might develop a pressure opposing the external pressure during processing.

The basic requirements for the envelope are that it should be relatively strong, gas tight, inert and plastic under the applied temperature and pressure conditions. It also has to be compatible with the material to be pressed so as to minimize diffusion reactions and to be readily removable. Various types of capsule can be utilized.

Sheet metal is the most widely used material. The sheets are generally of mild steel, stainless steel or nickel alloys. The container is leak tested before the powder is loaded. The envelope is evacuated (10^{-2}-10^{-4} Torr), at an elevated temperature (300-500 ^{0}C) for elimination of material contamination by vapour particles, and properly sealed by welding. After HIPing compaction, the sheet metal container can be removed by machining .

4.6.3 PROCEDURE OF THE HIPing CYCLE

For completeness the procedure for the HIPing cycle followed by HIP laboratory are as follows ;

1) Preparation; Components are placed on trays, and are suitably separated for expansion effects.
2) Loading; Individual trays are assembled into supporting furniture and the completed charge is lowered into the pressure vessel. The pressure vessel is closed.
3) Purging; The pressure vessel is evacuated and purged with the pressurizing gas.
4) Equalization; High-purity argon is admitted to the vessel from the storage system until the vessel pressure has risen to the storage pressure.
5) Compression; Gas is pumped via a compressor from the storage system to the vessel until the required 'start pressure' is reached. Heating may take place while this is occurring and this contributes to the pressurization.
6) Heating; The required HIPing temperature is achieved (usually after about 2-3 hours depending on the nature of the charge) and sustained for between 1 and 4 hours depending on the application.
7) Cooling; At the end of the sustain period, the furnace is allowed to

cool. This inevitably reduces the pressure but some excess pressure is important for cooling purposes. Cooling rates can be varied between 2 and 100 °C per minute.

4.6.4 SAMPLES PRODUCTION BY HIPing PROCESS

The production of samples was carried out through a contract at the Interdisciplinary Research Centre (IRC) of Birmingham university. The procedure followed is believed to be similar to that described above using a cycle time of two hours at 100 Mpa and 1100 °C.

The dimensions of the capsules before sintering were 15 mm in diameter by 100 mm in length. The capsule material was mild steel, and the final dimensions of the hipped samples were approximately 10 mm by 70mm, illustrated in Figure 4.7. The casing on the samples were machined off and samples were sectioned to size, using a diamond wheel slicing machine in preparation for testing of mechanical properties.

AS the mechanical properties of the samples produced by vacuum sintering indicated that samples of composition type 4, 7, and 8 were superior to the others in the group, only samples of this type and one of group 1, were used in the HIPing process.

4.6.5 TEST SPECIMEN PRODUCTION

Due to dimensional limitation it was not possible to use the HIPing facilities at IRC, therefore a contract through HIP limited was used. Due to the cost constraints the HIPing vessel was shared, and the supper alloy cycle which was not available at IRC was selected. This cycle had the added advantage of higher temperature (1200°C) and pressure (120 Mpa) and HIPing duration of four hours.

Although using the super alloy cycle had improved the attained

mechanical properties even further, the only critical effect in using this cycle may be due to the invariability of results from those obtained from samples.

Figure 4.8, illustrates the final geometry of the HIPed test specimen.

The cold compaction procedure of the powder particles for the test specimen (proclaimed by HIP Limited conducting the HIPing process) was carried out using an ultrasonic vibratory bed. The estimated pre-HIPing green density of 65 % was found. The final dimension of the HIPed component was reduced by over 30% with a side crinkle of the outer casing which is not an uncommon feature of the HIPing process.

4.7 MICROSTRUCTURE OF HIPed TiC COMPOSITE

The microstructural effects from the metallurgical point of the research are important both because of their influence on final properties and because the microstructural development (eg. grain growth influences densification). However, from the manufacturing point of the research, the concern was primarily due to homogeneity and the effects of particle distribution and densification through the material.

The three samples of composition Group two, (4, 7, and 8) and one of Group one processed by HIPing application were prepared and analyzed using a scanning electron microscope (SEM). The percentage dispersion of elements was as illustrated in Figures 4.9 through to 4.13.

The general observation of the Scanning Electron Microscope analyses indicate that a relatively consistent distribution through the composition was obtained. Isolated large chromium particles (Figure 4.11) entrapped within an area could alter the result of the dispersion analyses. These are considered to be due to such particles failing to be crushed during the milling process. However since only a few of such

entrapped particles were observed their effect on the final properties of the component should be minimal.

The spectrum of elements analyzed also indicate the presence of a very small quantity of impurity, namely silicon, which is believed to have been present in the supplied materials or present in the milling container. The effect of these impurities on the final mechanical properties of the end product (if any) is not fully understood.

4.8 EXPERIMENTAL PROCEDURE

The critical factors for the dynamic stability of the boring bar are the examination of equivalent stiffness E/ρ and the damping factor of the fabricated material. Using these quantities the natural frequency and mode shapes of a given geometry may be determined.

One of the classical methods of measuring the Elastic Modulus and specific damping (ψ) is to employ a specimen beam suspended at its nodal points and vibrated in the plane of the support strings.

If the strings are attached to the beam precisely at the nodes, the strings will be motionless, and there will be no damping due to the supporting strings (4.6). Although in practice it may be impossible to achieve the exact position through trial and error the effective error can be minimised to less than 0.1 %. Figure 4.14 illustrates the specimen positioned for measurement of flexural frequency using a free-free beam suspension method.

Due to the relatively small dimensions of the specimens and low amplitude of the exciting frequency, the effect of air damping was ignored. It may be argued that the damping factors obtained within the fabricated samples would not be representative of the designed boring bar, due to the composite construction. However, the purpose of carrying out the damping investigation of the samples was to characterise the internal friction of the samples. This result may be

used in examination of the application of such materials as the tool structure without the combination design. Moreover, a comparative analysis of the developed material to that of high damping alloys can be carried out.

4.8.1 MECHANICAL CHARACTERISTICS AND TESTING OF THE FABRICATED SAMPLES.

The Hot Isostatic Pressing (HIP) process was applied for the production of particulate titanium carbide and steel bonded matrix parts. The composite material is designated herewith (TC) with its appropriate sample number, for example (TC4).

Elastic properties, damping properties, density and hardness measurements were carried out on the densified products. Results confirm much better properties than that published in the literature (4.3) or those of sintered parts produced earlier under this investigation.

The procedure for testing the mechanical properties of the aforementioned fabricated samples described above for both the vacuum sintered and HIPed samples were similar in procedure.

Some of the tests for mechanical properties were carried out by the author at the Interdisciplinary Research Centre of Birmingham University. The examination procedure of the test samples were as follows;

Density

After slicing the samples to size the remainder of the sample was used for determination of the specific gravity. The sample density was measured using water as the reference substance, which was a measure of mass of a known volume of the sample to the mass of an equal volume of water. Results are given in tables 4.5 and 4.6.

Hardness

Hardness was measured using the Vickers diamond pyramid indentation technique on materials as described in BS472 part I. The load is applied mechanically by a lever and the application is hydraulically controlled so as to give the correct time of contact.

The samples, which had a highly polished surface, were mounted on a Vickers indentor fixture. Measurements were made on the C scale using a 10 Kg load. The measured hardness values of the samples are listed in tables 4.5 and 4.6.

Elastic and Damping Properties

Young's modulus, Poison's ratio, and damping, were measured at room temperature by a sonic velocity method as a function of relative density, using a free-free beam suspended at its nodes by two strings. Samples in the form of rectangular section prisms, typically 60.0 by 2.0 by 1.0 mm, were used for testing. The tests were conducted in an intermediate frequency range (100 to 2000 Hz) using the resonant bar equipment at IRC. The detailed theory and description of the technique adapted by the author for examination of elastic moduli and dynamic properties are detailed in Appendix "A".

4.9 RESULTS AND ANALYSES

From the experiments of material development, The samples fabricated through Hot Isostatic Process indicate that the (TC4) composition exhibits some essential dynamic properties that are superior to that of the conventional steel or Sintered Carbide tools.

The common solution in industry for the problems of chatter is to make use of Sintered Tungsten Carbide tools. Unfortunately, sintered carbides have a higher density than steel leading to only a marginal increase of the equivalent stiffness (14 %). Furthermore, according to the obtained analytical results of Table 8.6 in chapter eight, it can be observed that the fundamental natural frequency of a Tungsten carbide bar of a given geometry would be 20% lower than that of a steel bar. However, the TC4 bar developed as part of the work in this thesis would be expected to operate with a fundamental natural frequency 83% higher than that of a sintered carbide bar of the same geometry.

The progression of improvement towards material development entailed having powder compacts of two group compositions table 4.3.

These were sintered using Hot Isostatic Pressing (HIP) at 1400 °C and 120 MPa chamber pressure. The mechanical properties of the dense product were measured and the following results were obtained.

From Table's 4.3, 4.5 and 4.6, it can be seen that the mechanical property of the dense composite material was dependent on the percent composition as well as the processing technique.

Increasing the Titanium carbide content from 30 % (sample 2) to 35 % (sample 4), resulted in an increase in the Elastic Modules of the samples by a marginal 9.8%, for the sintered product and 15.3% in that of sample fabricated by The HIPing process.

The addition of Nickel and Chromium content (1%) (ie, TC4 composition) also shows an improvement in the percentage variations of the Elastic Modulus by a margin of 13.6 % for the sintered product and 28.9 % for the HIPed sample.

These results indicate that;

a) Both alloying elements and processing technique have a profound effect on the mechanical properties of the final product. And under the defined practice

b) The processing technique has a greater influence than variation in the constituent elements.

The comparative analyses on numerical values for the specific gravity from table 4.5 and 4.6, illustrates that;

Using the HIPing process results in a small increase of the density of the final product compared to vacuum sintering. The rise of 75 Kg / m^3 in specific gravity corresponds to only 1.4 % . This is due to the greater tendency of pore closure which is caused by the relatively high external pressure.

Although the natural frequency of a structure may be lowered with increased specific gravity, the effective dynamic compliance owing to the greater elastic modulus is significantly improved. Estimation of specific gravity at the design stage could be a useful parameter in tailoring the composition to suit a given requirement. The "rule of mixture" ($\rho_c = \Sigma\ \rho_i\ f_i$) was used to estimate the theoretical density of the composition.

The value of Poison's ratio (which is the ratio of lateral strain to the longitudinal strain) was approximated for use in estimation of damping parameters.

From Tables 4.5 and 4.6, it may be observed that the value of Poison's ratio of the HIPed samples is 8% less than that obtained for samples produced by vacuum sintering. These values could also be used as a further indicator of the enhanced elastic properties of samples produced through the HIPing process.

The elastic modulus and damping behaviour of HIPed composite specimens, as a function of strain amplitude, have been examined using

the free - free flexure test method at 100 to 2000 Hz, and strain amplitudes of 10^{-6} to 10^{-4},.

Examination of the mechanical properties of the sintered samples was initially carried out to identify the elastic modulus, density, hardness and equivalent stiffness. At the design stage the material to be developed was considered to be used as an integral part of a composite construction. Therefore, the quality of material damping may not be representative of the whole system. However, the results of specific damping capacity for the HIPed samples were obtained (Table 4.6) which indicate that the overall percentage loss factor of the developed compounds is comparable to the high damping metallic materials. For example, from Table 4.7, and Figures 4.15 and 4.16, on the comparative classification of high damping alloys it can be seen that the percentage loss factor of TC4 is over five times greater than that of steel.

In comparison with the high damping alloys table 4.7, it can be seen that the percent loss factor of the fabricated samples is almost similar to that of Sonoston. In addition they also exhibit the highest elastic modulus and equivalent stiffness in the group.

Although the TC1 sample has yielded the lowest elastic modulus and equivalent stiffness values it exhibits the greatest percent loss factor in the group. This observation may be treated as confirmation of the fact that higher damping is associated with materials of lower modulus.

Table 4.6, shows that the associated dynamic quality of the TC4 composition fabricated through HIP process is 40% higher than that of TC2, 17% better than TC3, and 447% higher than that of steel bar. This indicates the suitability of such material as a candidate for the proposed design.

Note that the specific damping capacity is frequency dependent over a given temperature range. The cutting operation however operates over a broad range of frequency. Therefore the effective damping of the

boring bar should be taken as quality of the finished product with respect to manufacturing achievement of the design. Hence, the material damping qualities may not be related to the loss factor in the design of the final construction.

For completeness Tables 4.8, 4.9 and 4.10 are presented in which the relative percentage variation in the mechanical properties of fabricated samples are compared. The results indicate that :

I) An overall improvement of dynamic properties has been observed with TC1, TC3 and TC4 irrespective of the processing technique. However, with the vacuum sintered specimen (sample 2) a 1.3 % reduction of elastic modulus and 5.7 % loss of equivalent stiffness are observed. The reduction in elastic modulus is not considered to be significant. Therefore variation of the alloying element due to the reduction in titanium carbide content is considered to be responsible.

II) An overall improvement in the properties of samples fabricated through HIP process is associated with mechanics on densification of materials. This is related to the simultaneous application of temperature and pressure. From the observation of the results in table 4.9 it may be concluded that the effect of the processing technique on average improves the elastic modulus of the blended composition by 13.5 percent. This effect cannot be observed from the properties of TC2 samples. This is considered to be due to an ineffective HIPing process. Observations of the mechanical hardness test results from table 4.6, are indicative of insufficient densification.

III) Tables 4.8 and 4.10, illustrate that the quality of the boring bar made of TC4 composition would be;

a) At least 27% better in elastic modulus and 85% greater in equivalent stiffness to that of steel bar fabricated by vacuum sintering process.

b) And 44% better in elastic modulus and 109% greater in equivalent stiffness to that of steel bar fabricated by HIP process.

Due to the defined objective of the investigation the effective mechanism involved for characterisation of damping capacity is not examined. However, according to reference (4.7), when the constituting elements of a high modulus material (such as ceramic titanium carbide TiC) are matched with high thermal conductivity metals, higher damping would be achieved due to inter-particle thermal mismatch. Researchers (4.7) have reported to have attained a 20 % loss factor for TiC and magnesium. Such a mechanism could also be responsible for the damping levels associated with the composition developed under this investigation.

4.10 CONCLUDING REMARKS

The amount of energy dissipated in each component of a composite system is equal to the damping coefficient multiplied by the maximum strain energy stored in that component, so increasing the system damping requires that the configuration used should increase the total strain energy in the high damping material (4.7).

Unfortunately, in all practically applicable materials increasing the damping factor always decreases the elastic modulus so that the only successful technique relies on increasing the strain level.

Increasing the strain level may be attained by composite construction of the boring bar. The documented design practice is developed by Finite Element modelling of the construction given in chapters seven and eight.

The "constraint layer" damping, was also applied as a design option as reported in the previous chapter. The criticism of using this method as a means of attenuation point to the difficulty of application

on the bar of a given curvature. A relatively varied result may be obtained if the bar is to operate over a large temperature range.

The composite material developed, designated herewith TC plus a Group Number, consists of ceramic particles namely titanium carbide dispersed through a particulate steel matrix. The Titanium carbide (TiC) imparts strength, and stiffness and the metal matrix provides toughness.

Powder compacts of TiC and steel matrix of the two groups given in table 4.3 were fabricated using sintering and HIP process. The effectiveness of these materials as a candidate for boring bar applications was investigated by measurement of the mechanical properties of the dense product.

Additions of Titanium carbide (TiC) to the steel forming matrix are experimentally demonstrated (table's 4.5 and 4.6) to produce a dense composite product with increased elastic modulus. The amount of increase in stiffness is not a linear function of the ceramic content but rather the majority of the stiffening effect is achieved by the initial addition of ceramic.

It was further shown that the important dynamic quantities E/ρ and the damping capacity of the composite are higher than that of conventional materials used for boring bar application. The examination of materials fabricated by the HIPing process shows the attained mechanical properties are better than those published in literature (U.S patent 2,752,666 (4.3)) on similar materials. The results of samples fabricated by sintering indicates that variation of the samples constituents could have a considerable effect on mechanical properties of the component.

The composite material TC4 developed in this thesis for boring bars with improved dynamic stiffness is considered to have much greater potential use than simply the boring bar application. The full

potential may be realised by a thorough investigation into other physical properties such as creep, plasticity and thermo-elastic Young's modulus at elevated temperature, thermal expansion coefficient, thermal and electrical conductivity and interface damping characteristics. It should be mentioned that at the time of material development the concern was solely for a solution to the problem of improving the equivalent stiffness. Therefore, experimentation was only made through the manufacturing engineering approach. The use of a metallurgical approach for material development was later realized to be more effective especially in respect of damping capacity at the interface for various material combinations (4.8 and 4.9). However, this was considered to be separate from the scope of the research. Methods to optimize the mechanisms responsible for damping characteristics require further investigation for clear documentation of the effects .

In terms of practical achievement due to material development, with reference to tables 4.5 and 4.6 it can be seen that all static and dynamic quantities that could influence the increase of natural frequency and reduce the static deflections and high amplitude of vibrations, ie, Elastic modulus, Equivalent Stiffness (E/ρ) and damping, have substantially been improved by a respective factor of 45%, 110% and 450% compared to the conventional steel. These improvements are further investigated and reported through practical and analytical consideration in the subsequent chapters.

Table 4.5 : Mechanical Properties of Vacuum Sintered,TiC Composite

Sample No.	Elastic Modulus (E)GN/m²	Density ρ Kg/M³	Equivalent Stiffness E/ρx 10⁶	Possion Ratio υ	Vickers Hardness
1	$238_{(TC1)}$	5519	43.12	0.24	50 - 53
2	235	5780	40.65	0.24	49 - 54
3	243	5250	46.28	0.24	48 - 60
4	$258_{(TC2)}$	5496	46.94	0.24	59 - 65
5	251	5570	45.06	0.24	60 - 67
6	253	5291	47.81	0.24	59 - 64
7	$261_{(TC3)}$	5389	48.43	0.22	61 - 66
8	$267_{(TC4)}$	5315	49.49	0.22	66 - 70

Table 4.6 : Mechanical Properties of HIP_{ed} TiC Composite.

HIP_{ed} Sample No.	Elastic Modulus (E)GN/m²	Density ρ Kg/M³	E/ρ x 10⁶	Possion Ratio υ	Vickers Hardness	Specific Damping (Ψ)	Loss Factor (η) %
TC1	267	5723	46.65	0.21	80-83	0.4297	6.84
TC2	272.2	5703	47.72	0.21	65-71	0.2185	3.48
TC3	294	5587	52.62	0.21	88-91	0.30	4.77
TC4	303	5392	56.19	0.20	93-98	0.3614	5.75

Table 4.7 : Mechanical Properties of high damping alloys and HIP_{ed} Composites.

Alloy	Elastic Modulus (E)GN/m²	Density ρ Kg/M³	Loss Factor (η) %	Equivalent Stiffness E/ρ x 10⁶
Aluminium	70	2698	0.85	25.94
Steel	210	7834	1.05	26.81
Cast Iron	110	7658	4.30	14.36
Nitinol	94	6526	5.15	13.79
Sonoston	105	5922	6.25	17.73
Proteus	90	7734	11.80	11.64
Gentalloy	190	8679	12.78	21.89
TC1	267	5723	6.84	46.65
TC2	272.2	5703	3.48	47.72
TC3	294	5587	4.77	52.62
TC4	303	5392	5.75	56.19

Table 4.8 : Comparative Analyses on Mechanical Properties, Composition of Group 1, with Respect to Those of Group 2. (Vacuum Sintered)

Sample No	percentage Variation	
	E %	(E / ρ) %
2	- 1.26	- 5.7
3	+ 2.10	+ 7.32
4	+ 8.40	+ 8.86
5	+ 5.46	+ 4.50
6	+ 6.30	+10.87
7	+ 9.66	+ 12.31
8	+12.18	+ 14.77
Steel	-21.34	- 45.84

Table 4.9 : Comparative Analyses on Mechanical Properties (TC1, TC2, TC3, TC4 Samples) of Vacuum Sintered Process to that of HIPed Process.

Sample No	percentage Variation	
	E %	(E / ρ) %
TC1	+ 12.18	8.18
TC2	+ 5.5	1.66
TC3	+ 12.64	8.65
TC4	+ 13.48	13.53

Table 4.10 : Percentage Variation on Mechanical Properties of HIP_{cd} TC4, with Respect to Composition of TC, Group, for both Vacuum sintered and HIP_{cd} Samples.

HIPed TC4 with respect to	percentage Variation	
	E %	(E / ρ) %
TC1 Vac	27.31	30.31
TC2 Vac	17.44	19.70
TC3 Vac	16.09	16.03
TC4 Vac	13.48	13.54
TC1 HIP	13.48	20.45
TC2 HIP	11.31	17 75
TC3 HIP	3.06	6.78
Steel	- 44.28	- 109.59

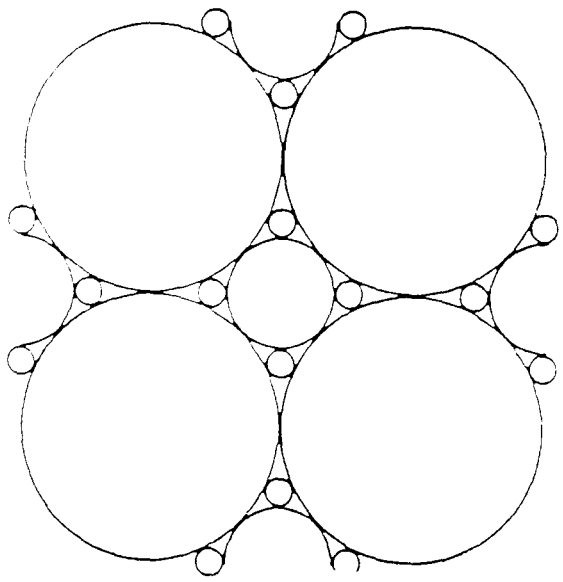

Figure 4.2 : REDUCTION OF POROSITY BY FILLING THE GAPS WITH SMALLER PARTICLES

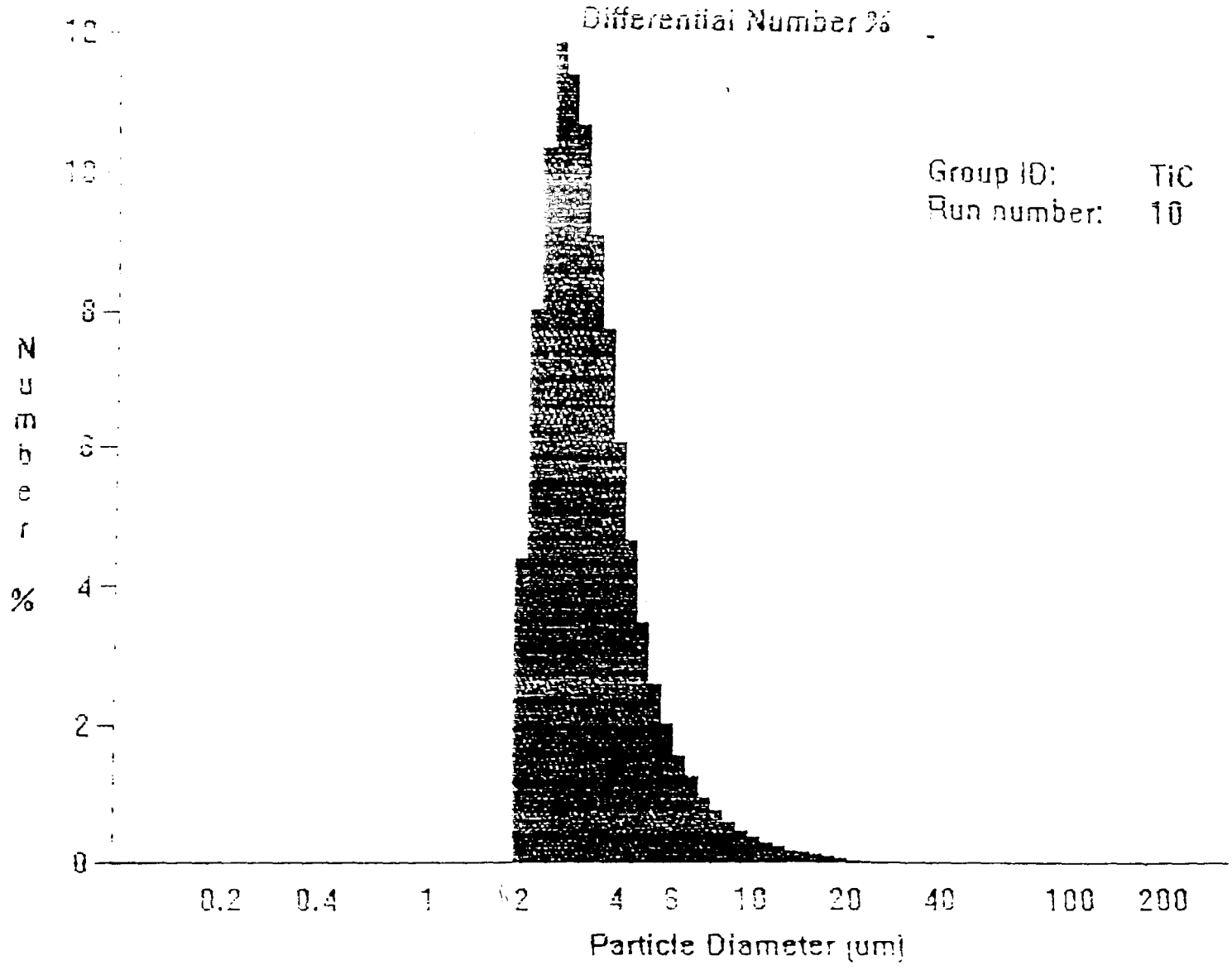

% >	10.00	25.00	50.00	75.00	90.00
Size um	5.336	3.880	3.001	2.462	2.151

Figure 4.3 : PARTICLE SIZE ANALYSIS OF THE SUPPLIED MATERIALS

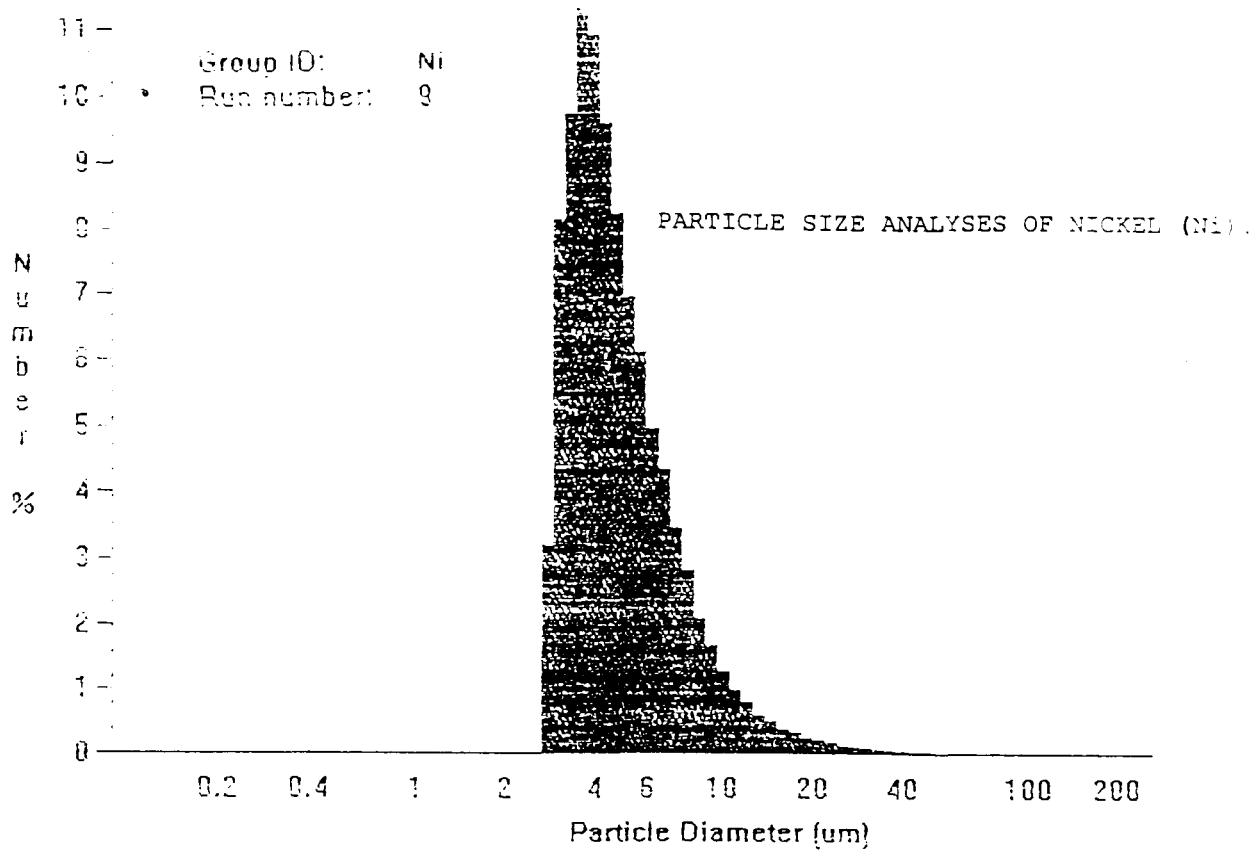

% >	10.00	25.00	50.00	75.00	90.00
Size um	8.592	6.059	4.446	3.595	3.134

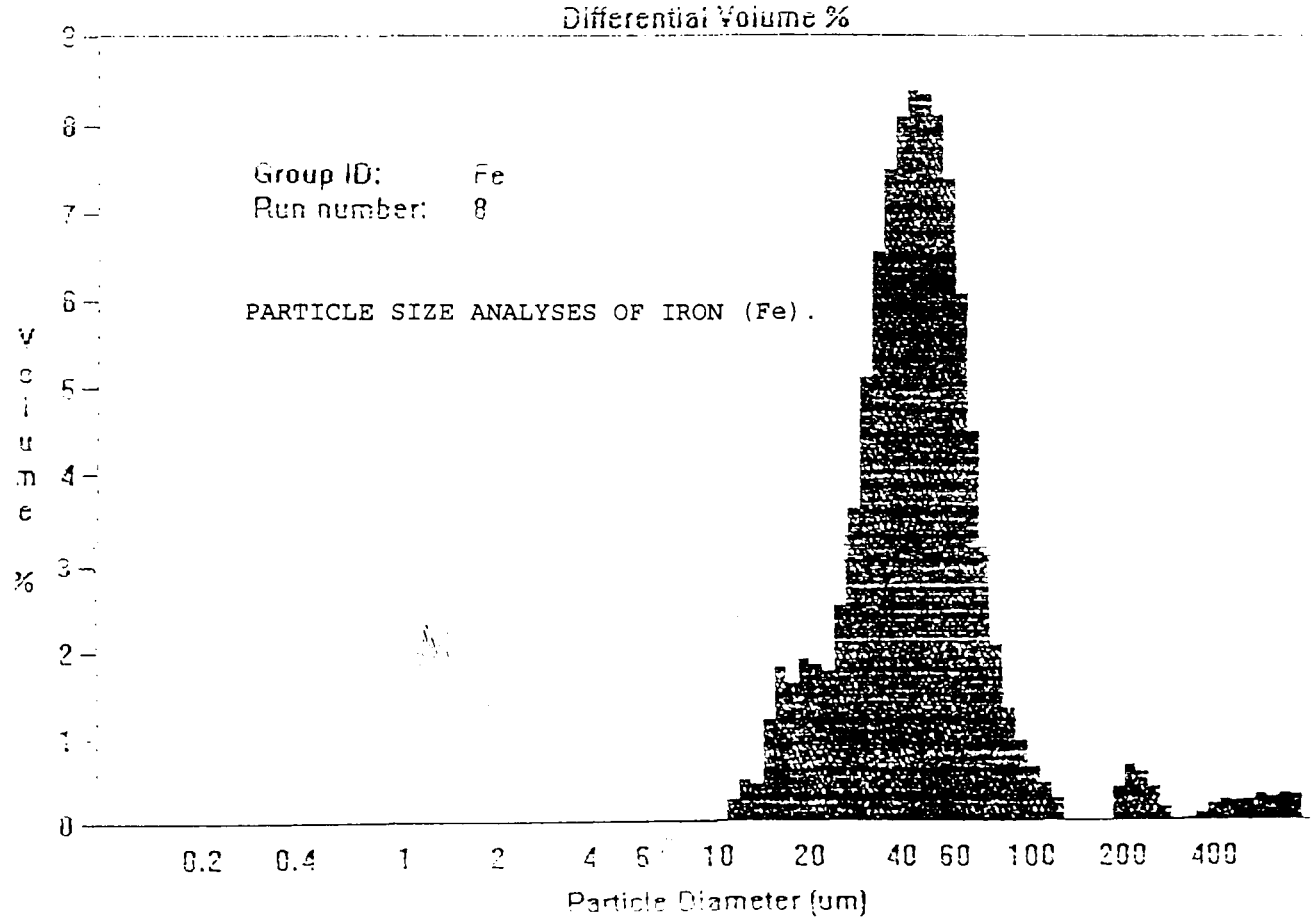

% >	10.00	25.00	50.00	75.00	90.00
Size um	84.03	63.04	47.49	35.35	28.48

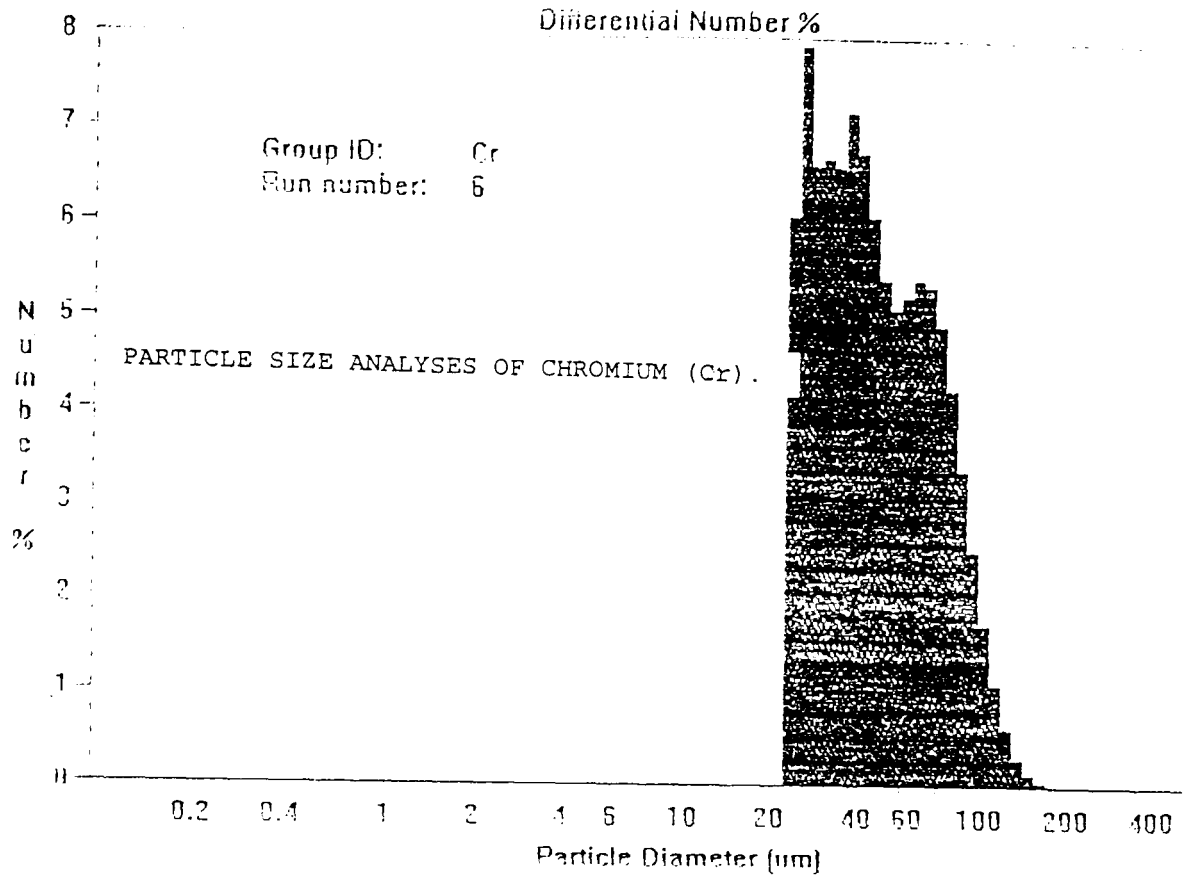

% >	10.00	25.00	50.00	75.00	90.00
Size um	92.20	69.82	45.98	32.89	27.04

PARTICLE SIZE ANALYSES OF MOLYBDENUM (Mo).

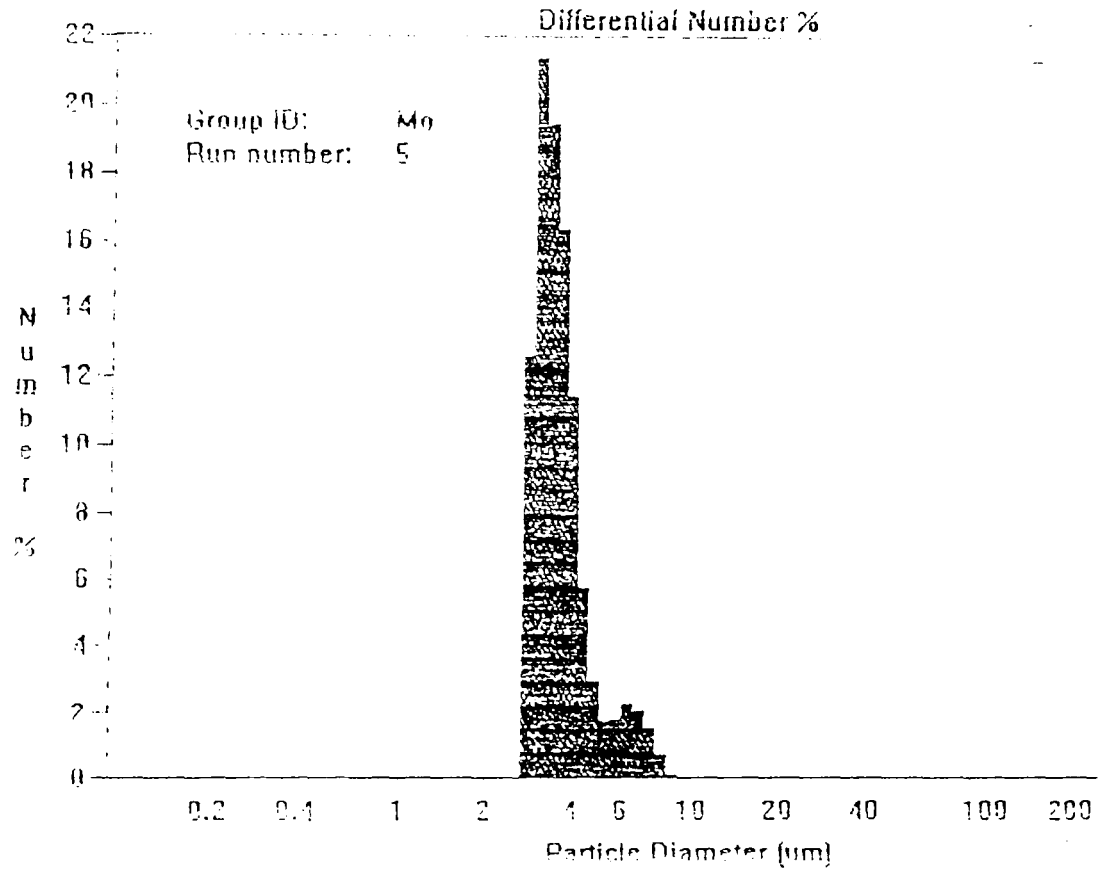

% >	10.00	25.00	50.00	75.00	90.00
Size um	5.023	3.980	3.430	3.065	2.852

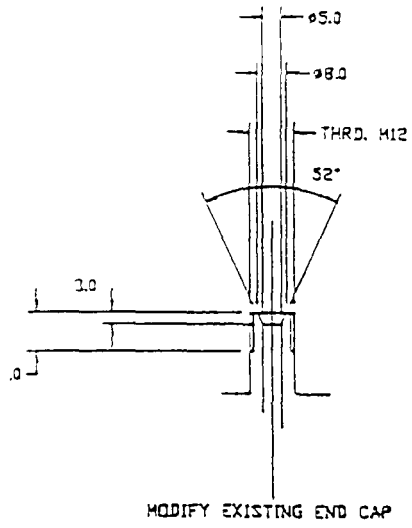

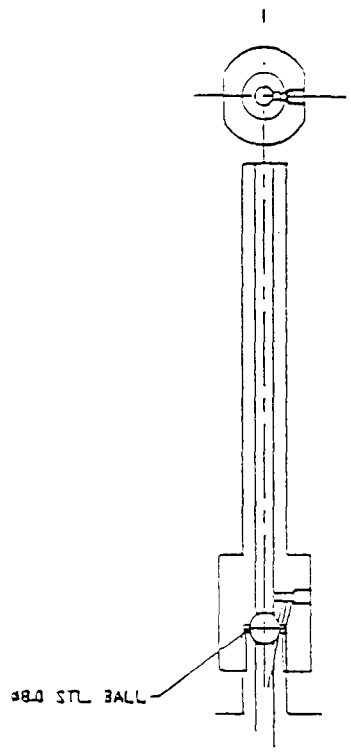

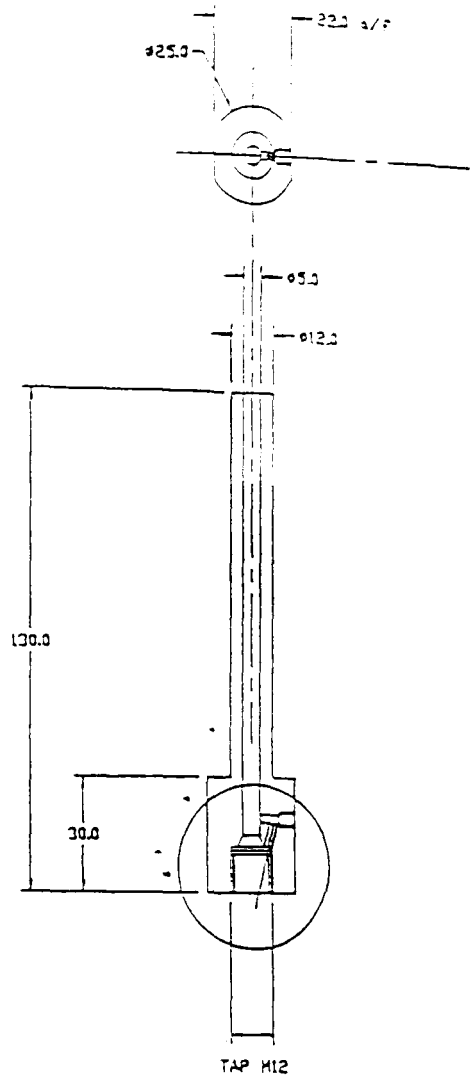

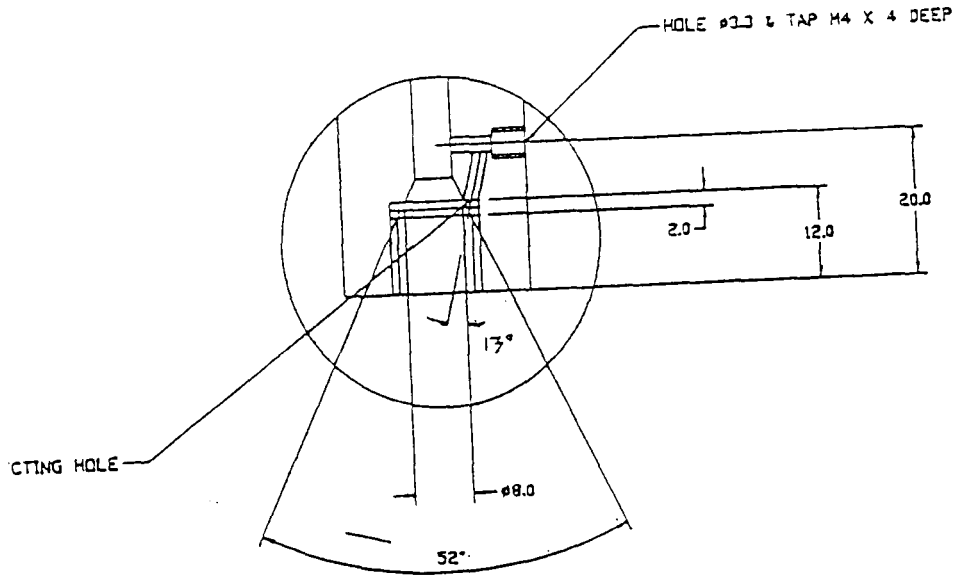

Figure 4.4 : DESIGN OF VACUUM CHAMBER MECHANISM

Figure 4.5 : Encapsulated compacted powder in vacuum chamber, prior to sintering

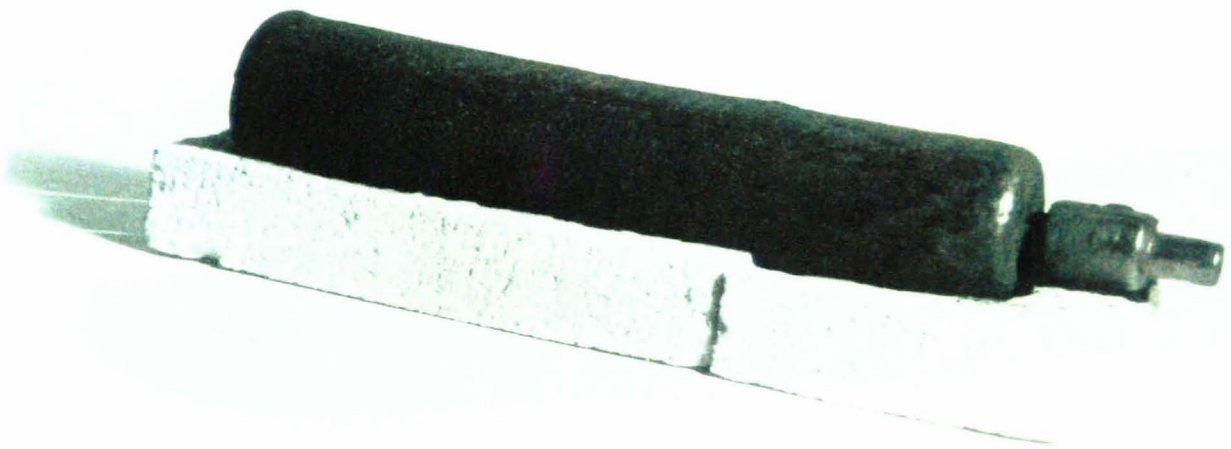

Figure 4.6 : Encapsulated compacted powder in vacuum chamber, after sintering

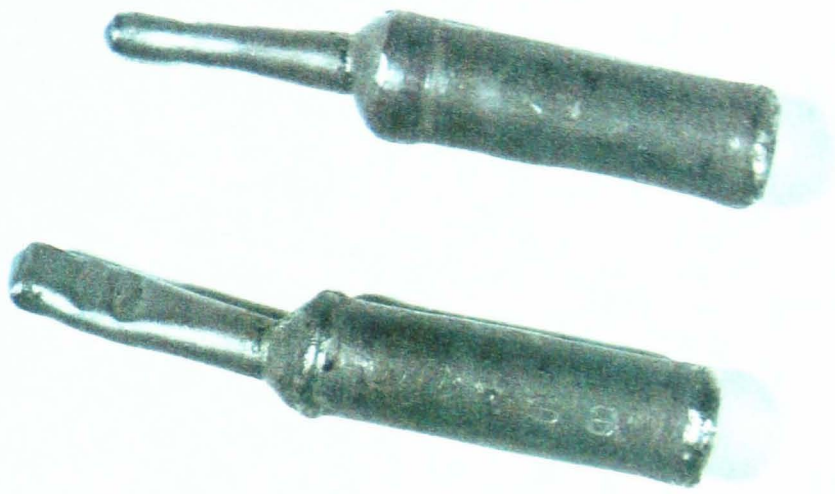

Figure 4.7 : FINAL SHAPE OF THE HIPed SAMPLES

Figure 4.8 : FINAL SHAPE OF THE HIPed TEST SPECIMEN

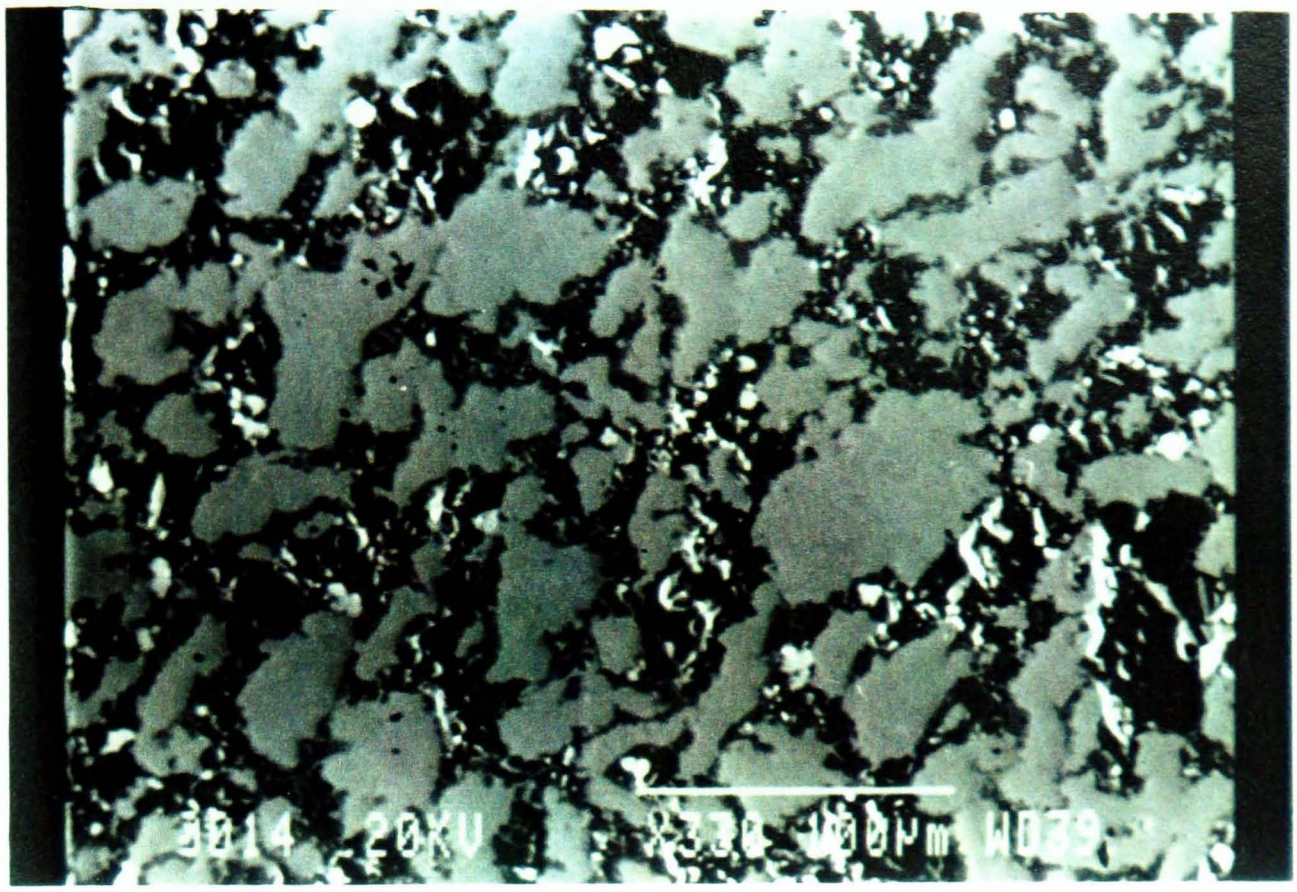

Figure 4.9 : SEM Micrograph of sample "1" (particle distribution).

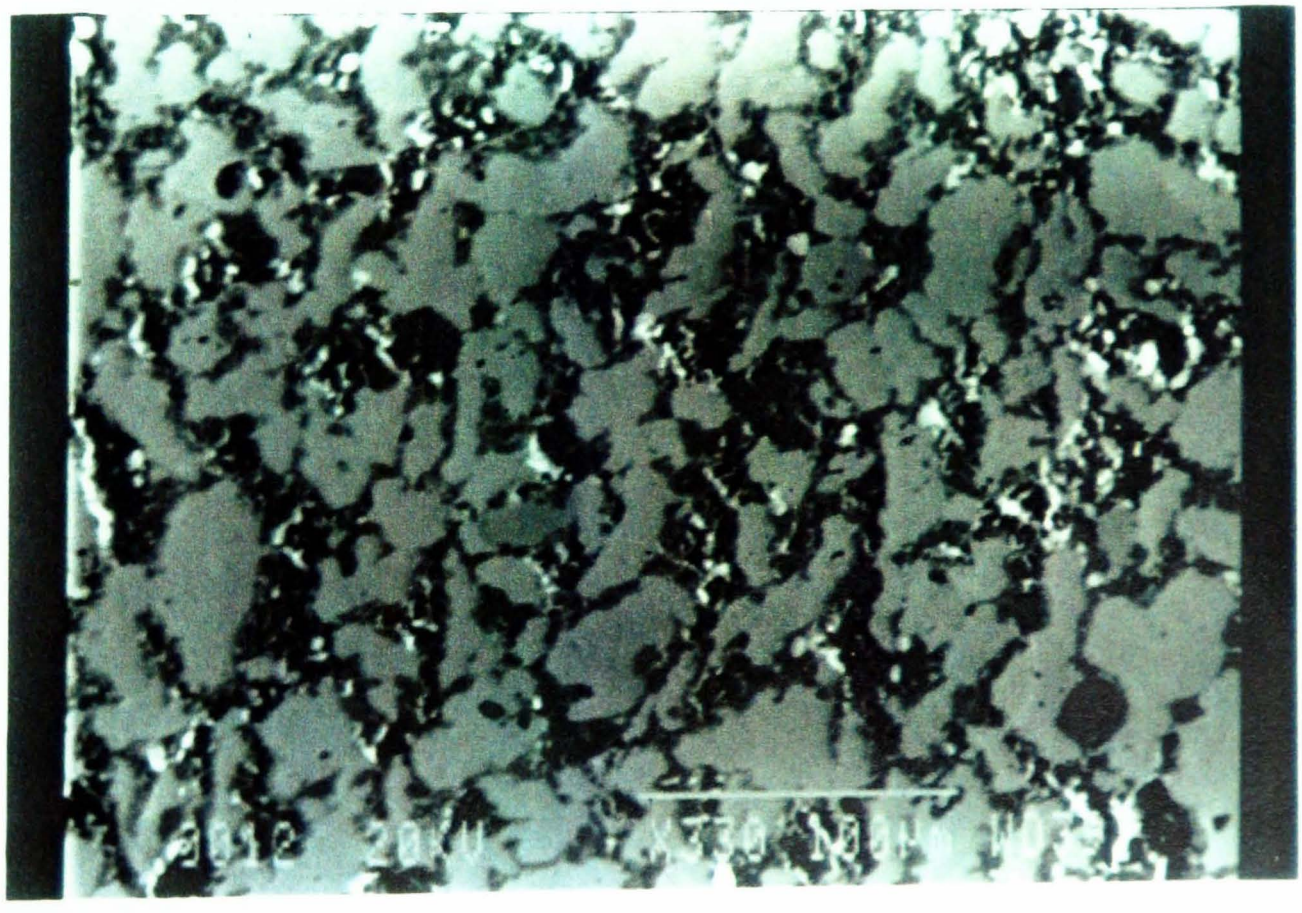

Figure 4.10 : SEM Micrograph of sample "4" illustrating particle distribution.

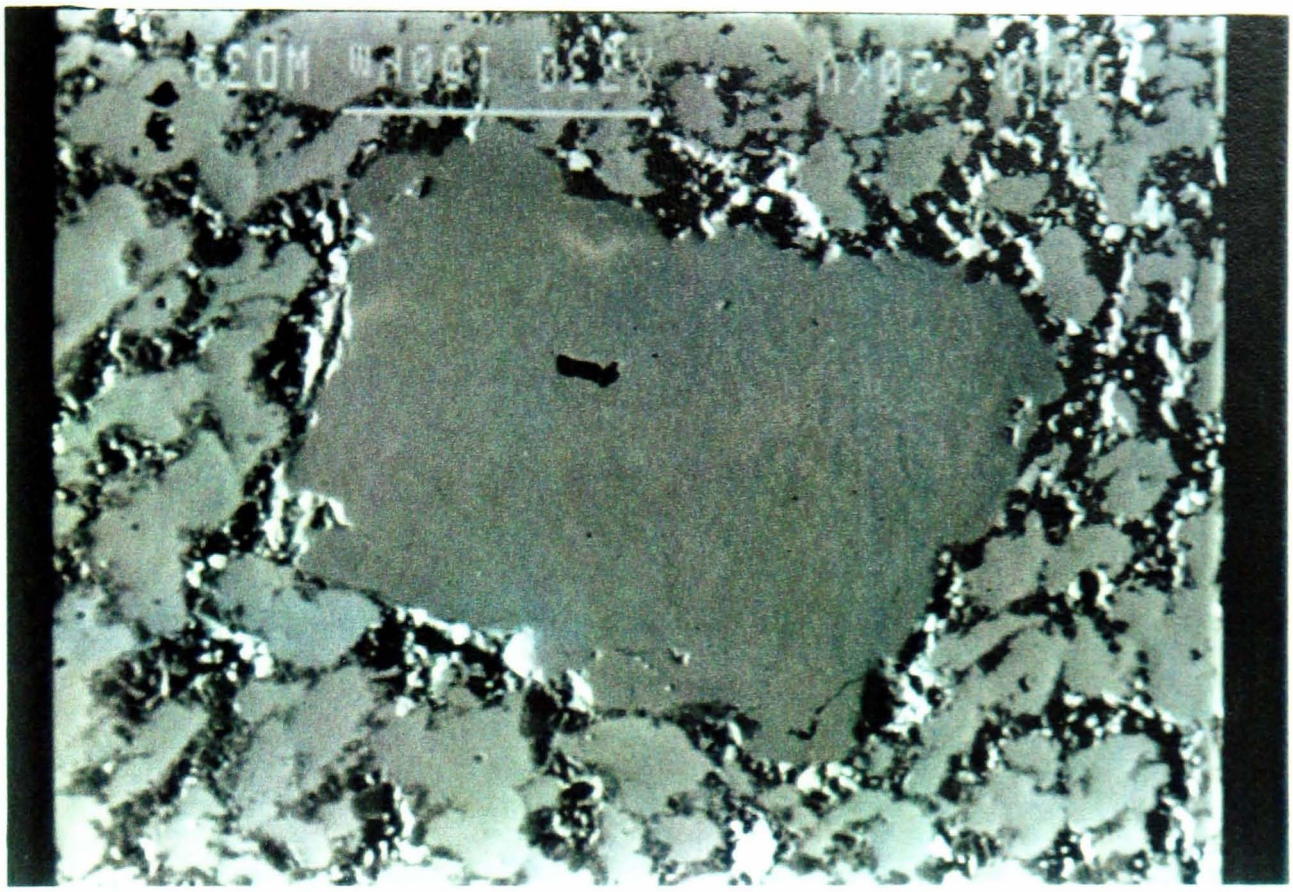

Figure 4.11 : SEM Micrograph of sample "7" illustrating entrapped large chromium particle .

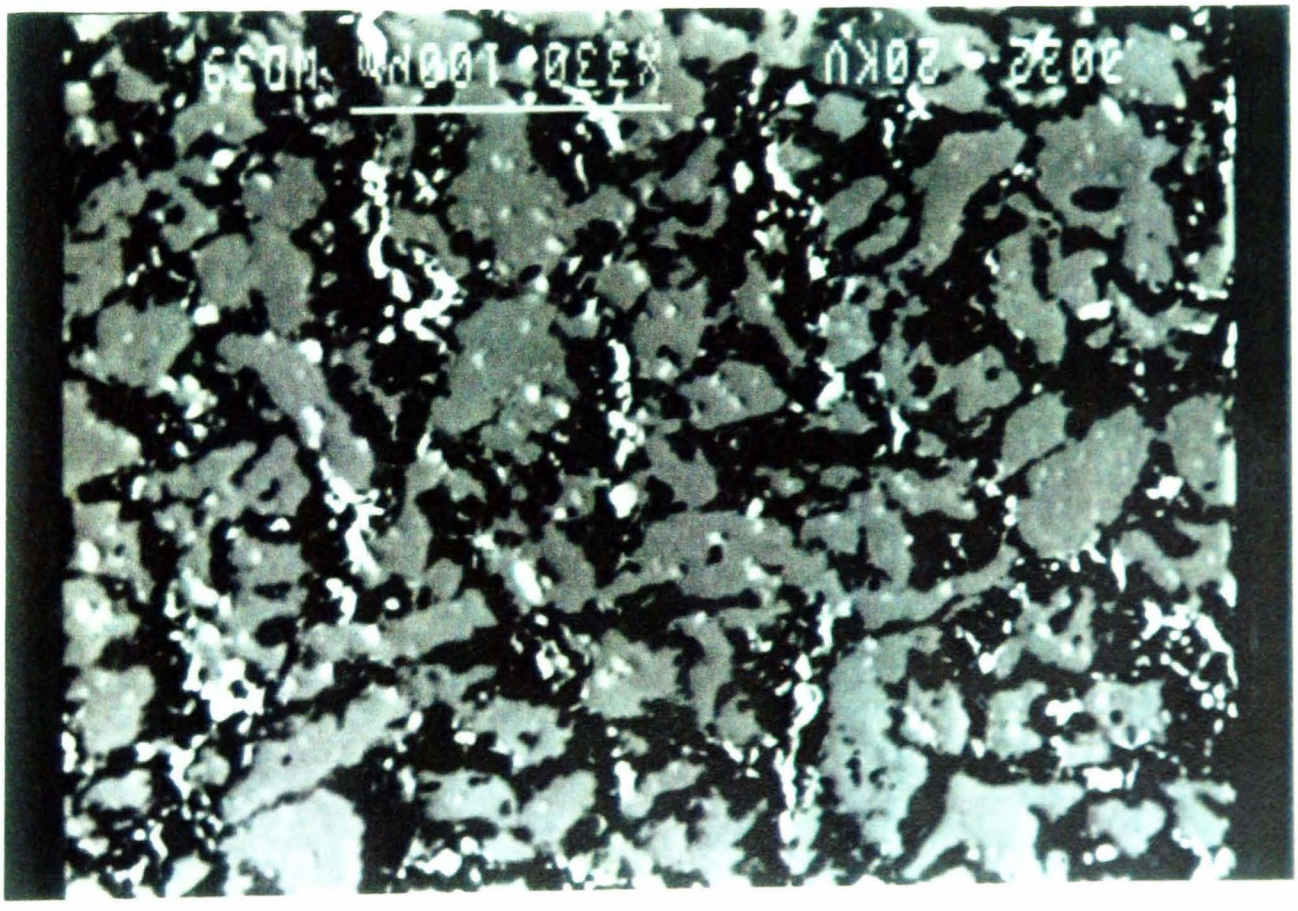

Figure 4.12 : SEM Micrograph of sample "8" illustrating particle distribution.

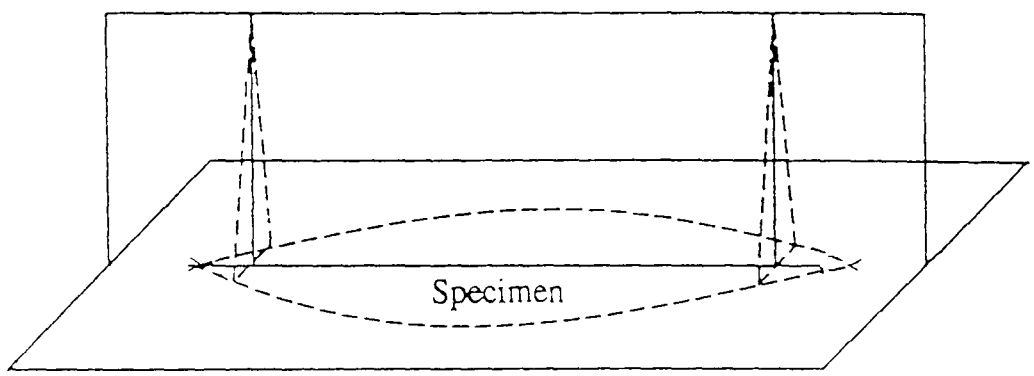

Figure 4.14 : Specimen Configuration for measurement of flexural frequency.

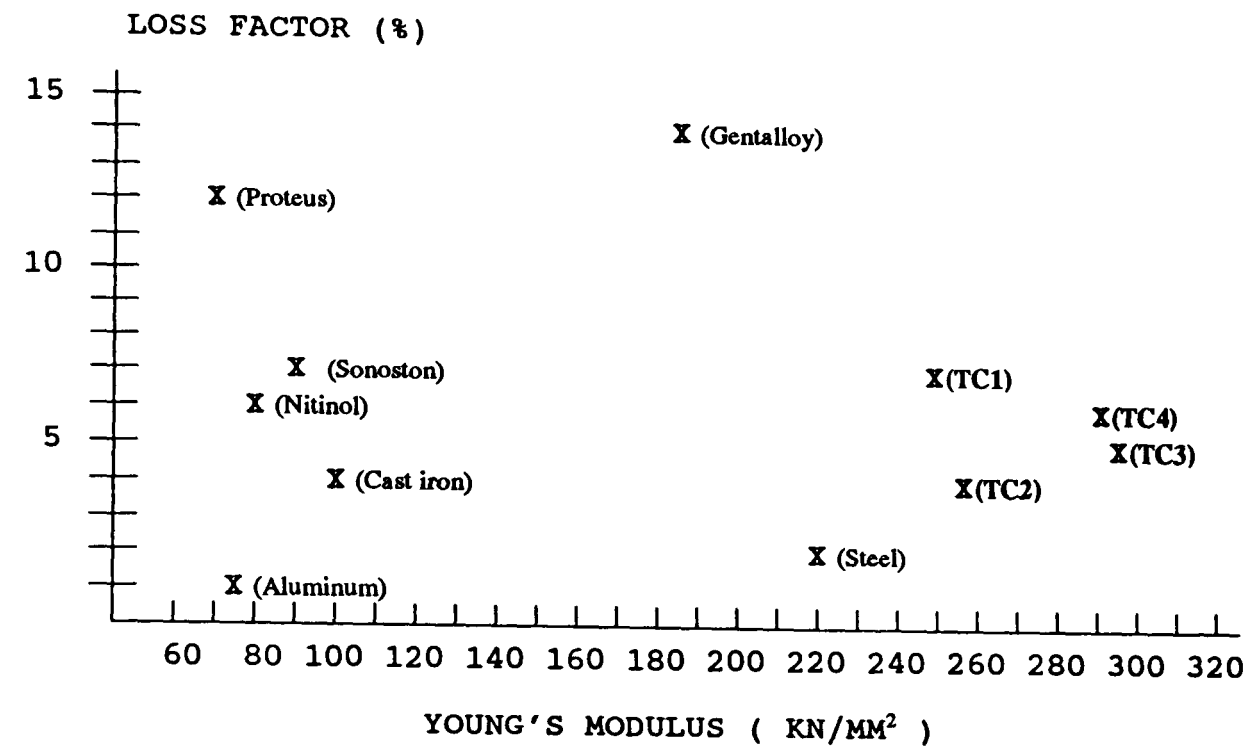

Figure 4.15 : Comparative Classification of high damping alloys with respect to Elastic Modulus.

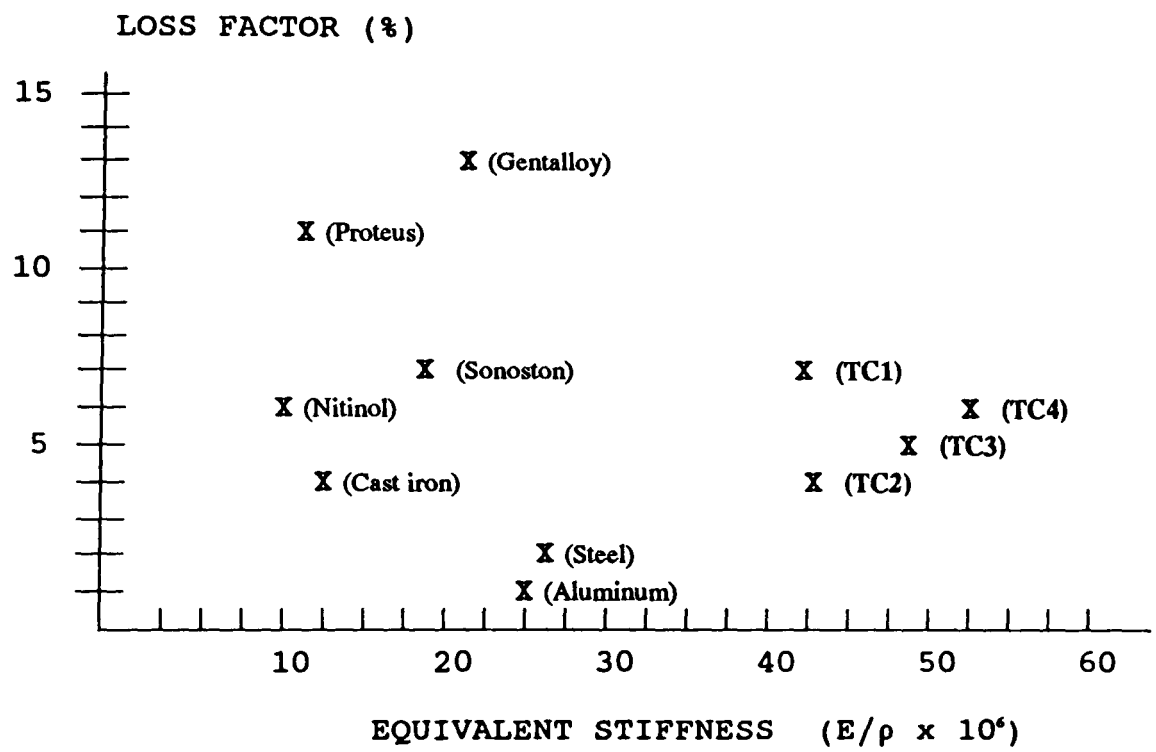

Figure 4.16 : Comparative Classification of high damping alloys with respect to Equivalent Stiffness E/ρ.

CHAPTER 5

5.0 EXPERIMENTAL PROCEDURE AND RESULTS

5.1 INTRODUCTION

In this study an assumption has been made that the random components of the surface profile could come from tool vibratory motion caused by random excitation. This random excitation in turn originates from the force variation caused by the non-homogeneous distribution of micro-hardness present in the workpiece material, or from chip breaking. The dynamic instability is further aggravated by the complex interaction of the cutting process and variation in tool geometry due to built up edge or undulation of surface quality of the tool. The boring bar structure responds to the change in the force applied on the cutting tool with a relative displacement between the tool and the workpiece. This displacement affects the values of the effective cutting angle, which in turn results in the further variation of the cutting force.

For the experimental procedure the dynamic compliance of the bar has been examined as a quality of attained finished boring, the surface finish of R_a = 3.00 μm was considered to be acceptable.

Finally ; the factorial design of experiments were not considered necessary since the most sensitive parameters that relate to the dynamic compliance of the tool was obvious.

5.2 EXPERIMENTAL INVESTIGATION

In chapter two, it was demonstrated that the roughness of the machined surface is a result of superposition of a random profile caused by the relative vibrations between the cutting edge and the workpiece. The surface topography observed after machining with a single-point tool originates from two parts of tool motion. The first part is the geometrical tool motion and the second part is the tool vibration about its dynamic equilibrium position (5.2).

The geometrical tool motion is deterministic in nature. In a turning operation, the motion can be described (5.3), as a spiral trajectory in space as shown in Figure 5.1. The three dimensions in Figure 5.1 represent the direction related to feed, cutting speed, and depth of cut. If the assumed tool vibratory motion is superimposed on the dynamic equilibrium position during machining this will lead to formation of the surface topography (as shown in Figure 5.2), that is normally observed in practice. This indicates that the tool vibratory motion may be studied through observations of the surface produced during machining.

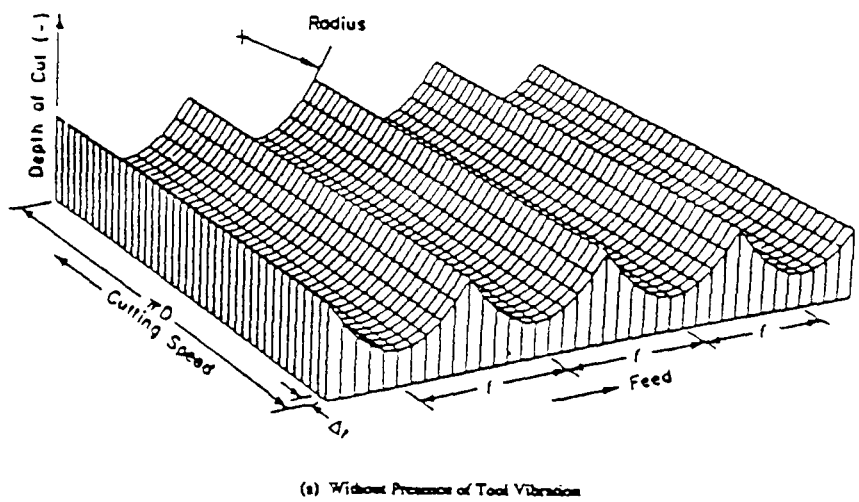

(a) Without Presence of Tool Vibration

Figure 5.1: Surface Topographies assumed to be generated during machining (without presence of tool vibration). (5.3)

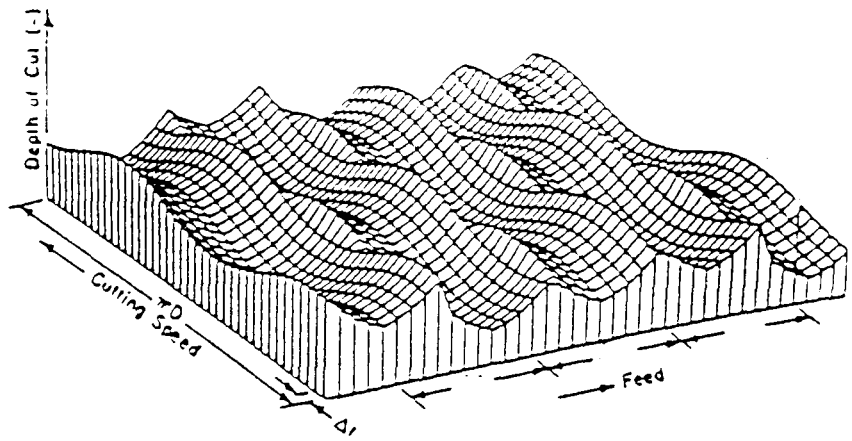

(b) Tool Vibration Motion $3 * \sin 50 t$ (μm) Assumed

Figure 5.2: Surface Topographies with assumed tool vibratory motion superimposed on the dynamic equilibrium mosition during machining.

5.3 PRECISION OF EXPERIMENTAL INVESTIGATION

Taking a profile trace on an internal surface such as a bored hole is difficult. The accuracy of the obtained measurements requires skilful inspection so a number of traces at various locations are taken to insure a reliable mean. There are also concerns due to the radial stresses applied by the chuck due to the reduced stiffness at the free end of the cantilever workpiece.

The design of a stable boring bar also requires a stiff clamping system so that the frequency of the vibrating tool does not coincide with the frequency of the clamping system. To fulfil this condition an adjustable stiff modular clamping mechanism detailed in section 3.9.1, was used to clamp the boring bar in the tool post.

The experimental tests were conducted to evaluate the effectiveness of the present approach in design compared to that of the conventional and tuned damper (Sandvic TNS bar) tools.

For the accuracy of experimental results, a total of three surface profile traces at various locations (approximately 120° apart) were obtained for each set of machined surfaces.

To ensure the accuracy of measurements, surface traces were taken towards the middle of the workpiece. A few pilot tests were carried out in order to get an appreciation of the extent of the machining chatter problems. This was used to select the specific cutting parameters (Cutting speed, feed rate, depth of cut and length to diameter ratio) required for observations of the dynamic qualities of the tool on the workpiece.

Using the selected experimental conditions, the dynamic quality of the workpiece was taken as a measure of the freshly cut surface using a portable stylus instrument (Surtronic 3).

To ensure consistency of the produced data the effect of excessive tool wear or built up edge had to be minimised. Therefore, all machining operations were performed with a new tip for a given cutting condition. Tables 5.1 to 5.12, tabulates the average R_a values measured in respect to variation of the machining conditions.

Three types of boring bars were tested. The selection was based on their corresponding geometrical configuration. The designed composite tools were analyzed and compared to those of Sandvic TNS tuned bars and conventional steel tool.

Tests were always repeated on the occurrence of abnormal or unpredictable results due to tool failure or chip jamming.

For every variation of length ratio or where characteristic chatter marks were present a rough cut was conducted. This was to eliminate the eccentricity between the tool and the workpiece as a result of diverse static deflection and to cut off any irregular shape in the bore of the workpiece.

5.4 CUTTING CONDITIONS

Single point boring tests were performed for length to diameter ratio's 5, 7, 9, and 11 with surface cutting speeds at the tool engaging point of 100, 135, 170, 210, and 250 m/min. The selected feed rates were 0.071, 0.09, 0.125, 0.17 mm/rev and depth of cuts used were 0.25, 0.5, 0.75, 1.00, 1.5, and 2 mm.

The effect of wear rate on the obtained results was minimised by employing a new cutting edge for each set of test run.

5.5 TOOL MATERIAL AND GEOMETRY

The indexable insert tool tip employed was a coated ceramic carbide material of ISO designation CCMM 09T304-270 P15/K15, supplied by SECO TOOLS Ltd. The inserts were 4 mm thick with a nose radius of 0.4 mm, and approach angle 90°. For boring operations the inserts were clamped in the tool holder via a clamping screw maintaining the following tool angles.

Approach angle	..... 90°
Back Rake	.....-15°
End Relief	..... 15°
Side Cutting Edge	..... 15°
Side Relief	..... 5°

5.6 WORKPIECE MATERIALS AND GEOMETRIES

The machined samples for the cutting tests were EN8 medium carbon steel. The workpieces were made from the same bar and the outer 5 mm of the bar stock as supplied was removed before workpieces were made. The bar was sectioned into three samples of 150 mm long and 200 mm outer diameter. The bars were then drilled through and bored to 60 mm internal diameter to accommodate the tool. To avoid excessive damage on

entry to the cut a chamfer was machined on the outer edge of the bored work material. This process provided a condition where the whole length of the cutting edge could be engaged simultaneously at the initiation of the cut.

The clamping force of the chuck and the clamping device of the boring bars were fixed by the torque wrench to give the same value at every experiment. In order to avoid any eccentricity between the workpiece and the cutting tool surface measurements were performed after the workpiece was machined without un-clamping the workpiece or the tool. The chatter initiation was detected by the an audible load noise and measured as a function of the quality of surface finish.

5.7 CUTTING TESTS

Experimental procedure for the conventional and designed tools was confined to a simple internal turning operation (boring). This required the design of fixtures illustrated in Figure 3.20, for setting up the test rig. All groups of tests used a stationary boring bar clamped on the fixture positioned on the tool post of the lathe.

Cutting tests were to represent finish boring and a surface finish equivalent to R_a = 3.00 μm was considered acceptable as a measure of attained machining qualities.

The geometry of the composite boring bars was 650 mm long and 50 mm in diameter, thus allowing a length to diameter (L/D) ratio of up to 11 times the diameter .

The tests were conducted on a Boehringer DM 640 centre lathe. This lathe had a variable feed selector ranging from 0.05 to 1.8 mm/rev., and the speed selection ranging from 5 to 2500 rpm. Simple cutting tests were preformed, so that for a given length to diameter ratio of a tool, the respective variation of feed, depth of cut and speed could be examined.

Boring was performed in both dry and wet conditions. The coolant used was a general purpose mineral soluble oil hysol G, and a flow rate of 3.75 lit/min. The observations from the pre-qualifying machining indicated no significant variations of results in machining with coolant, therefore, further experiments were performed in dry conditions.

Although the cutting inserts were provided with chip breaking facility, often at speeds of above 170 m/min the problem due to chip jamming would result in severe deterioration of surface roughness.

This is regarded as a common problem of the boring operation at high speed. Due to the inherent nature of the internal cutting process, the chips are produced towards the workpiece rather than away from it. This problem was overcome by removing the chips by the application of high pressure air inside the bored hole during machining.

The designed composite tool holders were made of three different sections allowing tests for different configurations in design. The base of the tool that would be constrained by the clamping unit was made of mild steel of grade EN8. The body or the middle portion where it was necessary to provide maximum possible equivalent stiffness was constructed of steel tube of 50 mm outer diameter and 38 mm inner diameter inserted with a TC4 composite bung at the fixed end with a shrunk-on fit. The front of the boring bar was fabricated from steel and aluminium to allow a combination of design alteration.

The combination of the design configurations of the fabricated tool were ;

Tool I) Fabricated tool with steel head.

Tool II) Fabricated tool with Aluminium head.

Tool III) Fabricated tool with aluminium head and Aluminium constrained layer damping.

The result from three different design configuration adapted on the fabricated tool were used for comparative analyses of attained machining qualities.

Measurements of tool tip vibrations are difficult for internal turning operations. Some of the problems associated with vibration measurements of the boring bar may be summarised as;

1- Direct measured vibrations have to be made away from the tool tip, resulting in much smaller measured amplitudes compared to those at the tool tip.

2- Possible error due to interpretation of base amplitudes.

3- Analyses of vibration measurements may not reveal the direct effect of tool vibration at the cutting edge due to damping errors initiated by the supporting apparatus.

Therefore, evaluation of the maximum amplitude of tool tip vibration was based on the quality of the finished workpiece. A SURTRONIC 3, was used to measure the average surface roughness (R_a) value. The mobility of this instrument eliminates the need for dismantling the workpiece from the chuck of the lathe.

To ensure consistent accuracy the instrument was calibrated prior to each measurement. Subsequently the moving stylus was positioned on the surface to be measured, perpendicular to the feed marks. Each surface was measured three times at different locations approximately 120° apart and then the average value was determined for further analysis.

5.8 PRIMARY EXPERIMENTAL OBSERVATIONS

The primary experiments provided the recognition of imposed limitations and the determination of the effects of machining variables for the onset of chatter. This was carried out through the systematic variation of the cutting parameters to observe parameters (such as overhang ratio, cutting speed and feed) that may have a profound effect on stabilizing the process.

5.9 EXPERIMENTAL RESULTS AND ANALYSES

In order to assess the dynamic rigidity of the tool holders during actual cutting a number of tests were made under the set up and cutting conditions mentioned above. Stability diagrams on the variation of depth of cut, length to diameter ratio, cutting feed rate and speed with respect to the quality of the finished workpiece were obtained for five types of tool holders.

5.9.1 VARIATION OF SURFACE ROUGHNESS WITH RESPECT TO CUTTING SPEED AND LENGTH TO DIAMETER RATIO.

In the case of the steel tool holder (Figure 5.4) although some marginal improvements of the surface roughness may be observed with increasing speed; the larger the L/D ratio the more unstable the tool is. This is because of the low damping capacity and low static stiffness of steel tool holder. The result also indicates that for finish boring the length of the tool would be unsuitable above four times the diameter without supporting elements.

In the case of a Sandvic TNS tool holder, Figure 5.5, the bar is provided with a vibration absorber. The absorber utilises the applied force input from the cutting edge to activate the damping mechanism. This tool exhibits a marked improvement on the amplitude of vibrations reflected on the surface of the workpiece. From Figure 5.5, it can be seen that up to L/D ratio equal to 9, (the stable zone for R_a = 3 μm) the tool holder on average operates 97% more efficiently than conventional steel tool. For L/D ratio equal to 11 this tool may be regarded as unstable. The inconsistent results are assumed to be due to exceeding the stability limit of the tool holder.

In the case of the combination tool holder (Tool I) Figure 5.6, up to L/D ratio equal to 9, the tool may be regarded as stable for all

examined cutting speeds. However, at L/D ratio = 11 judging from the slope of the graph the predicted qualifying stability region is expected to be at speeds of above 250 m/min.

The analysis in chapter eight, shows that the obtained natural frequency of the first mode of vibration for this tool is only 11% greater than that for conventional steel tool. The average quality of the surface roughness with respect to variation in cutting speed is 124% better than conventional steel tool. This is as a result of 42% improvement of the equivalent stiffness. Owing to an effective expansion of the coinciding frequencies of Tool II Figure 5.7 shows an improvement of 12%, on the quality of surface roughness.

From the observations of data in Table's 5.2 to 5.5 and Figure 5.8 (Tool III) it can be deduced that the effect of additional damping increases with L/D ratio and cutting speed. This is believed to be due to the properties of the high damping material: the smaller the strain, the lower the damping capacity. This result may also be traced to the effect of process damping associated with cutting speeds detailed in section 2.10.

The margins of improvement on the quality of the finished workpiece for this tool with respect to the undamped Tool II, at L/D ratio's of 7, 9 and 11 and speed of 250 m/s are found to be 1 %, 3 % and 9 % respectively.

5.9.2 VARIATION OF SURFACE ROUGHNESS WITH RESPECT TO DEPTH OF CUT AND LENGTH TO DIAMETER RATIO.

The stability diagram shown in Figure's 5.10 to 5.15, illustrates that the surface roughness, as an indicator of the amplitude of vibration, increases almost linearly with the depth of cut.

Assuming the quality of the stability boundary for R_a = 3 μm to be acceptable. From Figure 5.10, it can be observed that the steel tool

may be expected to operate within the specified limit at L/D = 5, for a depth of cut equal to 0.5 mm. Increasing the L/D ratio to 7, would result in reducing the depth of cut to 0.25 mm, and at L/D = 9 or 11 this tool may not be considered a viable option for finish boring. Obviously the reduction of metal removal rate has a direct influence on the lack of dynamic stiffness inherent in such tools.

In the case of Sandvic TNS tool holder, Figure 5.11, as with conventional steel tool, the larger the depth of cut the more unstable the tool. Although the static stiffness and the dynamic rigidity of the Sandvic tool is much the same as the conventional steel tool nevertheless, the dynamic vibration absorber within the tool is designed such that it will initiate a damping component under dynamic disturbance. From Figure 5.11, it can be seen that for the given machining variables this tool may be regarded as stable for up to L/D ratio of 7, for all the depth of cut examined. For L/D ratio's of 9 and 11 the prime depth of cut expected for stable cutting would be 1.0 mm and 0.5 mm respectively.

The combination boring bar Tool I, Figure 5.12, illustrates a distinct improvement with respect to the conventional steel tool holder. It is also a marginally finer quality of finished workpiece to that of tuned TNS bar.

Tool I, may generally be regarded to perform stable cutting with L/D ratio equal to 9 for all examined depth of cut variation. However, at L/D ratio = 11 and depth of cut above 0.75 mm some characteristic vibration deviations on the surface could be observed. From Table 5.9, a deterioration of nearly 123% on the quality of surface roughness between the initial test results and the final set of cut was observed. This is assumed to be due to the operating frequency of the machining process harmonising near the fundamental frequency of the tool holder.

In order to overcome this problem the effective steel mass of the front section of the tool was replaced with aluminium. Tool II, has resulted in a 27% improvement of the fundamental frequency. The

deviations on the finished workpiece were reduced from 123% to 85%, ie, a further 38% improvement on the quality of measured roughness value.

From the observations of Figure 5.15, it can also be concluded that the effect of additional damping increases with L/D ratio as well as increase in depth of cut. This also shows that the maximum allowable depth of cut for L/D Ratio equal to 11 would be 1.5 mm for Tool III. This is reduced to 1.00 mm for Tool II. Tool I may only be expected to operate at 0.25 mm for the same specification.

5.9.3 VARIATION OF SURFACE ROUGHNESS WITH RESPECT TO CUTTING FEED RATE AND L/D RATIO.

The performance diagram in Figures 5.16 to 5.21 indicates that the amplitude of vibrations increases almost linearly with cutting feed rate. It can be seen that the steel tool may not be expected to operate effectively at an L/D ratio of above 5 for even the lowest feed rate.

For the given machining variables Figure 5.17 shows that the Sandvic TNS tool holder may be regarded as stable for up to L/D = 7 for all the examined cutting feed rates. Furthermore although at above L/D = 9, this tool may be regarded as having exceeded the designed limit of stability an interesting demonstration of improved surface quality at L/D ratio of 11 and feed rate above 0.125 represents the dependence of the damping mechanism to the tuning of local optimum frequency. Figures 5.18, 5.19, and 5.20, represent the performance characteristics of Tool I, II, and III, with respect to variation of cutting feed rate and L/D ratio. Tool I and II may be expected to perform stable cutting for L/D = 9 and feed rates of up to 0.125. However, for feed rate of 0.17 and at L/D ratio above 9 the characteristic vibration deviations reflected on the finished workpiece surface exceed the required quality.

From Table 5.13, the deterioration of nearly 33% for Tool I and

42% for Tool II on the quality of surface roughness for the initial test results and the final set of cut are observed. This is can be attributed to the lack of effective damping and equivalent stiffness. This presumption was based on the degeneration in the quality of surface finish with increase of the fundamental natural frequency. This assumption may be verified from the observations of data in Tables 5.13 and Figure 5.21 (Tool III). The results indicate that additional damping not only increases with L/D ratio and cutting feed rate but also causes a 17% increase on the quality of measured roughness value. This fact corroborates the significance of the damping capacity.

5.10 COMPARATIVE ANALYSIS AND DISCUSSION.

The comparative stability performance in Table 5.1, as an indicator of the maximum amplitude of vibration, exhibits the variation of surface roughness, with L/D ratio.

From Figure 5.3, it can be seen that the steel tool holder does not qualify to be a viable option for the selected parameters with a length to diameter (L/D) ratio of 5. However, under the same cutting conditions the Sandvic TNS bar operates safely at its optimum tuning frequency for up to L/D ratio equal to 7. Moreover, the combination boring bars (Tool I) may operate under this limit for up to 9 times L/D ratio.

By changing the tool head of the combination boring bar from steel to aluminium, the natural frequency of the vibrating bar is increased. This eliminates the large amplitude response at resonance, if the limit of the operating frequency is less than the fundamental natural frequency of the bar. This effect is analyzed in chapter eight, (Table 8.17). The design variation influences the first mode of vibration which was increased from 111 Hz to 141 Hz. The result examined by comparative observation of Tool I, and Tool II at L/D = 11

(Table 5.1), indicates a 19% attained improvement of surface quality. These results vindicate the assumption made in the theoretical model.

Improving the damping quality of the combination boring bar (Tool II), through constrained layer damping (Tool III), would result in the absorption of a portion of the strain energies. This also results in lower amplitude responses with subsequent improvement of the surface roughness.

This method of damping lends itself most effectively, by its very nature, to systems with thin sections. However, from the observations of the results of Figure 5.3, (Tool III), an average improvement of about 7 % on quality of surface roughness may be observed.

Conclusively, It would be misleading to assume that Figure 5.3, may be used as a universal indicator of performance index. Variation of the cutting parameters may significantly alter the stability performance. Therefore, in providing a more acceptable performance index, further examination of the results with respect to evaluation of combined interaction of the machining parameters and structural response are required. The analyses in the subsequent sections aim to fulfil this objective.

5.10.1 COMPARATIVE STABILITY PERFORMANCE WITH RESPECT TO VARIATION OF CUTTING SPEED AND L/D RATIO.

From the primary experimental observations it can be predicted that as the cutting speed increases there is a marginal decrease in the chatter amplitude. This is assumed to be associated with the decrease in the cutting force. The reduction of cutting force is a result of softening and the damping effect due to increased temperature around the locality of the heat effected zone of the cutting edge on the workpiece. This result may also be traced to the effect of process damping associated with cutting speed, detailed in section 2.10.

The sensitivity of Tool II on the quality of workpiece was considered to be due to the coinciding frequency of cutting process with that of the resonance frequency of the tool holder. This principle was examined by comparative examination of Tool I, and Tool II, in Figure 5.9. This figure also signifies that the effect of additional damping increases with an increase in the cutting speed and the L/D ratio. To substantiate this effect the variation on the quality of the finished workpiece produced by Tool III to that of Tool II were estimated. These results indicated that at L/D ratio's of 7, 9 and 11 the growth of strain energy resulted in an increase of the quality of the finished workpiece by respective factors of 5, 9 and 11 % .

5.10.2 COMPARATIVE STABILITY PERFORMANCE WITH RESPECT TO VARIATION OF DEPTH OF CUT AND L/D RATIO.

Since the surface finish and the metal removal rate depend largely on the dynamic stiffness of the tool useful information about the dynamic stiffness can be obtained by varying the depth of cut in metal cutting tests. To validate the effectiveness of the fabricated tools the stability performance of individual holders was obtained.

The depth of cut also determines the limit of strain energies. Therefore, the effect of additional damping increases with L/D ratio and depth of cut. The performance variation of Tool II and Tool III with respect to depth of cut and L/D ratio is illustrated in the table 5a, below.

Table 5a : performance variation of Tool II and Tool III with respect to depth of cut and L/D ratio

	L/D RATIO 5	7	9	11	DEPTH OF CUT
PERCENT PERFORMANCE VARIATION TOOL II Vs. TOOL III	4.28	4.9	6.1	6.96	0.25
	-0.8	-1.58	1.24	6.85	0.50
	5.9	1.07	9.63	10.86	1.00
	6.84	1.90	11.23	14.23	1.50
	8.39	2.64	8.72	11.17	2.00

Although the variations in surface roughness are not all inconsistent with the expected increase at higher strains, the general trend on the available results support the fact that as the strain level rises either due to L/D ratio or depth of cut a higher damping capacity of the overall system results.

The quality of the finished workpiece may be regarded as a function of the combination of feed, depth of cut, speed, and tool geometry. The typical performance characteristics for the combination boring bar's Tool I, II, and III are plotted in Figure's 5.24 to 5.26. From these diagrams the stability criterion for selecting the maximum allowable depth of cut for a given L/D Ratio may be estimated to suit the required application. Figure 5.26, Tool III, also shows that the maximum allowable depth of cut for a L/D Ratio equal to 11, would be; 1.5 mm. This is reduced to 1.00 mm for Tool II, (Figure 5.25), and Tool I, may only be expected to operate at 0.25 mm for an acceptable quality of surface finish.

5.10.3 COMPARATIVE STABILITY PERFORMANCE WITH RESPECT TO VARIATION OF FEED RATE AND L/D RATIO.

One of the most important and informative test performed was that of the cutting rate variation. The study of increased feed rate due to enhanced stiffness and damping should demonstrate the process stability with respect to metal removal rate.

Each tool has to be examined individually under common machining conditions. The following assessment aims to characterize the stability performance with respect to feed rate variation.

From Figure 5.16 and 5.10, it can be observed that the surface roughness, as an indicator of the amplitude of vibration, increases almost linearly with the depth of cut and cutting feed rate. Moreover, the depth of cut has a greater effect on the chatter amplitude than the cutting feed rate as is evident from the respective slopes in Figure 5.16 and 5.10.

In the case of Sandvic TNS tool holder, Figure 5.17, as with conventional steel tool, the larger the feed or L/D ratio, the more unstable is the tool. However, the construction of a damped vibration absorber prevents the presence of large amplitude vibrations.

The comparative performance of the steel tool and TNS bar from Table 5.13 and Figure 5.21 shows that the variation in cutting feed rate from 0.071 to 0.17 results in an increase in the quality of surface finish from 81% to 121 %. This observation signifies that the system responses are strain dependent and will rise with an increase in the cutting force.

Results presented in Table's 5.10 to 5.13, and Figure's 5.18 to 5.21, indicate an overall improvement in the stability of the cutting process through the combination design of the tool holders. However, with the stability limit set at Ra = 3 μm, Tool I and II, may only be expected to perform stable cutting for up to L/D = 9, and feed rates of up to 0.125. Moreover, for feed rate of 0.17 and at L/D ratio above 9,

the characteristic vibration deviations reflected in the finished workpiece exceed the required quality.

The deterioration of nearly 33% for Tool I and 42% for Tool II between the initial test results and the final set of cut are attributed to lack of effective damping and equivalent stiffness. This presumption was based on degeneration in the quality of surface finish with increase of the fundamental natural frequency. This conclusion may also be verified from the observations of data in Table's 5.13 and Figure 5.21 (Tool III). A 17% increase on the quality of measured roughness value corroborate the significance of the damping capacity.

From Figure 5.21, it can be seen that at L/D = 11 Tool III may perform with an expected accuracy of Ra less than 4 μm, for all cutting feed rates examined. The margin of improvement in the quality of the finished workpiece for this tool with respect to the undamped Tool II, are shown in the table 5b, below:

Table 5b : Comparative performance variation for tool II and III with respect to the cutting feed rate variation.

	L/D RATIO 5	7	9	11	CUTTING FEED RATE
PERCENT PERFORMANCE VARIATION TOOL II Vs. TOOL III	5.9	1.07	9.63	10.86	0.075
	3.31	10.19	9.79	12.89	0.090
	7.4	14.28	11.23	13.97	0.125
	9.39	12.72	12.81	16.89	0.17

The general trend of the results obtained also verifies the fact that the rise in strain level is either due to the L/D ratio or to the feed rate and results in a higher damping capacity of the overall system.

The variations in surface roughness are not all consistent with the expected increase at higher strains, so some erratic results should

not be regarded as unexpected.

conclusively, the stability performance in Figures 5.3, 5.9, 5.15 and 5.21 with respect to variation of cutting process parameters and L/D ratio, illustrates the dynamic rigidity, and limitations of the constructed design. The composite boring bar with aluminium head and aluminium constraint layer damping demonstrates the widest stable zone.

The influence of the discrete configuration parameters with respect to dynamic compliance of the tool holders is further analyzed in chapters 7 and 8.

CUTTING SPEED = 135 m/min
COMMAND FEED = 0.071 mm/Rev
DEPTH OF CUT = 1.00 mm
RAKE ANGLE = 15°
SIDE CUTTING EDGE = 15°

TEST No.	1	2	3	4
L/D RATIO VARIATION	5	7	9	11

MACHINING QUALITY	TEST No.	DeVlieg STEEL	SANDVIC TNS BAR	TOOL I	TOOL II	TOOL III
	1	4.20	2.83	2.12	1.61	1.52
SURFACE	2	4.91	3.20	2.42	1.89	1.87
ROUGHNESS	3	6.05	3.91	2.87	2.39	2.18
R_a (μm)	4	7.72	4.26	3.67	2.96	2.67

TABLE 5.1 : COMPARATIVE PERFORMANCE OF TOOLS WITH RESPECT TO VARIATION OF L/D RATIO

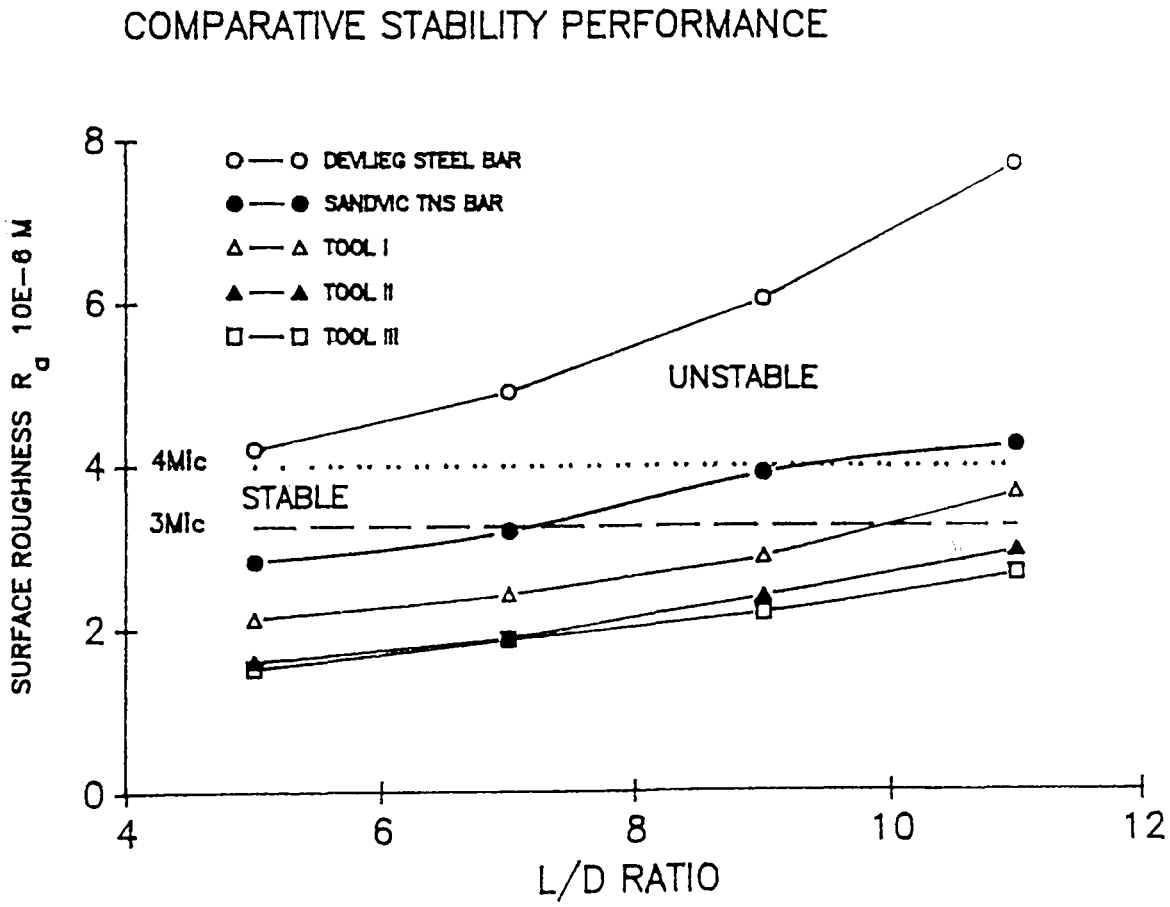

FIGURE 5.3 : L/D VARIATION OF EXAMINED BORING BARS WITH RESPECT TO SURFACE ROUGHNESS.

CUTTING SPEED VARIATION :
DEPTH OF CUT = 1.00 mm
COMMAND FEED = 0.071 mm/Rev

L/D RATIO = 5;

TEST No.	1	2	3	4	5
CUTTING SPEED VARIATION.(m/s)	100,	135	170	210	250

MACHINING QUALITY	TEST No.	DeVlieg STEEL	SANDVIC TNS BAR	TOOL I	TOOL II	TOOL III
	1	4.17	2.94	2.30	1.61	1.61
SURFACE	2	4.20	2.83	2.12	1.61	1.52
ROUGHNESS	3	4.13	2.85	2.09	1.49	1.47
R_a (μm)	4	4.06	2.79	1.99	1.41	1.44
	5	4.10	2.67	1.94	1.43	1.38

TABLE 5.2: COMPARATIVE PERFORMANCE OF TOOLS WITH RESPECT TO VARIATION CUTTING SPEED.

L/D RATIO = 7;

TEST No.	1	2	3	4	5
CUTTING SPEED VARIATION(m/s)	100	135	170	210	250

MACHINING QUALITY	TEST No.	DeVlieg STEEL	SANDVIC TNS BAR	TOOL I	TOOL II	TOOL III
	1	5.15	3.13	2.51	1.97	2.11
SURFACE	2	4.19	3.20	2.42	1.89	1.87
ROUGHNESS	3	5.03	3.02	2.39	1.87	1.95
R_a (μm)	4	4.88	2.77	2.38	1.91	2.01
	5	5.04	2.98	2.27	1.84	1.86

TABLE 5.3: COMPARATIVE PERFORMANCE OF TOOLS WITH RESPECT TO VARIATION CUTTING SPEED.

CUTTING SPEED VARIATION :
DEPTH OF CUT = 1.00 mm
COMMAND FEED = 0.071 mm/Rev

L/D RATIO = 9

TEST No.	1	2	3	4	5
CUTTING SPEED VARIATION(m/s)	100	135	170	210	250

MACHINING QUALITY	TEST No.	DeVlieg STEEL	SANDVIC TNS BAR	TOOL I	TOOL II	TOOL III
	1	6.19	3.87	2.89	2.54	2.48
	2	6.05	3.91	2.87	2.39	2.18
SURFACE	3	6.11	3.73	3.02	2.31	2.26
ROUGHNESS	4	5.93	3.27	2.69	2.28	2.31
R_a (μm)	5	6.10	3.41	2.84	2.36	2.29

TABLE 5.4: COMPARATIVE PERFORMANCE OF TOOLS WITH RESPECT TO VARIATION CUTTING SPEED.

L/D RATIO = 11

TEST No.	1	2	3	4	5
CUTTING SPEED VARIATION(m/s)	100	135	170	210	250

MACHINING QUALITY	TEST No.	DeVlieg STEEL	SANDVIC TNS BAR	TOOL I	TOOL II	TOOL III
	1	7.77	3.88	3.52	3.12	2.89
	2	7.72	4.26	3.67	2.96	2.67
SURFACE	3	7.64	4.12	3.44	3.07	2.73
ROUGHNESS	4	7.61	4.19	3.19	2.91	2.68
R_a (μm)	5	7.57	4.69	3.37	2.98	2.71

TABLE 5.5: COMPARATIVE PERFORMANCE OF TOOLS WITH RESPECT TO VARIATION CUTTING SPEED.

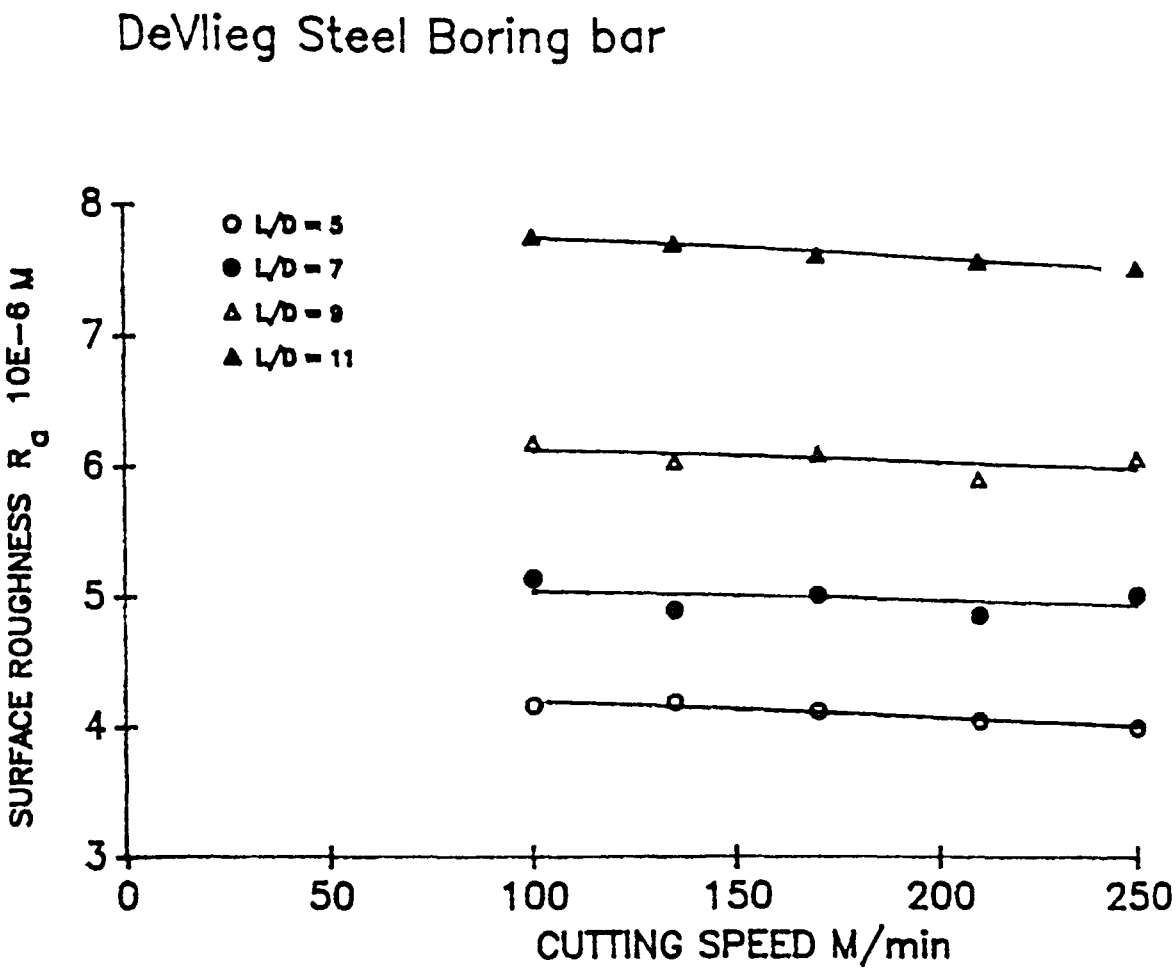

FIGURE 5.4 : VARIATION OF SURFACE ROUGHNESS WITH CUTTING SPEED AND L/D RATIO

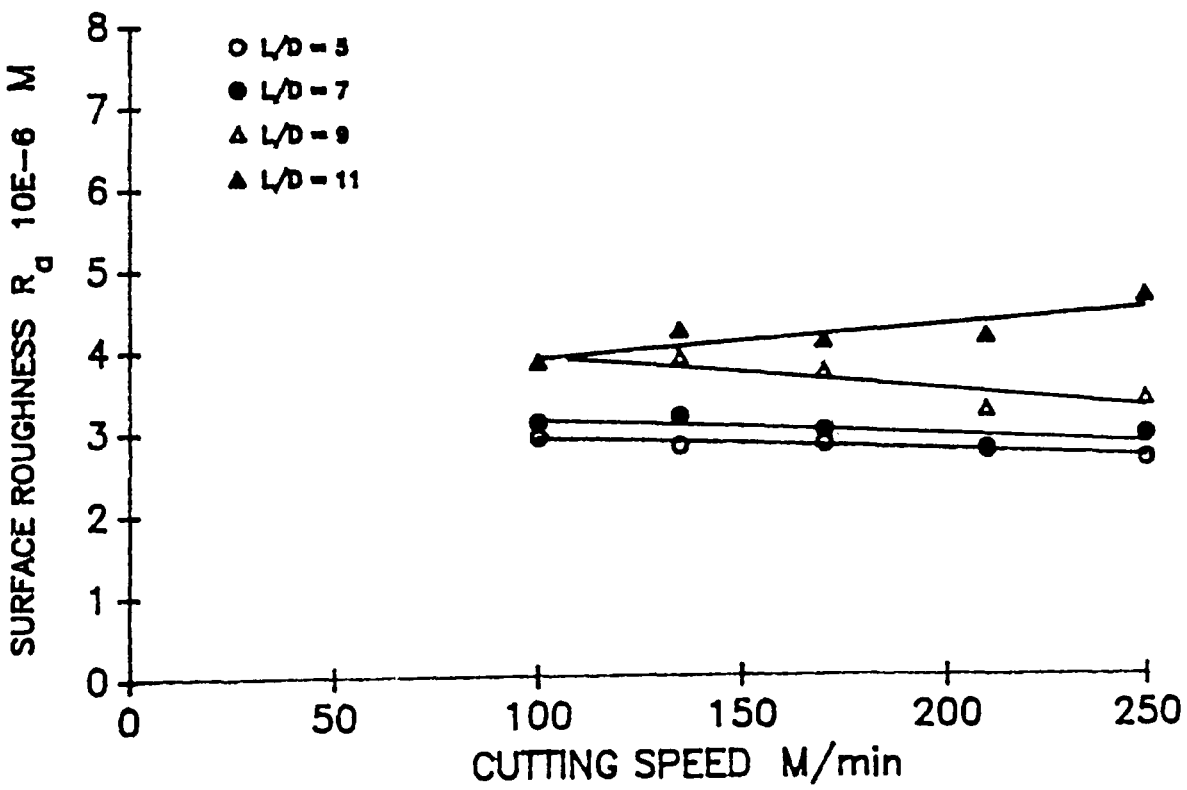

FIGURE 5.5 : VARIATION OF SURFACE ROUGHNESS WITH CUTTING SPEED AND L/D RATIO

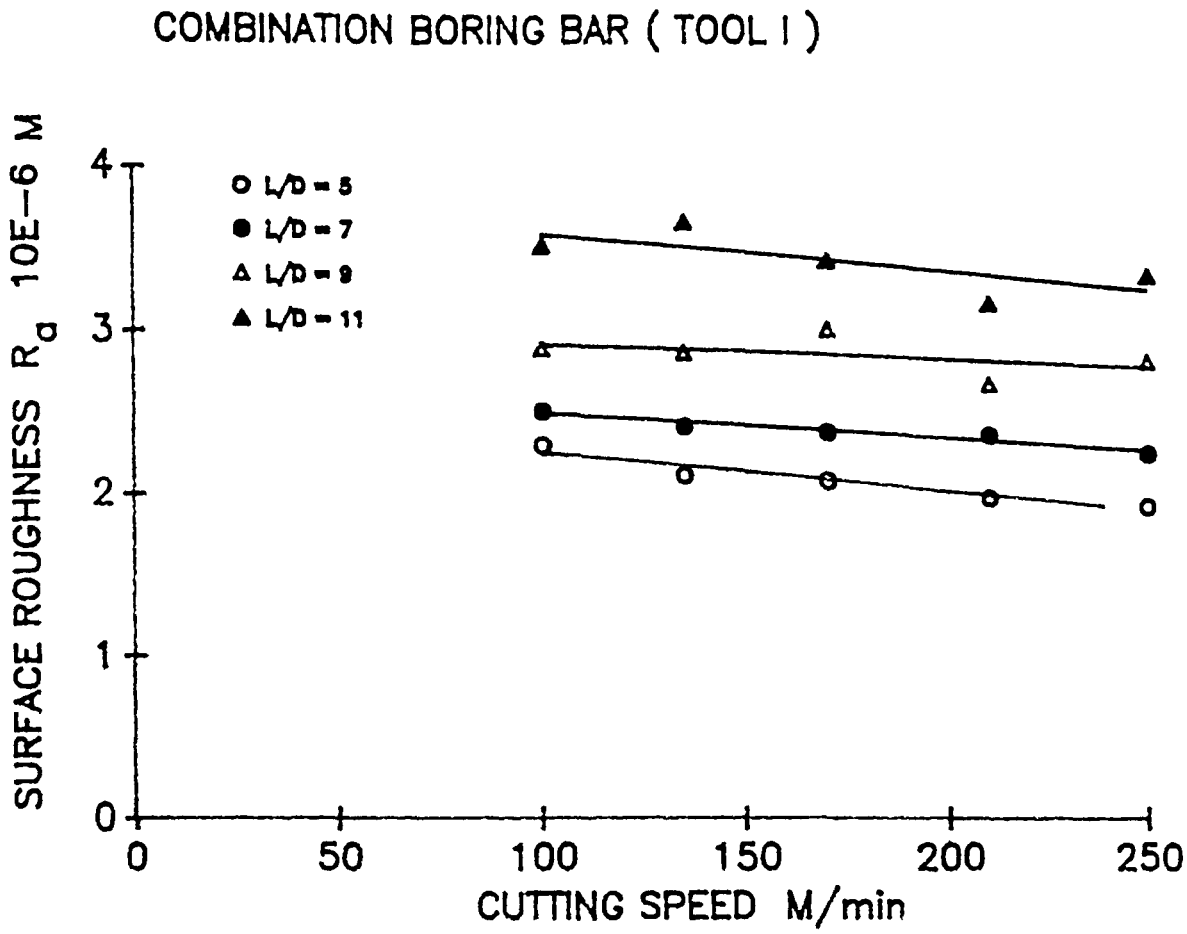

FIGURE 5.6 : VARIATION OF SURFACE ROUGHNESS WITH CUTTING SPEED AND L/D RATO

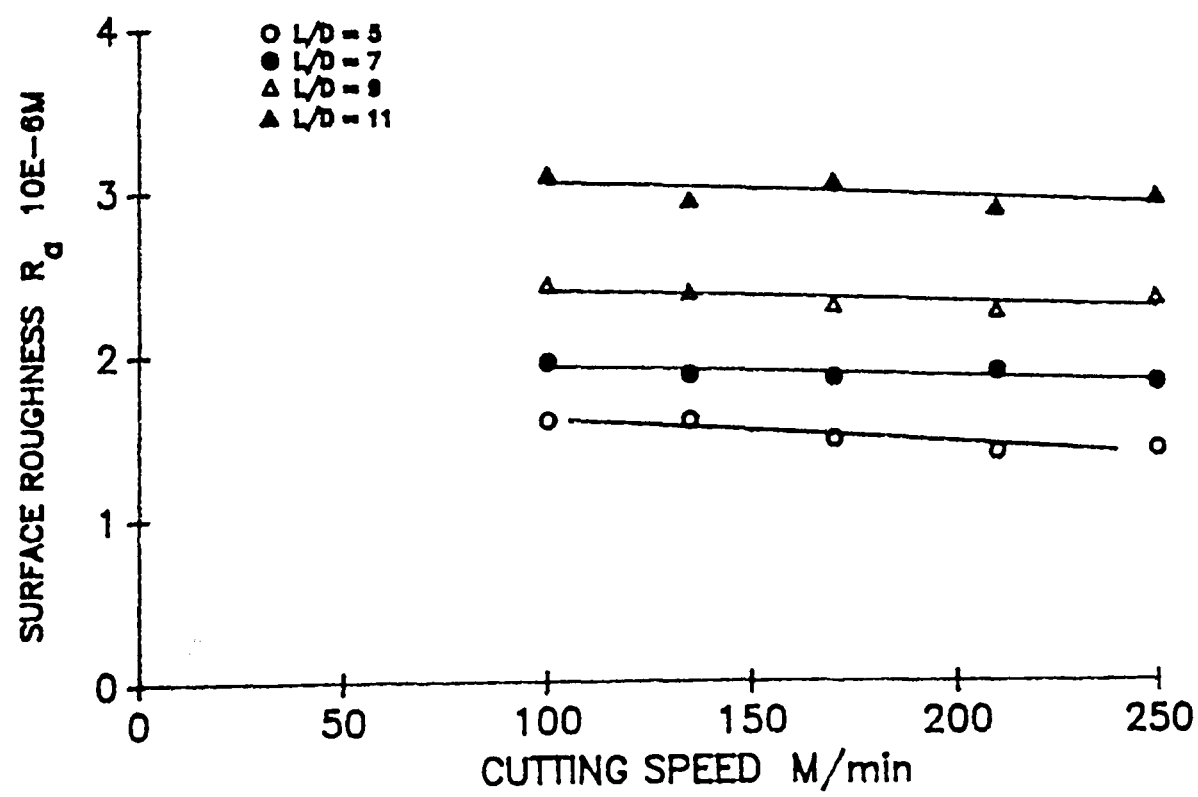

FIGURE 5.7 : VARIATION OF SURFACE ROUGHNESS WITH CUTTING SPEED AND L/D RATIO

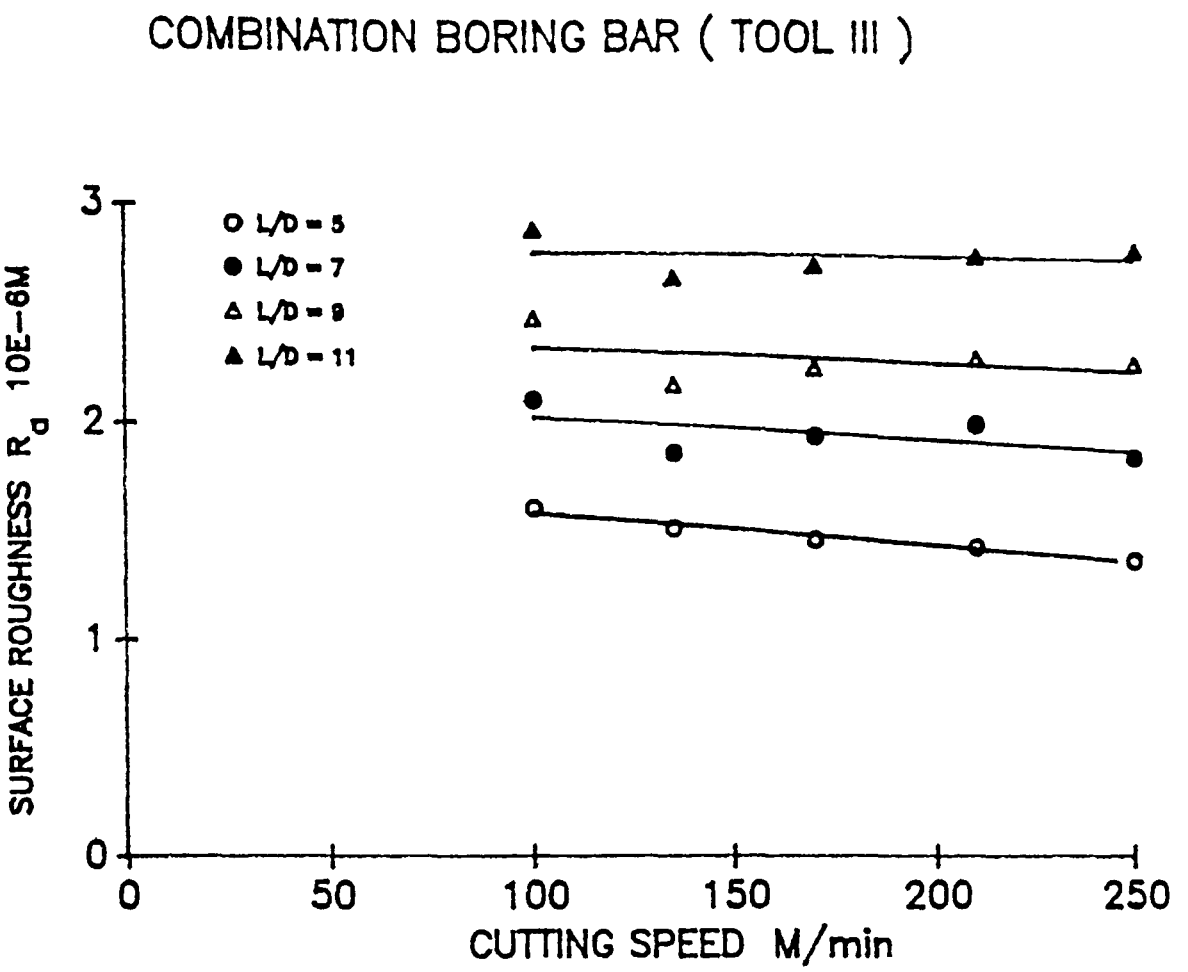

FIGURE 5.8 : VARIATION OF SURFACE ROUGHNESS WITH CUTTING SPEED AND L/D RATIO

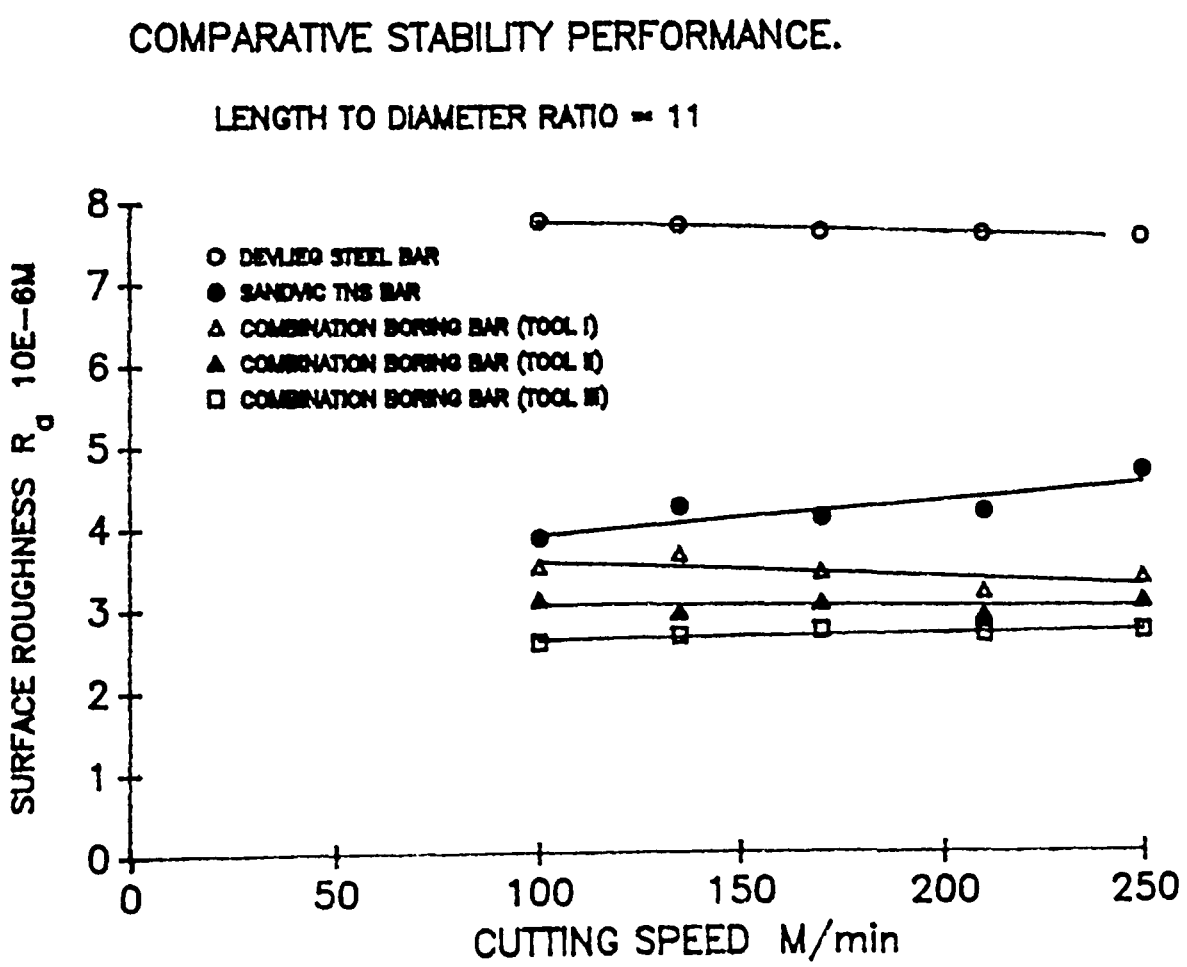

FIGURE 5.9 : COMPARETIVE CUTTING SPEED VARIATION OF THE EXAMINED TOOLS WITH RESPECT TO SURFACE ROUGHNESS.

DEPTH OF CUT VARIATION :
CUTTING SPEED = 135 m/min
COMMAND FEED = 0.071 mm/Rev

L/D RATIO = 5;

TEST No.	1	2	3	4	5	6
DEPTH OF CUT VARIATION (mm)	0.25	0.50	0.75	1.00	1.50	2.00

MACHINING QUALITY	TEST No.	DeVlieg STEEL	SANDVIC TNS BAR	TOOL I	TOOL II	TOOL III
	1	1.98	1.25	1.09	0.88	0.77
SURFACE	2	2.77	1.71	1.31	1.12	1.13
ROUGHNESS	3	3.49	2.34	1.74	1.32	1.28
R_a (μm)	4	4.20	2.83	2.12	1.61	1.52
	5	5.11	3.18	2.72	2.34	2.19
	6	6.25	3.43	3.29	2.97	2.74

TABLE 5.6: COMPARATIVE PERFORMANCE OF TOOLS WITH RESPECT TO VARIATION OF DEPTH OF CUT.

L/D RATIO = 7;

TEST No.	1	2	3	4	5	6
DEPTH OF CUT VARIATION (mm)	0.25	0.50	0.75	1.00	1.50	2.00

MACHINING QUALITY	TEST No.	DeVlieg STEEL	SANDVIC TNS BAR	TOOL I	TOOL II	TOOL III
	1	2.86	2.04	1.14	1.07	1.02
SURFACE	2	3.34	2.29	1.47	1.24	1.26
ROUGHNESS	3	4.17	2.64	1.89	1.39	1.54
R_a (μm)	4	4.19	3.20	2.42	1.89	1.87
	5	6.32	3.64	2.96	2.68	2.63
	6	7.42	3.96	3.58	3.11	3.03

TABLE 5.7: COMPARATIVE PERFORMANCE OF TOOLS WITH RESPECT TO VARIATION OF DEPTH OF CUT.

DEPTH OF CUT VARIATION :
CUTTING SPEED = 135 m/min
COMMAND FEED = 0.071 mm/Rev

L/D RATIO = 9;

TEST No.	1	2	3	4	5	6
DEPTH OF CUT VARIATION (mm)	0.25	0.50	0.75	1.00	1.50	2.00

MACHINING QUALITY	TEST No.	DeVlieg STEEL	SANDVIC TNS BAR	TOOL I	TOOL II	TOOL III
	1	3.86	2.59	1.66	1.39	1.31
	2	4.63	2.88	1.74	1.63	1.61
SURFACE	3	5.27	2.98	2.18	1.95	1.83
ROUGHNESS	4	6.05	3.91	2.87	2.39	2.18
R_a (μm)	5	7.46	4.56	3.52	3.07	2.76
	6	9.05	4.39	3.71	3.49	3.21

TABLE 5.8: COMPARATIVE PERFORMANCE OF TOOLS WITH RESPECT TO VARIATION OF DEPTH OF CUT.

L/D RATIO = 11;

TEST No.	1	2	3	4	5	6
DEPTH OF CUT VARIATION (mm)	0.25	0.50	0.75	1.00	1.50	2.00

MACHINING QUALITY	TEST No.	DeVlieg STEEL	SANDVIC TNS BAR	TOOL I	TOOL II	TOOL III
	1	4.86	3.06	2.16	2.15	2.01
	2	5.22	3.62	2.45	2.34	2.19
SURFACE	3	6.15	4.28	2.83	2.62	2.43
ROUGHNESS	4	7.72	4.26	3.67	2.96	2.67
R_a (μm)	5	8.79	4.74	4.26	3.45	3.02
	6	10.20	5.32	4.82	3.98	3.58

TABLE 5.9: COMPARATIVE PERFORMANCE OF TOOLS WITH RESPECT TO VARIATION OF DEPTH OF CUT.

DEVLIGE STEEL BAR

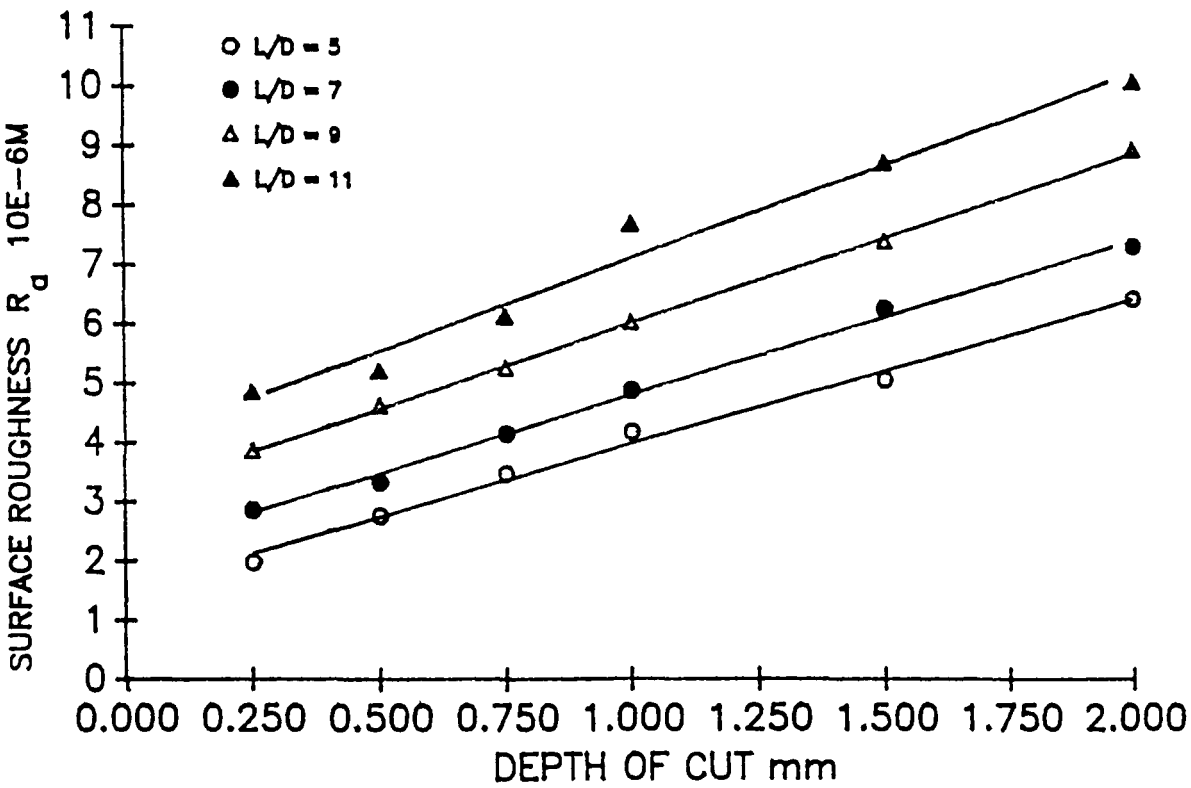

FIGURE 5.10 : VARIATION OF SURFACE ROUGHNESS WITH DEPTH OF CUT AND L/D RATIO

SANDVIC TNS BAR

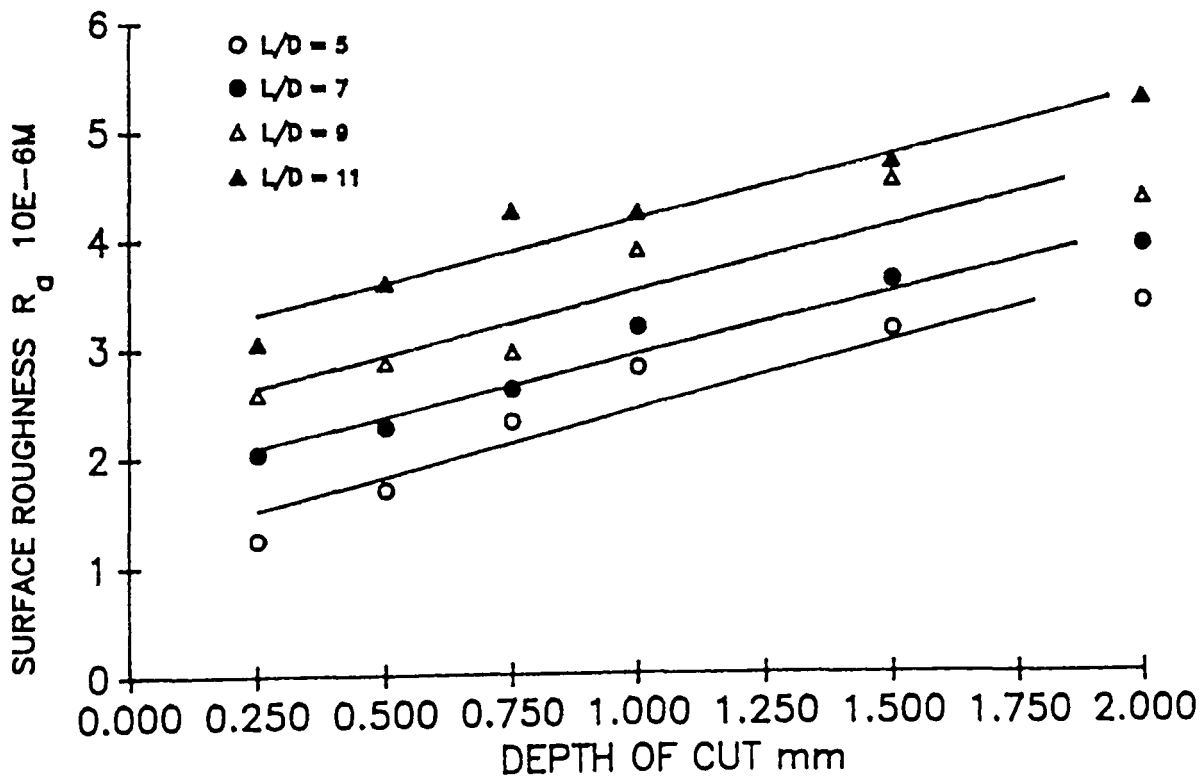

FIGURE 5.11 : VARIATION OF SURFACE ROUGHNESS WITH DEPTH OF CUT AND L/D RATIO.

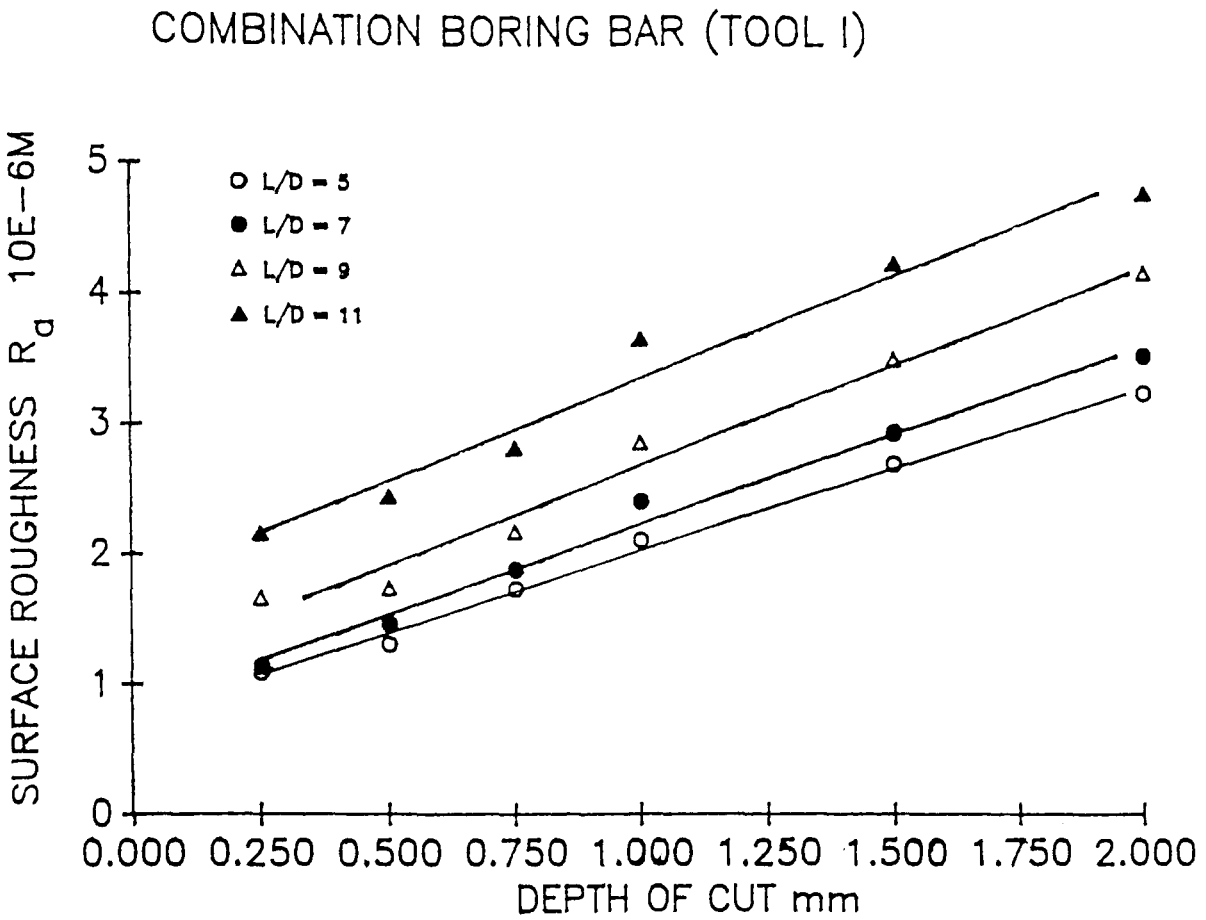

FIGURE 5.12 : VARIATION OF SURFACE ROUGHNESS WITH DEPTH OF CUT AND L/D RATIO

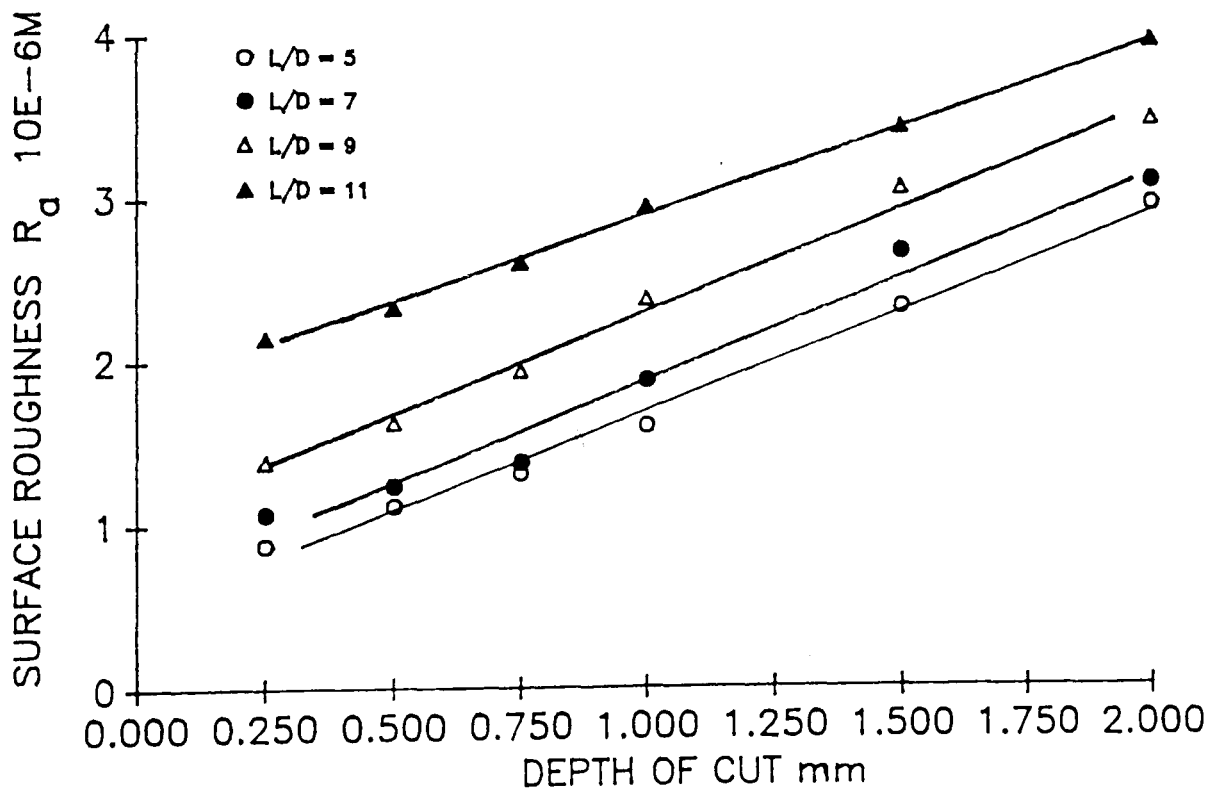

FIGURE 5.13 : VARIATION OF SURFACE ROUGHNESS WITH DEPTH OF CUT AND L/D RATIO

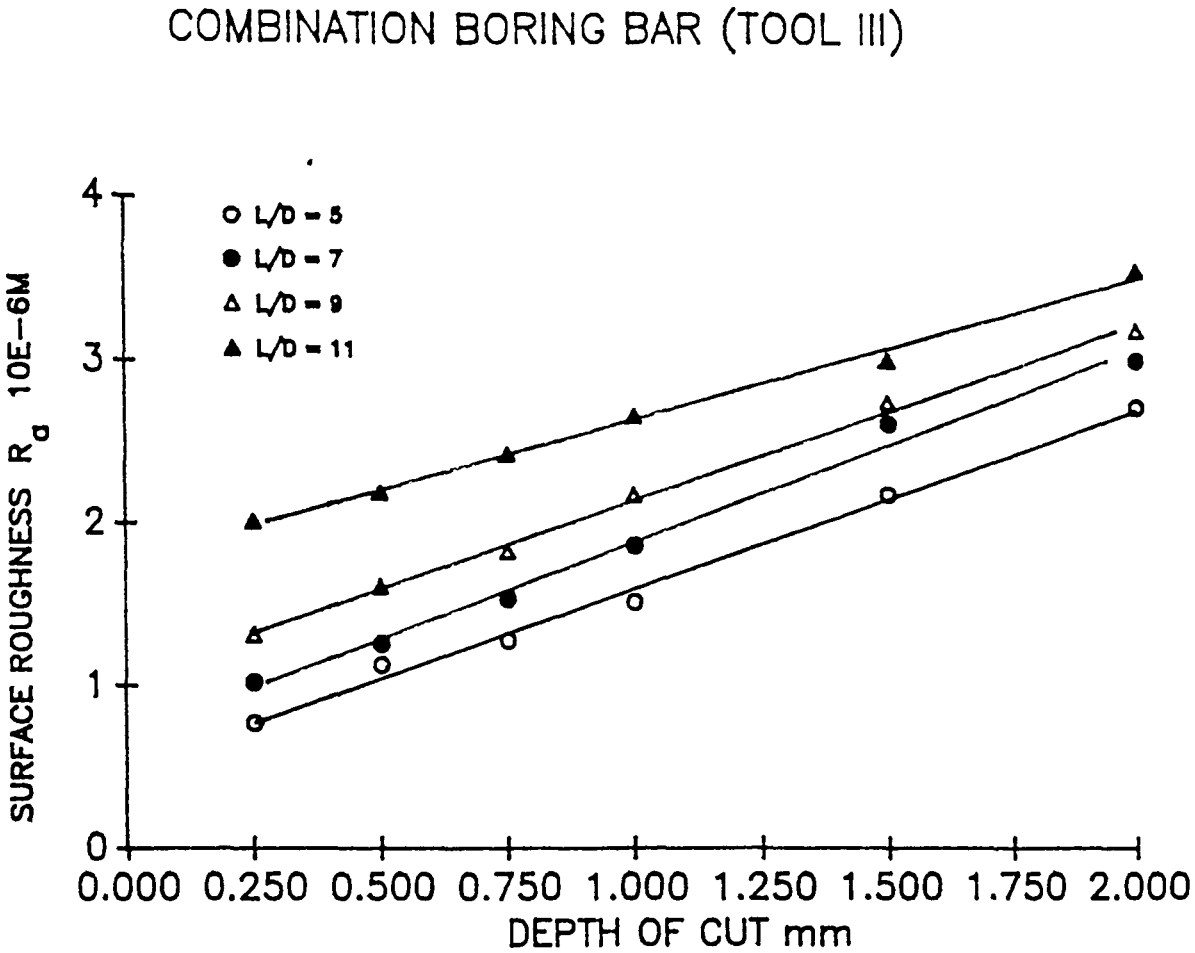

FIGURE 5.14 : VARIATION OF SURFACE ROUGHNESS WITH DEPTH OF CUT AND L/D RATIO

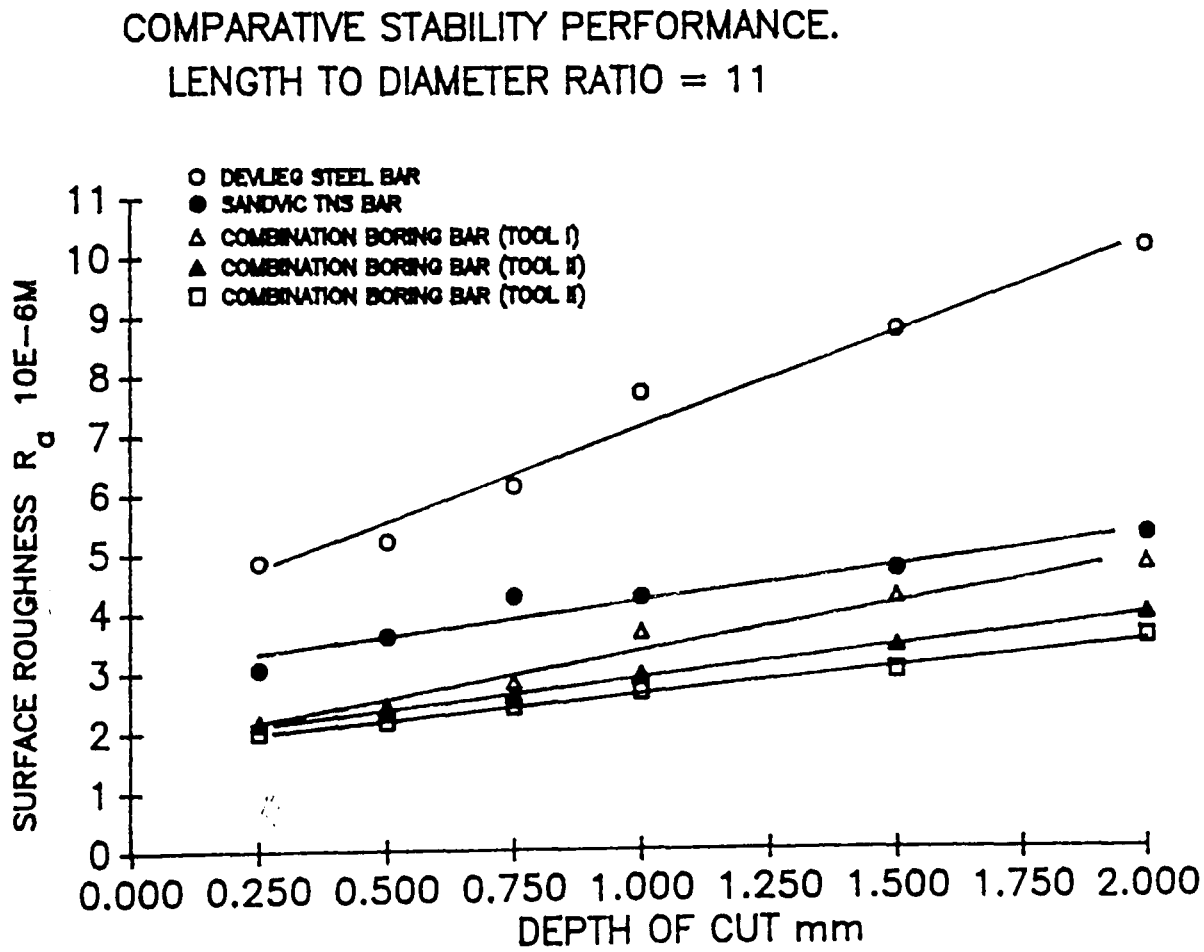

FIGURE 5.15 : COMPARATIVE DEPTH OF CUT VARIATION OF THE EXAMINED TOOLS WITH RESPECT TO SURFACE ROUGHNESS

COMMAND FEED VARIATION:
DEPTH OF CUT = 1.00 mm
CUTTING SPEED = 135 m/min

L/D RATIO = 5;

TEST No.	1	2	3	4
FEED VARIATION (mm/Rev)	0.071	0.09	0.125	0.17

MACHINING QUALITY	TEST No.	DeVlieg STEEL	SANDVIC TNS BAR	TOOL I	TOOL II	TOOL III
	1	4.20	2.83	2.12	1.61	1.52
SURFACE	2	4.43	3.05	2.32	1.87	1.81
ROUGHNESS	3	4.84	3.13	2.77	2.29	1.95
R_a (μm)	4	5.27	3.27	3.15	2.78	2.15

TABLE 5.10: COMPARATIVE PERFORMANCE OF TOOLS WITH RESPECT TO VARIATION OF FEED RATE.

L/D RATIO = 7;

TEST No.	1	2	3	4
FEED VARIATION (mm/Rev)	0.071	0.09	0.125	0.17

MACHINING QUALITY	TEST No.	DeVlieg STEEL	SANDVIC TNS BAR	TOOL I	TOOL II	TOOL III
	1	4.91	3.20	2.42	1.89	1.87
SURFACE	2	5.26	1.97	2.76	2.27	2.06
ROUGHNESS	3	5.73	2.64	3.14	2.64	2.31
R_a (μm)	4	6.51	3.13	3.68	3.27	2.57

TABLE 5.11: COMPARATIVE PERFORMANCE OF TOOLS WITH RESPECT TO VARIATION OF FEED RATE.

COMMAND FEED VARIATION:
DEPTH OF CUT = 1.00 mm
CUTTING SPEED = 135 m/min

L/D RATIO = 9;

TEST No.	1	2	3	4
FEED VARIATION (mm/Rev)	0.075	0.09	0.125	0.17

MACHINING QUALITY	TEST No.	DeVlieg STEEL	SANDVIC TNS BAR	TOOL I	TOOL II	TOOL III
	1	6.05	3.91	2.87	2.39	2.18
SURFACE	2	6.24	4.46	3.14	2.69	2.45
ROUGHNESS	3	6.99	4.77	3.68	3.18	2.79
R_a (µm)	4	7.79	5.39	4.25	3.82	2.98

TABLE 5.12: COMPARATIVE PERFORMANCE OF TOOLS WITH RESPECT TO VARIATION FEED RATE.

L/D RATIO = 11;

TEST No.	1	2	3	4
FEED VARIATION (mm/Rev)	0.071	0.09	0.125	0.17

MACHINING QUALITY	TEST No.	DeVlieg STEEL	SANDVIC TNS BAR	TOOL I	TOOL II	TOOL III
	1	7.72	4.26	3.67	2.96	2.67
SURFACE	2	8.27	4.40	3.84	3.24	2.87
ROUGHNESS	3	8.88	5.29	4.38	3.52	3.19
R_a (µm)	4	10.14	4.78	4.91	4.29	3.67

TABLE 5.13: COMPARATIVE PERFORMANCE OF TOOLS WITH RESPECT TO VARIATION FEED RATE.

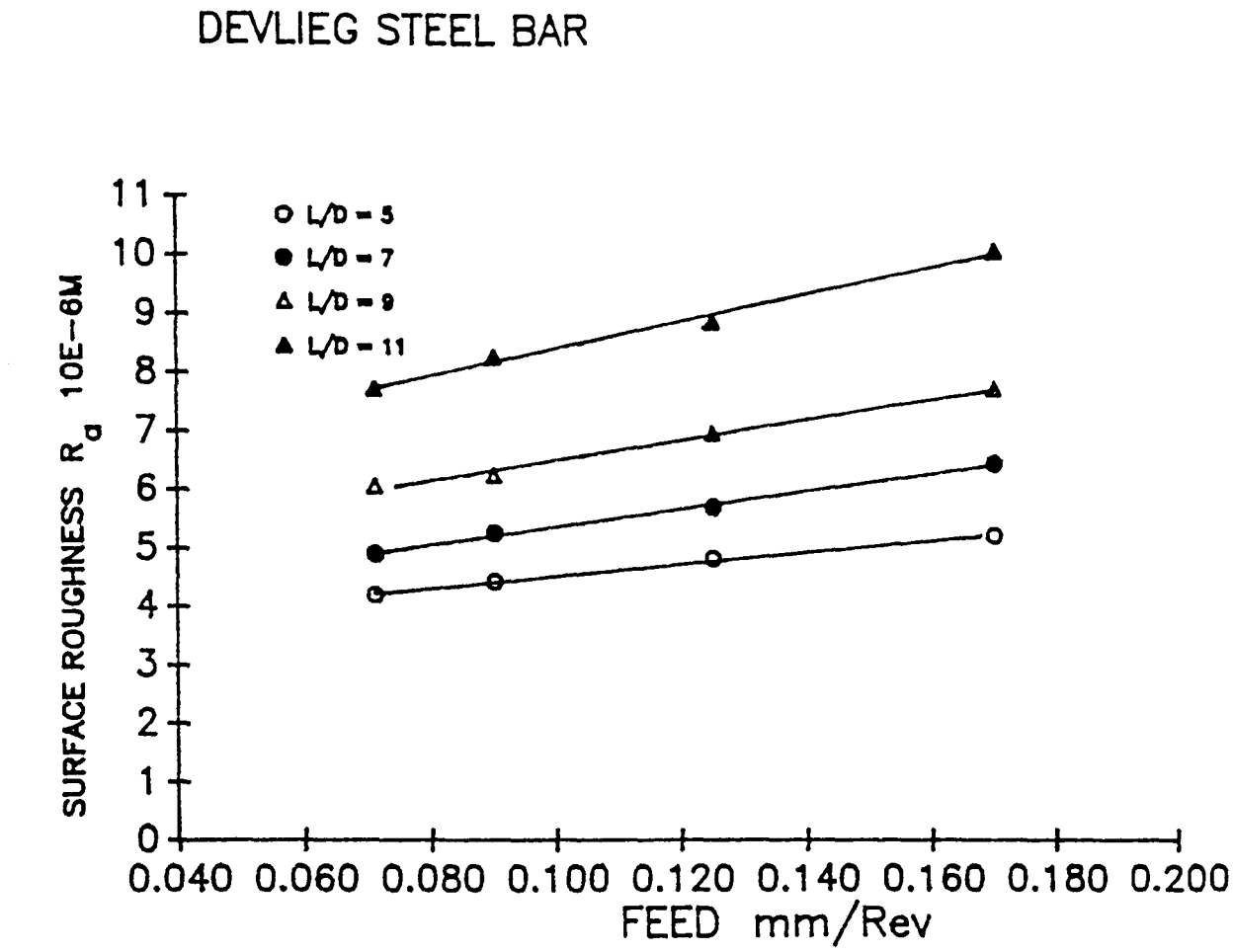

FIGURE 5.16 : VARIATION OF SURFACE ROUGHNESS WITH CUTTING FEED AND L/D RATIO

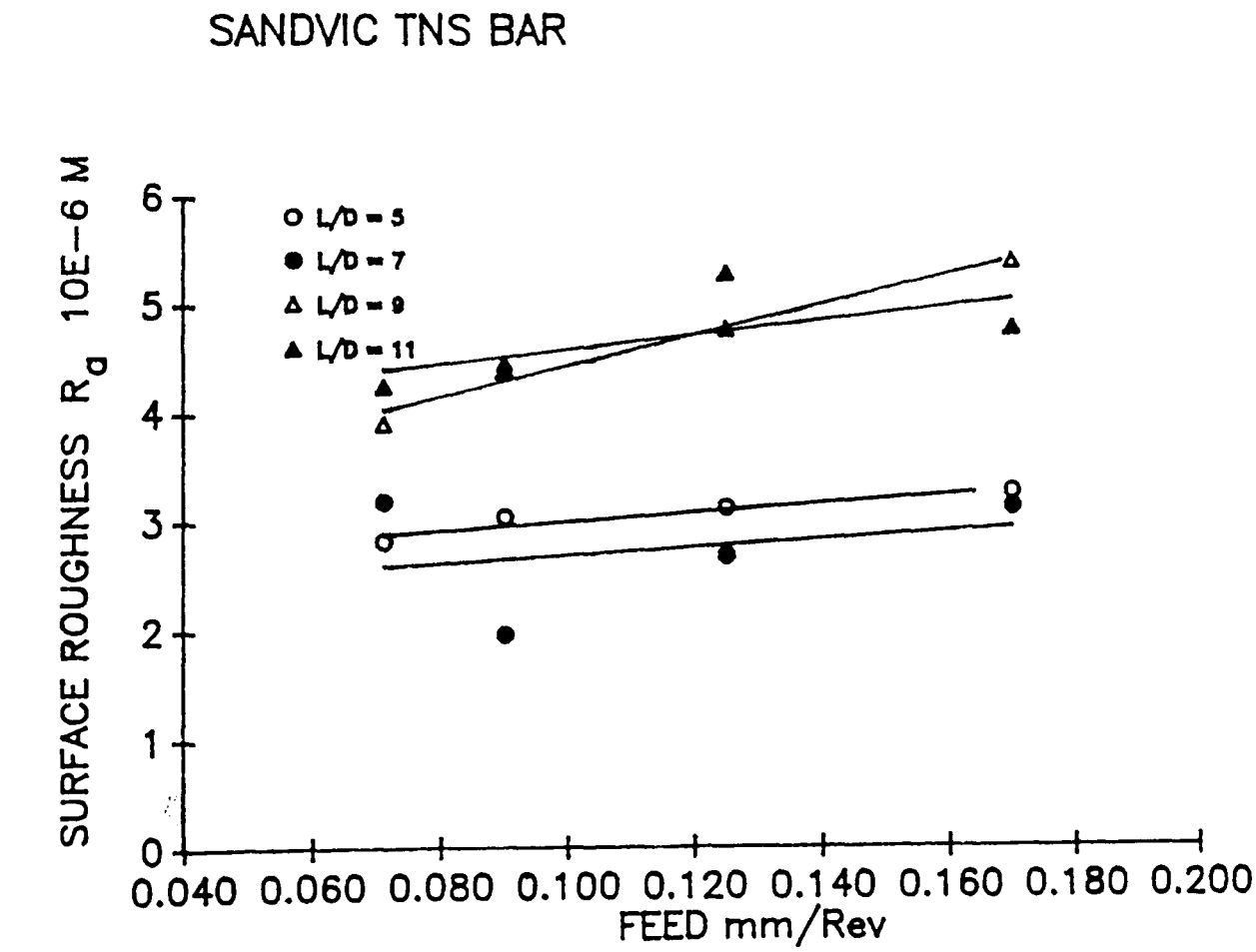

FIGURE 5.17 : VARIATION OF SURFACE ROUGHNESS WITH CUTTING FEED AND L/D RATIO

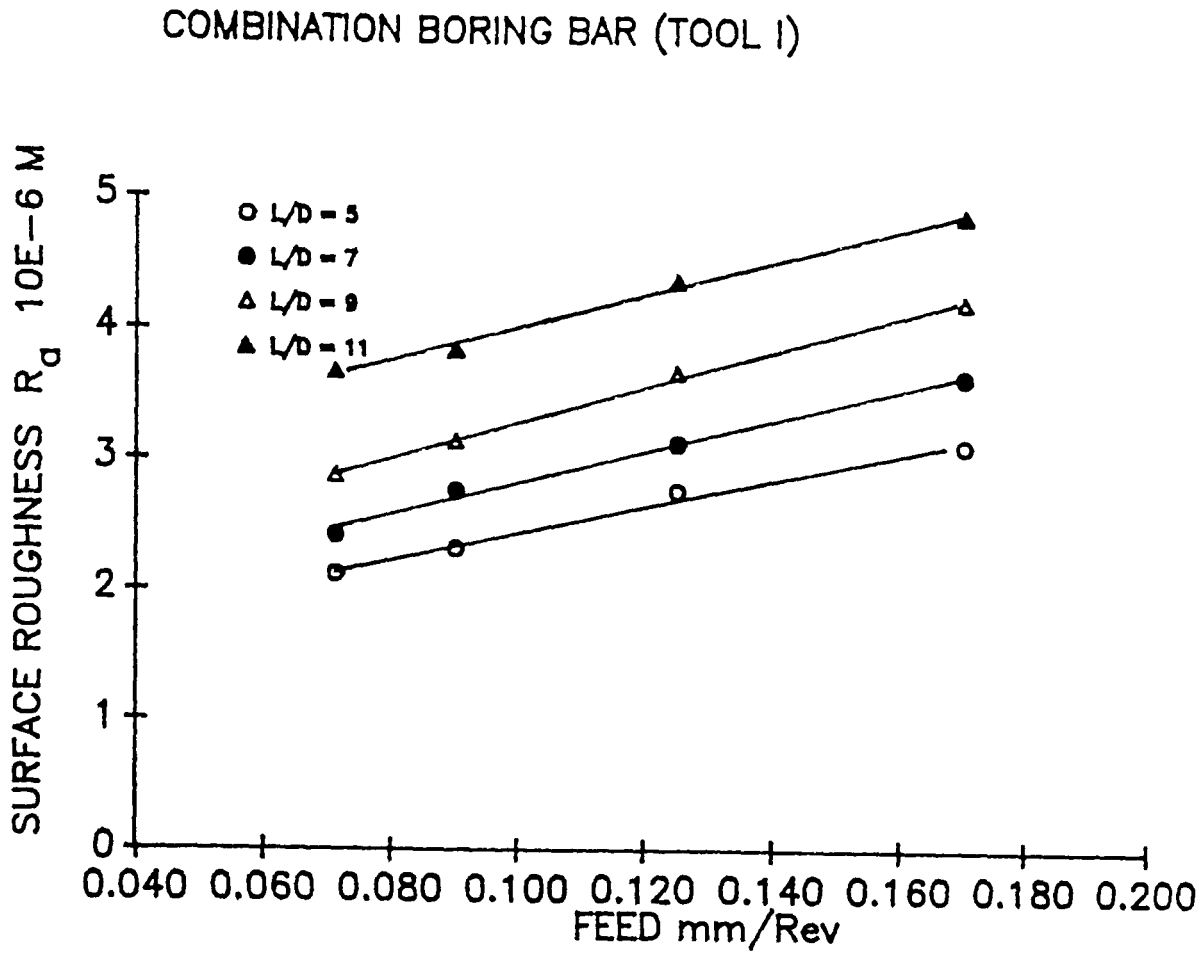

FIGURE 5.18 : VARIATION OF SURFACE ROUGHNESS WITH CUTTING FEED AND L/D RATIO.

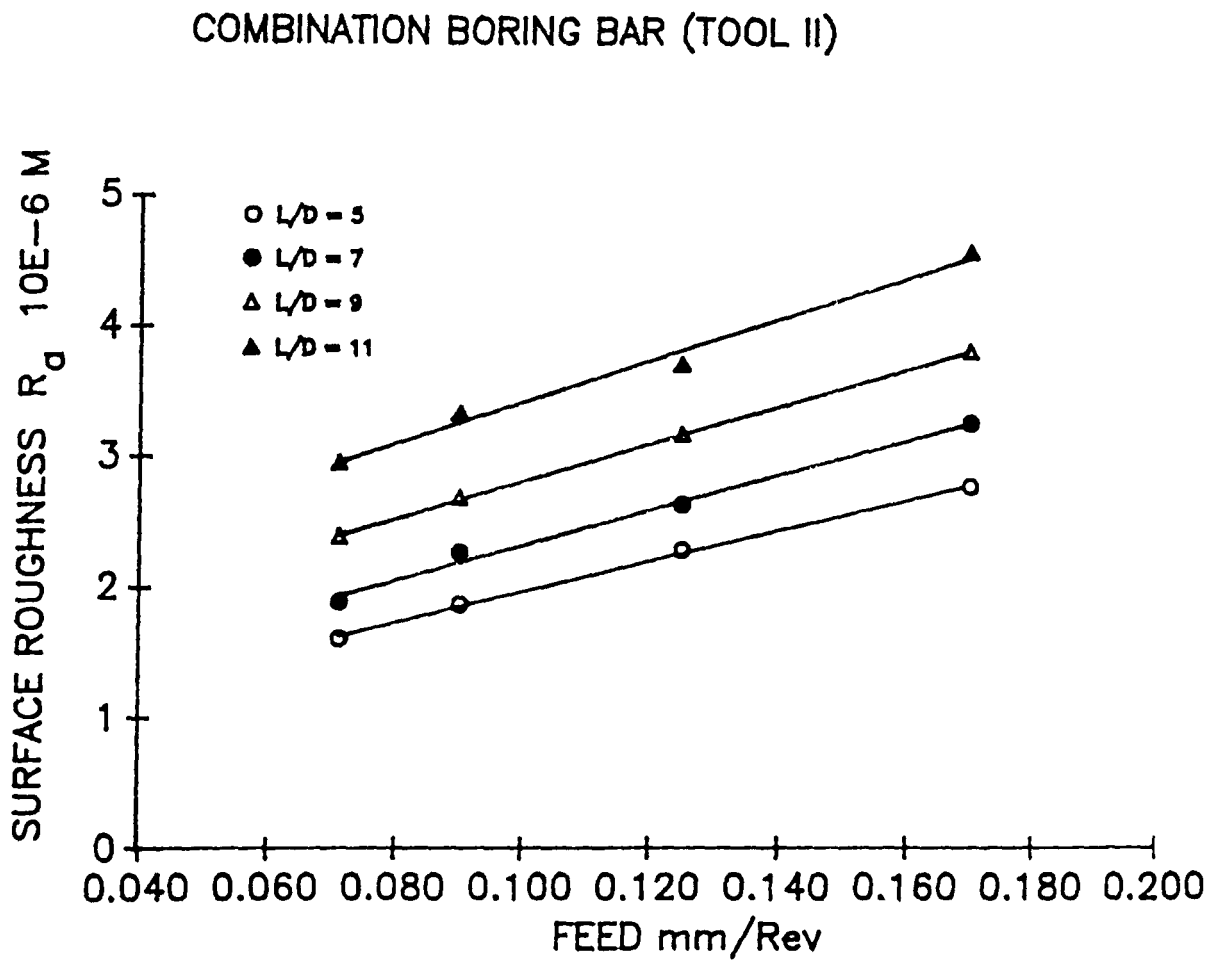

FIGURE 5.19 : VARIATION OF SURFACE ROUGHNESS WITH CUTTING FEED AND L/D RATIO.

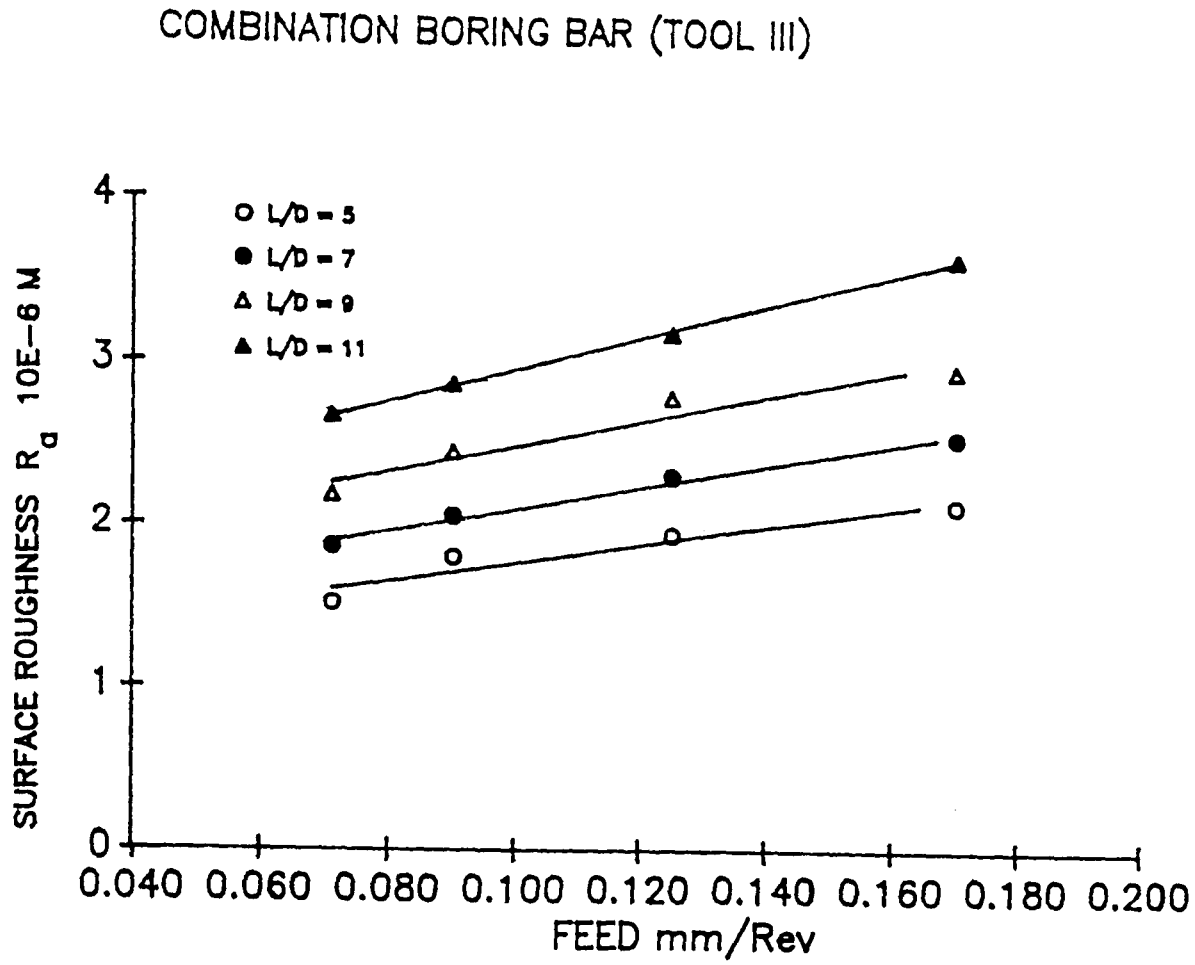

FIGURE 5.20 : VARIATION OF SURFACE ROUGHNESS WITH CUTTING FEED AND L/D RATIO.

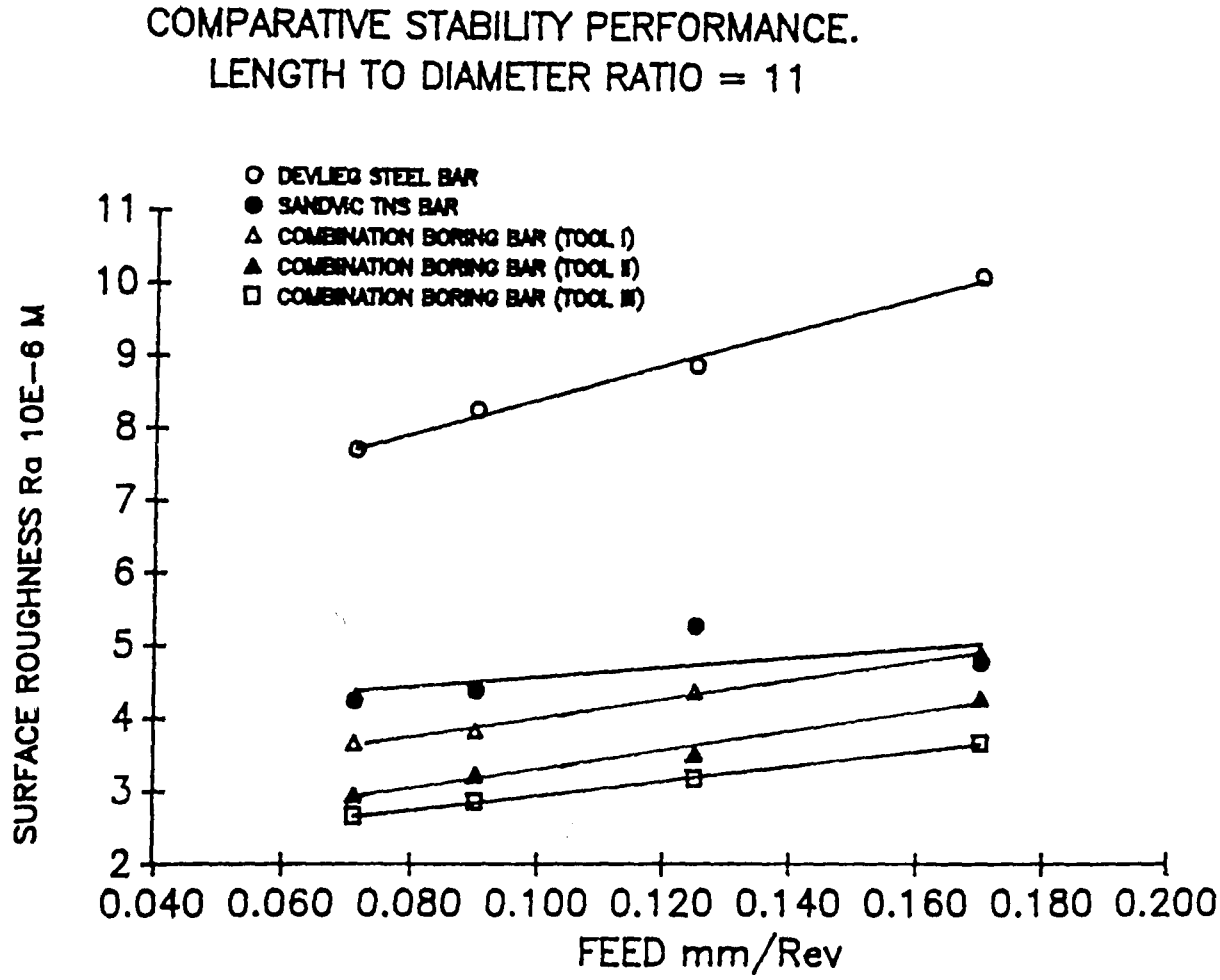

FIGURE 5.21 : COMPARATIVE VARIATION OF THE CUTTING FEED RATE OF THE EXAMINED TOOLS WITH RESPECT TO SURFACE ROUGHNESS.

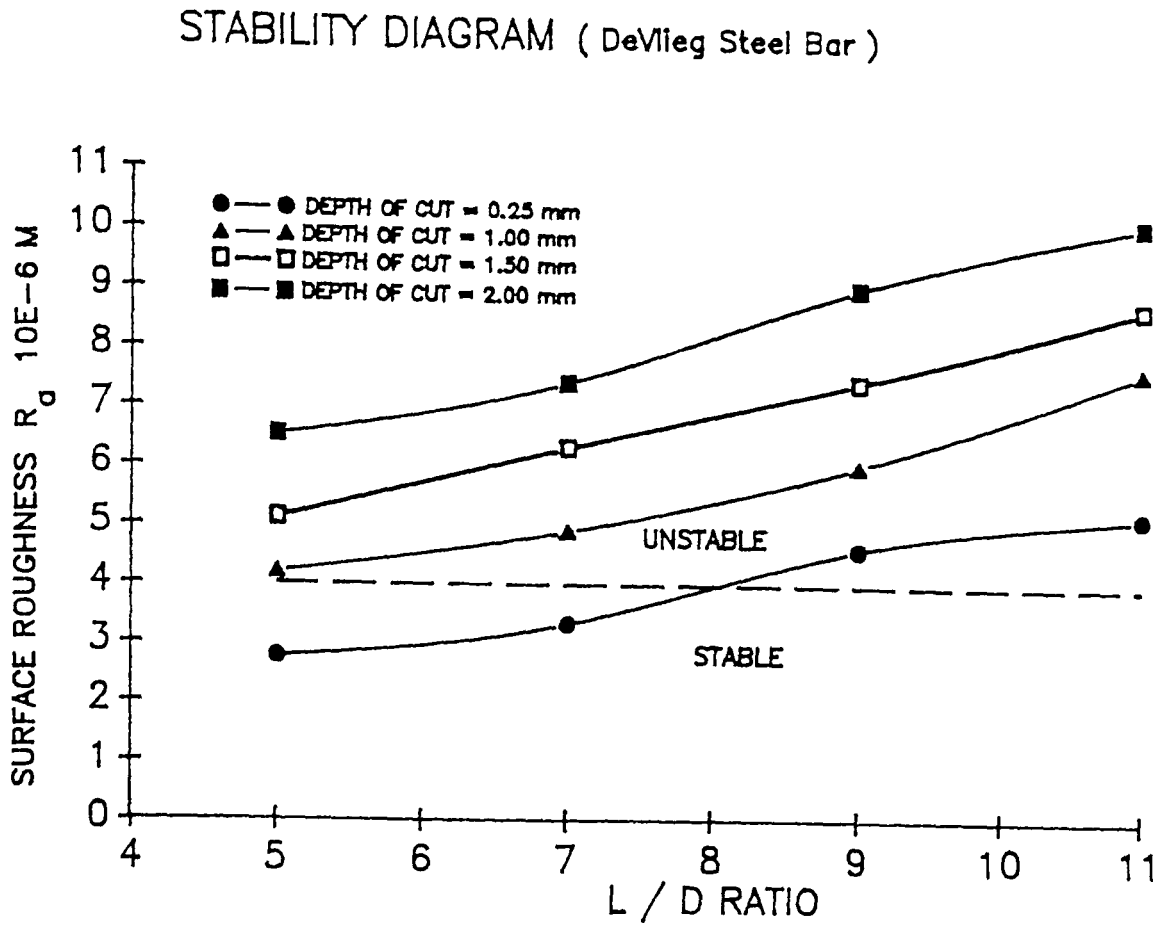

FIGURE 5.22 : PERFORMANCE CHARACTERISTICS OF DEVLIEG STEEL BAR FOR VARIATION OF L/D RATIO WITH RESPECT TO DEPTH OF CUT.

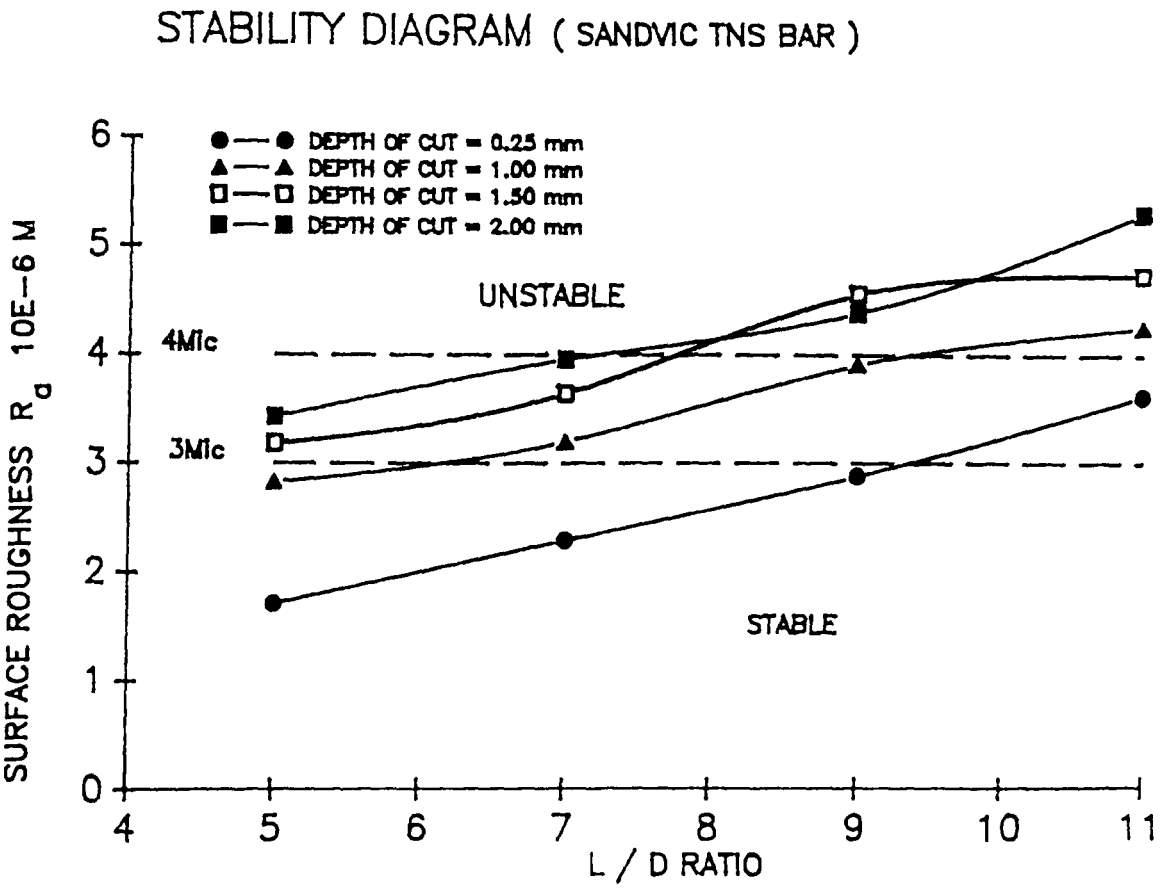

FIGURE 5.23 : PERFORMANCE CHARACTERISTICS OF SANDVIC TNS BAR FOR VARIATION OF L/D RATIO WITH RESPECT TO DEPTH OF CUT.

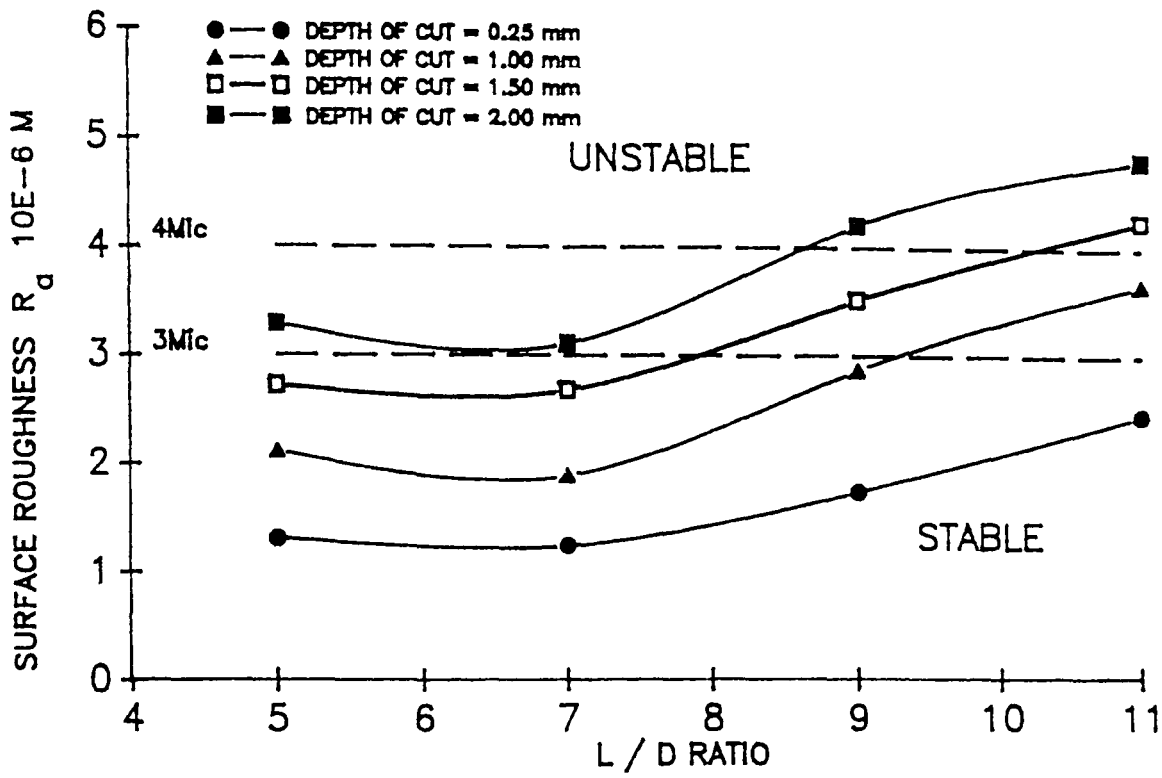

FIGURE 5.24 : PERFORMANCE CHARACTERISTICS OF THE COMBINATION BORING BAR (TOOL I) FOR VARIATION OF L/D RATIO WITH RESPECT TO DEPTH OF CUT.

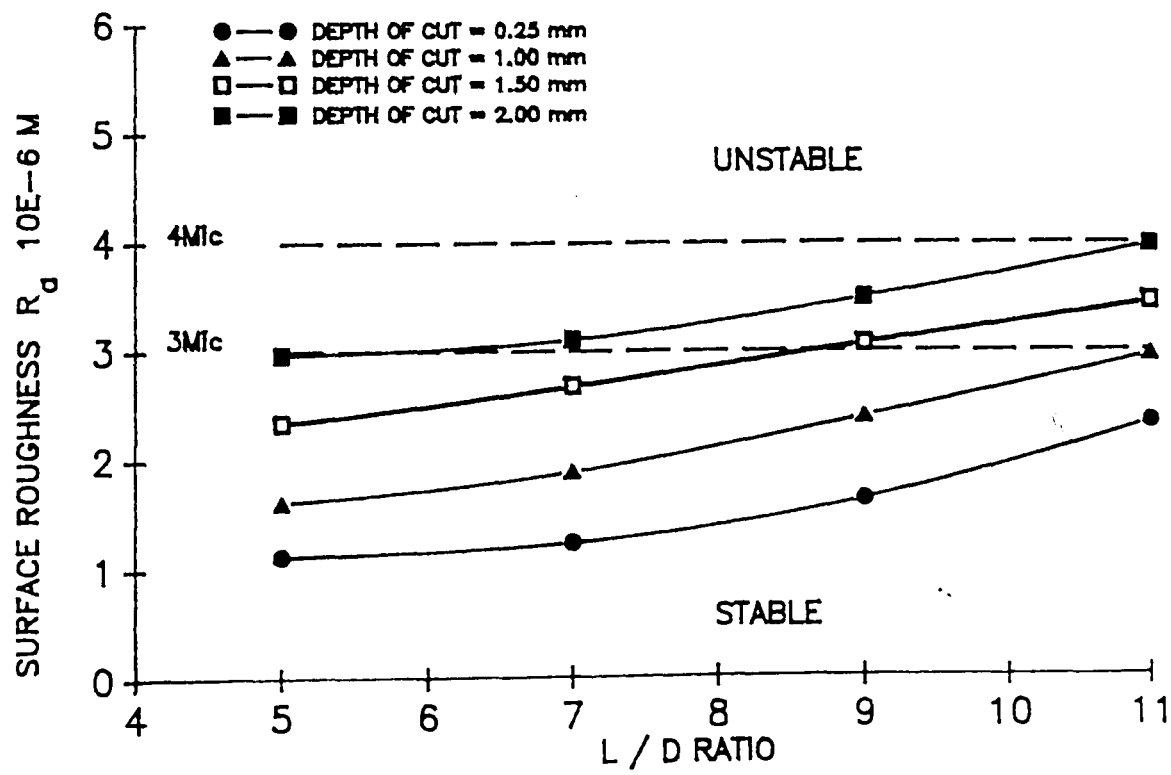

FIGURE 5.25 : PERFORMANCE CHARACTERISTIC OF COMBINATION BORING BAR (TOOL II) FOR VARIATION OF L/D RATIO WITH RESPECT TO DEPTH OF CUT.

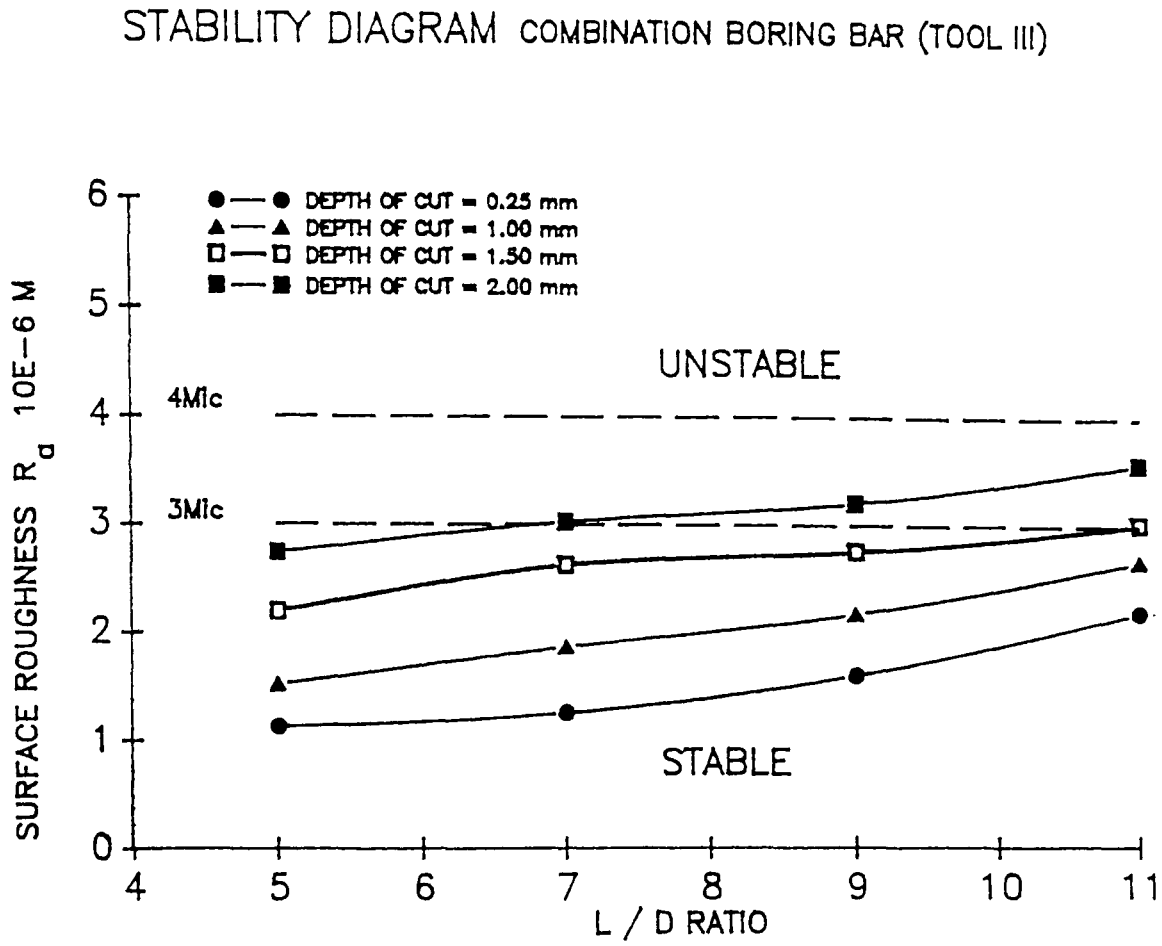

FIGURE 5.26 : PERFORMANCE CHARACTERISTIC OF COMBINATION BORING BAR (TOOL III) FOR VARIATION OF L/D RATIO WITH RESPECT TO DEPTH OF CUT.

CHAPTER 6

FINITE ELEMENT MODELLING

PART I: FINITE ELEMENT BACKGROUND AND THEORY

6.0 INTRODUCTION

To determine the response of engineering systems to an applied action the mathematical solutions may be employed. There are two common numerical methods which offers a convenient way of obtaining approximate yet acceptable solutions to certain engineering problems.

1) Finite difference method (FDM)
2) Finite element method (FEM)

Although the use of these methods in engineering and structural analysis are well established, to date there is no known literature on the application of FEM to the dynamic analysis of extended length tool holders. In this, and the subsequent chapters (chapters seven and eight) the procedure for modelling the tool together with results and analyses with respect to the static and dynamic response are demonstrated. Although the theory of Finite elements are well known, for completeness the basic principles with respect to the method and modelling technique using ANSYS (6.1) and referenced literature are included.

6.1 HISTORICAL PERSPECTIVE

The roots of the modern day finite element method (FEM) developed around the turn of this century with the use of lattice analogy to solve solid continuum structural problems. With this technique, the structure was divided into a regular mesh of elastic beams. Beam theory was then used to approximate the true solution of the structure.

In the early 1940's mathematicians adapted the Rayleigh-Ritz approach where the structure is divided into triangular subregions. Courant (6.2) described each subregion by polynomial functions to approximate the exact solution. However the practicability of Courant's method was limited because there were no digital computers to do the tedious calculations.

Interest in FEM increased dramatically in 1956 with a publication by Turner, Clough, Martin and Topp (6.3), in which the actual solution of plane stress problems by means of triangular elements whose properties were determined from the equations of elastic theory was given. The use of the method in the 1960s was mainly limited to structural analysis. The general purpose finite element programmes emerged during the late 1960's - early 1970's period. These general programmes combined the special features of many small programs into analysis packages.

By 1973 with the introduction of digital computers that could solve large simultaneous equations, the now feasible matrix methods became popular in engineering circles, especially in the aerospace industry.

The finite element code ANSYS (used in this research) was introduced by Swanson Analysis Systems, Institute (SASI) in 1970, gave analysts the capability to perform static and dynamic calculations in a single program.

The proliferation of super-minis with interactive operating systems and graphics terminals also brought about changes in the FE codes. The codes had to be reconstructed for use in an interactive environment. In the case of the ANSYS program the solution modules were maintained as basically batch operations. However, data preparation (preprocessing and results evaluation (postprocessing) were created to be used interactively.

The finite element method (FEM) is widely regarded as the more

powerful method of the two for the solution of continuum problems in physics and engineering. The basic concept of FEM is that the structure to be analyzed is considered to be an assemblage of discrete pieces, called elements, that are connected together at a finite number of points or nodes. Each node has a degree of freedom (DOF) which in the case of structural static and dynamic analysis is the stress, strains, displacement and response of the node.

For structural analysis, having represented the model by three-dimensional elements, the displacements within the element are related to the displacement of the nodes by interpolation function.

A stiffness matrix, which relates the nodal stress and strains of an element, is a combination of the forcing function and material properties of the element.

By imposing equilibrium at every node, the individual element displacement, velocity or acceleration matrices are assembled into a set of linear simultaneous equations. The solution of the equation set determines the quantities such as force responses, displacements, strain energies.

In this chapter the methods developed to generate the finite element models necessary to design the cutting tools are demonstrated.

The chapter is divided into two sections:

Part I) The general interpretation of ANSYS finite element.

Part II) Generation of the cutting tool assembly.

6.2 THE FINITE ELEMENT METHOD FOR DESIGN AND ANALYSIS

In the past, designers have used classical analysis techniques. These, although useful for rough predictions for simple components, are inadequate for analysis of complex dynamic system such as the prediction of the compliance of machine tool elements or the induced stresses due to interface pressure. Hence, the traditional approach to

a new system was to design it using traditional techniques and to rely heavily on testing. The failed components were redesigned and retested.

In this investigation the powerful feature of the FE method was explored by construction of realistic FE models, including all the details that may effect the stability performance of the extended length boring bars.

The overall objective of FE dynamic analysis is to help and ensure the overall 'integrity' of the design, before prototype manufacture and testing. Although it would be ideal to incorporate the complete machining parameters during an analysis, certain simplifications must be accepted.

6.3 THE METHOD

The name finite element summarises the basic concept of the method. The transformation of an engineering system with infinite number of unknowns (the response at every location in a system) to one that has a finite number of unknowns related to each other by elements of finite size. The unknowns, called degrees of freedom, represent the responses to applied actions. Typical degrees of freedom with corresponding actions and applications are listed in Table 6.1.

TYPE OF DEGREE OF FREEDOM	ACTION	APPLICATION
Displacement	Force	Structural
Temperature	Heat flow rate	Heat transfer
Volt	Current	Electrical
Magnetic potential	Current	Magnetic
Pressure	Fluid flow rate	Fluid flow

Table 6.1 - The degrees of freedom, actions and applications

The degree of freedom and the actions are related by a set of basic equations. The purpose of the finite element method is to determine the solution to these across the entire engineering system being analyzed. The simplest form of a basic equation is as follows;

$$[K]\ \{d\} = \{A\} \qquad (6.1)$$

Where {d} is the degree of freedom vector, {A} is the action vector, and [K] is the stiffness matrix relating {d} to {A}.

In general [K] and {A} are unknown, and {d} is initially unknown. The actual form of a basic equation is determined by the type of analysis being performed.

In order to solve the basic equation across the entire engineering system the system must be represented (modelled) by discrete, interconnection pieces (elements). Once the stiffness matrix [K] is determined for each element all of the individual [K] matrices are assembled to form the set of simultaneous equations. Solution of the simultaneous equations gives response values at every degree of freedom across the entire system.

The execution of the finite element method usually follows a step-by-step procedure parts of which may be invisible to the user if a modern packages is used. The following list describes the steps involved.

1 Model characterisation (1-d, 2-d, 3-d, time varying etc).
2 Element type specification (triangular, quadrilateral, tetrahedron).
3 Definition of physical properties.
4 Discretisation - creation of interconnected pieces (elements).
5 Definition of boundary conditions.
6 Formation of the element equations.
7 Formation of the system equations.
8 Solution of the equations.
9 Postprocessing to analyze the results.

In the commercially available packages it is a common practice to execute the steps 6 to 9 in a batch form such that it is not visible to

the user.

6.4 THE ELEMENT AND ELEMENT TYPES

The element is the critical part of the FEM. The element interconnects degrees of freedom, establishes how they act together, and determines how they respond to applied actions. Every element has one or more nodes that lie along its boundary. Nodes are the points where other elements can be connected and also at which the degrees of freedom are located. Information is passed from element to element only at common (shared) nodes. The number of degrees of freedom (DOF) at a node and their meaning (for example displacement) are determined by the element type.

The type of element used depends upon the problem. The element [K] matrix relates the applied action to the degrees of freedom in the element. In order to determine the [K] matrix element shape functions must be determined for each type of element. An element shape function maps values of a degree of freedom from the nodes to points within the element. This is important because the FEM solves for degree of freedom values only at the nodes.

For example considering a four-node 2-D solid element for which the values of the degrees of freedom at its four nodes have been established. Furthermore consider a quadratic distribution of degree of freedom values shown against the edge of an element Figure 6.1a. A single element with a linear shape function would do a poor job of capturing the actual quadratic nature of the response Figure 6.1b. Better results could be obtained with a greater number of elements Figure 6.1c. A single element that has a quadratic shape function can capture the actual distribution Figure 6.1d. Note that in each of these examples, the DOF were actually matched at the nodes, but not always within the elements.

Additional solution data, such as structural stress and frequency response, are usually derived from the DOF solutions by calculating

derivatives of the shape function. Therefore, if the DOF solution captured by the shape function within the element is inaccurate, the derived results will also be inaccurate. Once the shape function has been assumed, the [K] matrix can be derived.

6.5 THE ELEMENT MESH DENSITY

In the early development of the finite element method the programmers were using simple elements, having linear approximation functions. Employing such elements necessitates using a finely divided mesh if results were to be accurate. Since, generally, as the number of elements is increased in a mesh the accuracy of the solution is also increased.

At present, programmers can use element that offer high accuracy therefore reducing the number of elements. Such elements employ higher order quadratic or cubic approximation functions which normally have mid-side nodes.

6.6 PROPERTIES OF ELEMENTS

After the discretisation of the continuum and selection of the their interpolation functions, the matrix equations are determined by expressing the properties of the individual elements. For this, one of the four approaches of

a) direct approach,

b) variational approach,

c) weighted residual approach,

d) energy balance approach can be used.

The approach used depends entirely on the nature of the problem. The first approach to obtain the element properties is called the

'direct approach' because its origin is traceable to the direct stiffness method of structural analysis. The direct approach can be used only for relatively simple problems.

6.6.1 ELEMENT EQUATIONS ASSEMBLY

The properties of the overall system can be constructed by "assembling" all the element properties or combining the matrix equations expressing the behaviour of the entire solution region or system. The overall equilibrium equation can be formulated as follows for a problem in elasticity:

$$[k]\ u' = p'$$

where

[k]	is the assembled stiffness matrix
u'	is the vector of nodal displacements
p'	is the vector of nodal forces for the entire system

The assembly procedure is based on the continuity principal that, at a node where elements are connected, the values of the field variable is the same for each element sharing that node. The assembly process gives a set of linear simultaneous equations that must next be modified to incorporate the boundary conditions and constraints of the problem and thereafter can be solved in order to obtain the unknown nodal values of the field variable.

6.6.2 SOLVING THE SYSTEM EQUATIONS

For linear problems the equations can be solved by using a number of standard techniques. But for non-linear problems the solution must be obtained iteratively, each step involving the modification of the stiffness matrix [k] and/or the load vector p'. Non-linearities arise,

for example, when material properties are function of temperature.

Finally, it may be required to use the solution of the system equations to calculate other important parameters such as strains and stresses from displacements or frequency response from stiffness and material properties.

6.7 THE FINITE-ELEMENT PACKAGES RELEVANT BACKGROUND

The current trend of performing an analysis is to operate the pre-processing and the post-processing phases interactively.

The finite element method is an important part of computer aided engineering (CAE), starting from the sketches of the designer, to the analyses, eventually leading to the design of the finished product. The capability to assess the design in detail prior to prototype testing could also result in substantial time saving.

6.7.1 INTRODUCTION TO ANSYS

ANSYS is a self-contained general purpose finite element program developed and maintained by Swanson Analysis Systems Inc (6.1). The program contains many routines, all inter-related, together they provide solutions to modern engineering problems by finite element method.

ANSYS may be executed in either of two modes: 1) interactive, or 2) batch. An analysis execution may be "all batch", "all interactive", or a combination of both. The element library provides more than forty element types, for static and dynamic analyses. This variety of elements gives the ANSYS program the capability of analysing many engineering problems. Loading on the structures may be force,

displacements, pressures, or response spectra.

An engineering problem is usually solved in three phases: preprocessing, solution phase and postprocessing.

The preprocessing phase involves defining the model geometry, generating a mesh and applying boundary conditions and material properties. This phase may consist of input from different preprocessing routines.

The ANSYS package has two preprocessing routines available, known as PREP7 and PREP6.

PREP6 is used to generate load step data for multiple load step or transient analyses.

PREP7 is used to generate nodes, elements, material properties, constraints and loads that describe the problem.

Once the preprocessing is performed and the model definition is complete, the solution phase may begin.

The solution phase involves operation on the model data to produce solutions for the unknowns at the nodes in the model. The solution phase may consist of several solutions in series, such as a stress or modal solution followed by harmonic solution.

Once the solution phase is completed various postprocessing operations may be performed on the results. This provides interrogation of the results from the solution phase.

The ANSYS program has several routines for postprocessing analysis of the results. The routines are POST1, POST26, POST29 and POST30.

POST1 is a General Database Results Post-processor.

POST26 is a Time-History Results Post-processor.

POST29 is a harmonic solid element post-processor and

POST30 is a harmonic shell element post-processor.

The ANSYS element library consists of 78 distinct element types. The elements are grouped into categories such as fluids, thermal or structural (for static and dynamic analyses).

6.7.2 ISOPARAMETRIC STRESS SOLID - (STIF, 45)

This element is used for the three-dimensional modelling of solid structures. It is defined by eight nodal points and the appropriate material properties.

The geometry, nodal locations, face numbers, loading, and the coordinate system for this element are shown in Figure 6.2. The element loading may be input as any combination of nodal forces (for stress calculation) or face pressures.

In stress analysis, the three degrees of freedom per node are the displacements UX, UY, and UZ. The element has plastic, creep, swelling, stress stiffening and large rotation capabilities.

The output data may be per element, per node or per face. The post processing data includes element volume, stresses and strains. The nodal outputs include displacements and principal stresses.

6.7.3 THREE-DIMENSIONAL INTERFACE ELEMENT - (STIF, 52)

The three-dimensional gap element represents two surfaces which may maintain or break physical contact. They may also slide relative to each other. The element has three degrees of freedom at each node: translations in the nodal x, y and z directions. A specified stiffness acts in the normal and tangential directions when the gap is closed and not sliding.

The element is defined by two nodal points, an interface stiffness (k), an initial gap (or interference), and an initial element status. The geometry, nodal point locations, and the coordinate system for the interface element are shown in Figure 6.3.

The only material property used is the coefficient of friction μ at interface. The coefficient of friction μ for the present simulation was assumed to be μ = 0.5, (6.1), across core/shank interface.

6.7.4 COMBINATION ELEMENT - (STIF, 40)

This element is a combination of a spring-slider and a damper in parallel, coupled to a gap in series. A mass can be associated with one or both nodal points. The element has one degree of freedom at each node, either a nodal translation, rotation, pressure.

The combination element is shown in Figure 6.4. The element is defined by two nodes, two spring constants K_1 and K_2, a damping coefficient C, a mass M, a gap size "Gap" or a limiting sliding force FSLIDE. In this work, the mass M was assigned to the second node and the gap and slider were also removed.

6.8 STATIC ANALYSIS

The static analysis capability in the ANSYS program is used to determine the displacements, stresses and strains that occur in a structure. This analysis is limited for solving problems in which the time-dependent effects of inertia and damping do not affect the structure's response. Therefore, only a brief summary of the analyzed results will be discussed. The program resolves the static problems by applying the numerical techniques to the basic engineering concepts as discussed in chapter 3.

6.9 DYNAMIC ANALYSIS

Dynamic analysis may be used to determine the compliance of the structure to the applied loads. Dynamic analyses is useful for problems of structures subjected to time-varying loads and where damping characteristics are of importance. The dynamic analysis in the finite element program are based on the following general equation of motion:

$$[M]\ \{\ddot{U}(t)\} + [C]\ \{\dot{U}(t)\} + [k]\{U(t)\} = \{F(t)\} \qquad (6.2)$$

Where:

[M] is the structure mass matrix, [C] is the structure damping matrix,

[K] is the structure stiffness matrix, {Ü} is the nodal acceleration vector,

{U̇} is the nodal velocity vector, {U} is the nodal displacement vector,

{F} is the forcing function, and t is time.

Through this equation, the program determines the value of the unknowns ({U}) which satisfy equilibrium at time t, with inertia and damping effects included.

6.10 HARMONIC RESPONSE ANALYSIS

Harmonic response analysis is used to determine the steady-state response of a linear structure to a sinusoidal forcing function. This analysis is useful for studying the effects of load conditions that vary harmonically with time. Such responses may be assumed to be associated with the extended tools and their supporting elements.

The governing equation for harmonic response analysis is a special case of the equation of motion, in which the forcing function [F] is a known function of time, varying sinusoidally with a known amplitude F_0 at a known frequency ω.

$$\{F\} = F_0\ Cos(\ \omega t + \phi\ ) + i\ Sin\ (\ \omega t + \phi\ ) \qquad (6.3)$$

The displacements are also assumed to vary sinusoidally at the same frequency ω, but not necessarily in phase with the forcing function.

Loading can be in the form of nodal forces or imposed displacements. The displacement solution can be obtained at

user-specified frequencies in terms of amplitudes and phase angles or real and imaginary parts.

The solution may be obtained by using either the direct (integration) method or the mode superposition method. The solution is a two-step procedure. The displacement pass, solves for nodal displacements at master degrees of freedom. The stress pass, resolves the solution to expand the desired frequency-point.

In this work, the reduced harmonic response analysis was used. This was achieved by defining a total of six master of degrees of freedoms at the cutting edge or the tool tip, and the base of the tip for three directions of x, y and z. as shown in Figure 6.8.

6.11 MODAL ANALYSIS

The mode-frequency analysis was used to extract the natural frequencies and mode shapes of the defined structure. Modal analysis is an important precursor to any dynamic analysis. The knowledge of the structure's modes and frequencies can be used to characterize its dynamic response. The results of this analyses also helps to determine the position on the tool most influenced by the successive flexure. This data may be used in determination of the most effective location on the bar for the application of constraint layer damping.

For the modal analysis, the program assumes free, undamped vibrations. The governing equation of this analyses is:

$$[M]\{\ddot{U}\} + [K]\{U\} = 0 \qquad (6.4)$$

Formulating as an eigen value, thus :

$$([K] - \omega^2[M])\{U\} = 0 \qquad (6.5)$$

Where

ω^2, is the square of natural frequencies

and eigen vectors {U}, represents the mode shapes.

Modal analysis is useful for any application in which the natural frequencies of a structure are of interest. For example, the natural frequencies of a cutting tool should be determined in order to produce a design that will prevent the component from vibrating at one its fundamental modes under operating conditions.

6.12 MODEL GENERATION IN ANSYS

In ANSYS, mesh generation may be performed by either: a) direct generation or, b) automatic generation. In direct generation, the designer makes use of standard ANSYS commands, such as N, FILL and NGEN to generate nodes and EGEN to generate elements. Automatic mesh generation in ANSYS uses solid modelling concepts to mesh portions of a model. A region once generated may be modified, or partially regenerated. The automatic mesh generation procedure may be used in conjunction with the direct generation procedure.

During the model generation, in particular using, direct generation, the designer may be forced to generate element of poor quality such as element with large twisting. In this case, triangular elements may offer a better solution. Triangular elements may also be employed for modelling transition regions between fine and coarse grids or for modelling irregular structures.

6.12.1 PARAMETRIC APPROACH IN ANSYS

After the mesh generation and submission of the model to the solution phase, the calculated results may be extracted and analyzed. In some cases, the analysis of the data may indicate that part or whole of the model is not of sufficient accuracy and therefore it should be modified and re-meshed. In other cases, the designer may need to

generate several models of similar geometry. In such cases, the global control features of the ANSYS program may be used to control the model generation based on specified variables and/or selected analysis criteria. The global controls may be used to control many aspects of the model such as mesh refinement and interrogation of the obtained results. To this end, these controls gives the designer the capability to run an analysis virtually automated. These features are known as parameters and repeat routines. The latter consist of macros, branching and user files. The combination of control features are :
a) parameters, b) branching, c) repeated functions and abbreviations, d) macros, e) user files and f) user routines.

The parametric approach can be adopted to minimize the effort needed to generate different models for different geometries. Figure 6.5 shows the cutting tool parameters.

The parametric approach was used in this investigation to conveniently perform calculations and to define the boundary conditions such as physical and material properties in the most convenient and sensible way for tool design.

PART II CUTTING TOOL MODEL GENERATION

6.13 METHOD OF TOOL GENERATION

In this work a finite element model of the definitive design of the cutting tool is described. The model was needed to examine the static and dynamic compliance of the tool and assembly with respect to design variations. The analysis of the results was used in adapting a definitive optimised configuration for the design and fabrication of the test specimen. Although with every design there is a limit on the stability performance the objective in this thesis has been taken to design for a L/D ratio of 11. This is designated in the results by abbreviation "def" . In order to investigate the behaviour of the

cutting tool assembly four types of model were used;

1) The assembly of tip and homogeneous solid shank ("**Solid Tool**")
2) The assembly of tip, and composite shank ("**Bonded Composite Tool**"). In this case, part of the inner volume of the shank is converted to a new material. The core fully occupies the inner volume of the hollow shank and are assumed bonded (merged).
3) The assembly of tip and hollow shank ("**Hollow Tool**").
4) The assembly of the tip, hollow shank and it's core ("**Inserted Composite Tool**"). In this case, the core is firmly held by the shank through interface elements.

The schematic diagrams of these tools are shown in Figure 6.6. In practice the shank would be clamped by some type of fixture. To simplify the model the tool shank was assumed to be fully constrained.

6.13.1 MASTER MODEL

The external profiles of the boring bar are assumed to be identical in the model. The main difference lies in the variation of the inner portion of the shank volume. Since the models have similar configurations a "master model" was generated which contains all the features of the other models. A flexible program was developed so that when the master model was generated it could be modified into one of the four configuration described above. Once the master model and the necessary routines were established, specific variation in the model were obtained simply by changing the required design parameter. The model can be modified for variations in materials, geometry and position of constraints (ie, L/D ratio).

The program was to analyze for the following variation:

1) material variation.

2) Real constant variation. A 'real constant' is data such as interface stiffness.

3) combining and/or deleting any of the components.

The elements and nodes are identified by their respective numbers, which also defines their position. Grouping into sets is made through the element numbering, included in the programming of the model generation. This was achieved by dividing the model into components or blocks that share the same material number and each group of elements can be brought under a distinctive name or set. The material type numbers also define their properties.

In ANSYS, the link between the block name and its respective property number can be established by the use of user files. The user files have the distinct name of the block and inside it a property parameter is defined. Therefore, whenever one of these user files is called it resets that property parameter to a specified number which can be used to select its respective element set. Other related types of link may also be included in such files. As an example, the user file named MTIP, where letter M indicates the material link and TIP indicates the tip,

```
MTIP
======================
*SET,MAT,3
*ABBR,MATT,*USE,STEL,3
/EOF
======================
```

As an example, this file sets the parameter named MAT 3 (ie, The 3rd material in the group). Then all elements having the material number 3 can be selected. Material properties are defined in a different user file, such as:

```
STEL
======================
EX,ARG1,200E+9     Elastic Modulus = 200 GPa.
GXY,ARG1,80E+9     Shear Modulus   = 80  GPa.
NUXY,ARG1,0.28     Possion Ratio   = 0.28
DENS,ARG1,7840     Density         = 7840 Kg/m³
/EOF
======================
```

The cutting tools are not symmetrical relative to any plane therefore the whole of the tool geometry had to be modelled. The modelling was further simplified by dividing the cutting tool into several regions, as shown in Figure 6.4. For the ease of identification these regions are named 'shank', 'tip','hole' and 'core'. This figure also shows the parametric geometrical variables for the cutting tool. Table 6.2 lists the material numbers and the material links used for these regions.

Figure 6.7 illustrates the cross section of the master model around the end of the hole before it is modified to an inserted tool model. On this figure, the numbers 1, 5 and 6 indicate the shank, hole and core material numbers which were used to identify each region. Therefore, during conversion of this intermediate model to its intended inserted tool material number 5 was used to delete elements constituting the 'hole' region.

Finally, the model was parametised to facilitate the variation of the tool lengths and sizes. Figure 6.8 illustrates examples of the cutting tool model geometry variations. In all the examined models, the geometry and material of the tip is the same. Figure 6.9 shows the model of the tip and part of the shank.

In order to simulate the secure grip of the holder, the interface of the shank with the holder was assumed to be fully constrained. To resemble the practical design the axial length of the constrained section was set at 4 times the diameter of the tool. Up to and including overhangs of 11 times the diameter the variations in the tool length were obtained by moving the position of the "clamping constraints" to achieve the required overhang. This is illustrated in

Figure 6.8. For the configuration of overhang above 11 times the diameter, the front section of the tool is extended to achieve the desired ratio.

6.14 SUMMARY

1) In this chapter the techniques developed for generating the finite element models of the cutting tool were explained.
2) The parametric approach was used to generated the cutting tool model.
3) The cutting tools were developed by:
   a) Combining the four models into a single 'master' model.
   b) The 'master' model was decomposed into a series of block elements and material link mechanisms were established for ease of components recognition, selection and modification during the model generation.

Tool Region	Material No.	Material Link
Tool shank	1	MSHK
Tip	3	MTIP
Hole	5	MHOL
Core	6	MCOR

Table 6.2 - Tool material (region) identification.

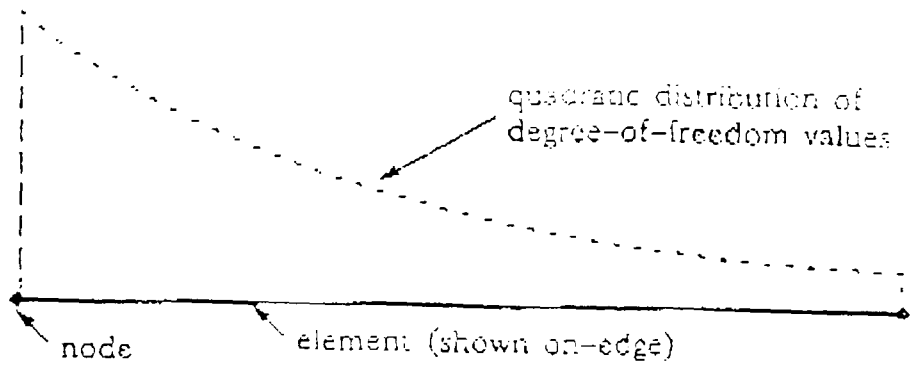

FIGURE 6.1a - ASSUMED QUADRATIC FUNCTION

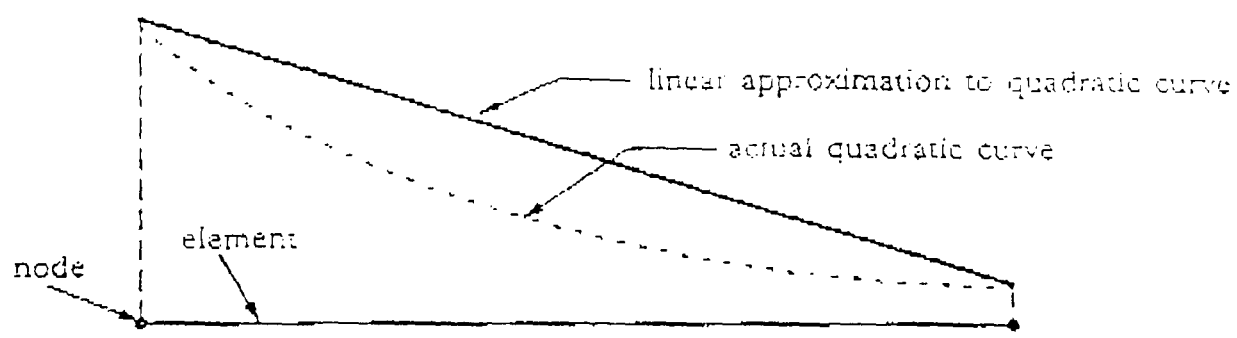

FIGURE 6.1b - LINEAR APPROXIMATION

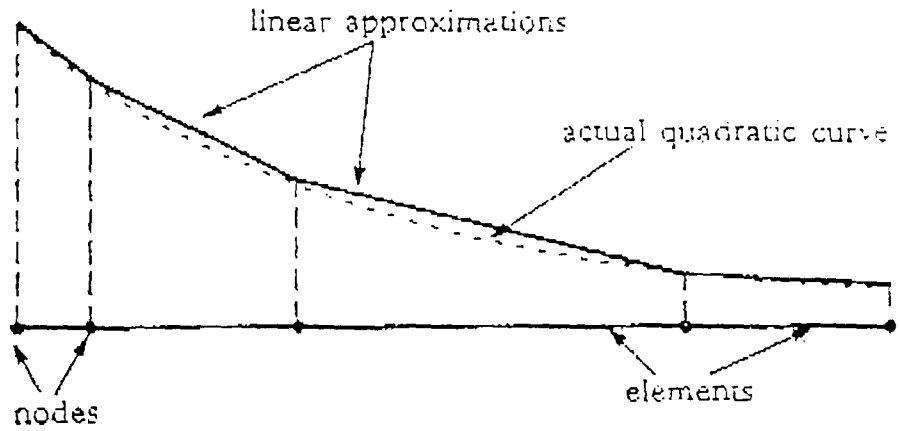

FIGURE 6.1c - SEVERAL LINEAR APPROXIMATION

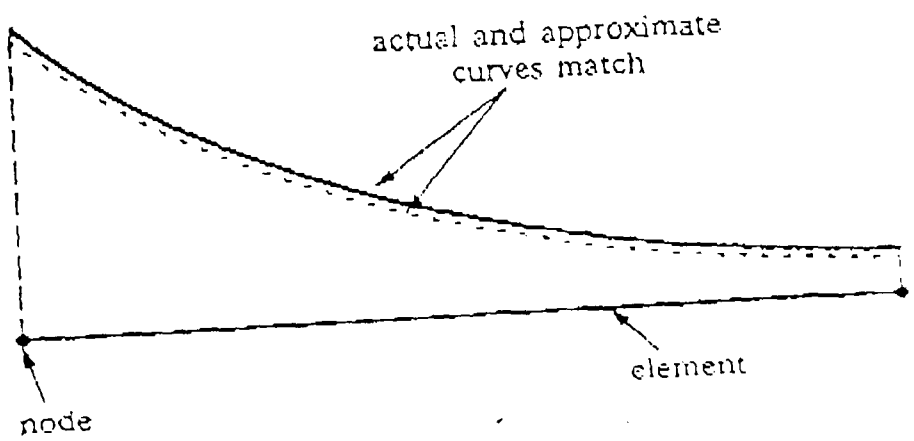

FIGURE 6.1d- ACTUAL SHAPE FUNCTION

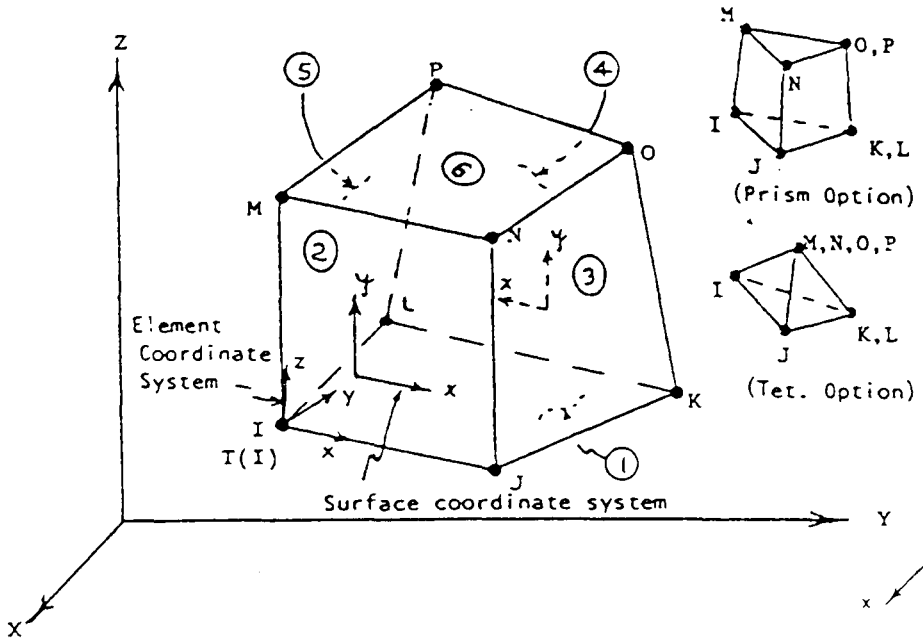

Figure 6.2 : - 3-Dimensional Isoparametric Stress Solid (STIF, 45)

-

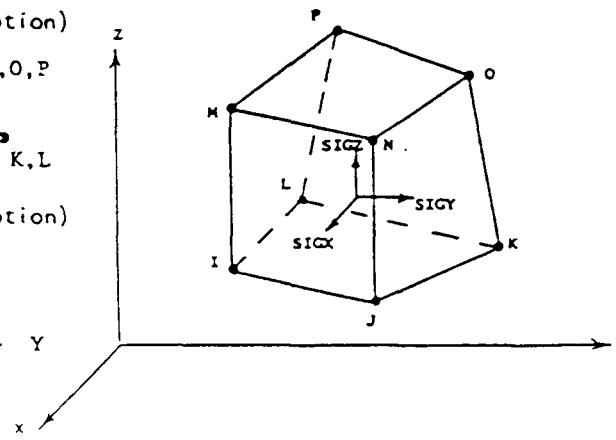

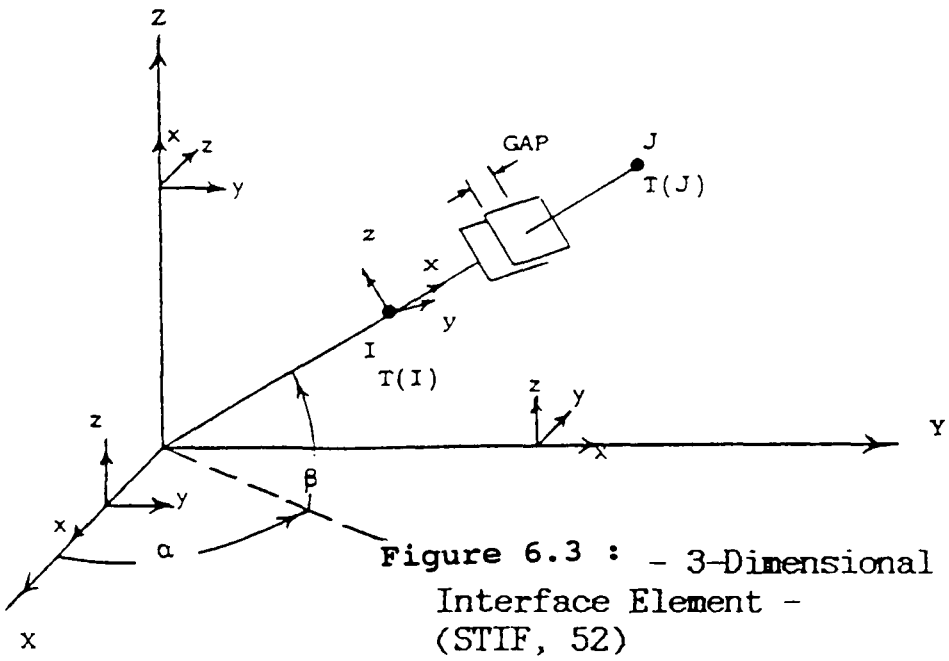

Figure 6.3 : - 3-Dimensional Interface Element - (STIF, 52)

-

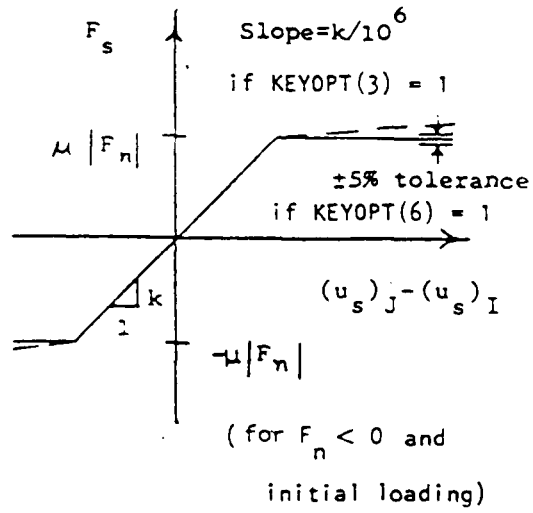

3-D Interface Output

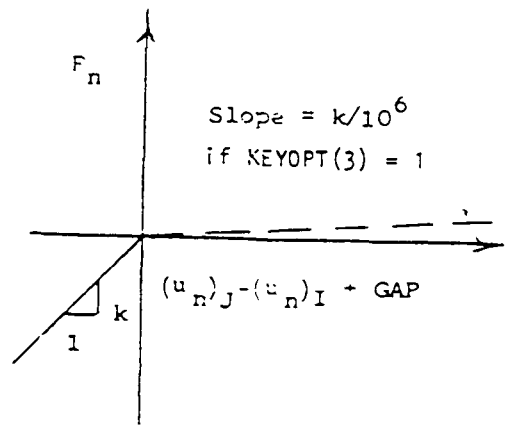

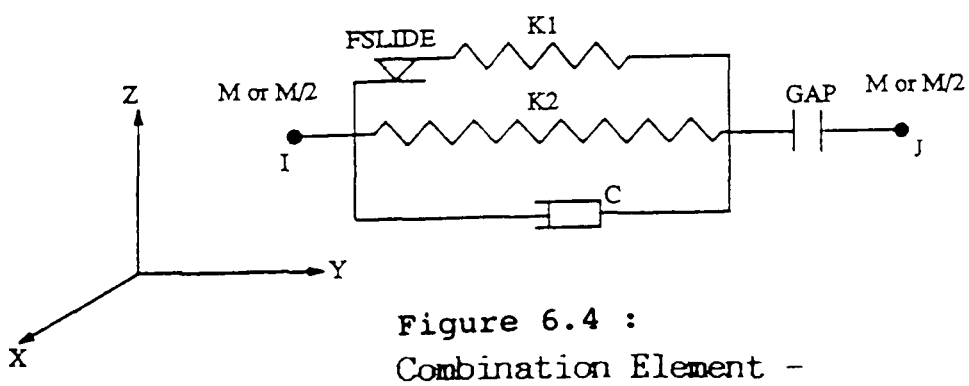

Figure 6.4 :
Combination Element - (STIF, 40)

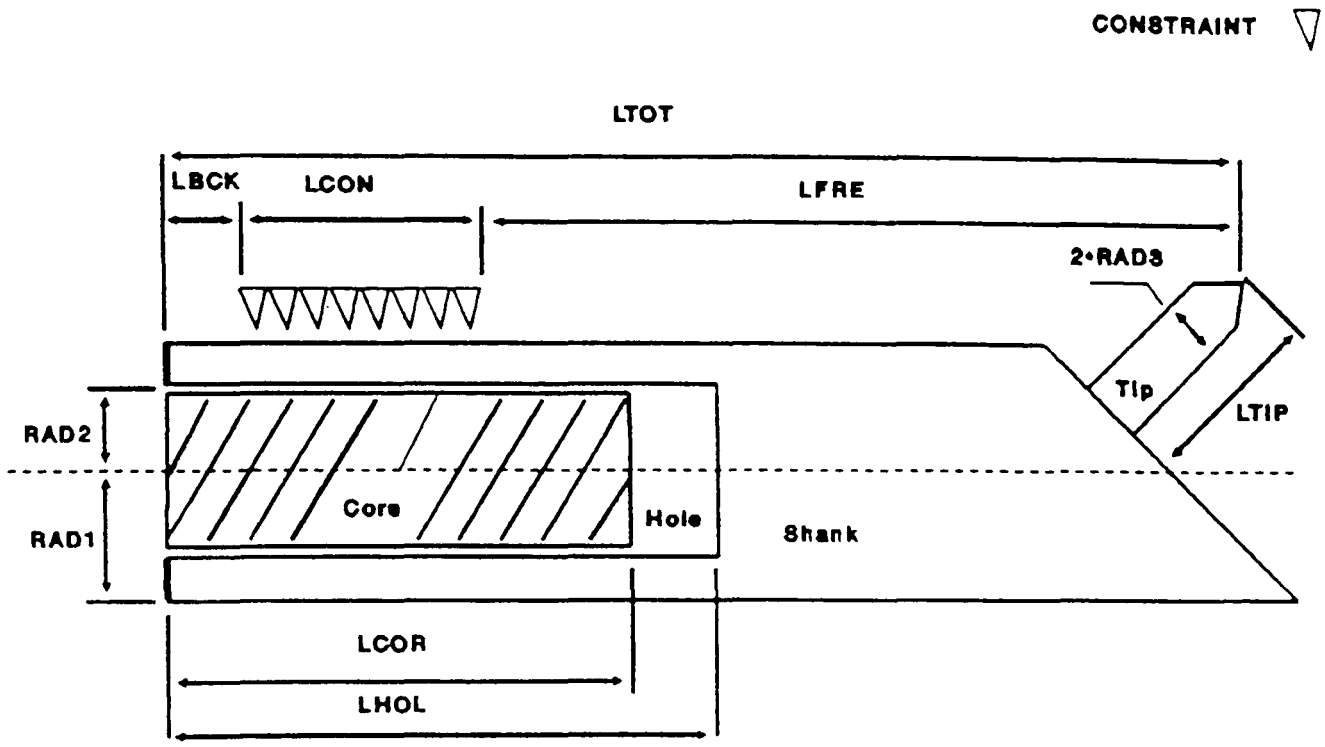

Figure 6.5 : - Geometrical Parameters of the Cutting Tool and Material Identification

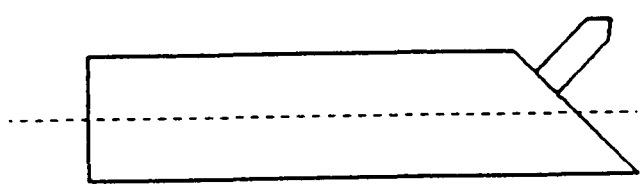

Figure 6.6.a - Model Number 1 (Solid Tool)

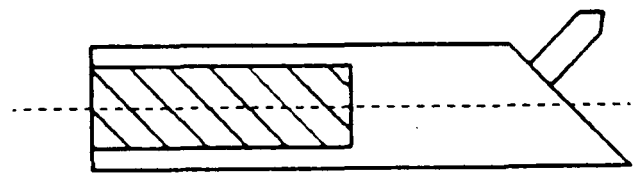

Figure 6.6.b - Model Number 2 (Composite Tool)

Figure 6.6 : - Schematic Diagrams of Different Types of Tools

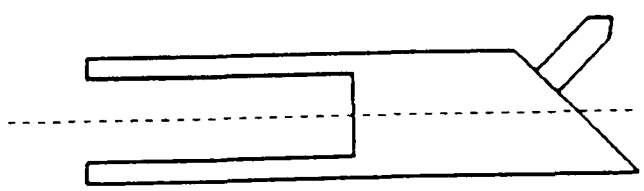

Figure 6.6.c - Model Number 3 (Hollow Tool)

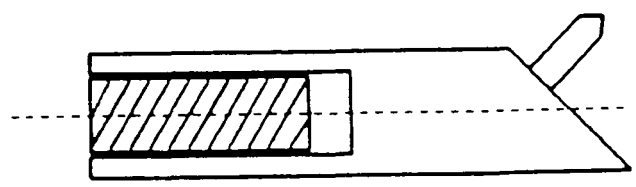

Figure 6.6.d - Model Number 4 (Inserted Tool)

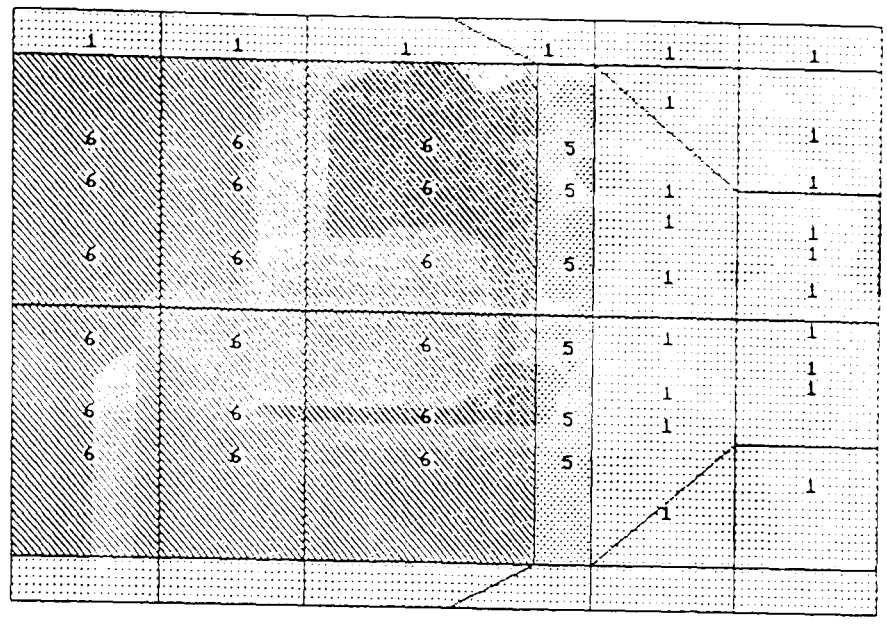

Figure 6.7 : – Cross–section of the Master Model Around the End of the Hole.

Figure 6.8.a – Overhang 8 Times the Radius

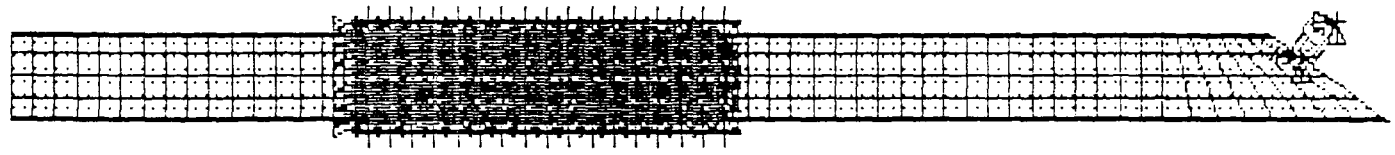

Figure 6.8.b – Overhang 14 Times the Radius

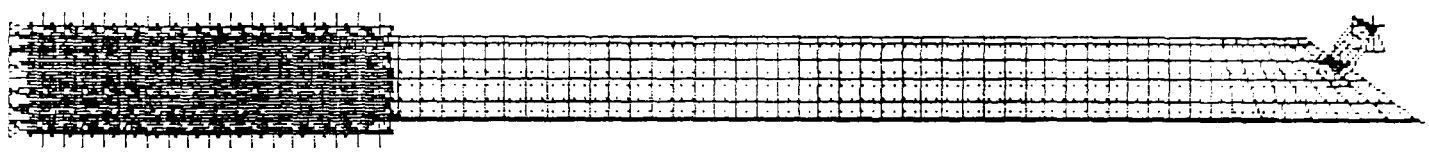

Figure 6.8.c – Overhang 22 Times the Radius

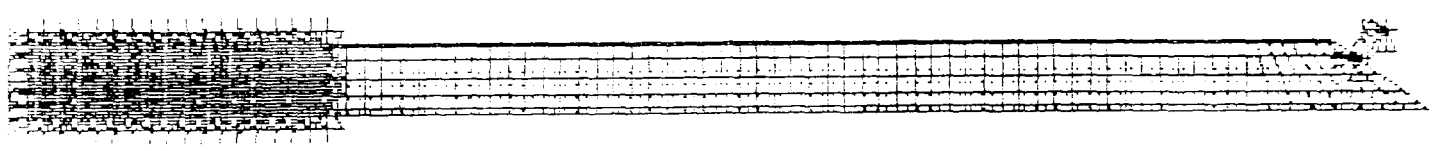

Figure 6.8.d – Overhang 30 "

Figure 6.8 : – Examples of the Model Geometry.

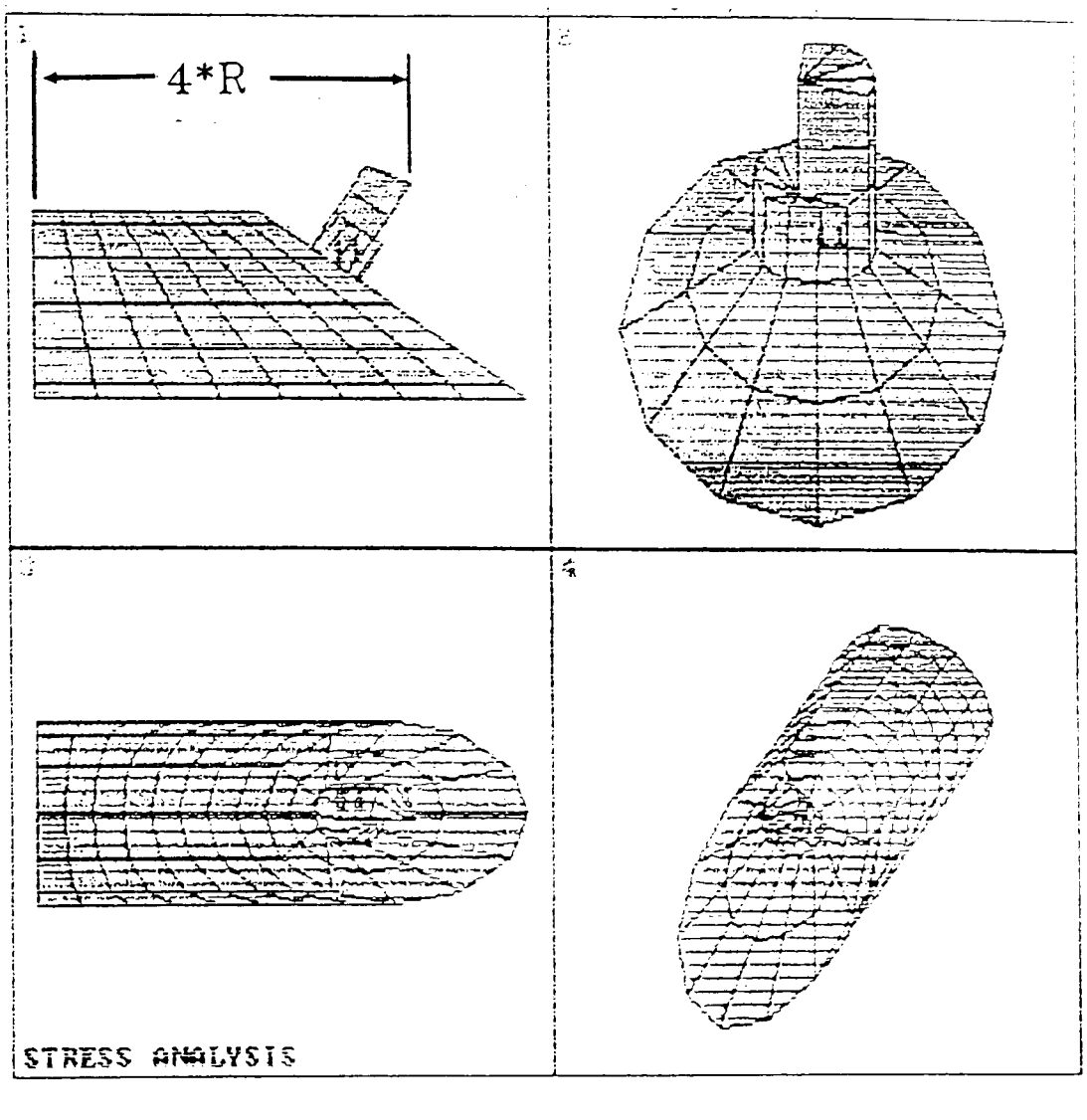

Figure 6.9 :

Finite Element Model of the Front of the Tool.

CHAPTER 7

COMPOSITE TOOL STATIC ANALYSIS

7.0 INTRODUCTION

In this section comparative analyses of combination boring bars with respect to the various factors of importance are presented. The analyses are based on comparative examination of tip deflections, strain energies and shank/core interface pressure.

The variation of the parameters for an optimised design are as follows :

a) Interference variation; the inserted steel tools having the same overhang and subjected to the same cutting force,

b) Cutting force variation with respect to default case,

c) Shank material variation with respect to default case,

d) Core material variation with respect to default case,

e) Core length variation with respect to default case,

f) Overhang variation for inserted steel tools subjected to the same cutting force and having the same level of shank/core interference.

The relevant design parameters of the combination boring bar are illustrated in Table 7.3. The tool with an overhang of 11 times the diameter is defined as the baseline tool and the inserted tool with this overhang and the force case number 16 (ie, 1500 N) is defined as the default case. For comparative analyses in the tables of results this case is highlighted by the abbreviate "def" . For the default case, the tip material was steel and the core was TC4 and the designed length of the TC4 core inside the shank is set at 60 % of the overhang length. For comparative analyses only one design parameter is changed every time.

7.1 THE FINITE ELEMENT MODEL

This study is confined to the examination of the inserted composite tool and a special case of the bonded composite tool. With the inserted composite tool the core and shank are joined together through interface elements. On the other hand, in the bonded composite tool the core and shank are bonded together with no relative movements between the core and shank.

The force components were categorised into three directional groups as listed in Table 7.1. The magnitude of the static forces were based on the practical results obtained from the primary experiments. The force variation analysis, was based on application of force cases 2, 11, 13, 16 and 18 .

Six shank materials, steel (STEL), Aluminium Alloy (ALAL), three type of combination boring bars with inserted Titanium Carbide composite (TC2, TC3, TC4) and Tungsten Carbide (TNGC) were examined. For the default case, the tip material was steel and core was TC4. The mechanical properties of these materials are listed in Table 7.2.

Throughout this analysis, the tip maintains the same geometry and material as the baseline tool (the baseline tool is the solid model with steel shank). Similarly, the radius and length of internal cavity remains constant to resemble more closely the physical model. The internal diameter of the cavity is set at 38 mm and the length of internal cavity designed for over 60% of the effective overhang was 8 times the external diameter to simulate a typical practical case.

In order to simulate a secure grip of the tool holder, the interface of the shank and mounting was assumed to be fully constrained. The axial length of the constrained section was kept to 4 times the diameter of the tool to resemble the tool mounting used for practical examination.

Up to and including L/D ratio of 11 times the diameter length variations were obtained by generating a single length tool (of total

length 15 times the diameter). By shifting the position of the "mounting" (constraints) the required tool overhang was achieved. This is graphically represented in Figure 7.1.

The degree of interference between the core and shank determines the respective interface pressure along the contact area. This was modelled by means of interface elements between the two contacting surfaces. A contact stiffness was assumed to correspond to an initial interference fit in order to ensure that the compliance of the connecting surfaces are always positive. When steady state is reached, the final local interference level is different from the initial interference level. This determines the local contact pressure. For simplicity, the minimum, maximum and average interference levels were determined for each case. Average interface pressure and interference levels are presented in Tables 7.4.c to 7.9.c. Figure 7.2, demonstrates an example of the FE model of the solid tool with the respective constraint and forces applied on the tool.

The cutting forces are assumed to be composed of static and dynamic components. The cylindricity of the finished workpiece is equated to the static component of the cutting force while the surface finish of the workpiece is related to the dynamic component of the cutting force. Up to the overhang of 4 times the diameter the core is not protruding into the overhang region while at L/D = 11 the radius (and above) the length of the back section is zero. The final average interference and average interface pressure were calculated for the entire length of the contact.

The strain energies are categorised into two main groups:

a) The strain energies stored in the solid elements of the tool.

b) The strain energy stored in the gap elements (shank-core interface).

The computed percentage contribution of the strain energies (solid, gap, shank and core) with respect to the total strain energy of

the system are tabulated in Tables 7.4.b to 7.9.b.

7.2 DATA ANALYSES OF THE DEFAULT CASE

The default case "def" is composed of a steel shank and the TC4 core with L/D ratio equal to 11. The initial interference between the shank and the core is equal to 84 micrometre, which resembles the practical values. This initial case is subjected to the force case number 16 (1500 N), which results in respective tip deflections of 1.173 mm, -1.031 mm and 0.129 mm along x (tangential), y (radial) and z (axial) directions respectively (negative values indicate direction).

Compared with the solid tool the result indicates that the tip deflections along x and y directions have reduced by 16.7% and 17.6% while along z has increased by 14%.

This demonstrate that the baseline inserted tool has a higher lateral stiffness than the baseline solid tool. The increased axial deflection can mainly be attributed to the poison effect resulting from the combined effect of the interface pressure on the inner and constraints on the outer surface of the shank. Figure 7.3 a and b shows the model of the baseline tool before and after the application of force. The example with the baseline tool showed that its final interference level would average 17.6 micrometre along its entire length. This level of interference resulted in an average compressive contact pressure of 502 mN/m^2.

The observation of the results on strain energies for the default case show that the strain energy contribution of the bar (953 W) is 67% of the total strain energy. And the strain energy contribution by the interface is (465 W) 33% of the total strain energy. The percentage contribution of the former can also be subdivided into shank (26%) and core (42%). These proportions indicate that the interface restrain

about one third of the total strain energy. Moreover, the strain energy of the tip is only 0.16% (2.3 W), indicating that the contribution of the tip is insignificant compared to the base of the tool.

Compared to the solid tool, the inserted tool shows a significant rise in the level of strain energies. This can be attributed to the existence of the pre-stressed condition along the shank-core interface. It also indicates that the distribution of strain energy in the inserted tools are different from the solid tool.

Figure 7.4, illustrates the strain energy distribution of baseline steel tool when subjected to the force case 16.

Figure 7.5 shows the change of the strain energy along the shank, Where A represents radii of zero "centre line" B and E are 1/3, C and F are 2/3 radius and D and G "surface" (see figure 7.5). Conclusively, The result demonstrate that the shank's strain energy distribution is:

a) Dependent upon the direction of forces.

b) Varies disproportionably across the shank (radially). The maximum is located on the surface and the minimum at the centre.

c) Varies disproportionably along the shank (axially), where the maximum is located near the holder.

Figure's 7.6 and 7.7, demonstrate the distribution and graduation of strain energy along the length of the inserted tool. The distribution plots along the axial cross section of the shank demonstrate that:

a) The strain energies are relatively constant for each section.

b) While under the envelope of the constraints the strain energy of the core are much higher than the shank.

c) In the unconstrained region the strain energies decay rapidly to reach their steady value. This decay occurs towards the fixed end of the tool as expected since maximum potential energies are concentrated at this region.

7.3 INITIAL INTERFERENCE VARIATION

The initial interference of the core and the shank was changed from 84 Micron to 64 and 104 micrometre. The results indicate that the initial interference level can significantly affect the final status of contact pressure. The effect of the interference variation showed that the average interface pressure and average interference level were changed by 119.5 MPa and 4.18 micrometer respectively, see Table 7.4.c.

Figure 7.8.a, illustrates that the interference level has little or no affect on the tip deflections along x and y directions while decreasing or increasing the initial interference level by 20 micrometre will decrease or increase the deflections along z direction (axial) by 5.7%, (see also Table 7.4.a). The former suggests that the interference variation does not change the lateral stiffness of the tool, while the later is due to the Poison effect resulting from the increased internal pressure in the shank.

The effect of variation in contact pressure causes the strain energies of both sections to change accordingly (For 64 micrometer : 554 Watt and for 104 micrometer: 1460 W). However, the proportionality of 67% and 33% with respect to strain energies remains constant. these results are tabulated in Table 7.4.b.

This relationship indicates that while the value of the average pressure is significant in determining the level of the strain energies it will not affect its distribution.

The interface pressure distribution may also depend on the other design parameters such as materials and the geometry of the workpiece, for example the length of the core. These factors will be examined in detail in the following sections.

7.4 FORCE VARIATION

Force variation analyses were used to examine the comparative displacement and respective effect on interface pressure variation.

Table 7.5.c and Figure 7.9 demonstrate that force variation has a negligible effect on the final interference or average compressive contact pressure level (502 MN/m^2).

The difference of 17.5% on the values of strain energies between the solid and inserted tool (ie, from 3.3 to 2.8) are considered to be due to variation on the static stiffness of the tool material, ie, for steel E = 200 GN/m^2 and for the TC4 core E=303 GN/m^2. This result illustrates the fact that the static stiffness of the baseline inserted tool is higher than the baseline solid tool.

Table 7.5.a demonstrates that changing the force case will increase the tip deflections by the respective force factor. The displacements display a linear relationship.

It is also interesting to note that although the static stiffness of the inserted tool is higher than the solid tool the axial deflections of the former is higher than the later. This can be attributed to the Poisson effect acting on the shank.

7.5 CORE MATERIAL VARIATION

In this analyses the geometrical configuration are similar to the "def" case and the design variable is the material of the inner casing of the tool.

Table 7.7 c, shows that changing the core material from TC4 to TNGC will increase the interface pressure by only 1.4 MN/m^2. Although this is insignificant, this rise is due to the small increase in the modulus of elasticity (TC4:303 GN/m^2, TNGC:305 GN/m^2) (see Table 7.7 b).

Table 7.7 a, demonstrates that increasing the modulus of elasticity of core from TC4 to TNGC will reduce all three tip deflections by less than 0.3 percent. These results demonstrate that a significant change in strain energies levels or tip deflections can only be achieved if the core's modulus of elasticity is significantly altered. However, in chapter eight it is shown that due to the high density of tungsten carbide the effective equivalent stiffness of such a configuration would be lower.

7.6 CORE LENGTH VARIATION

From the analyses of results, the influence of geometry and material on the level of interference and pressure between the core and the tool has been determined. In this analyses the effect of the variation of core length is examined.

Considering the default case and removing its TC4 core (ie, making it a hollow tool) reveals a total strain energy of 3.381 W. From Table 7.8 c and Figure 7.13 it is observed that more than 99% of this energy relates to the body of the tool and the remainder to the tip section. This is an important design parameter since the point of maximum energy concentration is the potential location for maximum stiffness and damping application point.

Figure 7.14, demonstrates the strain energy variation along the length of the hollow tool. Compared to the default case of the solid tool the hollow tool exhibits a 45 % higher total strain energy .

Introducing the TC4 core up to the full length of the constrained section will cause the strain energy in the interface to increase to 449 W. The distribution of strain energies when the core length is eight times the radius are shown in Figure 7.15. These results demonstrate that while the core is not protruding into the overhang region it will not increase the lateral stiffness of the shank hence,

the tip deflections along x or y directions will not change from that of the hollow tool.

Increasing the length of the core over the full designed length ie, 8 times the diameter will result to an average interference and pressure drop of 17.6 micrometre (40%) and 502 MPa (42.7%) respectively.

Figures 7.16 and 7.18, demonstrate that beyond the edge of the constraints the level of the strain energies decay very rapidly and they attain steady values. The average pressure of the unconstrained section also drops to 82.9% of the constrained section after a distance of twice the radius from the edge of the constraints. Increasing the core length also reduces the tip deflections along x, y and z directions, this is illustrated, in table 7.8.a.

These results indicate that the root portion of the bar has a dominating influence on its deflection at the tool end. On the other hand, the influence on deflection of the portion of the bar which is close to the tool head is minimal. Therefore, the TC4 core should be extended as far as the designed length of the overhang region for a compromised optimum solution.

The design was modelled for a special case when the core fully occupied the hole (insert length = depth of hole=16*R) with no relative movement between the two materials. Comparing this tool to the baseline inserted tool (core length = 15.8*R) revealed that the tip deflections along x, y and z reduced by 4%, 4.2% and 26.8% respectively. This result is of important value for the design, it shows the significance of the increased stiffness due to elimination of relative displacement of the core especially along z direction. Since the bar is modelled as a bonded composite case the increased stiffness along z direction is also attributed to the removal of internal pressure.

7.7 OVERHANG VARIATION

In this section, the effect of the overhang by progressive variation of the position of the constraints on the inserted tools are analyzed to determine the effect and significance of L/D ratio on the composite tool physical parameters.

Up to and including L/D ratio of 11 times the diameter, length variations were obtained by generating a single length tool and shifting the position of the constraints along the shank. For tools of overhang above 11 times the diameter the front section of the tool was extended to achieve the desired ratio.In this analysis, the depth of the hole and the length of the TC4 core were kept the same as the baseline inserted tool at 8 times the diameter.

From Table 7.9.c and Figure 7.19, it is observed that increasing the overhang length from 11 to 15 times the diameter, will not change the average interference (17.6 micrometre) or pressure (502 MN/m^2). Therefore, the interface strain energies also remains the same (465 W). This is because the optimum designed length of TC4 core was only modelled for L/D ratio of 11 times the diameter. However, It is interesting to note that the same overhang variation for the baseline solid tool resulted the total strain energy of the solid tool to increase by 156% . Knowing that the interface status has not changed, the difference can mainly be attributed to the substitution of the core of the tool material from the steel to TC4.

This level of overhang variation will subject the tool to an increase of tip deflections along x, y and z directions by 2.6, 2.7 and 1.7 fold. This result signifies the importance of reducing the L/D ratio as much as possible. Moreover, the tool which was designed and developed for practical examination may not be expected to perform much beyond the designed overhang ratio (11 times the diameter) without a proportional increase of the TC4 core length. Reducing the overhang to 8 times the diameter will reduce the protrusion of the core into the

overhang. The distribution and variation of strain energy along the tool when the length of overhang is 8 times the diameter is illustrate in Figure 7.20 and Figure 7.21.

At the overhang of 7 times the diameter, the front edge of the constraint section and the core are aligned with each other. This removes the edge loading at the front of the constraint section. Therefore, the average contact pressure drops to 483.6 MN/m^2 and, similarly, the solid portion and interface strain energies reduce to 910.6 W and 454.9 W or by 4.5 and 2.2 percent compared with the default case.

As far as the tip deflections are concerned, reducing the overhang to 7 times the diameter will reduce the tip deflections along x, y and z directions by 65.9, 69.2 and 64.7 percent, see Table 7.9.a.

7.8 SUMMARY

Increasing or decreasing the initial interference level by 20 micrometer will :

a) Cause the average contact pressure and average interference level to change by 119.5 MPa and 4.18 micrometre.

b) Has little or no affect on the tip deflections.

c) Cause the strain energies of both solid and interface to change while keeping their proportionality. (at 67.2 % and 32.8 % of total).

Taking the baseline inserted tool and varying the forces acting on the tip :

a) Had a negligible effect on the final interference or average pressure level (502 MN/m^2).

b) Did not changed the strain energy stored in the interface and increased the strain energy in solid elements by only 2.8 W

(0.29%).

Increasing the modulus of elasticity of the shank or core:

a) Reduces the tip deflections along x, y and z direction,

b) Increases the interface pressure,

c) Increases the strain energy of both solid elements and the gap,

d) Reduces the percentage strain energy contribution by the solid elements, and increases the percentage contribution of the gap,

e) A significant change in strain energies levels or tip deflections can only be achieved if the modulus of elasticity of either component is significantly altered.

Introducing the TC4 core up to the full designed length of the constrained section will :

a) Result in an average interface pressure of 876 MPa,

b) Cause the strain energy in the solids and interface to increase by about 100 W and 55 W for every unit length (radius) increase of the core,

Also :-

c) The bonded composite tool demonstrated a total strain energy of 1.51 W which is lower than the total strain energies of the baseline solid tool by 18.29%.

d) The bonded composite tool exhibited lower tip deflections, when compared with baseline inserted tool, by 4%, 4.2% and 26.8% along x, y and z directions.

Extending the length of overhang from 11 to 15 times the diameter :

a) Will not change the average interference (17.57 micron) or its average interface pressure (502 MN/m^2)

b) Will not change the interface strain energy (465.1 W), but increased the solid portion by only 2.6 W (0.27%),

c) It increased the tip deflections along x, y and z directions by 2.56, 2.68 and 1.73 folds,

Reducing the overhang from 11 to 8 times the radius will:

a) Increase the contact pressure by 5 MN/m^2 (1%)

b) Increase the strain energy of the shank and core by 0.66 and 1.52 percent,

In conclusion, the results of the static analyses indicate a marked improvement on the values of tip deflection for the combination boring bar compared to the solid tool and similar to that of tungsten carbide tool. Furthermore, the main factors for enhancing such tools at the design stage may be summarised as follows;

1) Greater static stability may be achieved by reduced L/D ratio.
2) The combination boring bar is most effective when the TC4 core protrudes up to maximum designed length (53.2% of the overhang length) and fully occupies the hollow shank with interference fit such that the tool may be assumed to be a bonded composite tool.
3) The locations of maximum strain energies must be used to incorporate high stiff materials.
4) The performance of every design can be estimated using this model preferably before fabrication.
5) If the dynamic components such as resonance frequencies are not of interest the tool with the highest static stiffness (solid TC4) will produce the best result.

NOTE;- The units of measure for strain energy values in ANSYS FE package are in Watt (W) which are the same as Joules/Second.

Force Case Number	Force Components on The Tip (N)		
	Fx (Tangential)	Fy (Radial)	Fz (Axial)
0	0	0	0
1	80	-80	-100
2	100	-100	-120
3	120	-120	-140
4	140	-140	-160
5	160	-160	-180
6	200	-200	-240
7	240	-230	-275
8	280	-290	-310
9	300	-300	-330
10	350	-350	-385
11	400	-400	-440
12	800	-800	-850
13	1000	-1000	-1050
14	1200	-1200	-1250
15	1400	-1400	-1490
16 (Def)	1500	-1500	-1600
17	1800	-1800	-1850
18	2000	-2000	-2050

Table 7.1 - Static Force Components and Case Numbers.

Material	Young's Modulus GN/M^2	Shear Modulus GN/M^2	Poison's Ratio	Density Kg/M^3
STEL *	200	80	0.28	7840
ALAL	70	27	0.33	2800
TC2	272.2	-	0.22	6560
TC3	294	-	0.22	5160
TC4	303	-	0.20	5132
TNGC	305	-	-	17500

* STEL = Steel (baseline material)
ALAL = Aluminum alloy
TC2, TC3, TC4 = Titanium Carbide composite type 2 to 4
TNGC = Tungsten Carbide

Table 7.2 - Material Property Table.

Design parameter	Value
Radius:	
Outer (R)	25.00 mm
Internal	19.00 mm
Length:	
Overhang	22* R
Hole	16.0*R
Core	15.8*R
Interface:	
Interference	84 Micron
Friction Coeff.	0.5
Gap Stiffness	5E+9 N/m^2
Material:	
Shank	Steel
Tip	Steel
Core	TC4

Table 7.3 - Inserted Tool Design Parameters.

Initial Interf. (Micron)	Tip Deflections (mm)		
	X (Tangential)	Y (Radial)	Z (Axial)
64	1.173	-1.031	1.217E-1
84	1.173	-1.031	1.291E-1
(Def) 104	1.173	-1.031	1.365E-1

Table 7.4.a - Tip Deflections for Various Interference Levels.(Inserted Tool)

Initial Interf. (Micron)	Strain Energy					
	Total Solid (W)	Total Gap (W)	Total solid %	Total gap %	Shank %	Core %
64	553.9	270.0	67.23	32.77	25.61	41.62
84	953.1	465.1	67.20	32.80	25.58	41.62
104	1460.0	713.0	67.19	32.81	25.57	41.62

Table 7.4.b - Strain Energy Distribution for Various shank/core interference levels.(Inserted Tool)

Initial Interference (Micron)	Contact Interference (Micron)			Contact Pressure (MN/m^2)
	Average	Maximum	Minimum	
64	-13.38	-23.79	-2.334	-382.5
84 **(Def)**	-17.57	-31.23	-3.081	-502.0
104	-21.75	-38.66	-3.828	-621.5

Table 7.4.c - Interface Pressure for Various Initial Shank/Core Interference Levels (Inserted Tool).

Force Case	Tip Deflections (mm)		
	X (Tangential)	Y (Radial)	Z (Axial)
2	7.807E-2	-6.769E-2	3.746E-2
11	3.127E-1	-2.739E-1	5.704E-2
13	7.823E-1	-6.886E-1	9.684E-2
16	1.173	-1.031	1.291E-1
(Def)	1.565	-1.381	1.635E-1
18			

Table 7.5.a - Tip Deflections for Various Force Cases.(Inserted Tool)

Force Case	Strain Energy					
	Total Solid (W)	Total Gap (W)	Total solid %	Total gap %	Shank %	Core %
2	951.5		67.17	32.83	25.55	
11	951.6		67.17	32.83	25.55	
13	952.2	465.1	67.18	32.82	25.56	41.62
16	953.1		67.20	32.80	25.58	
(Def)	954.3		67.23	32.77	25.61	
18						

Table 7.5.b - Strain Energy Distribution for Various Force Cases.(Inserted Tool)

Shank Material	Tip Deflections (mm)		
	X (Tangential)	Y (Radial)	Z (Axial)
ALAL	2.168	-1.886	2.269E-1
STEL	1.173	-1.031	1.291E-1
(Def)	9.773E-1	-8.586E-1	1.074E-1
TC2	9.327E-1	-8.194E-1	1.028E-1
TC3	9.157E-1	-8.043E-1	1.011E-1
TC4	9.120E-1	-8.011E-1	1.007E-1

Table 7.6.a - Tip Deflections for Various Shank Materials. (Inserted Tool)

Shank Material	Strain Energy					
	Total Solid (W)	Total Gap (W)	Total Solid %	Total Gap %	Shank %	Core %
ALAL	771.5	282.4	73.2	26.8	38.63	34.57
STEL	953.1	465.1	67.2	32.8	25.58	41.62
(Def)	1011	522.7	65.93	34.07	22.82	43.10
TC2	1026	535.0	65.73	34.27	22.40	43.32
TC3	1032	539.7	65.65	34.35	22.25	43.40
TC4	1033	540.7	65.64	34.36	22.22	43.42

Table 7.6.b - Strain Energy Distribution for Various Shank Materials.(Inserted Tool)

Shank Material	Contact Interference (Micron)			Contact Pressure (MN/m^2)
	Average	Maximum	Minimum	
ALAL	-13.03	-24.64	-1.25	-372.4
STEL	-17.57	-31.23	-3.08	-502.0
(Def)	-19.01	-32.92	-4.12	-543.1
TC2	-19.34	-33.24	-4.41	-552.7
TC3	-19.47	-33.37	-4.53	-556.4
TC4	-19.50	-33.39	-4.56	-557.2
TNGC				

Table 7.6.c - Interface Pressure for Various Shank Materials. (Inserted Tool)

Core Material	Tip Deflections (mm)		
	X (Tangential)	Y (Radial)	Z (Axial)
TC4 (Def)	1.173	-1.031	1.291E-1
TNGC	1.170	-1.028	1.289E-1

Table 7.7.a- Tip Deflections for Various core Materials.(Inserted Tool)

Core Material	Strain Energy					
	Total Solid (W)	Total Gap (W)	Total Solid %	Total Gap %	Shank %	Core %
TC4	953.1	465.1	67.2	32.8	25.58	41.62
(Def)	954.2	467.9	67.10	32.9	25.62	41.48

Table 7.7.b - Strain Energy Distribution for Various Core Materials.(Inserted Tool)

Core Material	Contact Interference (Micron)			Contact Pressure (MN/m^2)
	Average	Maximum	Minimum	
TC4 (Def)	-17.57	-31.23	-3.08	-502.0
TNGC	-17.62	-31.32	-3.08	-503.4

Table 7.7.c - Interface Pressure for Various Core Materials. (Inserted Tool)

Core Length (* Radius)	Tip Deflections (mm)		
	X (Tangential)	Y (Radial)	Z (Axial)
0 (Hollow)	2.472	-2.233	1.848E-1
4	2.472	-2.233	1.848E-1
8	2.461	-2.222	1.966E-1
10	2.111	-1.919	1.944E-1
12	1.733	-1.544	1.704E-1
14	1.431	-1.271	1.495E-1
15	1.307	-1.149	1.404E-1
15.8 (Def)	1.173	-1.031	1.291E-1
16 (Bonded)	1.126	-9.881E-1	9.400E-2

Table 7.8.a - Tip Deflections for Various Core Lengths.(Inserted Tool)

Core Length (* Radius)	Strain Energy					
	Total Solid (W)	Total Gap (W)	Total solid %	Total gap %	Shank %	Core %
(Hollow)	412	216.1	100	---	99.35	---
4	807	449.0	65.63	34.37	18.58	47.05
8	849	460.2	64.25	35.75	18.14	46.11
10	883	461.5	64.86	35.14	20.41	44.46
12	917	463.2	65.69	34.31	22.24	43.44
14	934	463.8	66.45	33.55	23.98	42.47
15	953	465.1	66.83	33.17	24.83	42.00
15.8 (Def)	1.51	---	67.20	32.80	25.58	41.62
			100	---	55.46	---

Table 7.8.b - Strain Energy distribution for Various Core Lengths.

Core Length (* Radius)	Contact Interference (Micron)			Contact Pressure (MN/m ^{2})
	Average	Maximum	Minimum	
0	---.	---	---	---
(Hollow)	-27.58	-31.03	-15.94	-875.5
4	-29.25	-31.23	-15.95	-876.8
8	-24.69	-31.23	-3.18	-731.5
10	-21.31	-31.23	-3.08	-626.3
12	-18.86	-31.23	-3.08	-551.2
14	-17.87	-31.23	-3.08	-521.2
15	-17.57	-31.23	-3.08	-502.0
15.8 (Def)	---	---	---	---
16 (Bonded)				

Table 7.8.c - Shank/Core Final Interference and Interface Pressure for Various Core Lengths.(Inserted Tool)

Tool Overhang (*Radius)	Tip Deflections (mm)		
	X (Tangential)	Y (Radial)	Z (Axial)
8	1.019E-1	-5.594E-2	1.455E-2
10	1.646E-1	-1.085E-1	2.226E-2
12	2.570E-1	-1.890E-1	3.203E-2
14	4.007E-1	-3.173E-1	4.555E-2
16	5.558E-1	-4.579E-1	8.725E-2
18	7.202E-1	-6.089E-1	9.955E-2
20	9.244E-1	-7.983E-1	1.136E-1
22 (Def)	1.173	-1.031	1.291E-1
24	1.525	-1.361	1.495E-1
26	1.944	-1.756	1.719E-1
28	2.436	-2.222	1.964E-1
30	3.007	-2.765	2.229E-1

Table 7.9.a - Tip Deflections for Various Tool Overhangs. (Inserted Tool)

Tool Overhang (*radius)	Strain Energy					
	Total Solid (W)	Total Gap (W)	Total solid %	Total gap %	Shank %	Core %
8	423.0	109.3	79.46	20.54	52.02	27.44
10	583.4	223.1	72.33	27.67	37.31	35.02
12	746.8	339.0	68.78	31.22	29.84	38.94
14	910.6	454.9	66.69	33.31	25.40	41.29
16	959.4	472.2	67.02	32.98	25.41	41.61
18	960.0	472.5	67.01	32.99	25.39	41.62
20	960.6	473.1	67.00	33.00	25.36	41.64
22 (Def)	953.1	465.1	67.20	32.80	25.58	41.62
24	953.6	465.1	67.21	32.79	25.60	41.61
26	954.2	465.1	67.23	32.77	25.62	41.61
28	954.9	465.1	67.24	32.76	25.64	41.60
30	955.7	465.1	67.26	32.74	25.67	41.59

Table 7.9.b - Strain Energy Distribution for Various Tool Overhangs.

Tool Overhang (* Radius)	Contact Interference (Micron)			Contact Pressure (MN/m^2)
	Average	Maximum	Minimum	
8	-6.597	-33.72	-1.566	-188.5
10	-9.998	-34.97	-1.563	-285.7
12	-13.46	-35.05	-1.561	-384.6
14	-16.92	-35.08	-1.557	-483.6
16	-17.74	-31.21	-1.553	-507.0
18	-17.75	-31.21	-1.546	-507.2
20	-17.76	-31.21	-1.521	-507.5
22 **(Def)**	-17.57	-31.23	-3.081	-502.0
24	-17.57	-31.23	-3.076	-502.0
26	-17.57	-31.23	-3.071	-502.0
28	-17.57	-31.23	-3.066	-502.0
30	-17.57	-31.23	-3.060	-502.0

Table 7.9.c - Interface Pressure for Various Tool Overhangs.

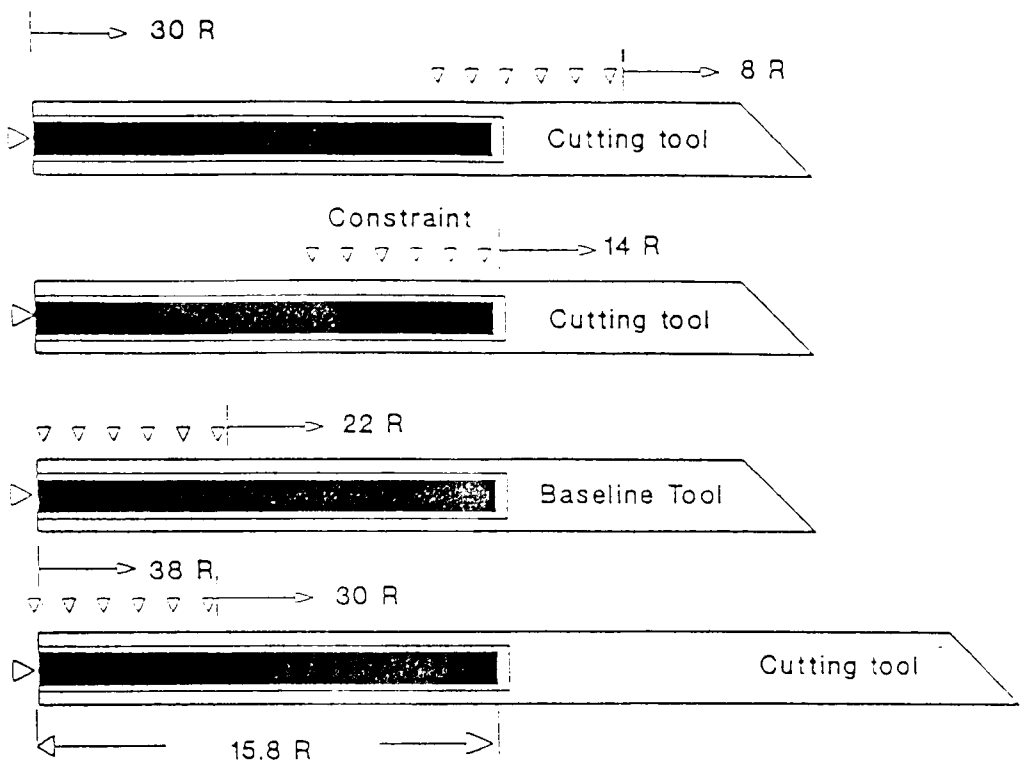

Figure 7.1
Schematic Diagram of Overhang
Variation (Inserted Tool).

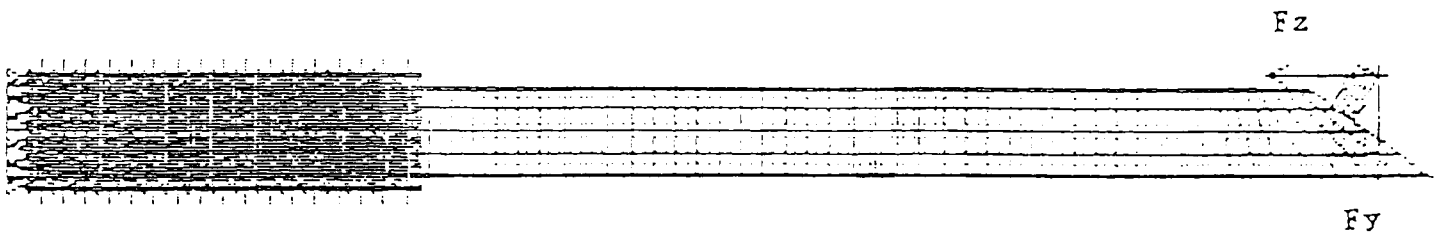

Figure 7.2 -
Finite Element Model of the
Baseline Solid Tool.

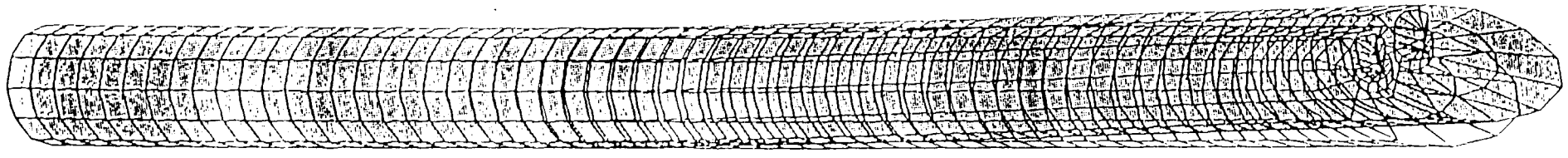

Figure 7.3 a Solid Tool Displacement Plot.(Fcase=16)

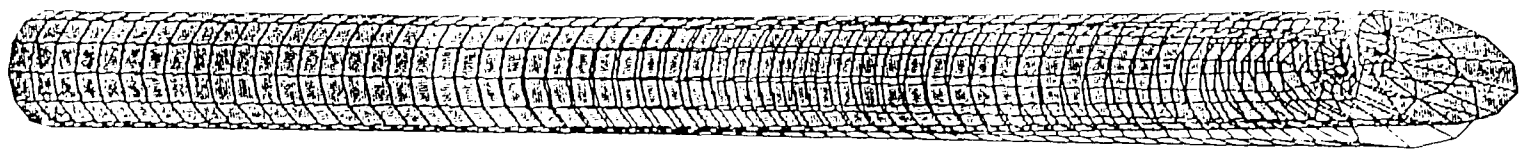

Figure 7.3 b -
Baseline Inserted Tool
Displacement Plot.
(Fcase=16)

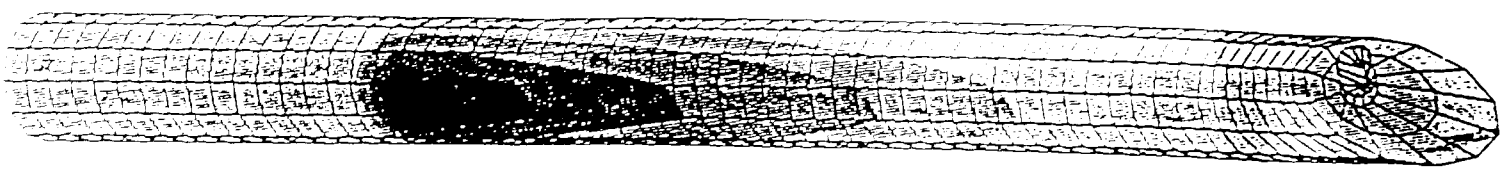

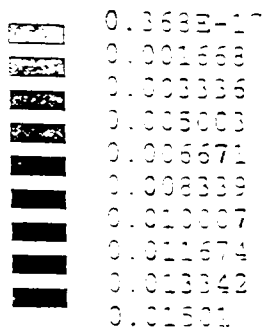

Figure 7.4 -
Strain Energy Distribution
of Baseline Tool.
(Solid Tool, Fcase=16)

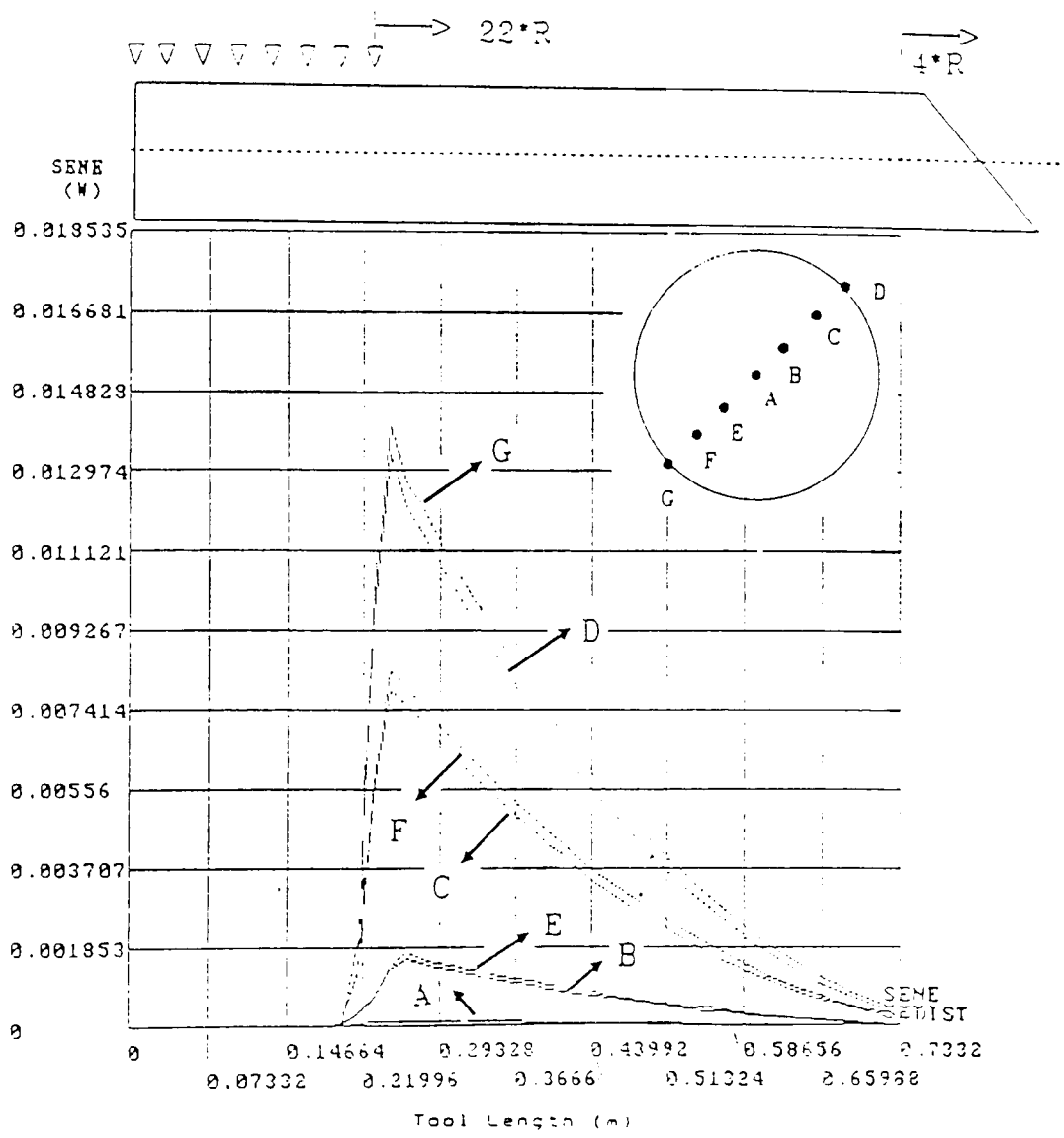

Figure 7.5 -
Strain Energy graduation
along the Baseline Tool.
(Solid Tool, Fcase=16)

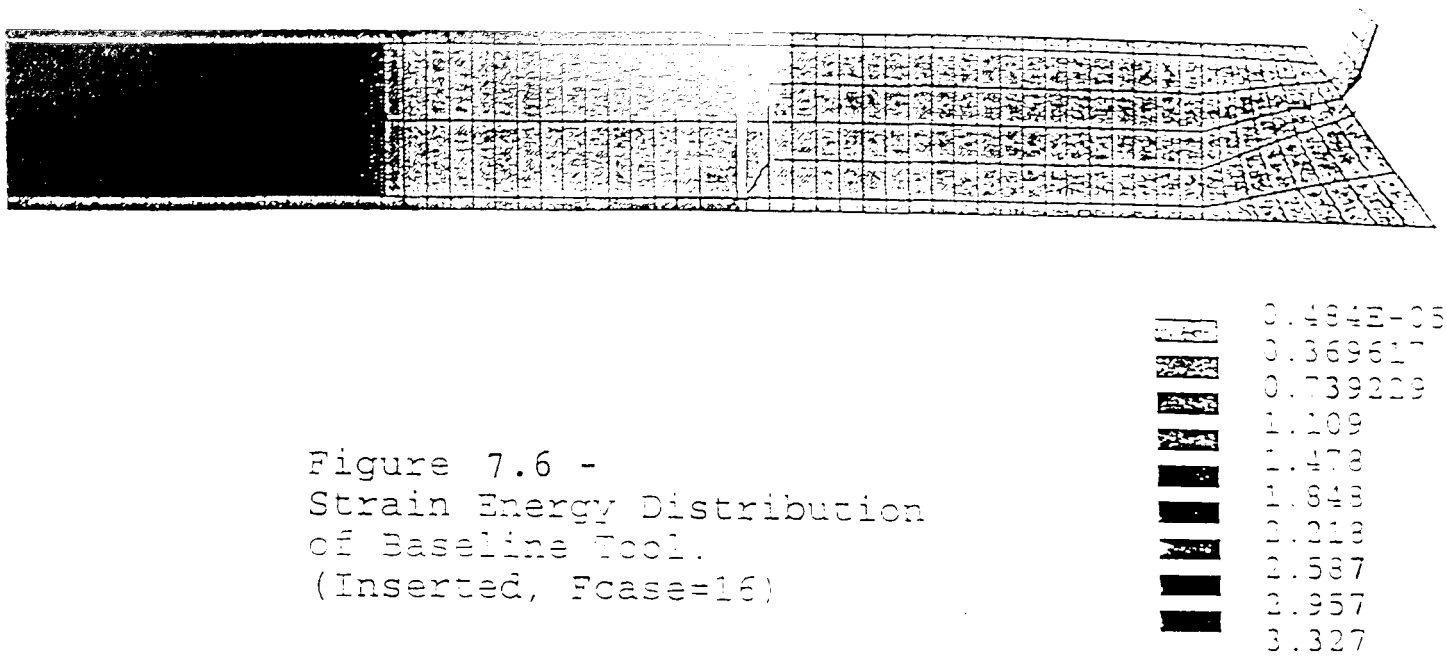

Figure 7.6 -
Strain Energy Distribution
of Baseline Tool.
(Inserted, Fcase=16)

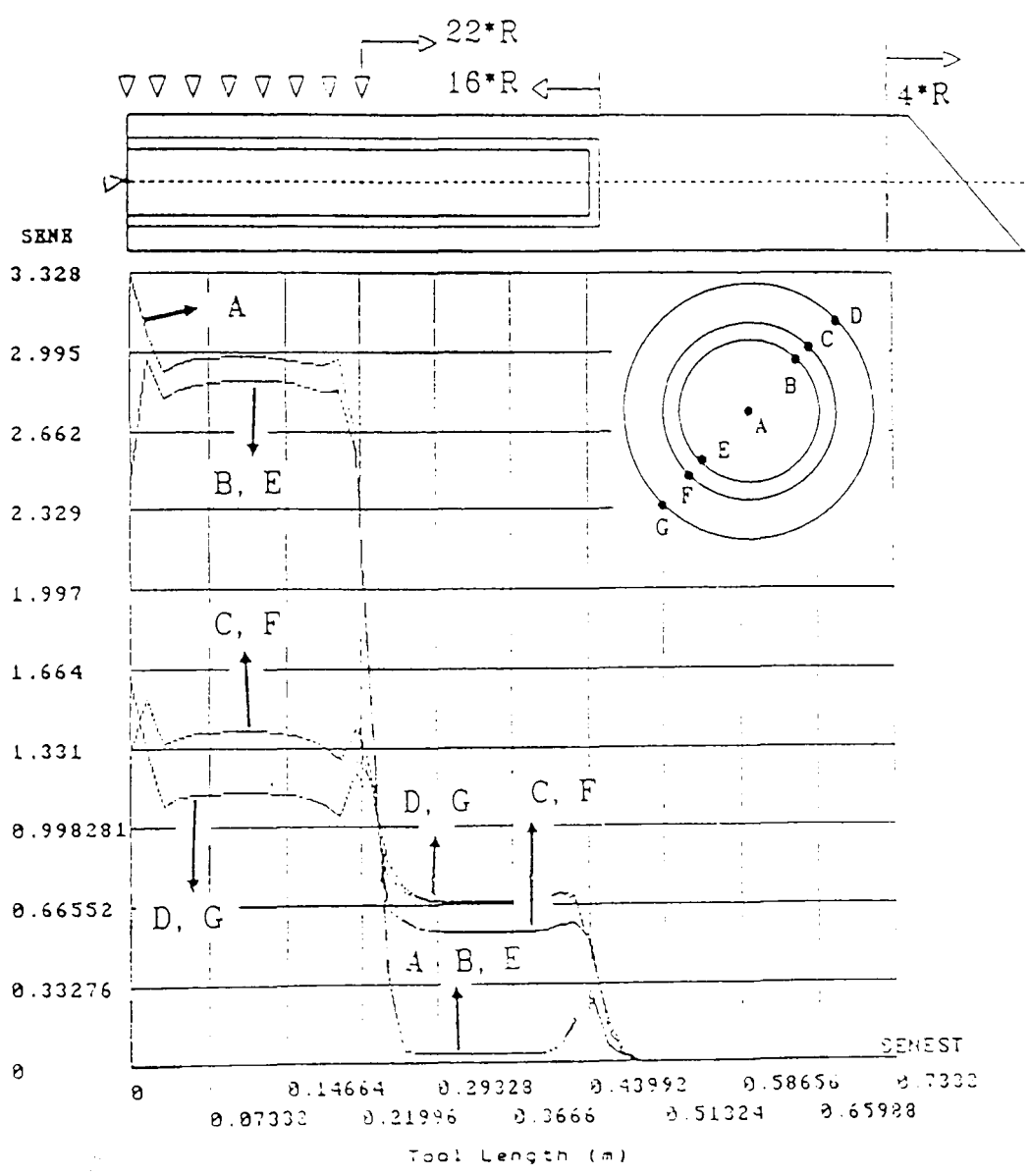

Figure 7.7 -
Strain Energy graduation
along the Baseline Tool.
(Inserted, Fcase=16)

Figure 7.8a Tip Deflections

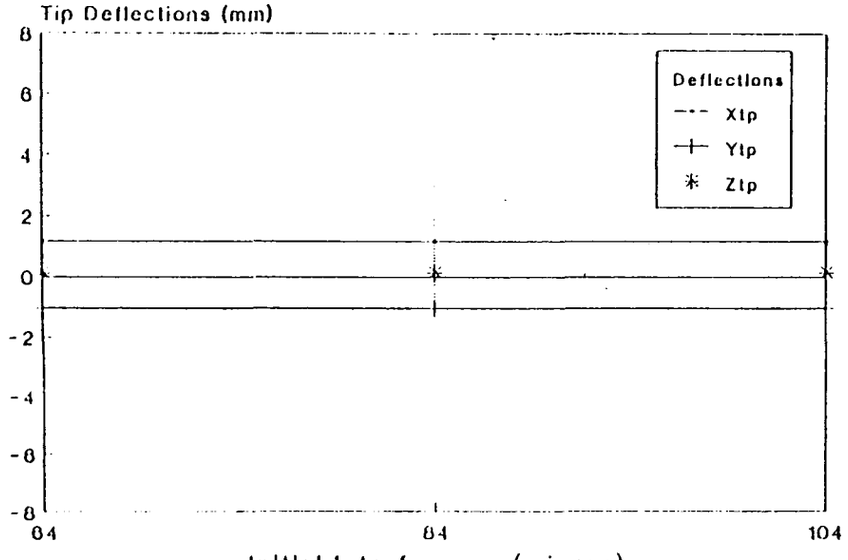

Figure 7.8b Strain Energy

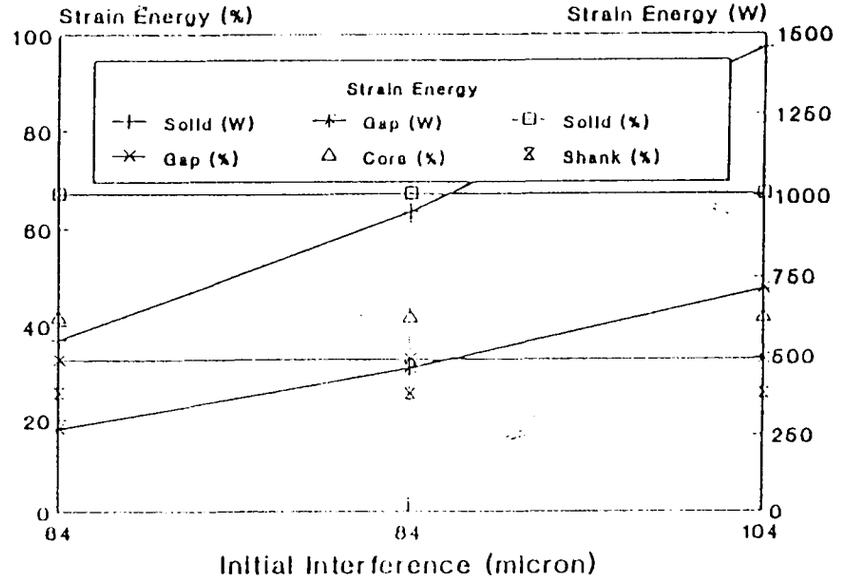

Figure 7.8c Interface

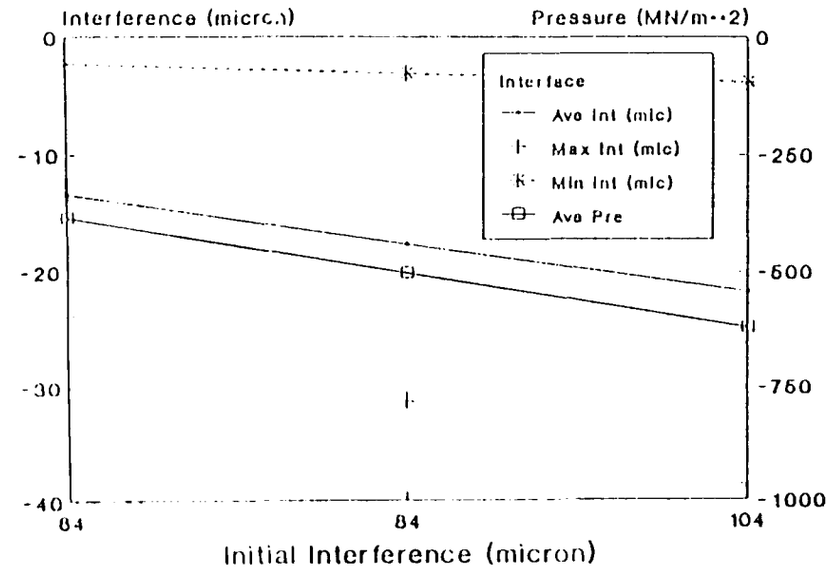

Effect of Initial Interference Variation. (Inserted Tool).

Figure 7.9a - Tip Deflections

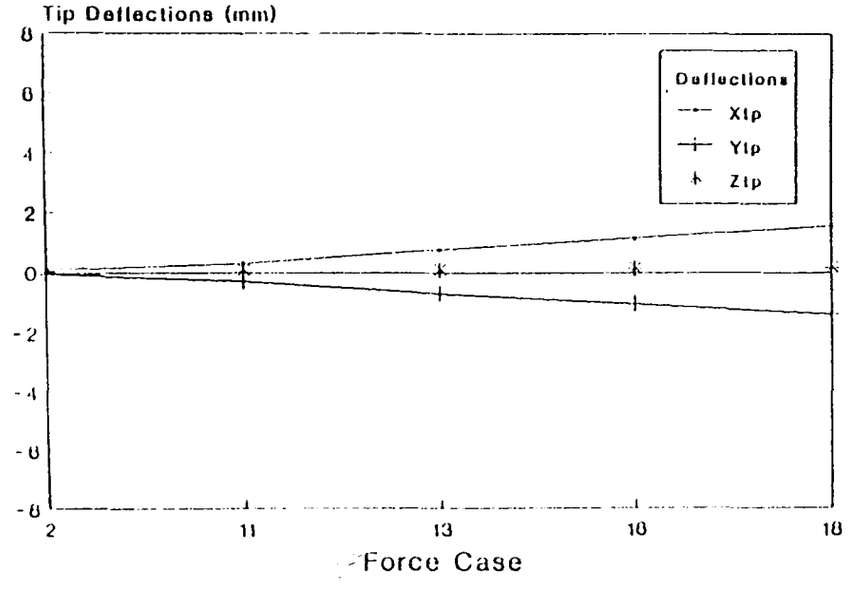

Figure 7.9b - Strain Energy

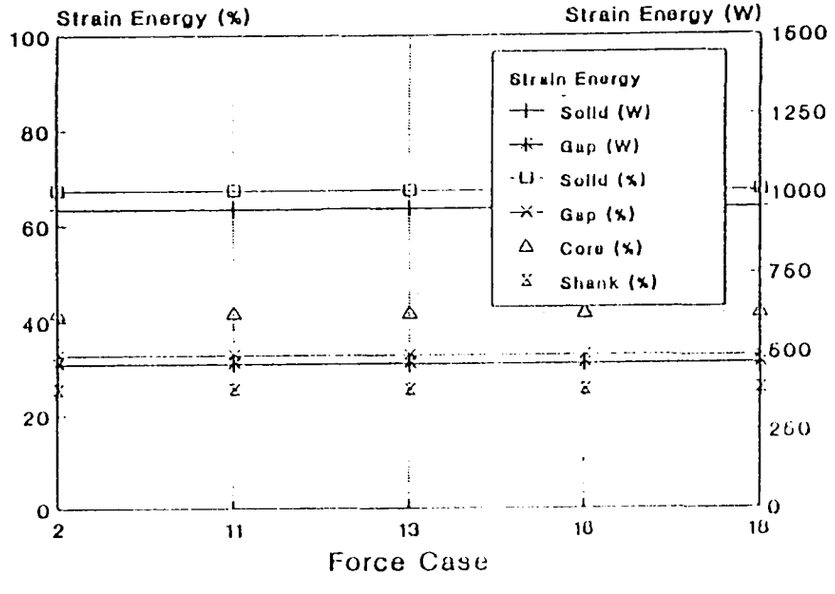

Figure 7.9c - Interface

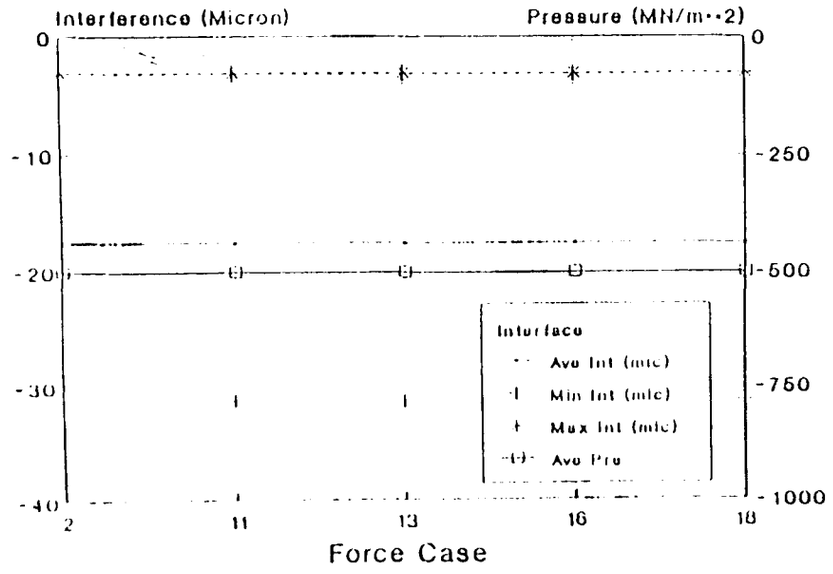

Effect of Force Variation.
(Inserted Tool).

Figure 7.10a· Tip Deflections

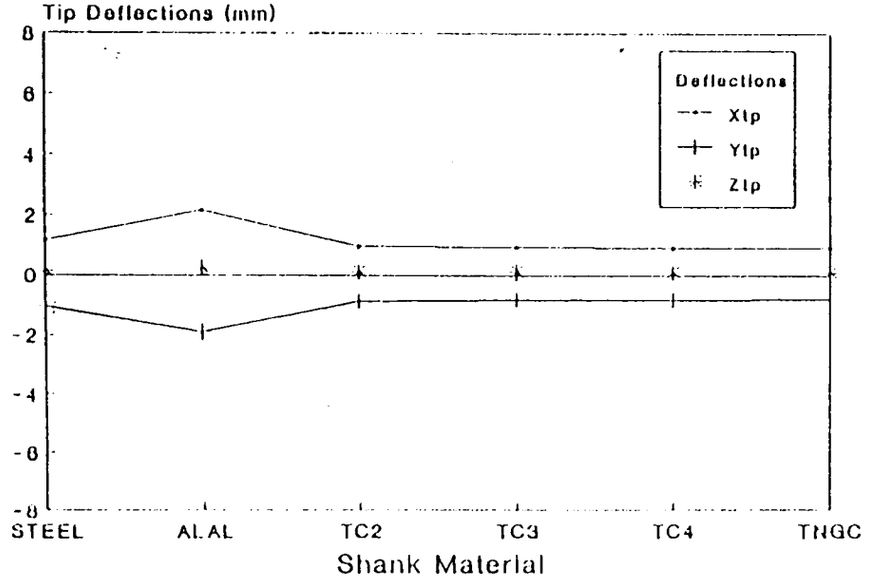

Figure 7.10b Strain Energy

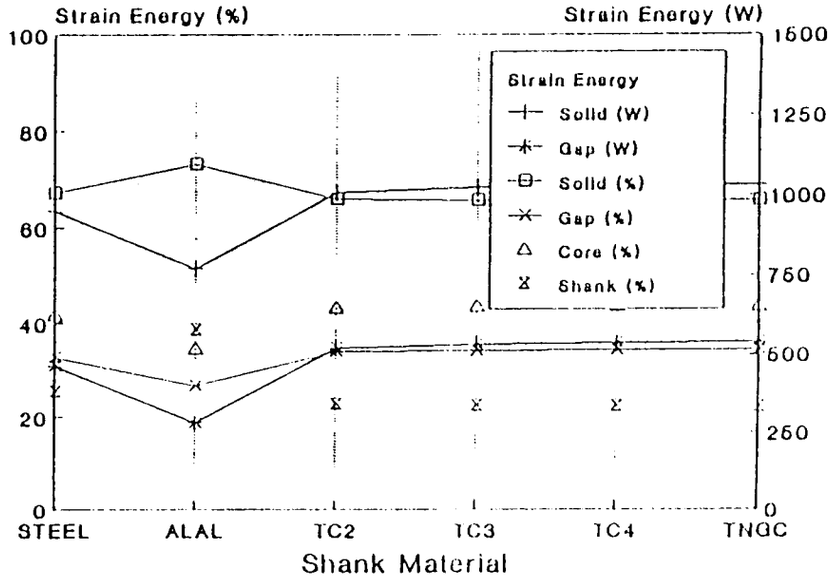

Figure 7.10c- Interface

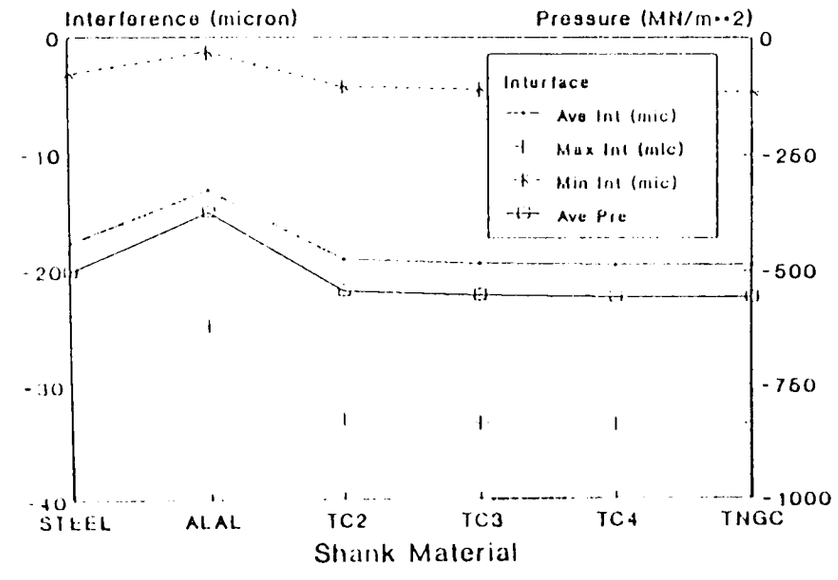

Effect of Shank Material Variation.(Inserted Tool).

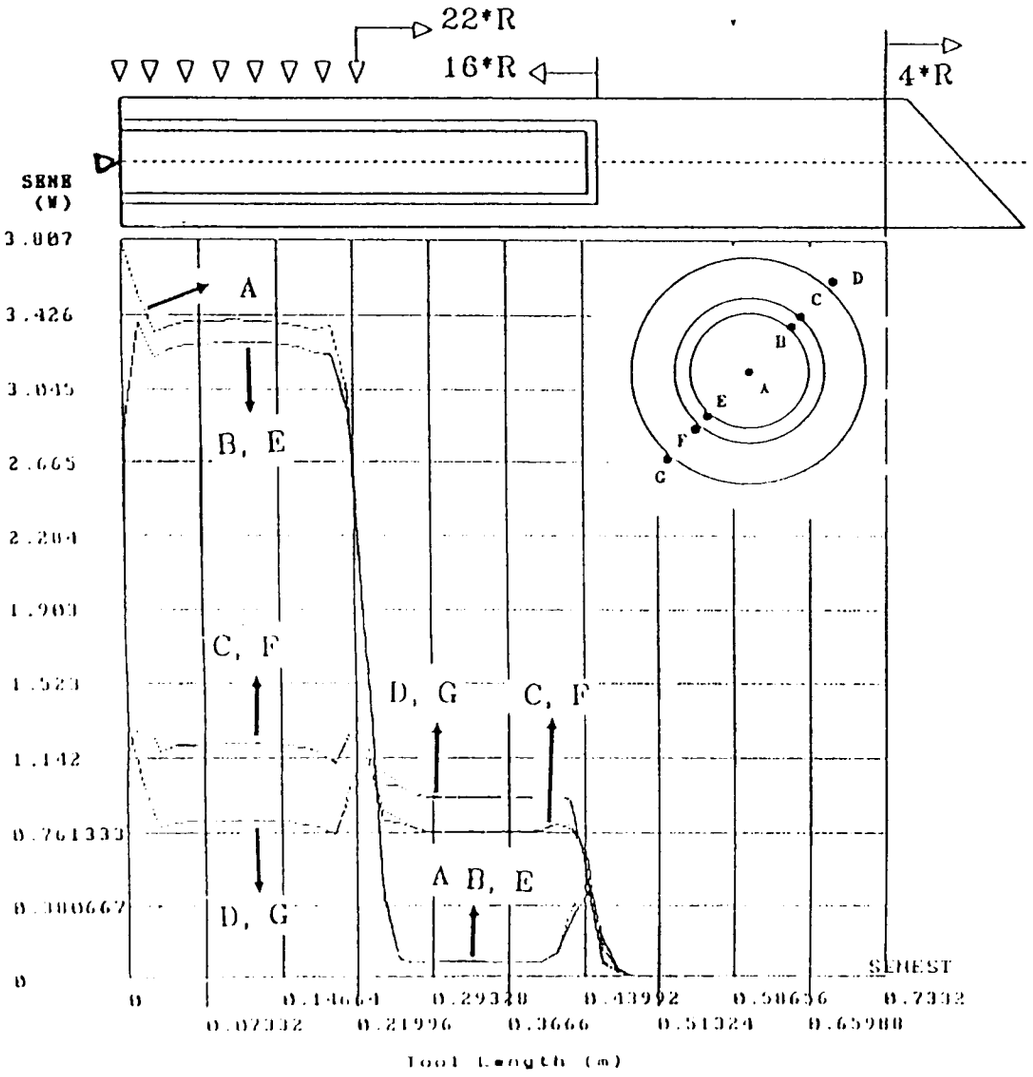

Figure 7.12 -
Strain Energy graduation
along the TNGC Tool.
(Inserted, Fcase=16)

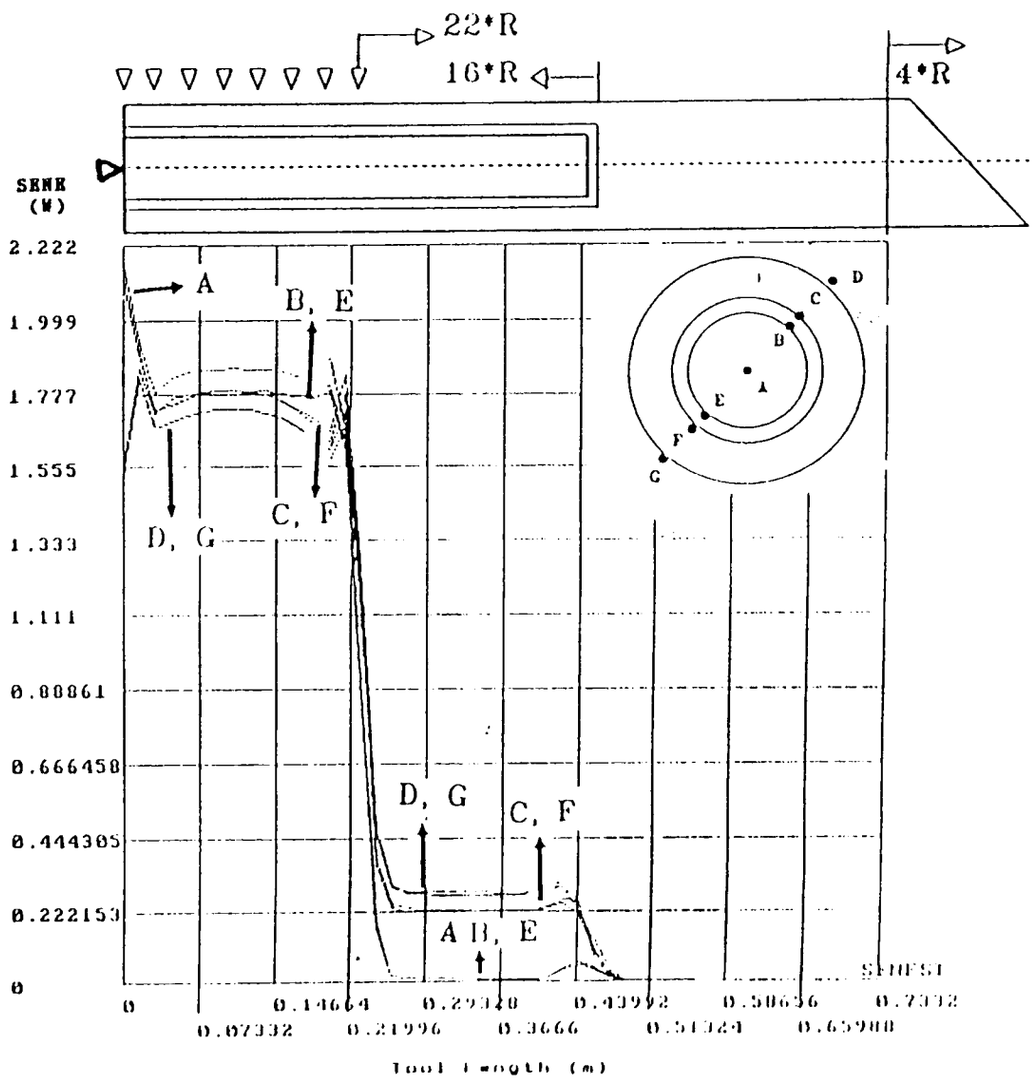

Figure 7.11 -
Strain Energy graduation
along the ALAL Tool.
(Inserted, Fcase=16)

Figure 7.13a Tip Deflections

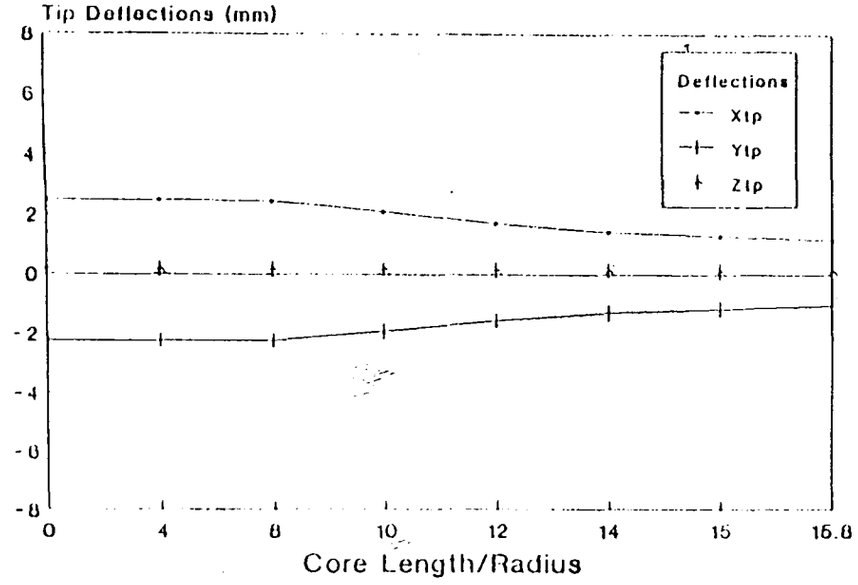

Figure 7.13b Strain Energy

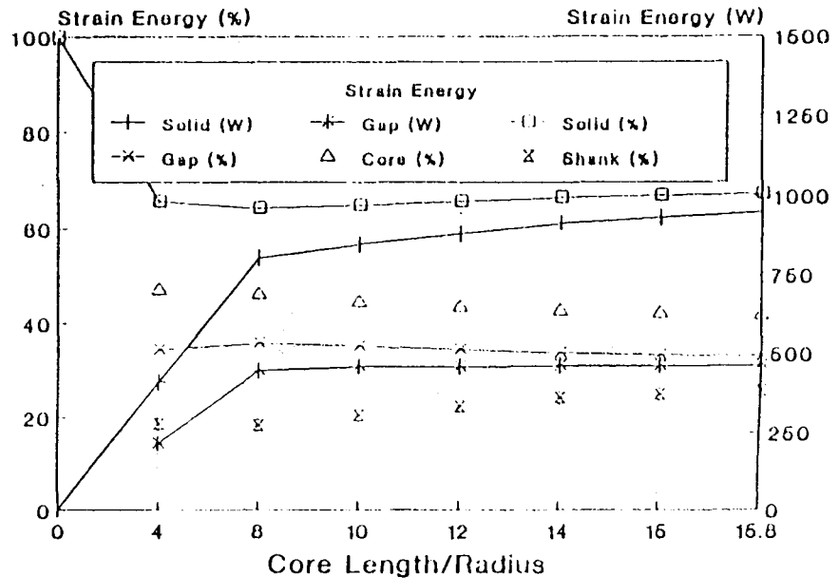

Figure 7.13c Interface

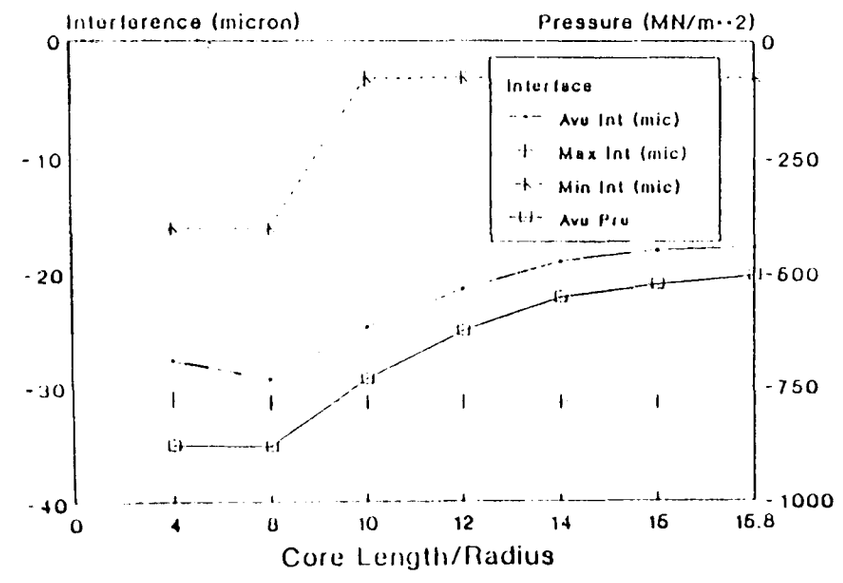

Effect of Core Length Variation.
(Inserted Tool, Pcase=16).

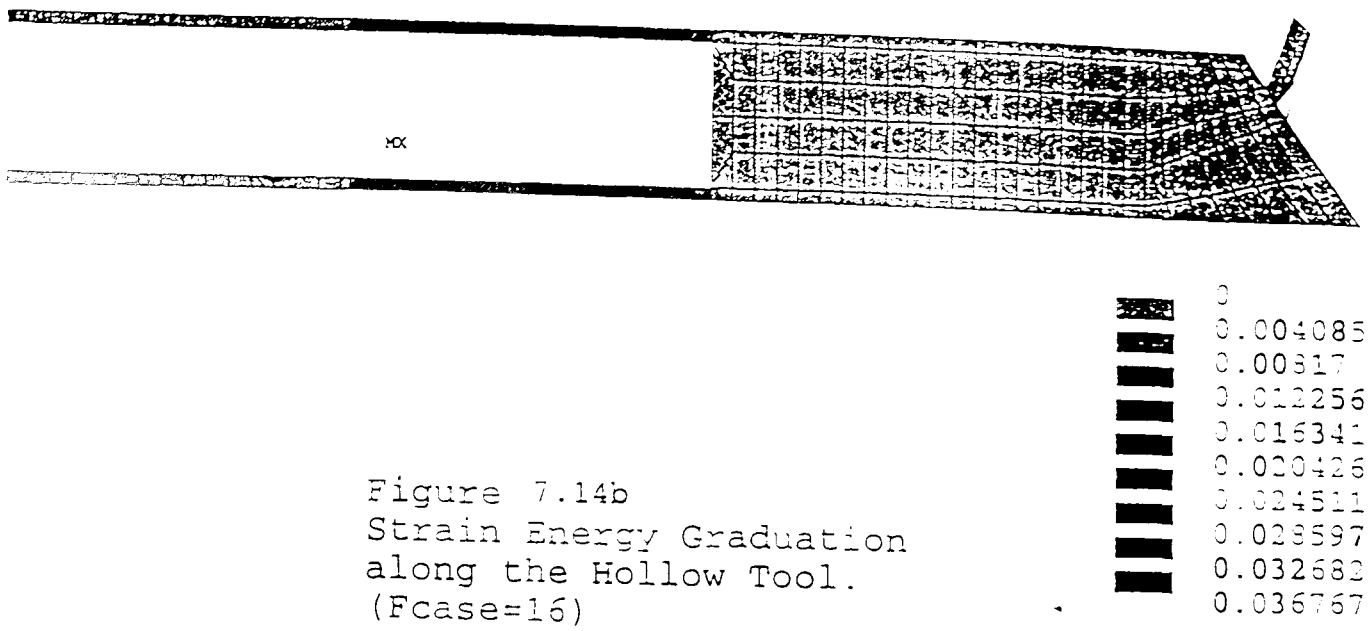

Figure 7.14b
Strain Energy Graduation
along the Hollow Tool.
(Fcase=16)

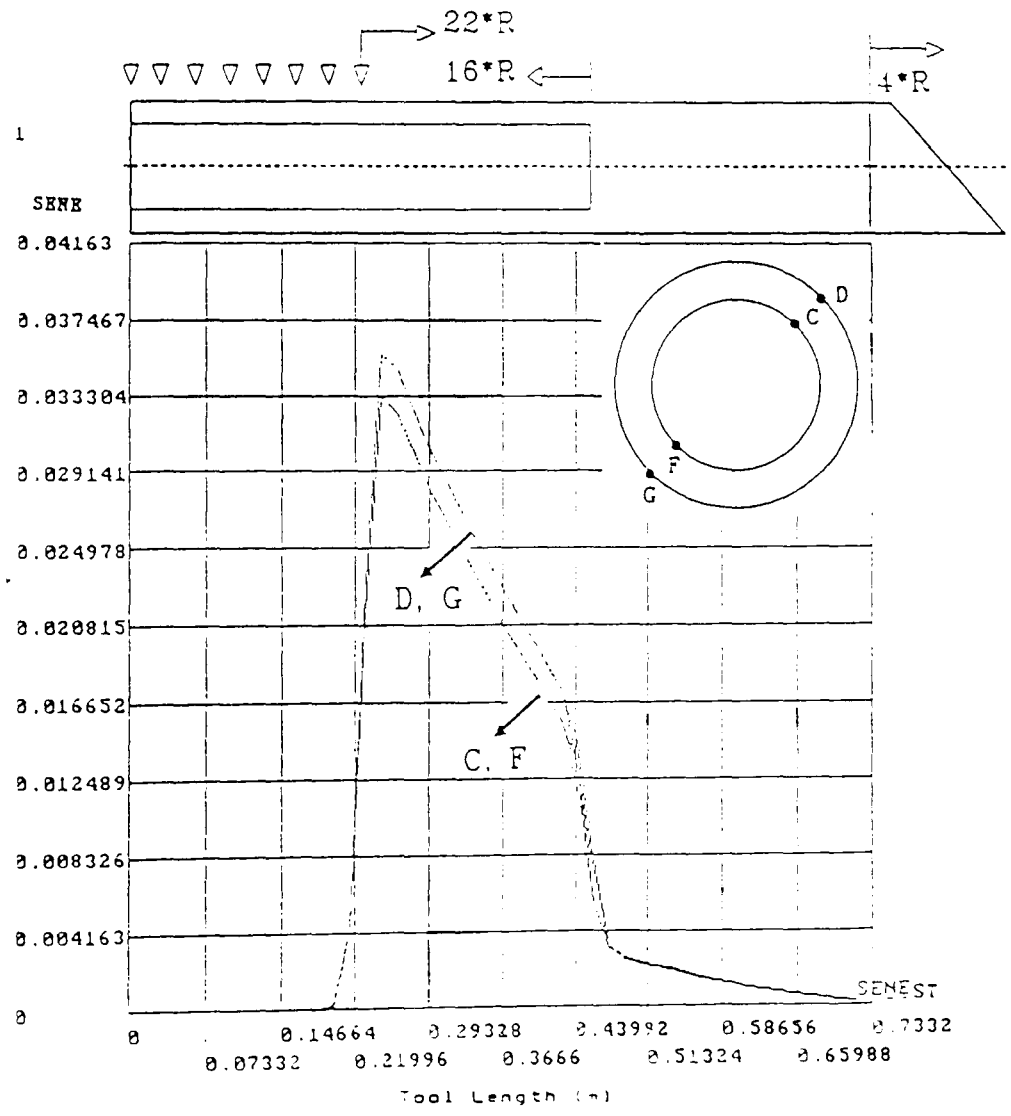

Figure 7.14a
Hollow Tool Strain Energy
Distribution.(Fcase=16)

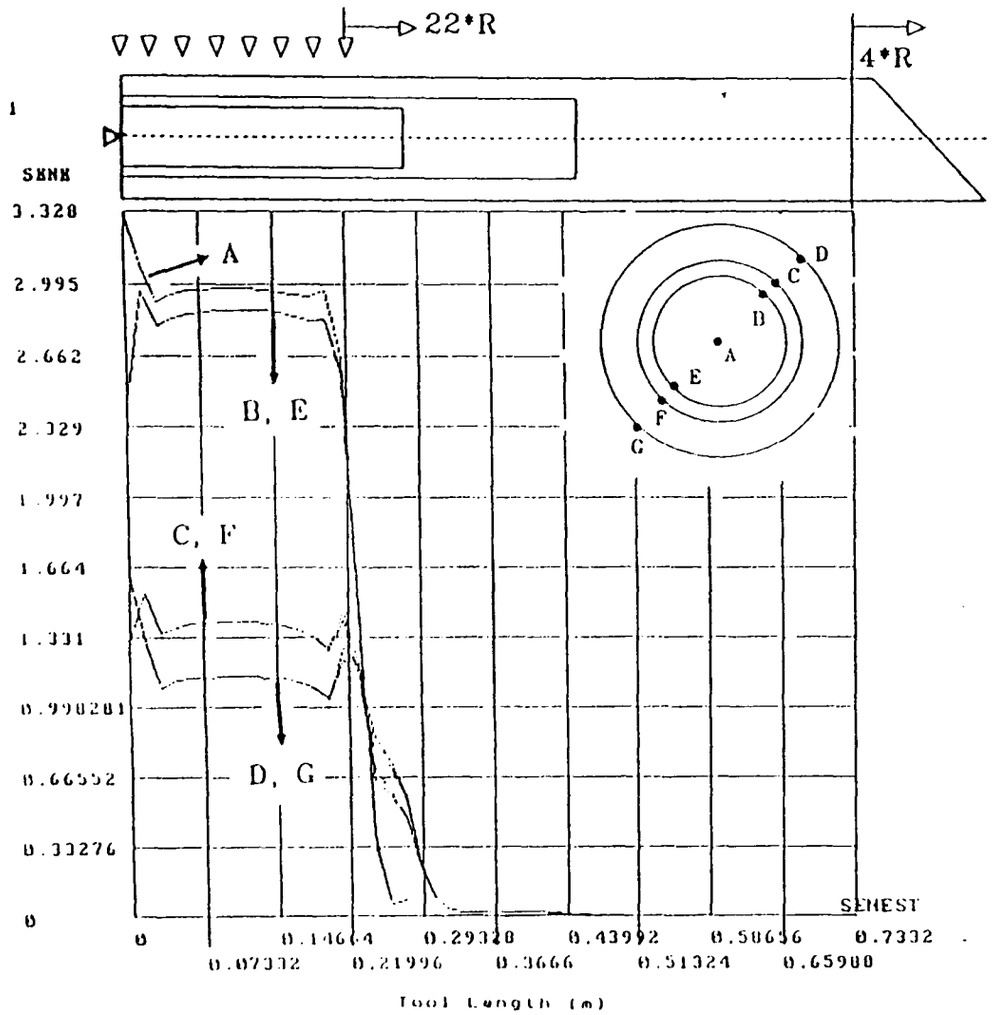

Figure 7.16 -
Strain Energy Graduation
along the Inserted Steel Tool.
(Core Length=10*R, Fcase=16)

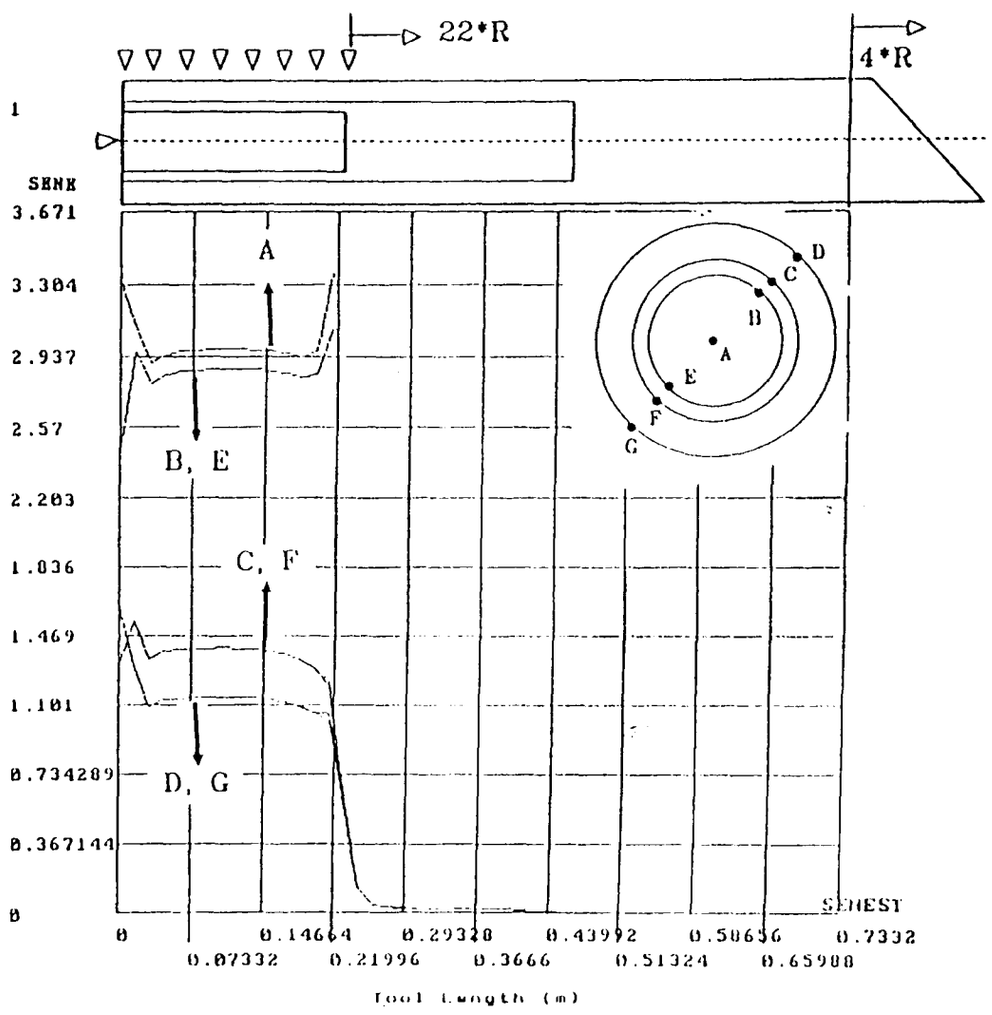

Figure 7.15 -
Strain Energy Graduation
along the Inserted Steel Tool.
(Core Length=8*R, Fcase=16)

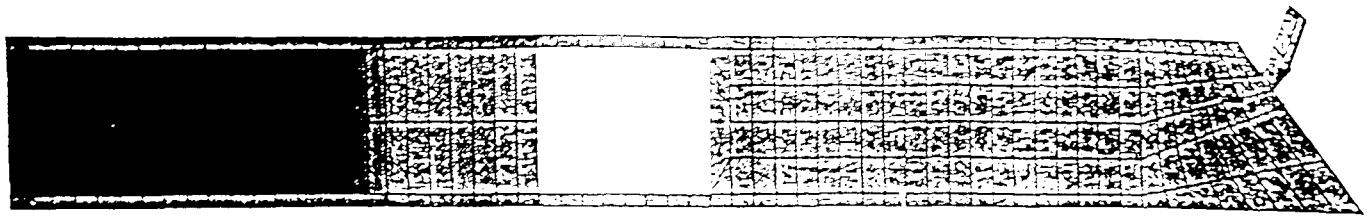

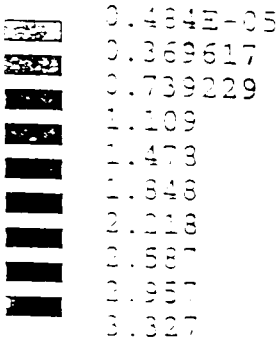

Figure 7.17 -
Strain Energy Distribution
along the Inserted Steel Tool.
(Core Length=12*R, Fcase=16)

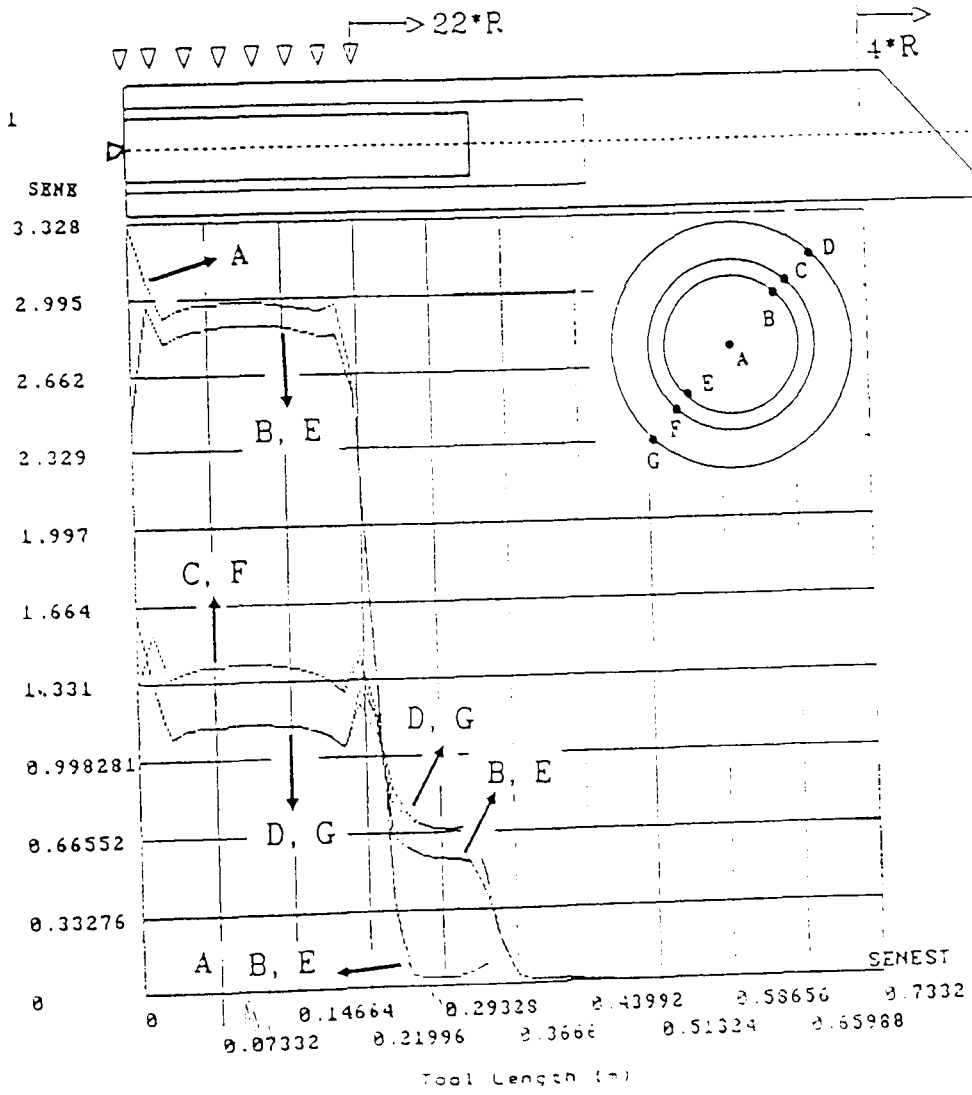

Figure 7.18 -
Strain Energy graduation
along the Inserted Steel Tool.
(Core Length=12*R, Fcase=16)

Figure 7.19a- Tip Deflections

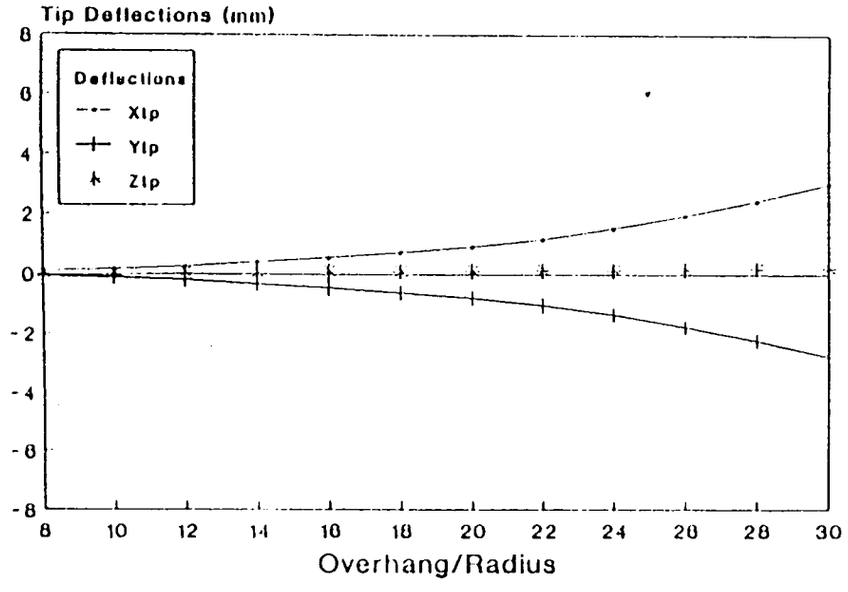

Figure 7.19b- Strain Energy

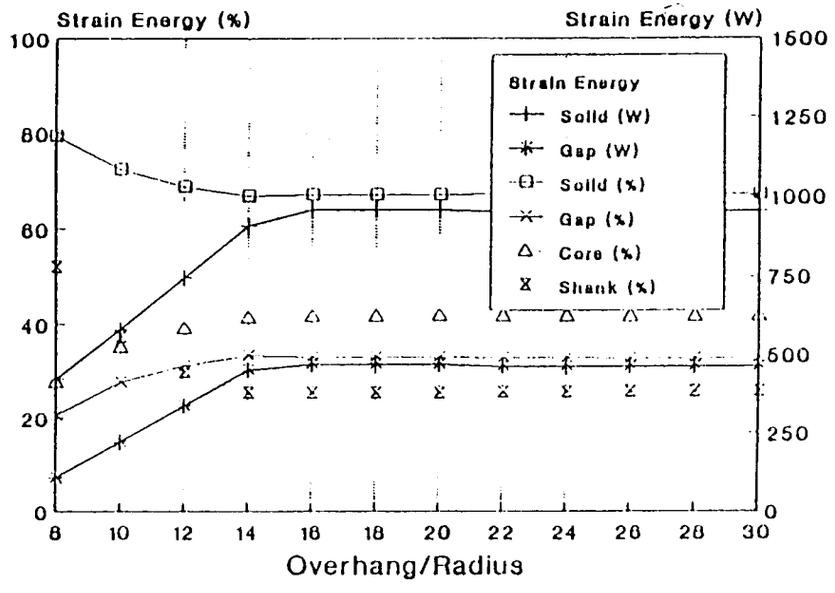

Figure 7.19c- Interface

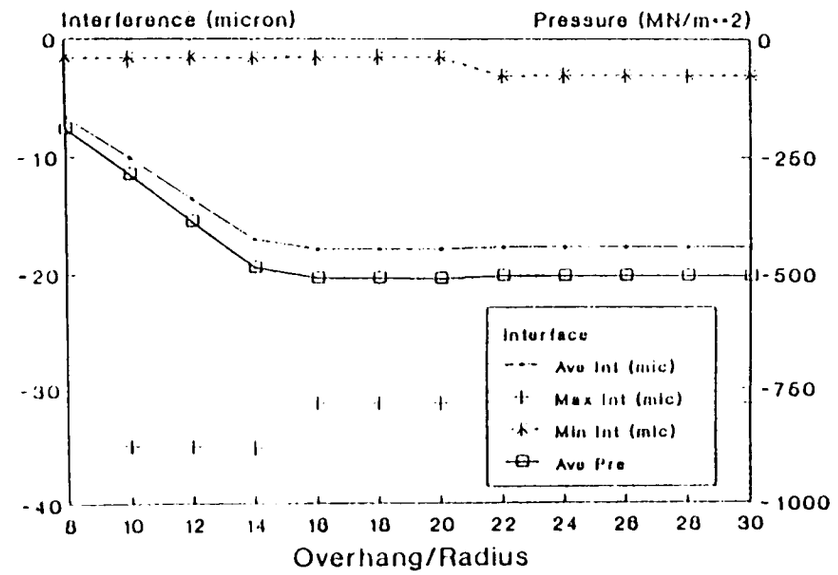

Effect of Overhang Variation of Inserted Steel Tool. (Fcase=16).

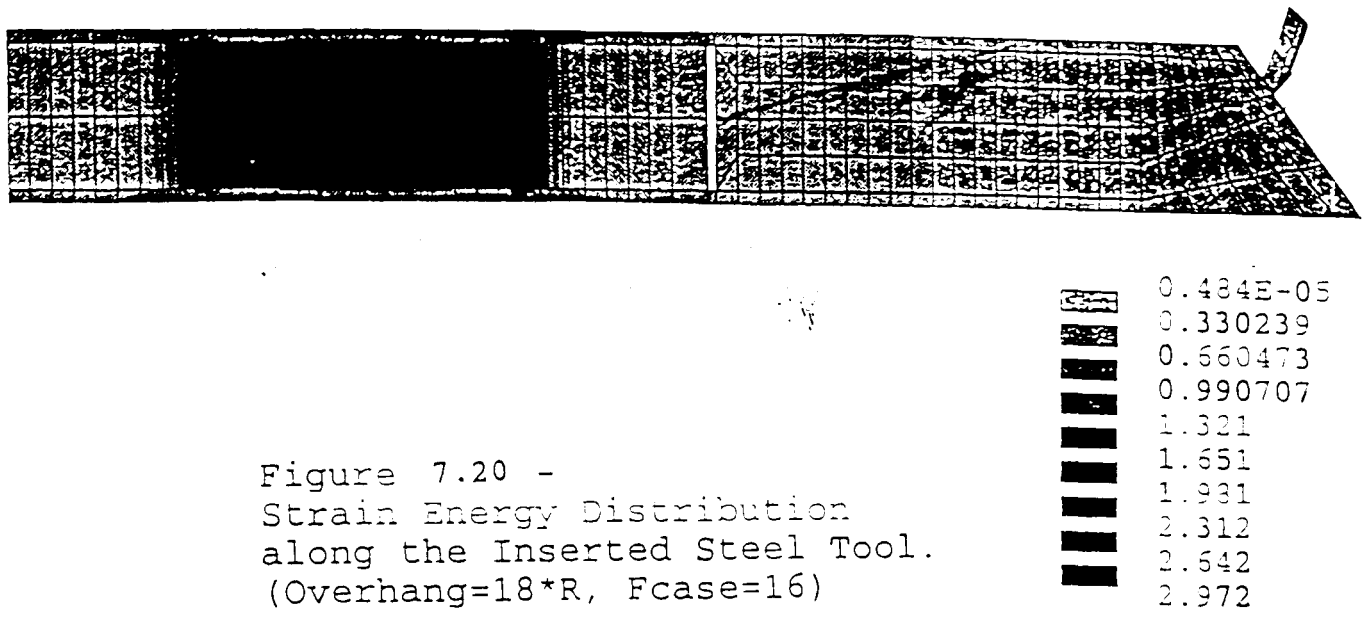

Figure 7.20 -
Strain Energy Distribution
along the Inserted Steel Tool.
(Overhang=18*R, Fcase=16)

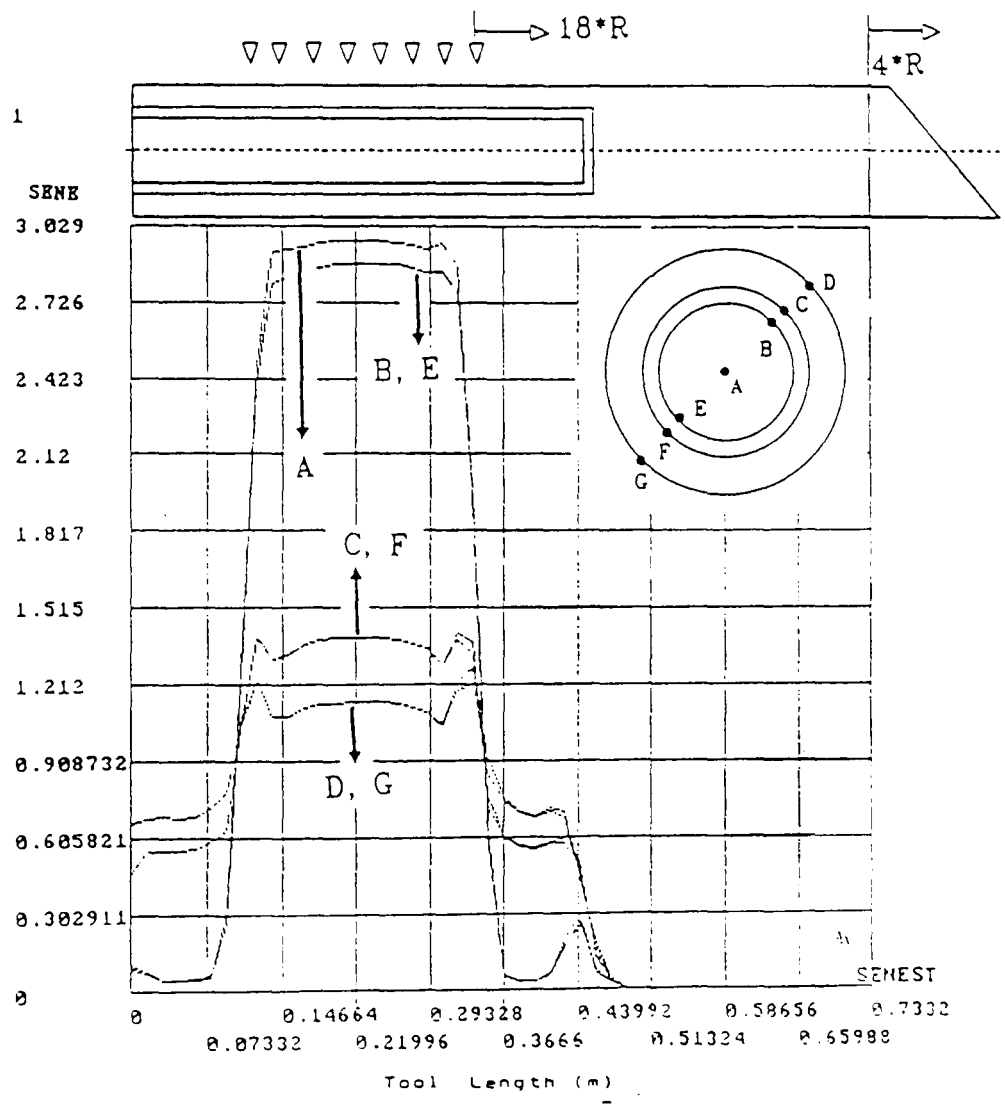

Figure 7.21 -
Strain Energy graduation
along the Inserted Steel Tool.
(Overhang=18*R, Fcase=16)

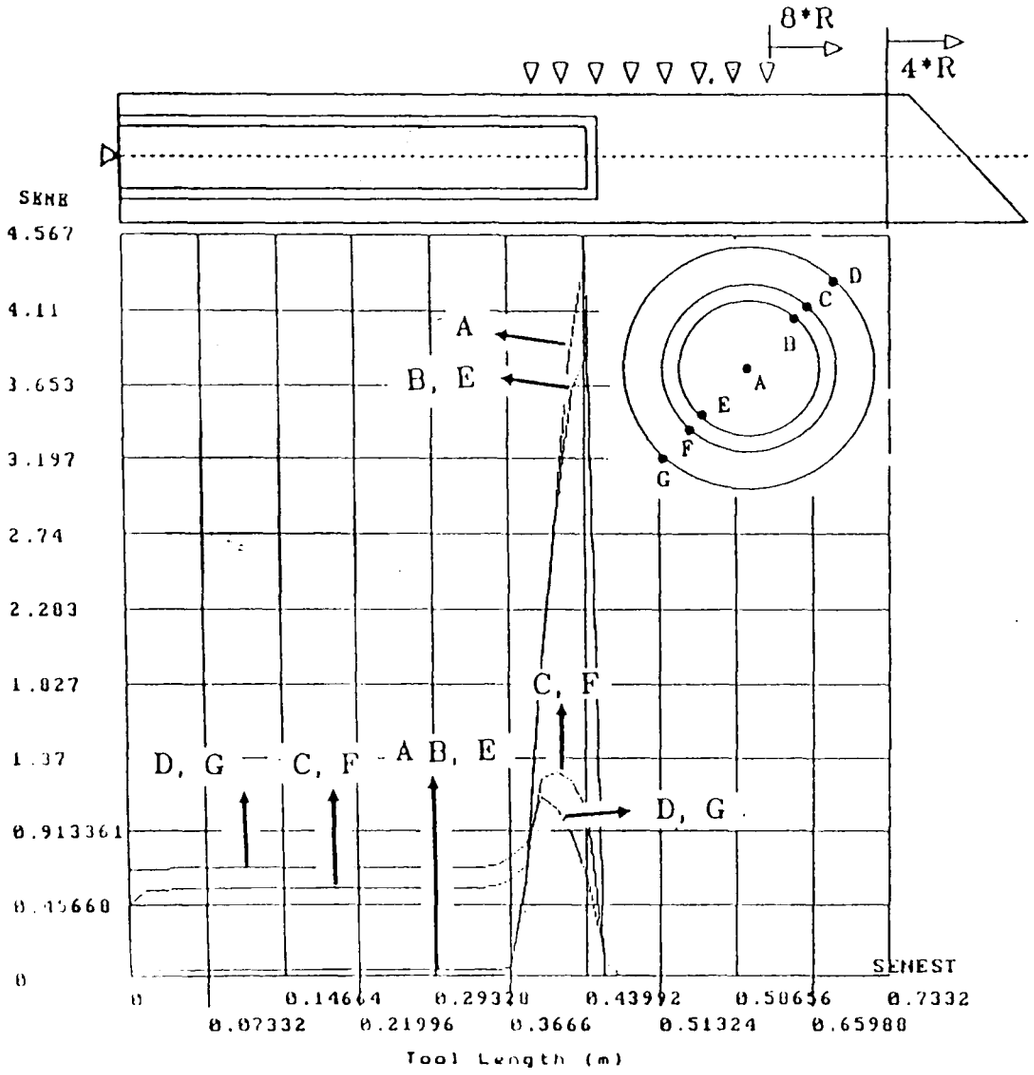

Figure 7.23 -
Strain Energy graduation
along the Inserted Steel Tool.
(Overhang=8*R, Fcase=16)

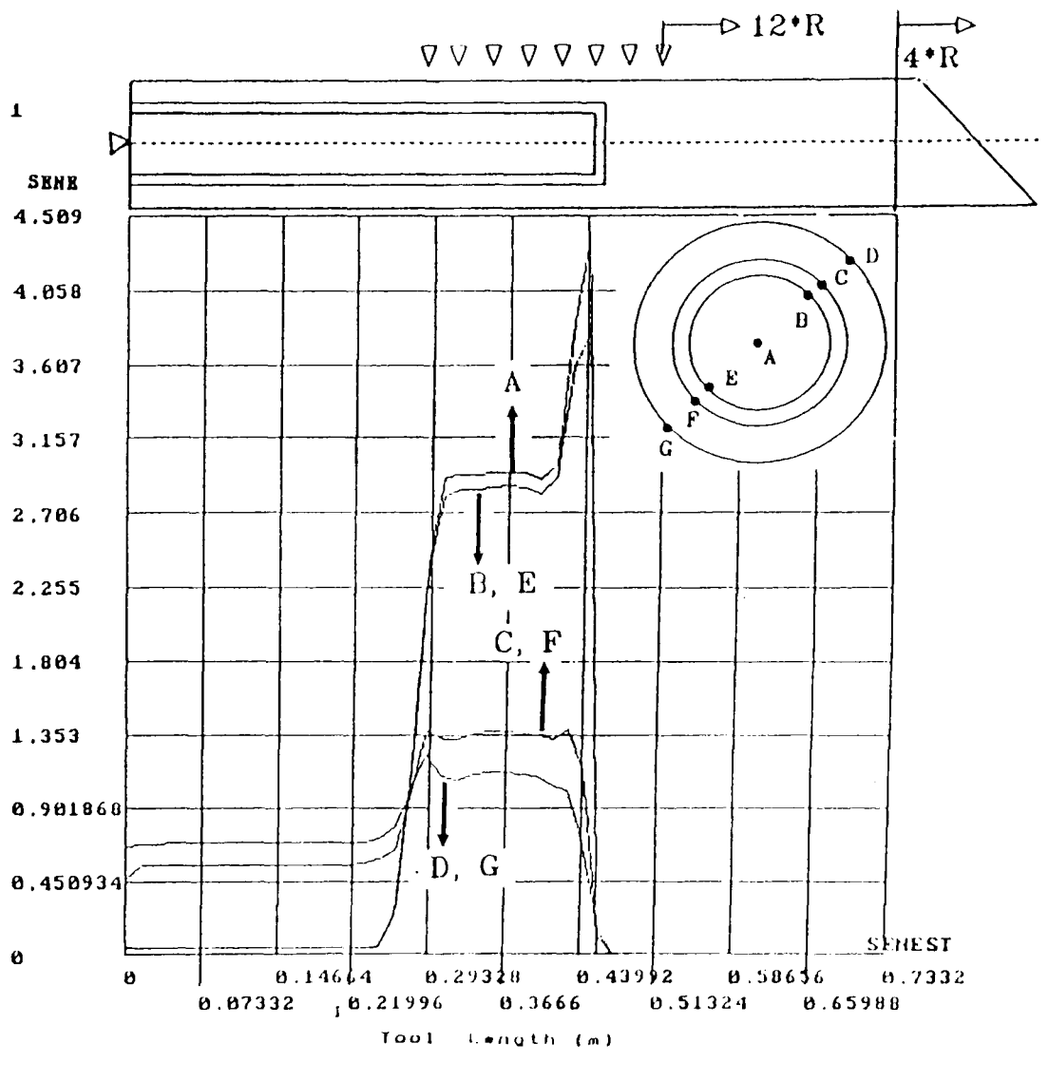

Figure 7.22 -
Strain Energy graduation
along the Inserted Steel Tool.
(Overhang=12*R, Fcase=16)

CHAPTER 8

DYNAMIC ANALYSIS OF THE CANTILEVER BORING BARS

8.0 INTRODUCTION

In this chapter the dynamic stability analyses of the boring bar model with respect to various design parameters are examined.

The dynamic compliance of the tools are confined to modal (for frequency and mode behaviour) and harmonic (for response amplitude) analysis of the solid and the composite bar. The design optimisation is based on tip response with respect to variation of fundamental determinants. This entails comparison and analysis of the results for the following design options:

a) Damping variation .

b) Overhang variation for tools subjected to the same cutting force and damping.

c) cutting force variation.

d) shank material variation for tools subjected to the same cutting force and damping.

e) Core length variation for combination boring bars.

8.1 THE FINITE ELEMENT MODEL

The finite element model for the dynamic analyses, corresponds to that of static analysis. Hence, the tool with the overhang of 11 times the diameter is defined as the baseline tool. In this analysis, the amplitude of the sinusoidal force input is assumed to be 10 percent of the respective static force. The default case is subjected to a force

case '16' with 5 percent damping.

It may be useful to mention that although the geometry of the model of the tool was simulated as a function length to radius ratio, in the analyses of the results this is taken to be as L/D ratio.

8.2 MODAL ANALYSIS OF CANTILEVER BORING BARS

If a system does not have much damping, then it is necessary to try and avoid resonance if large amplitudes of vibration are to be prevented. If the natural frequency of the boring bar is close to the forcing frequency of the cutting process increasing the stiffness "K" or reducing mass "m" of the tool holder would move the operating point of the response away from the peak resonance. In a typical system with little damping, this would greatly reduce the vibration amplitude.

Often the frequency of an exciting force is linked to the speed of rotation or process instability. During starting and stopping the force frequency changes between zero and its normal operating value. If the natural frequency of the tool is less than the forcing frequency during normal cutting the system has to pass through resonance during starting and stopping. This requires higher damping levels so that the peak amplitude is not too great.

Modal, or mode-frequency analysis is used to determine the natural frequencies and mode shapes of a structure subjected to dynamic loading. The cutting tool should be designed such that it does not "chatter" under varying cutting conditions. The dynamic response data is required to examine, and bypass the resonance frequency of the vibrating member at the design stage.

The tool is considered to be a beam with distributed mass and stiffness. Thus; The infinite number of frequencies is given by;

$$\omega_n = \frac{C_0}{L^2}\sqrt{\frac{E\,I}{\rho A}} \qquad (8.1)$$

Where ω_n = the nth natural frequency, E = the elastic modulus, I = area moment of inertia ($\pi.R^4/4$) and ρ = the mass density of the system and L = length of beam. The value of C_0 for the first five modes are shown in Table 8.1.

Equation 8.1, assumes that the beam is homogeneous, its area moment of inertia is constant throughout its length, it is axially symmetric, and the effect of rotary inertia is negligible. In a real situation it is probable that none of these conditions will be met. Nevertheless, the simulation may be used in practice as a best estimate. Hence; Substituting I ($\pi.R^4/4$) in equation (8.1) gives ;

$$\omega_n = C_0\sqrt{\pi}\ \left[\frac{(\frac{E}{\rho})^{\frac{1}{2}}}{(\frac{L}{R})^2}\right] \qquad (8.2)$$

Equation (8.2) indicates that ω_n is

a) Dependent upon C_0.

b) Varies inversely with length to radius ratio by a power of 2.

c) Varies with (E/ρ) ratio by the power of 0.5.

In equation (8.2) all parameters except C_0 are constant therefore the natural frequency will be a function of the end conditions and the material properties.

Stiffness can be expressed in terms of static or dynamic components. The Dynamic stiffness is the bar's ability to withstand the oscillating forces. This is a measure of the restoring force of the boring bar expressed as the ratio (E/ρ) and the damping capacity of the tool under dynamic loading.

The mode shapes and Eigenvalue of the first 8 modes of the

baseline solid tool examined through the generated finite element model are illustrated in Figure 8.1, and Table 8.2 respectively. It can be seen that the natural frequency of mode 1 and 2 are very close to each other and the dominating modes are in a plane parallel to the tangential force 'x' and radial force 'y'. The plane of the vibrating fundamental modes are perpendicular in the direction of feed.

Examining the frequency of the dominant modes with respect to the overhang variation (Figure 8.2) allows the following observations to be made;

a) Modes 1 and 2 are the dominant natural frequencies of the tool along x any y directions. They indicate the susceptibility of the limit of cutting tool stability .

b) Because the magnitudes of modes 1 and 2, also 3 and 4 are very close to each other (less than 1 Hz, For clarity, mode 2 and 4 are omitted from Figure 8.2).

c) All modal magnitudes increase hyperbolically, indicating that bypassing the fundamental mode of the vibrating tool may significantly reduce the oscillating response of the cutting process .

d) The fundamental mode shape of the tool illustrates the position of maximum flexure of the bar in x, y or z direction. This shape factor may be used to determine the position most appropriate for the application of the constraint layer damping for ideal performance.

Similarly, Figure 8.5, illustrates the first eight natural frequencies of the inserted tool with respect to various design parameters. The identical similarities on the pattern of mode shapes with respect to overhang to radius ratio in Figures 8.2, and 8.5.a, validates the same deduction as above. The comparative observations of these diagrams also represents the relative expansion on the level of resonance frequency through composite design of the boring bar for various length to radius ratios.

8.2.1 OVERHANG VARIATION

One of the physical parameters that influence the modal frequency (eigen values) and mode shapes (eigen vectors) of the boring bar construction is the geometry of the tool. Equation (8.2) shows that increasing the overhang will cause the natural frequencies to reduce inversely with the power of two of the overhang. However, the first eight modes of natural frequencies with respect to overhang variations in Figure 8.2.a illustrates a more complex picture. This complexity is considered to be as a result of the superimposed modes of the back section of the bar, and not purely due to the overhang section. As the length of the front section of the tool increases, the associated natural frequencies would reduce, but at the same time the natural frequencies of the back section increases. Reflecting this analogy on Figure 8.2.a, all the decreasing lines are associated with the overhang while, the increasing lines can be identified with the back section.

The first four mode shapes of the solid tools for overhangs of 4 and 7 times the diameter are shown in Figures 8.3 and 8.4. At some tool overhangs, the natural frequencies of the front and back would cross over each other. Figure 8.2.a also shows that at overhang of L/D = 5.5 times the diameter, all the mode numbers of the back section meet their respective mode number of the front section.

Although tuning by frequency impulse does not change the natural frequency of the tool, however, theoretically it may be possible to reduce the magnitude of the tool response provided that the magnitudes and direction of the tuning function is equal and opposite to that of the overhang section. Since in any practical machining the dynamic magnitude of the force components are unknown and variable this method of process attenuation was not considered as a viable option

It should be pointed out that the natural frequencies for overhang of 11 times the diameter and above are associated with the extended front section, since the length of the back section is zero.

Table 8.3, tabulates the fundamental natural frequencies of the solid tool at different overhangs. The comparative power rate of change of the first natural frequency for various design parameters in Table 8.4 indicate that the extended length of the front section are most sensitive to the threshold of natural frequency and varies with the power of 2 of the overhang.

The shank and core materials of the model for the inserted composite tool are steel and TC4, respectively. The frequency variation of these tools with respect to overhang variation are shown in Figure 8.5a. They indicates that the frequencies of the inserted model are higher than the solid tools. The comparative variation of frequencies of the solid and the inserted tools with respect to L/D ratio in Table 8.3, signify that at L/D ratio's of 11 and 15 times the diameter, the inserted tool display a 9.3% (10.4 Hz) and 7.5% (4.4 Hz) higher frequency than the solid tool. Although the increase of 9.3% may not be sufficient to justify such a design at this stage. However, the improved static stiffness of 53.64 % in the radial (y) direction and 17 % in (x) direction are indicators of improved dynamic compliance. Furthermore, in the following analysis it will be shown that, with reference to equation (8.1), it should be possible to modify (E/ρ) such that substantial improvements of the natural frequency may be achieved.

It should also be noted that the TC4 core protrudes into the overhang section after overhang of 4 times the diameter, hence the dynamic stiffness of the overhang would not be fully realised until there was an overhang of 11 times the diameter (designed length). Between 11 to 15 times the diameter the front section of the tool is extended, while the length of the core remains constant. This causes the percentage difference of the frequencies of the solid and inserted tools to reduce to 7.5% .

Although, the geometries of the overhang and the back section are different from each other (towards the tip), nonetheless, the results on the frequency and response of the back can be used as a precursor to

indicate the expected increase in the fundamental frequency of the overhang when the length of the TC4 core is extended to its maximum possible design length. The comparative variation of the inserted and the solid tool with respect to overhang variation illustrated in Figures 8.6 and Table 8.7, demonstrate that, for the back length of 4 and 7 times the diameter, the inserted tool would have a 30.4% and 31.7% higher natural frequency to that of the solid tool. Therefore, extending the TC4 core to its maximum design length would increase the fundamental frequency of the overhang by more than 30 percent of its respective solid tool. This percentage difference is expected to increase for higher overhang lengths.

8.2.2 SHANK MATERIAL VARIATION

Table 8.5, and Figure 8.2.b, illustrates the variation of (E/ρ) and the modal frequencies for different shank materials respectively. They demonstrates that the fundamental natural frequency of the overhang vary with the power of 0.5 of (E/ρ) of the shank and complies with the expected theoretical power. The results also indicate that the best way to increase the natural frequencies is to select a shorter tool length. However, because employing an extended length tool is a manufacturing necessity then selecting shank materials with higher (E/ρ) is the best way forward. Utilizing tools with very high static stiffness will normally increase the cost of tooling as well as the effective mass of the bar. Therefore a combination design through structural optimisation and development of high stiffness low mass material would result in a system compromise with respect to dynamic stability and improved frequency response for specific applications.

Figure 8.5.b and Table 8.6, similarly illustrate the natural frequencies of the inserted tool. They demonstrates that, by reducing the density of the shank material and increasing the elastic modulus of

the core material the modal frequencies will also increase. For example, modifying the material of the shank from Tungsten Carbide ($E=305$ GN/m^2, $\rho=17500$ Kg/m^3, N.Freq.= 84.31 Hz.) to TC4 ($E=303$ GN/m^2, $\rho=5132$ kg/m^3, N.Freq.= 153.8 Hz.) will increase the fundamental frequency by 82.4 %. . This indicates that the density of the shank material is a significant design parameter, specially towards the free end of the cutting tool.

8.2.3 CORE LENGTH VARIATION

Figure's 8.5.c, 8.5.d, and Table 8.8 illustrate the effect of core length variation on natural frequencies for the baseline composite tool. From these figures it can be observed that extending the core length up to 60% of the overhang length will increase the natural frequencies of the tool by up to 53 %. Comparing the baseline inserted tool with the bonded tool where the model assumes no relative movement between the core and the shank the results show an increase of only 2 Hz or 1.8 % on the fundamental natural frequency. This result shows that the 84 μm interference does in fact provide the required contact stiffness by practically eliminating the joining influence on the deflection of the bar. When the designed elastic modulus of the core is higher than the shank it may be concluded that a significant increase in the natural frequencies may be achieved if the length of the TC4 core is extended to its maximum designed length. The observation of the above results indicate that the maximum designed core length would approximately be 53.2 % of the overhang length. However, for practical applications as the tool would be expected to perform for various length to diameter ratios rather than an optimum set L/D ratio the emphasised designed length of the core should be based on the minimum expected L/D ratio to enable greater flexibility in selecting various L/D ratios for optimum performance.

Figure 8.5.d illustrate the effect of core length variation on the natural frequencies when the shank material is Aluminum. This illustration demonstrates that increasing the core length to 15.8 times the radius will increase the fundamental natural frequency by 99 % . Moreover, extending the core to fill the cavity shows that the fundamental natural frequency has increased by a further 7 % . These results are in agreement with the previous conclusion for the shank material variation.

These results indicate substantial improvement of the fundamental modal frequency. However, the dynamic compliance of a machining process is time dependent and the oscillating energy input of the system could vary throughout a cutting process. Since there is no direct method of adjusting the physical parameters with in the process such a design would be more suitable for an extended range of mass produced components where the whole manufacturing system is not expected to change.

8.3 HARMONIC ANALYSIS OF THE SOLID TOOL RESPONSE

8.3.1 DAMPING VARIATION

The cantilever boring bar will have many natural frequencies, each of which will have a resonance peak associated with it. Therefore, it may be difficult to avoid resonance, particularly if the exciting force has components at a number of different frequencies. For example, the exciting force may vary with varying machining conditions, variation of surface quality due to earlier processes, existence and disappearance of built up edge or metallurgical homogeneity of the workpiece materials. Ideally the lowest natural frequency must be higher than the highest exciting frequency, thereby ensuring that resonance does not occur. In circumstances where this may not be possible the damping treatments may be required for more satisfactory

control of vibration amplitude.

The experimental investigation on the developed TC4 material, revealed marked improvement on the damping qualities. In order to demonstrate the effect of damping on the amplitude response of the process, the finite element model was examined for variation in levels of damping (between 1 to 5 %). This is the expected range of practical damping qualities for steel and TC4 composite respectively. The effect of zero damping is also examined.

Figure 8.7 illustrates the natural frequencies of the baseline tool in the x direction for levels of damping "0, 1, 3 and 5" percent. It is obvious that the solid steel tool will exhibit higher tip vibration amplitude for all levels of damping. Moreover, damping has a greater effect on the reduction of tip amplitudes at higher frequencies. In this section, the dynamic analysis of the solid tools were based upon the variation of tip response at the fundamental frequency (the lowest frequency associated with resonance).

Table 8.9 and Figure 8.8, show that, while the tip responses along x and y directions are similar to each other they differ appreciably with the tip response along the z direction by a factor of 12. Hence, the axial response of the tool is insignificant compared to radial and tangential amplitudes.

The significance of damping on the response of the tool may observed by comparative analyses of Table 8.9 . While at 1 % damping, the fundamental mode along x direction shows a response of 6.25 mm peak amplitude, at 3 and 5 % damping it exhibits tip responses of 2.14 mm and 1.3 mm which translates to a reduction of 92, and 95 percent respectively. This also indicates that reducing the level of damping below 3 percent would substantially increase the tip response. Therefore, tip responses at the damping levels of 3, 1 and zero were estimated to be 1.7, 4.9 and 20 times the tip response at 5 percent damping.

Table 8.13 and Figure 8.10 presents the amplitude responses of

the baseline inserted tool in "x" direction with respect to damping variation. Increasing the damping level from 0 to 1, 3 and 5 percent would reduce the fundamental tip responses by 322 %, 1134 % and 1952 % respectively. Compared to solid steel tool with 1 % damping, The amplitude tip responses of the inserted tool in "x" "y" and "z" direction at these damping levels was estimated to be 1.7, 4.8 and 18.91 times lower tip response, at 5 percent damping.

Compared to the baseline solid tool the inserted steel tool exhibits lower tip responses and higher natural frequencies. For example, at 1 % percent damping (the expected damping factor for steel) the amplitude response at the fundamental mode of the solid tool along x direction is 6.27 mm (101 Hz) whilst for the inserted tool it is 1.091 mm (111 Hz).

It is important to note the significance of the above results which indicate an improvement of at least five fold through the initial design of the combination configuration (steel head) compared to the amplitude response of the solid steel bar.

8.3.2 OVERHANG VARIATION

Both resonance frequency and amplitude response of the cutting tools are influenced by changes in the overhang. Table 8.10 and Figure 8.9.a illustrate the amplitude responses for the solid steel tool for various tool overhangs at 5 percent damping. They show that the tip responses grow disproportionately with increasing the tool overhang.

Figure 8.9.a also reveals that the tip amplitude response along 'x' and 'y' directions varies to the power of 2.96 and 3.01 of the overhang while along z direction varies to the power of 2.1. These values are compatible with their respective static overhang variations of 2.89, 3.07 and 2.03 respectively, (section 7.2.1).

Figure 8.11.a illustrates the inserted tool response for various

overhangs at 5 percent damping. Similar to the solid tool they show that the tip responses grow disproportionately with increasing the tool overhang. For example, increasing the overhang from 10 to 20 and then 30 times the radius would result in the tip response along x axis increasing by 7 and then 23 fold. For an overhang of above 22 times the radius, the length of TC4 core stays constant but the length of the steel shank increases therefore the stiffness contribution of the TC4 core to the overhang remains constant in comparison to the contribution of the shank. *This result indicate that in order to improve the dynamic stiffness of the tool, the length of the TC4 core should be extended to its maximum designed length.*

8.3.3 FORCE VARIATION

Table 8.12 and Figure 8.9.b present the amplitude responses for the solid tool with respect to the force variation at 5 % damping. They demonstrate that tip responses in x, y and z directions vary linearly with force. From Table 8.12, the equivalent dynamic stiffness of the tool are estimated to be 116, 126 and 1502 KN/m. These are an order of magnitude lower than their respective equivalent static stiffness (1.1, 1.23 and 13.55 MN/m).

Table 8.15 and Figure 8.11.b presents the composite tool responses with respect to the force variations. These tables indicates that the dynamic stiffness for the inserted tool are 137, 149 and 1732 KN/m along x, y and z directions, which are about 9 times lower than their equivalent static stiffness (1.2, 1.45 and 15 MN/m). The baseline inserted tool exhibits higher dynamic stiffness to that of the baseline solid tool (116, 126 and 1502 KN/m) by 15.1, 15.4 and 13.3 percent respectively. It should also be mentioned that, reducing the damping level will increase the amplitude tip responses which, in turn will reduce the estimated dynamic stiffness.

8.3.4 SHANK MATERIAL VARIATION

Figure 8.9.c and Table 8.12 illustrate tool response with respect to the modulus of elasticity of the shank material. They shows that shank materials with lower modulus of elasticity will result in higher tip responses. For example, the tip responses along x direction for ALAL (E=70E+9 N/m^2), steel (E=200E+9 N/m^2) and TNGC (E=305E+9 N/m^2) are 3.6 mm, 1.3 mm and 0.8 mm, which are lower than their respective static deflections (3.8 mm, 1.36 mm and 0.91 mm). This is expected, since at 5 percent damping, the amplitude of the sinusoidal forces are an order of magnitude less than the static forces. The equivalent dynamic stiffness of the tool at this level of damping is an order of magnitude greater than the equivalent static stiffness of the tool.

Comparing the amplitude tip response of the inserted tool with that of the solid tool shows that as the ratio of (E_{core}/E_{shank}) of the inserted tool approaches unity the effect of the core will diminish, while below unity the inserted tools exhibit higher tool responses. For example, the ALAL and steel inserted tools show tip response reduction of 87.8 and 17.8 percent along the x direction. While for the TNGC it has increased by 0.8 percent.

Table 8.17 indicate that the amplitude tip responses along x, y and z direction vary inversely with the power of 0.59, 0.58 and 0.67 of the modulus of elasticity of the shank.

8.3.5 CORE LENGTH VARIATION

Table 8.18.a and 8.18.b present tip response at fundamental frequency of inserted tools at 5 % damping for steel and ALAL. They indicate that existence of the TC4 core does not have any effect on the tip responses, unless the core protrudes into the overhang region.

Increasing the length of the core beyond the constraint section

to 15.8 times the radius will reduce the tip responses in x, y and z directions by 53.8, 54.2 and 49.5 percent. Similar core length variation for ALAL shank will reduce the tip responses along x, y and z directions by 69.8, 70.3 and 63.7 percent respectively. These results indicate that incorporation and extension of the TC4 core in the ALAL tool will result in greater reduction of the tip response than the steel tool. Moreover, it can be deduced that the length of the core should be extended to the maximum design length. This is in agreement with the previous studies of both static and dynamic analyses. With the strain energy analysis of the solid tools (section 7.4) it was shown that 90 percent of the total strain energy of the tool is stored in the 52.3 percent of the shank from the fixed end. This suggests that the maximum design length of the core would be 52.3 percent of the overhang. Therefore, in order to investigate the effect of higher TC4 core lengths on the dynamic behaviour of the tool the length of the core was increased from 15.8 to 16.8, 17.8, and 19.8, keeping the clearance of the core and hole constant. The progressive improvements towards optimum designed length of the core are shown in Table 8.19.a and 8.19.b for steel and ALAL shank materials.

8.4 DISCUSSION FOR OPTIMUM DESIGN

Optimum improvement in the final design of the boring bar is based on maximizing the threshold of the natural frequency and reducing the amplitude levels. Increasing the natural frequency will reduce the possibility of the chatter vibrations while a reduction in amplitude levels will improve the dimensional accuracy of the workpiece at resonance.

The natural frequencies of a given tool is an inherent characteristic of the tool and is independent of imposed cutting force. But the tip amplitude response can be adjusted by either: a) changing

the load levels, b) incorporating damping or, c) Increasing stiffness, d) correlating the cutting process parameters, e) Incorporating vibration absorbers.

If the self-excited quantity during machining, is at or above the natural frequency of the tool chatter is inevitable. Therefore, in any tool design the fundamental natural frequency of the tool should be set as high as possible. However, at resonance or under steady state cutting, vibrations do exist, and the damping characteristics of the tool enables cutting to be performed at lower vibration amplitude levels hence enabling a better surface finish to be obtained.

A comparative study based on percentage improvement of both amplitude and frequency of selected design options is presented in Tables 8.20 and 8.21. A negative value of the tip response signifies an improvement of the amplitude levels while improvement of the natural frequency is positive.

Table 8.20 illustrates the performance of the TC4 solid tool, solid steel and tungsten carbide tool with respect to tip responses and natural frequency. The TC4 solid tools exhibit similar tip responses compared to TNGC solid tools, however the natural frequency of the TC4 bar is 82.1 percent greater than that of the sintered carbide bar. This signifies a substantial improvement of the dynamic stability of the TC4 tool.

Comparing with the solid steel tool the TC4 solid tool improves both the frequency and response levels by 51.5 and 34%, respectively with 1 % damping. However, although the expected damping level for steel is between 1 and 3 %, the damping of the TC4 is found to be above 5%, therefore from comparative observations of tables 8.10 and 8.13 it is estimated that the amplitude response of the TC4 solid tool to be at least 300 % lower than that of steel tool.

In order to reduce the cost of manufacturing and further to improve the natural frequency a subsequent design study resulted in a modification of the structural design of the tool which incorporated a

core (TC4), inserted within the cavity of the tool. Analysis for variation of overhang, core length and material, resulted in two more possibilities that performed close to or better than that of solid TC4 with respect to its natural frequency.

Table 8.19 and 8.20 and Figure 8.12 illustrates the comparative performance of the following selected design tools:

a) Composite inserted aluminium Tool with a TC4 core protruding 52.3 percent of the overhang .

b) Composite inserted steel tool with a TC4 core protruding 52.3 percent of overhang .

c) TC4 solid tool.

Comparing (a) above with a conventional solid steel tool (Figure 8.12) indicates an improvement of 59 percent in the fundamental natural frequency with a marginal 15 percent increase of amplitude levels. Since the dynamic stability of any tool is a function of (E/ρ) ratio and damping tool (a) exhibits maximum (E/ρ) ratio and any further improvement of this tool should be aimed towards improving the damping characteristics.

Although the effective (E/ρ) values of tool (a) is marginally higher than the solid TC4 tool the overall static stiffness (EI) of TC4 is higher than that of (a). Figure 8.12 illustrates this effect with a marginal improvement of natural frequency of about 5 % of tool (a). However, from Table 8.21.b it can be observed that a TC4 solid tool would have 73 percent lower amplitude response than tool (a). This result suggests that where the cutting operations are not frequency sensitive the use of solid TC4 would significantly improve the dynamic stiffness and therefore is most desirable for finishing operations.

Similar conclusions can be drawn for solid tungsten carbide (TNGC) tools where the response amplitudes are substantially lower. Examination of TNGC with Tool (a), (Figure 8.12), show that TNGC tools would be frequency sensitive and tool (a) would outperform solid

tungsten carbide by as much as 91.7 percent.

Changing the shank material from aluminium to steel would also result in an improvement of conventional tools with greater static stiffness but lower (E/ρ) ratio. For example, comparing tool (c) with solid steel tool would result in a 20 percent reduction in amplitude response levels and 3.86 percent increase in natural frequency. This tool would also out perform the solid TNGC by 36.9 percent. However, Tool (c) is not recommended to replace ALAL (19.8) since the measure of the fundamental natural frequency is 40 percent less than that of tool (a) and compared to TC4 both the amplitude response and chatter frequency are worse (Amp:21.5% higher, Freq:24.84 Lower).

Although the above values authenticate significant improvement of the dynamic qualities, the presented assessment assumes similar levels of damping for all materials. The combined damping effect of the composite boring bar, through TC4 core, constraint layer damping and column damping at interface is considered to have improved the response beyond the analyzed values.

Finally; although the first literature to be published on this investigation is currently under review, there has been industrial interests in the design both in terms of material development and combination structure.

Mode No.	End Conditions (C_0)					
	H-H * Simply Supported	C-F Cantilever	C-C	F-F	C-H	H-F
1	9.87	3.52	22.2	22.2	15.4	15.4
2	39.5	22.2	61.7	61.7	50.0	50.0
3	88.9	61.7	121	121	104	104
4	158	121	200	200	178	178
5	247	200	298	298	272	272
* H = Hinged C = Clamped F = Free						

Table 8.1 - Values of C_0 for Variety of End Conditions.

MODE	FREQUENCY (CYCLES/TIME)	
	Solid Tool	Inserted Tool
1	101.243	111.698
2	101.246	111.704
3	617.918	652.697
4	617.960	653.048
5	1332.296	1390.775
6	1680.973	1852.794
7	1694.049	1861.838
8	2337.768	2244.667

Table 8.2 - Eigen values of the 1^{st} Modes, of the Baseline Solid and Inserted Tools.

Overhang (*R)	Fundamental Overhang Natural Frequency	
	Solid Tool	Inserted Tool
8	745.3 Hz	739.7 Hz
14	248.6	240.9
15	216.8	210.0
22 (Base)	101.3	111.7
30	54.53	58.95

Table 8.3 - Variation of the Fundamental Natural Frequency with respect to Overhang Variation. (Shank Material=Steel)

Material	E (MPa)	ρ (Kg/M^3)	E/ρ (MNm/Kg)
ALAL	70	2800	25
STEL (Base)	200	7840	25.5
TC2	271.2	6500	34.72
TC3	249	5160	56.2
TC4	303	5132	59
TNGC	305	17500	17.43

Table 8.4 - Modulus of Elasticity (E), Density (ρ) and Static Stiffness (E/ρ) for Different Materials.

Description	Natural Frequency of overhang - Shank Materials					
Shank Material	TNGC	ALAL	STEL (Base)	TC2	TC3	TC4
(E/ρ) of Shank	17.43E+6 (Nm/Kg)	25E+6	25.5E+6	34.72E+6	56.2E+6	59E+6
Solid Tool:	Hz	Hz	Hz	Hz	Hz	Hz
Mode No. 1	84.06	99.22	101.24	129.02	150.85	153.55
Mode No. 3	512.4	606.69	617.92	787.34	920.92	937.41
Inserted Tool:						
Mode No. 1	84.31	141.83	111.7	132.41	152.1	153.8
Mode No. 3	532.94	687.56	652.7	801.76	918.9	932.6

Table 8.5 - The Effect of Shank Material Variation on the Natural Frequencies.(L/R=22)

Length of Back (*R)	Respective Overhang (*R)	Fundamental Natural Frequency of the Back Section	
		Solid Tool	Inserted Tool
14	8	245.4 Hz	323.2 Hz
8	14	732.7	955.5

Table 8.6 - Fundamental Frequency of the Back Section

Mode Numbers	Core Material - Natural Frequencies	
	TC4 (Base)	TNGC
1st Mode	111.7 Hz	111.25 Hz
3rd Mode	652.7	597.48

Table 8.7 - Effect of Core Material Substitution on the Natural Frequencies (Inserted tool).(L/R=22, Shank Material=Steel)

Mode No.s	Core length - (Model type)			
	0 (Hollow)	8*R (Inserted)	15.8*R (Inserted)	16*R (Composite)
STEEL Shank:				
1 Mode	72.86 Hz	73.06 Hz	111.7 Hz	113.88 Hz
3 Mode	564.22	566.47	652.7	660.29
ALAL Shank:				
1 Mode	71.37	71.67	141.83	146.89
3 Mode	553.2	555.67	687.56	690.17

Table 8.8 - Effect of Core Length on the Natural Frequencies.(L/R=22, Core material=TC4)

damping	Tip Response (mm)			Natural Frequency (Hz)		
	X	Y	Z	Fx	Fy	Fz
0	26.37	24.55	2.093	101	101	101
1	6.247	5.757	0.491	101	101	101
3	2.137	1.968	0.168	101	101	101
5 (Def)	1.285	1.183	0.101	101	101	101

Table 8.9 - Tip Response of the Baseline Solid Tool at Various Levels of Damping (Fundamental mode, Steel Shank, Fcase=16, L=22*R).

L/R ratio	Tip Response (mm)			Natural Frequency (Hz)		
	X	Y	Z	Fx	Fy	Fz
8	0.00644	0.00505	0.001177	744	743	743
9	0.0902	0.07350	0.001524	590	592	592
10	0.123	0.1020	0.001906	481	481	481
11	0.163	0.1377	0.002340	399	399	399
12	0.2108	0.1807	0.002817	336	336	336
13	0.2678	0.2321	0.003343	287	287	287
14	0.3333	0.2926	0.003914	248	248	248
15	0.4095	0.3623	0.004527	216	216	216
16	0.4963	0.4427	0.005188	190	190	190
17	0.5943	0.5339	0.005888	169	169	169
18	0.7039	0.6364	0.006630	151	151	151
19	0.8286	0.7530	0.007438	135	135	135
20	0.9661	0.8822	0.008280	122	122	122
21	1.117	1.025	0.009157	111	111	111
22	1.285	1.183	0.1010	101	101	101
(Def)	1.462	1.351	0.1104	92	92	92
23	1.666	1.545	0.1209	85	85	85
24	2.370	2.216	0.1543	67	67	67
27	1.879	1.748	0.1314	78	78	78
25	2.930	2.754	0.1785	58	58	58
29	3.219	3.031	0.1901	54	54	54

Table 8.10 - Tip Responses of the Baseline Solid Tool at Various Overhangs. (5% Damping, Fcase=16,).

Force Case	Tip Response (mm)			Natural Frequency (Hz)		
	X	Y	Z	Fx	Fy	Fz
2	0.0856	0.0780	0.006657	101	101	101
11	0.3425	0.3146	0.02685	101	101	101
13	0.8565	0.7899	0.06741	101	101	101
16 (Def)	1.285	1.1832	0.1010	101	101	101
18	1.713	1.5833	0.1351	101	101	101

Table 8.11- Tip Response of the Baseline Solid Tool for Various Force Cases (5% Damping, L=22*R).

Shank Material	Tip Response (mm)			Natural Frequency (Hz)		
	X	Y	Z	Fx	Fy	Fz
ALAL	3.663	3.3719	0.2886	99	99	99
STEL (Def)	1.285	1.1832	0.1010	101	101	101
TC2	0.9421	0.8677	0.07407	129	129	129
TC3	0.8725	0.8031	0.06866	150	150	150
TC4	0.8478	0.7805	0.06671	153	153	153
TNGC	0.8404	0.7743	0.06602	84	84	84

Table 8.12 - Tip Responses of the Baseline Solid Tool for Various Shank Materials (5% Damping, Fcase=16, L=22*R).

Damping	Tip Response (mm)			Natural Frequency (Hz)		
	X	Y	Z	Fx	Fy	Fz
0	20.623	18.583	1.6420	112	112	112
1	5.2594	4.8254	0.4259	112	112	112
3	1.8061	1.6590	0.1464	112	112	112
5 (Def)	1.0905	1.0011	0.08848	111	111	111

Table 8.13 - Tip Response of the Baseline Inserted Tool at Various Levels of Damping (TC4 Core, Fcase=16, L=22*R).

Overhang Length (*R)	Tip Response (mm)			Natural Frequency (Hz)		
	X	Y	Z	Fx	Fy	Fz
8	0.06471	0.05076	0.011791	739	737	737
9	0.09091	0.07383	0.015263	587	588	588
10	0.12370	0.10282	0.019151	478	479	479
11	0.16393	0.13860	0.02350	397	397	397
12	0.21202	0.18183	0.028281	335	335	335
13	0.26868	0.23324	0.033522	286	286	286
14	0.35033	0.30775	0.04060	240	240	240
15	0.43139	0.38235	0.047192	209	209	209
16	0.49954	0.44555	0.052368	190	190	190
17	0.57419	0.51501	0.057662	173	173	173
18	0.65718	0.59268	0.063189	158	158	158
19	0.75044	0.68014	0.069107	144	144	144
20	0.85363	0.77739	0.075294	132	132	132
21	0.96762	0.88495	0.081815	121	121	121
22 (Def)	1.09051	1.00109	0.088477	111	111	111
23	1.2518	1.15425	0.097459	102	102	102
24	1.43295	1.32545	0.107307	93	93	93
25	1.61909	1.50335	0.116702	86	86	86
26	1.83813	1.71101	0.127754	79	79	79
27	2.06734	1.92945	0.138705	73	73	73
28	2.30877	2.16061	0.149628	68	68	68
29	2.58116	2.42074	0.161898	63	63	63
30	2.8595	2.68837	0.173619	59	59	59

Table 8.14 - Tip Response of the Inserted Tool for Various Overhang Lengths (5% Damping, TC4 Core, Fcase=16).

Force Case	Tip Response (mm)			Natural Frequency (Hz)		
	X	Y	Z	Fx	Fy	Fz
2	0.07266	0.06593	0.00583	111	111	111
11	0.2908	0.2662	0.02353	111	111	111
13	0.7271	0.6684	0.05907	111	111	111
16 (def)	1.0905	1.0011	0.08848	111	111	111
18	1.4544	1.3398	0.1184	111	111	111

Table 8.15 - Tip Response of the Baseline Inserted Tool for Various Force Cases (5% Damping, TC4 Core, L=22*R).

Shank Material	Tip Response (mm)			Natural Frequency (Hz)		
	X	Y	Z	Fx	Fy	Fz
ALAL	2.0149	1.8312	0.1795	141	141	141
STEL (Def)	1.0905	1.0011	0.08848	111	111	111
TC2	0.9090	0.8361	0.07232	132	132	132
TC3	0.8665	0.7973	0.06863	152	152	152
TC4	0.8503	0.7824	0.06728	153	153	153
TNGC	0.8473	0.7801	0.06698	84	84	84

Table 8.16 - Tip Response of the Inserted Tool for Various Shank Materials (5% Damping, TC4 Core, Fcase=16, L=22*R).

Core Length (*R)	Tip Response (mm)			Natural Frequency (Hz)		
	X	Y	Z	Fx	Fy	Fz
8	2.3628	2.1880	0.1750	73	73	73
15.8 (Def)	1.0905	1.0011	0.0885	111	111	111

Table 8.17.a - Tip Response of the Inserted Tool for Various Core lengths (5% Damping, TC4 Core, Fcase=16,)

Core Length (*R)	Tip Response (mm)			Natural Frequency (Hz)		
	X	Y	Z	Fx	Fy	Fz
8	6.66	6.17	0.49	71	71	71
15.8	2.01	1.83	0.17	141	141	141

Table 8.17.b - Tip Response of the Inserted Tool for Various Core Lengths (5% Damping, ALAL Shank, TC4 Core).

Length (*R)		Tip Response (mm)			Natural Frequency (Hz)		
Core	Hole	X	Y	Z	Fx	Fy	Fz
15.8 (Def)	16	1.09	1.00	0.088	111	111	111
16.8	17	1.06	0.98	0.086	113	113	113
17.8	18	1.05	0.96	0.085	114	114	114
19.8	20	1.03	0.93	0.084	115	115	115

Table 8.18.a - Tip Response of the Inserted Tool for Various Core Lengths (5% Damping, TC4 Core, Fcase=16)

Length (*R)		Tip Response (mm)			Natural Frequency (Hz)		
Core	Hole	X	Y	Z	Fx	Fy	Fz
15.8	16 (Def)	2.01	1.83	0.17	141	141	141
16.8	17	1.86	1.69	0.16	146	146	146
17.8	18	1.74	1.58	0.15	151	151	151
19.8	20	1.47	1.39	0.13	161	161	161

Table 8.18.b - Tip Response of the Inserted Tool for Various Core/Hole Lengths (5% Damping, ALAL Shank, TC4 Core,).

Structural and Material Design Option	Amplitude Performance			Frequency Performance
	X	Y	Z	Frequency
SOLID:				
STEEL	-34 %	-34 %	-34 %	51.5 %
TNGC	0.9	0.8	1	82.1

Table 8.19 - Amplitude and Frequency Performance of the Solid TC4 Tool with Respect to Different Solid Tools at 1% damping.

Structural and Material Design Option	Amplitude Performance			Frequency Performance
	X	Y	Z	Fx, Fy, Fz
SOLIDS:				
STEEL	-19.83 %	-21.10 %	-16.73 %	13.86 %
TC4	21.51	19.60	26.07	-24.84
TNGC	22.58	20.56	27.39	36.90
INSERTED:				
STEEL	-5.53	-6.75	-4.97	3.60
ALAL (15.8)	-48.87	-49.02	-53.15	-18.44

Table 8.20.a - Amplitude and Frequency Performance of the Inserted Steel Tool (Core Length=19.8*R) for Different Tools.

Structural and Material Design Option	Amplitude Performance			Frequency Performance
	X	Y	Z	Fx, Fy, Fz
SOLIDS:				
STEEL	14.56 %	17.93 %	34.06 %	59.41 %
TC4	73.64	78.78	102.97	5.23
TNGC	75.17	80.21	105.09	91.67
INSERTED:				
STEEL	34.99	39.39	52.99	45.05
ALAL (15.8)	-26.94	-23.80	-24.57	14.18
STEEL (19.8)	42.89	49.48	61.00	40.00

Table 8.20.b - Amplitude and Frequency Performance of the Inserted ALAL Tool (Core Length=19.8*R) for Different Tools.

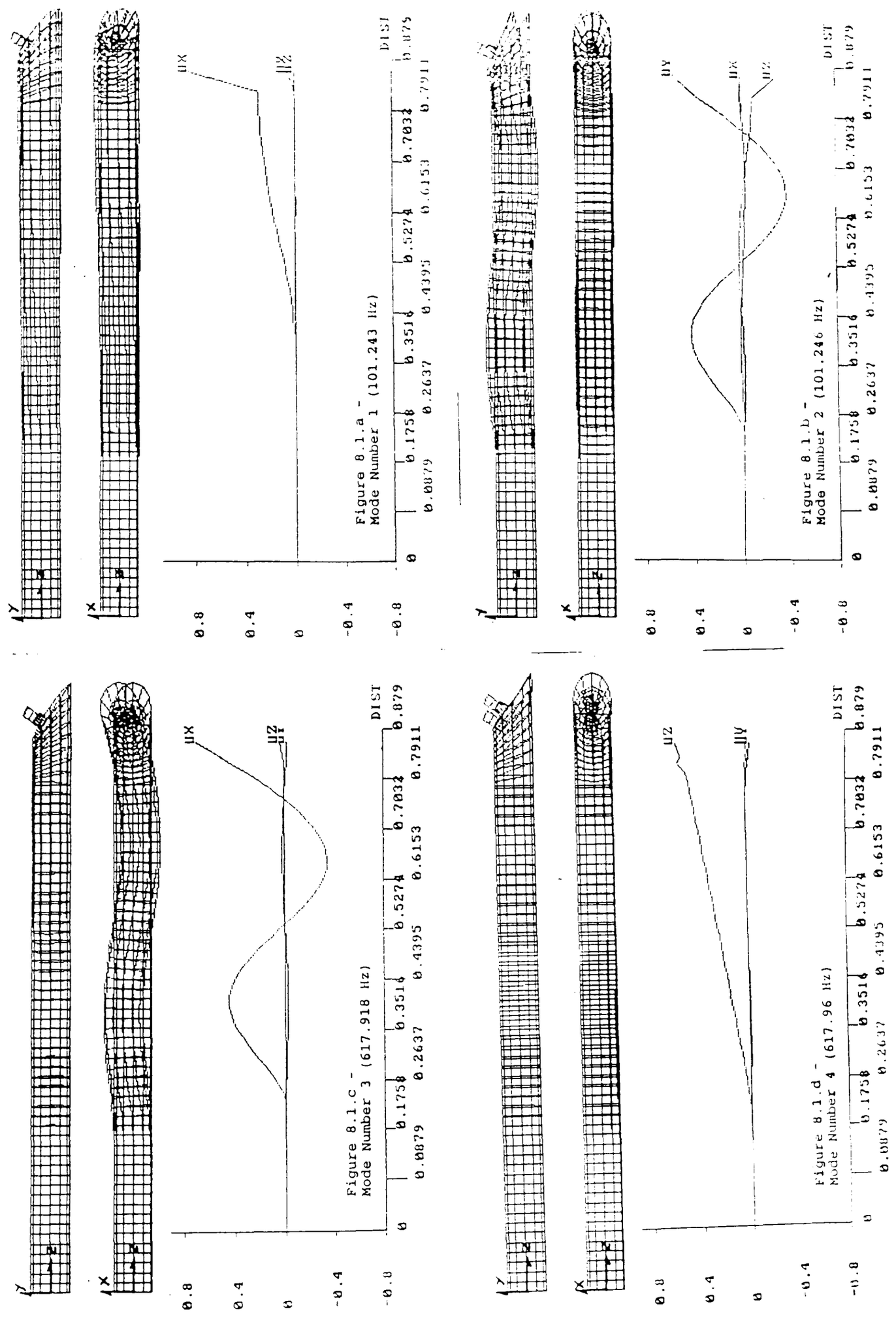

Figure 8.1 - Mode Shapes of the First Eight Modes of Baseline Solid Tool.

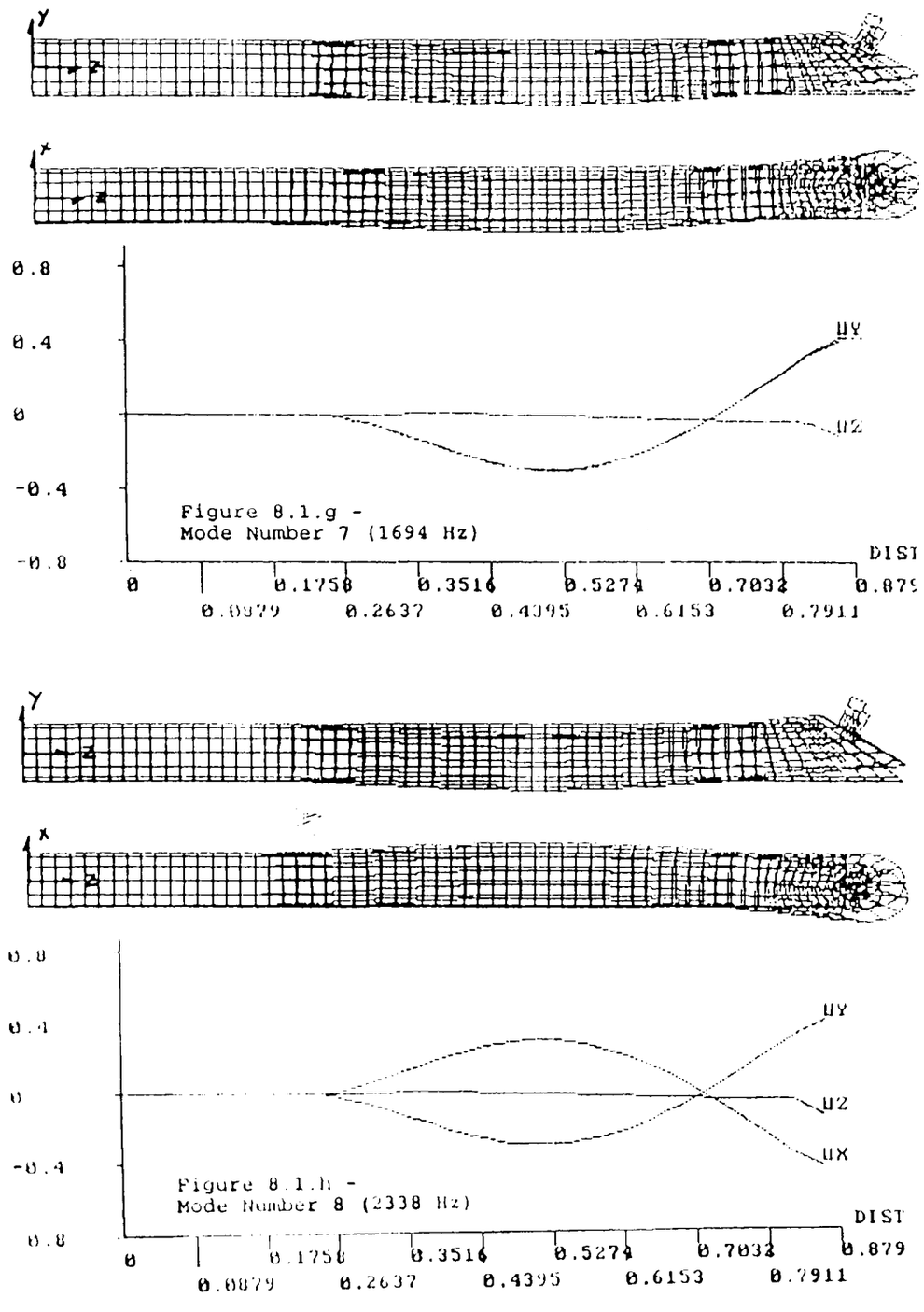

Figure 8.1.g -
Mode Number 7 (1694 Hz)

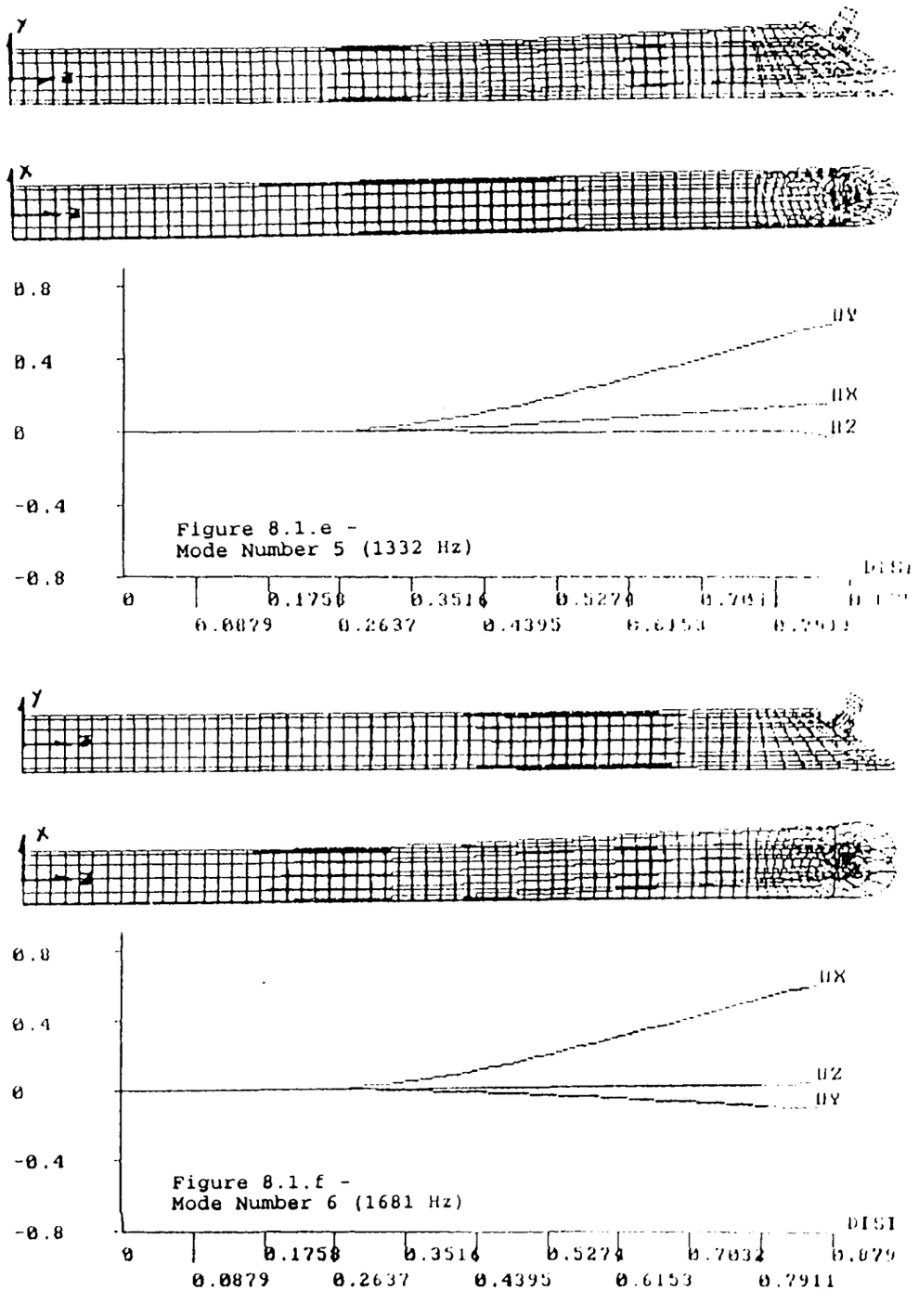

Figure 8.1.e -
Mode Number 5 (1332 Hz)

Figure 8.1.h -
Mode Number 8 (2338 Hz)

Figure 8.1.f -
Mode Number 6 (1681 Hz)

Figure 8.3- The First Four Mode Shapes of the Solid Tool With Overhang Eight Times the Radius.

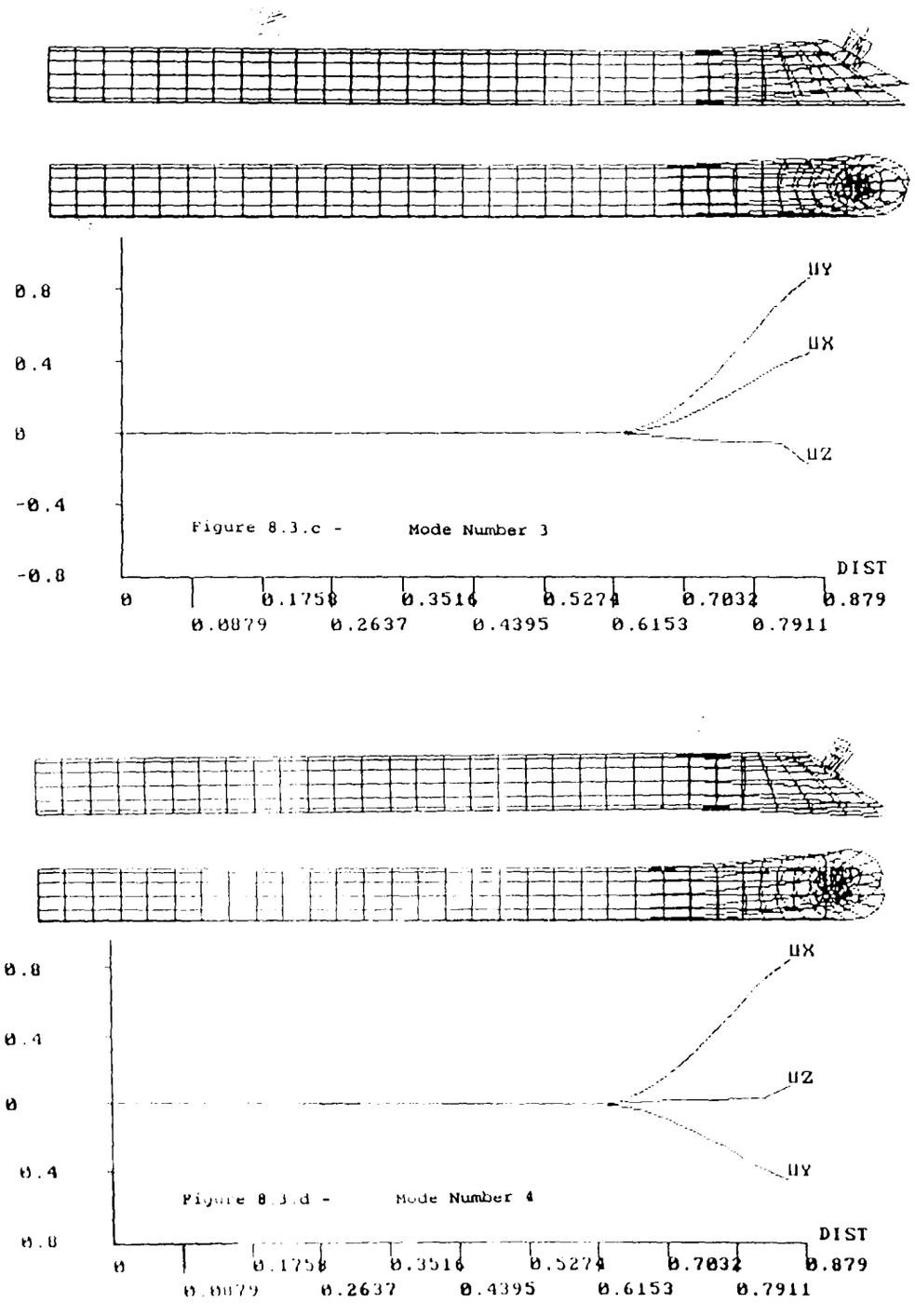

Figure 8.3.c - Mode Number 3

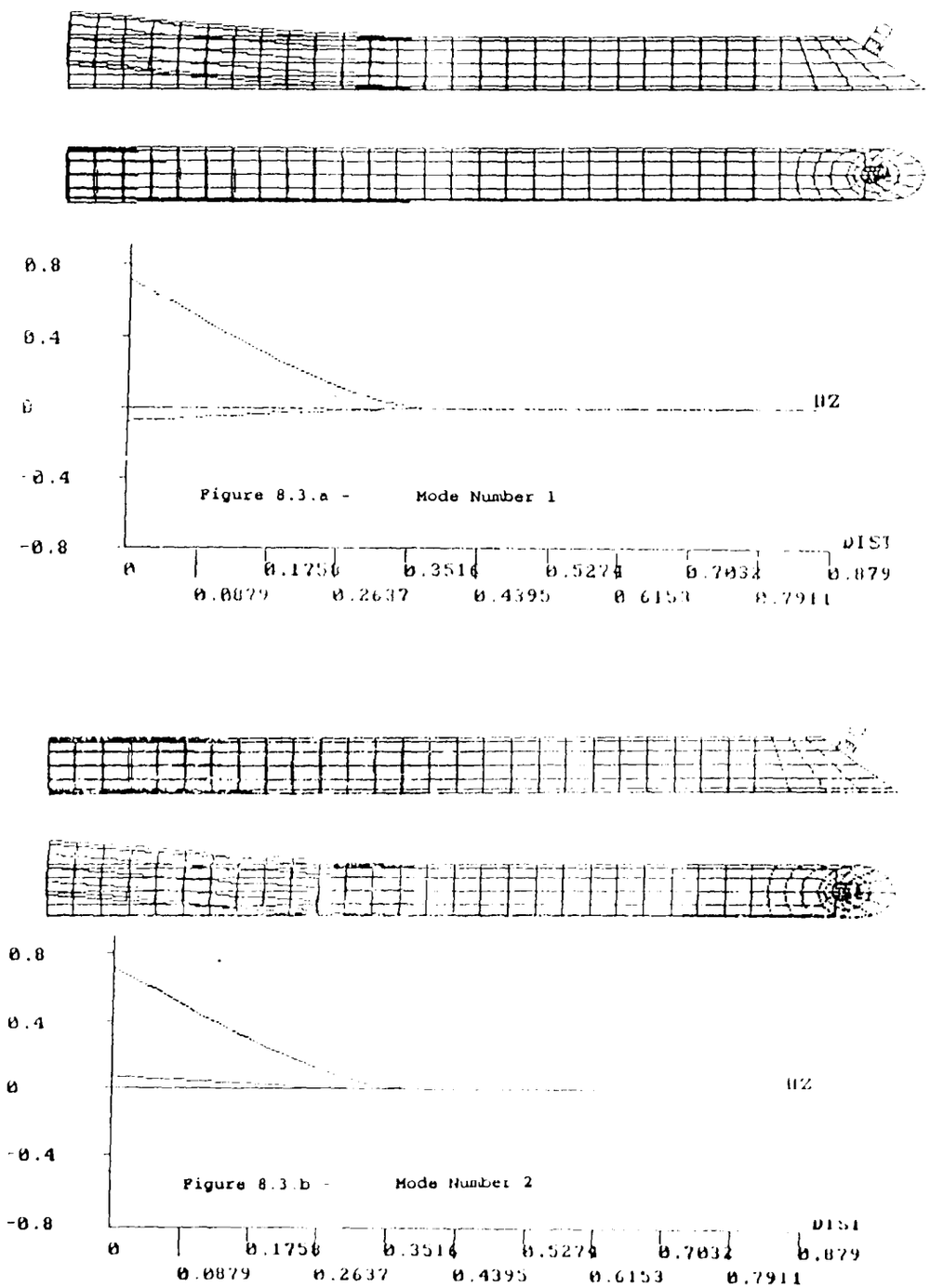

Figure 8.3.a - Mode Number 1

Figure 8.3.d - Mode Number 4

Figure 8.3.b - Mode Number 2

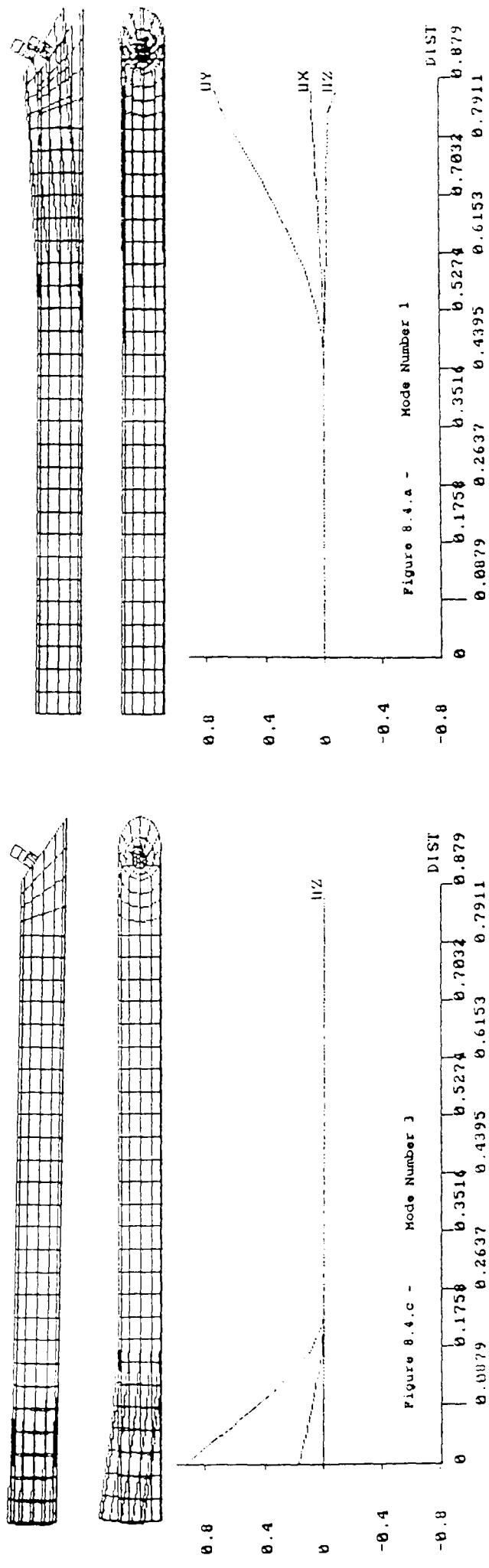

Figure 8.4- The First Four Mode Shapes of the Solid Tool With Overhang Fourteen Times the Radius.

Figure 8.2.a – Overhang Variation
(Solid Tool)

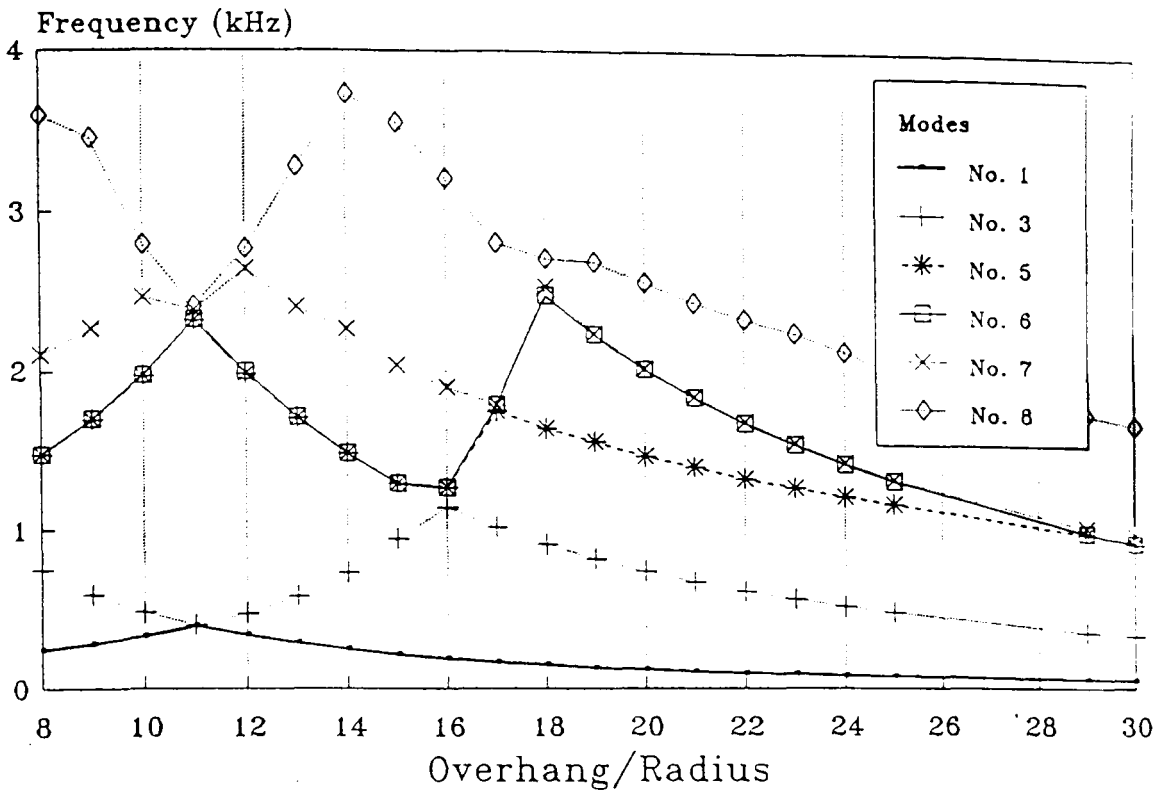

Figure 8.2a

Variation of the Eigenvalues (Natural Frequency) of the Solid Tool with Respect to Various Tool Design Parameters.

Figure 8.2.b – Shank Material Variation
(Solid Tool)

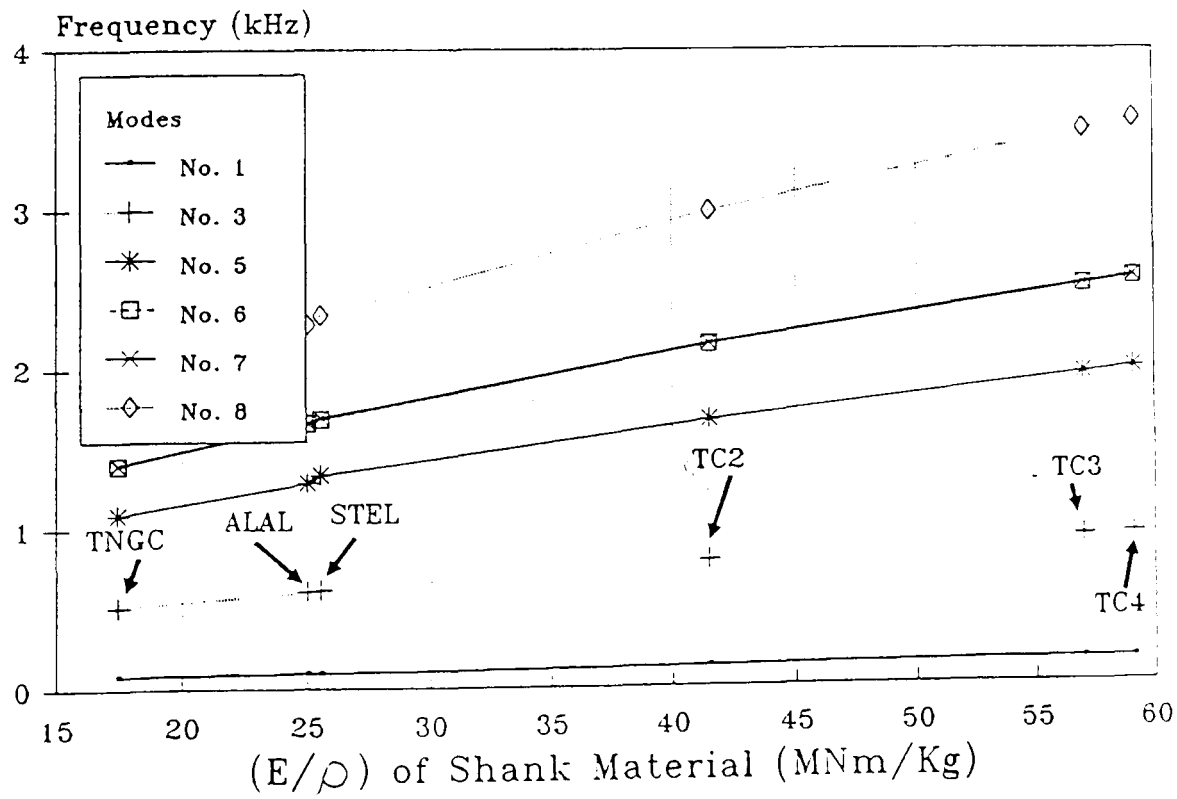

Figure 8.5.a – Overhang Variation
(Inserted Tool)

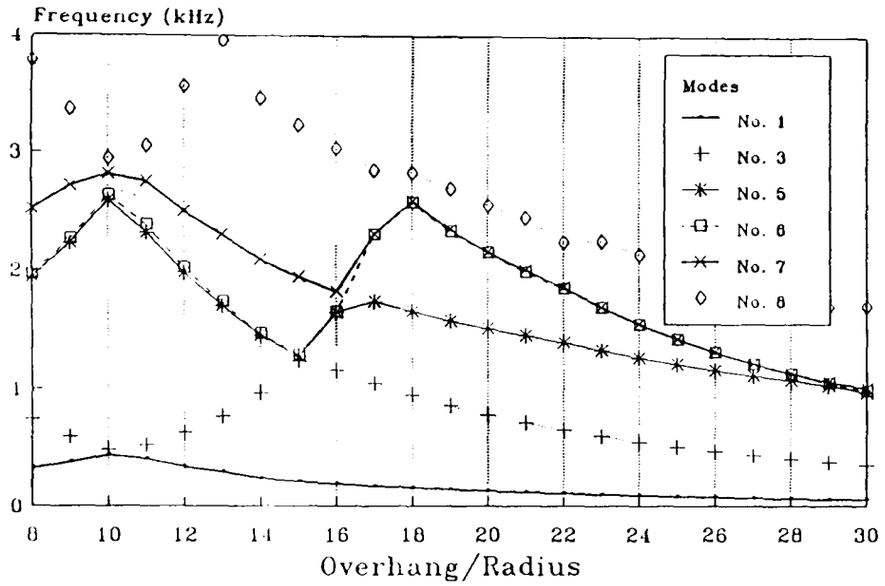

Figure 8.5.b – Shank Material Variation
(Inserted Tool)

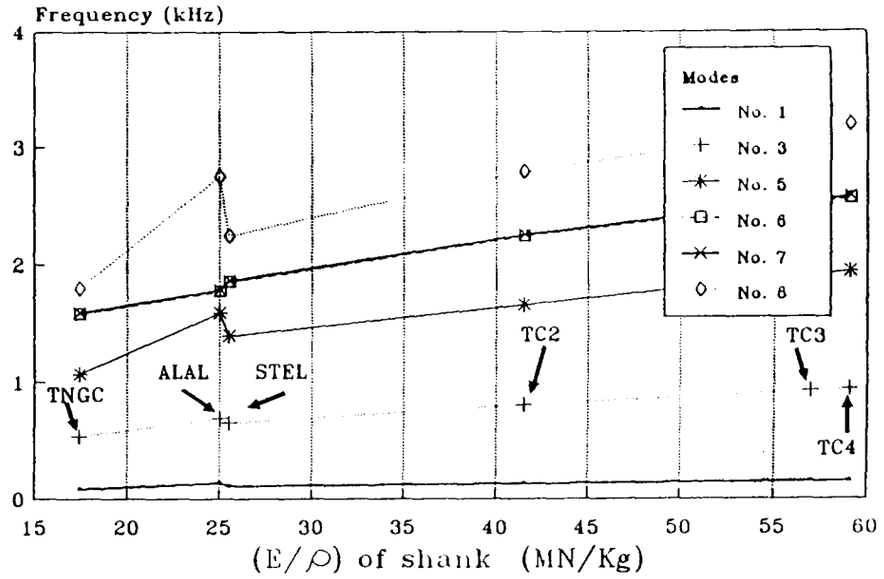

Figure 8.5 – Mode–Frequency Variation of Inserted Tools.

Figure 8.5.c – Core Length Variation
(Inserted Tool) Steel Shank

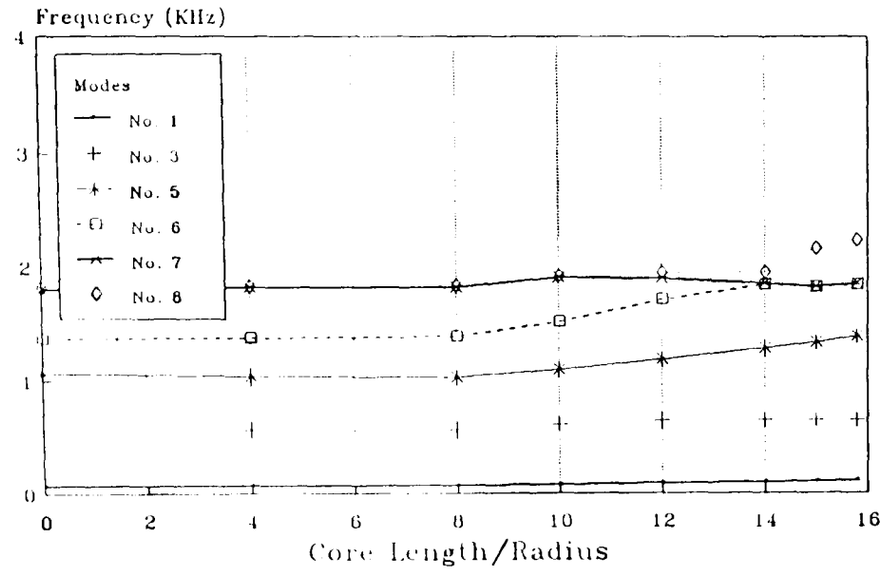

Figure 8.5.d – Core Length Variation
(Inserted Tool) ALAL Shank

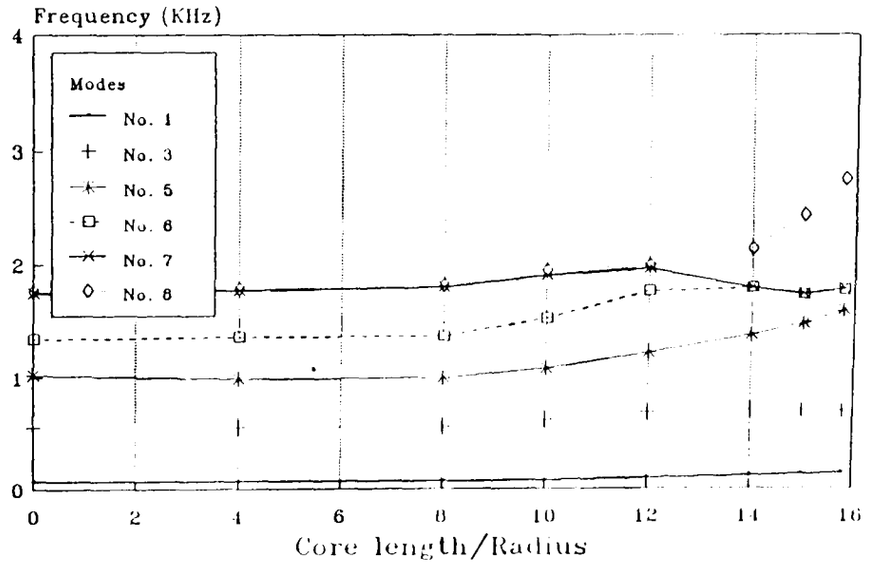

Figure 8.6– Fundemental Frequency Variation of Solid and Inserted Tools.

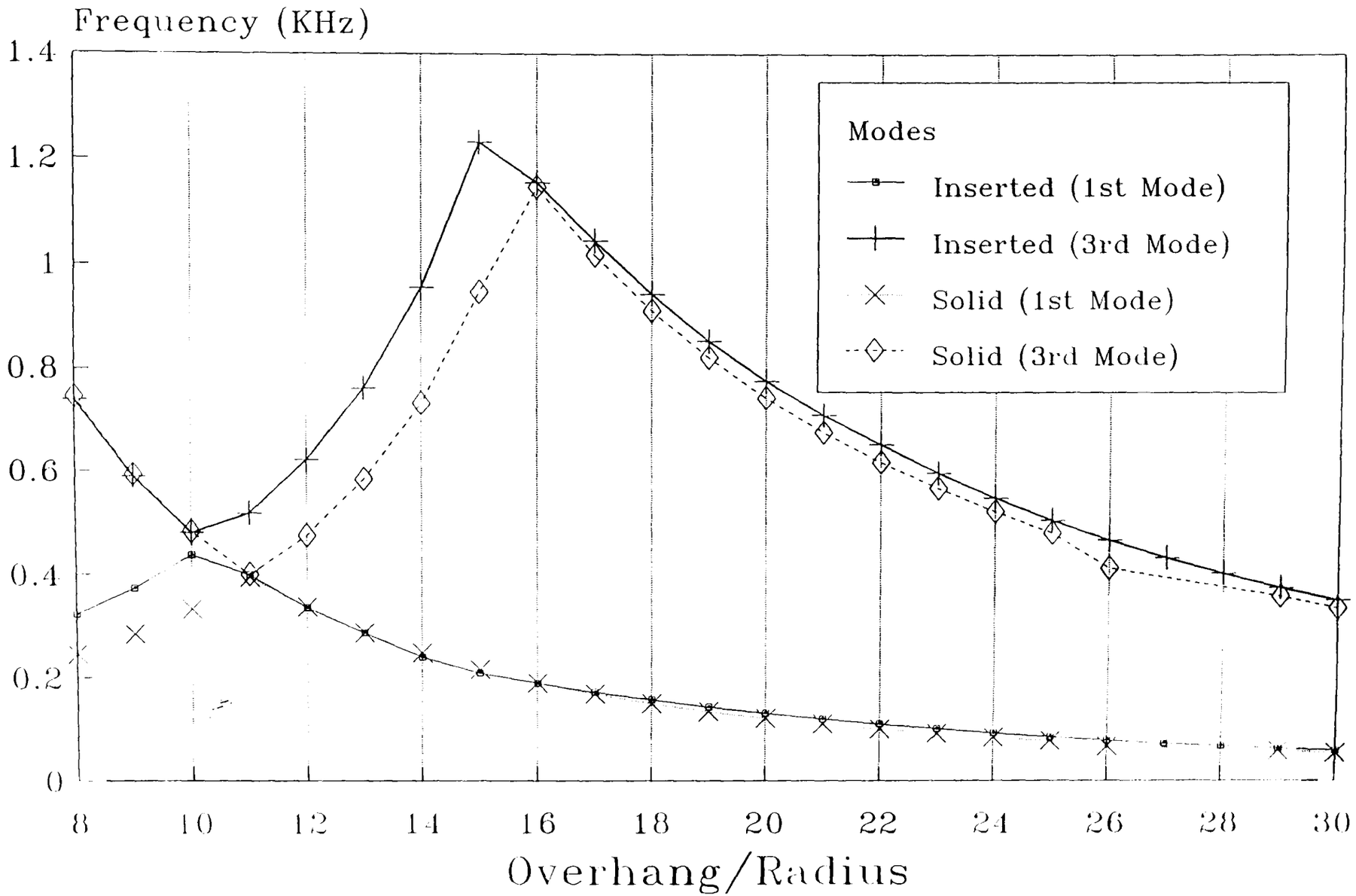

Figure 8.7.a– Tip Response at 0% Damping

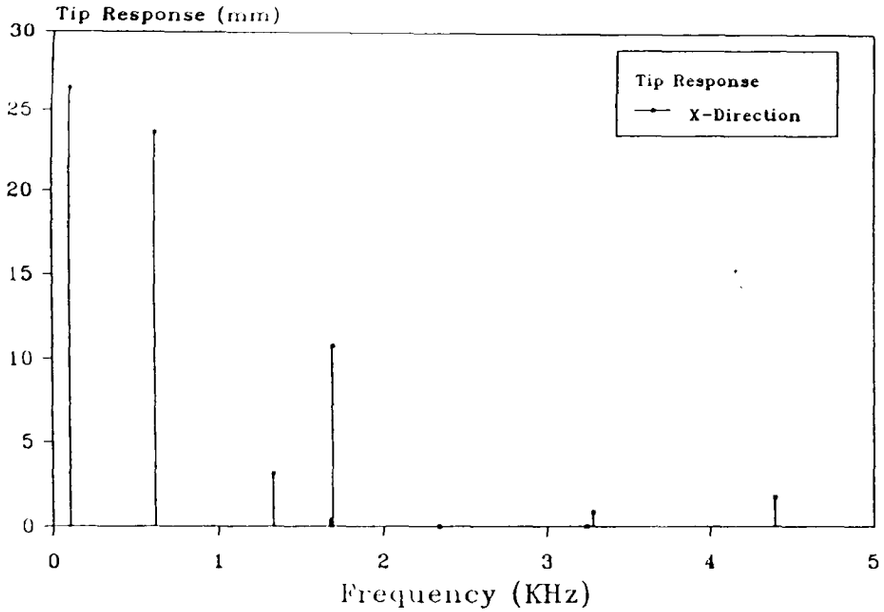

Figure 8.7.b– Tip Response at 1% Damping

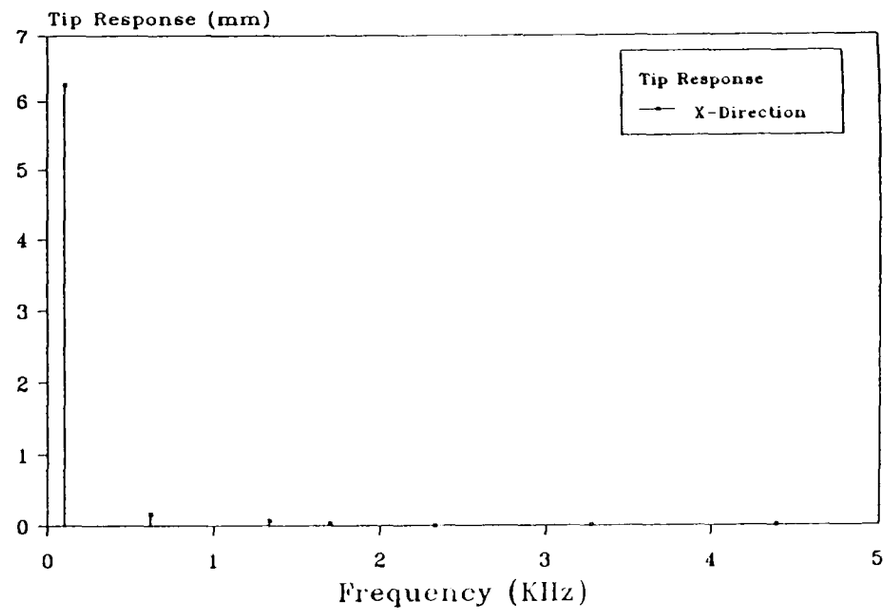

Figure 8.7–Tip Response at various Damping Levels (Solid)

Figure 8.7.c– Tip Response at 3% Damping

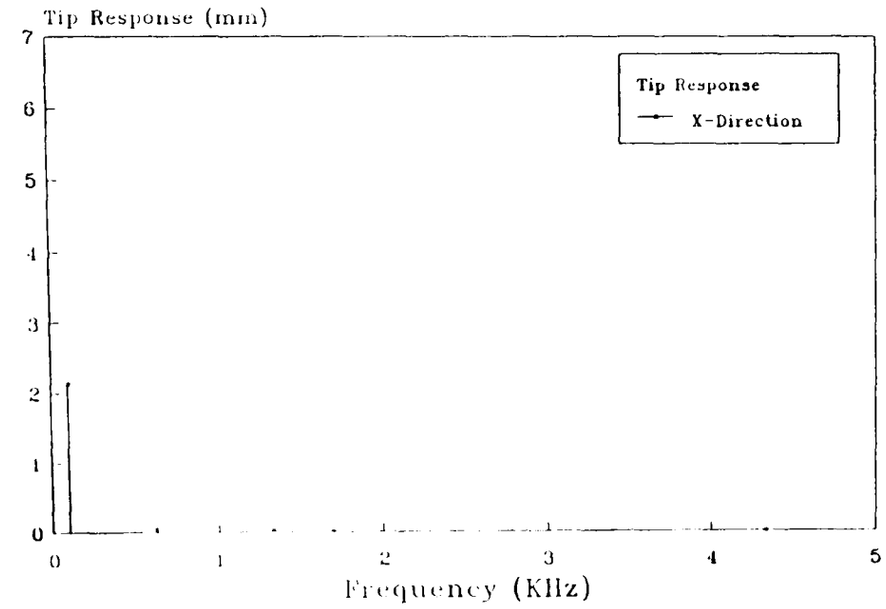

Figure 8.7.d– Tip Response at 5% Damping

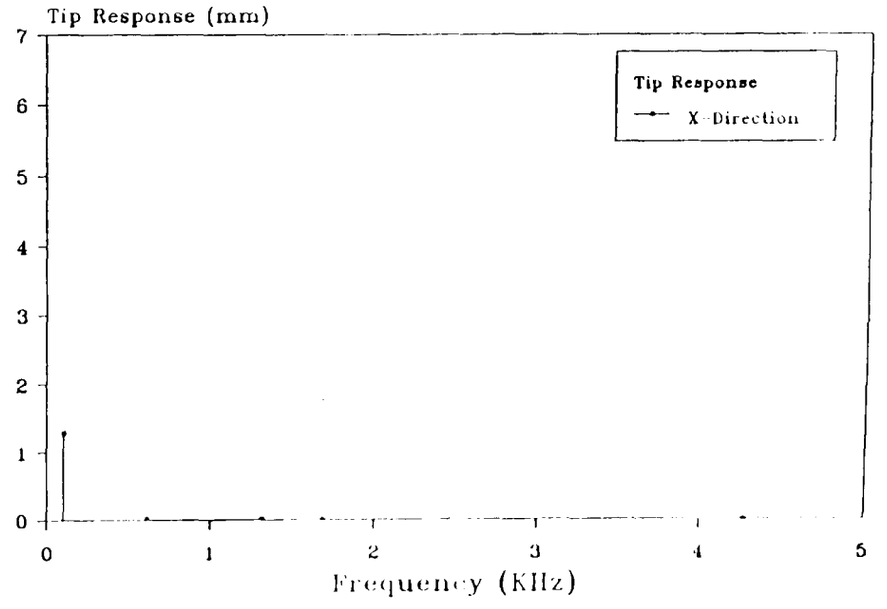

Figure 8.8–Tip Amplitude at fundemental Frequency for various Damping Levels.

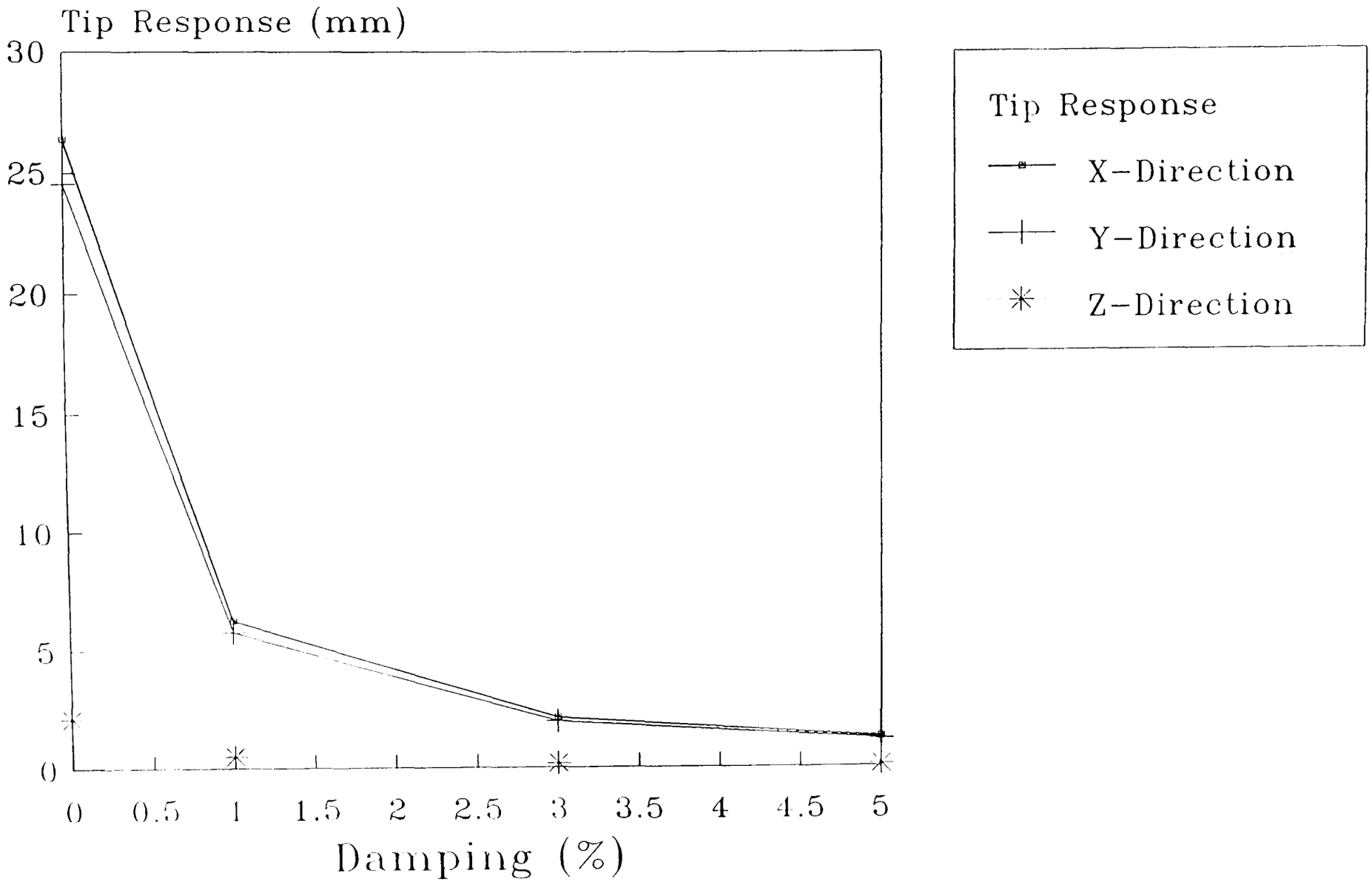

Figure 8.10.a–Tip Response at 0% Damping

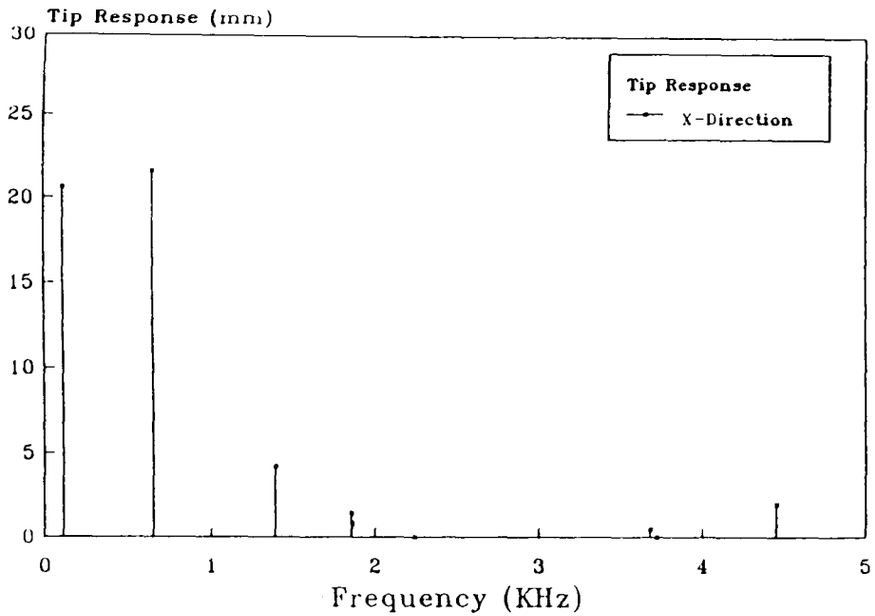

Figure 8.10.b–Tip Response at 1% Damping

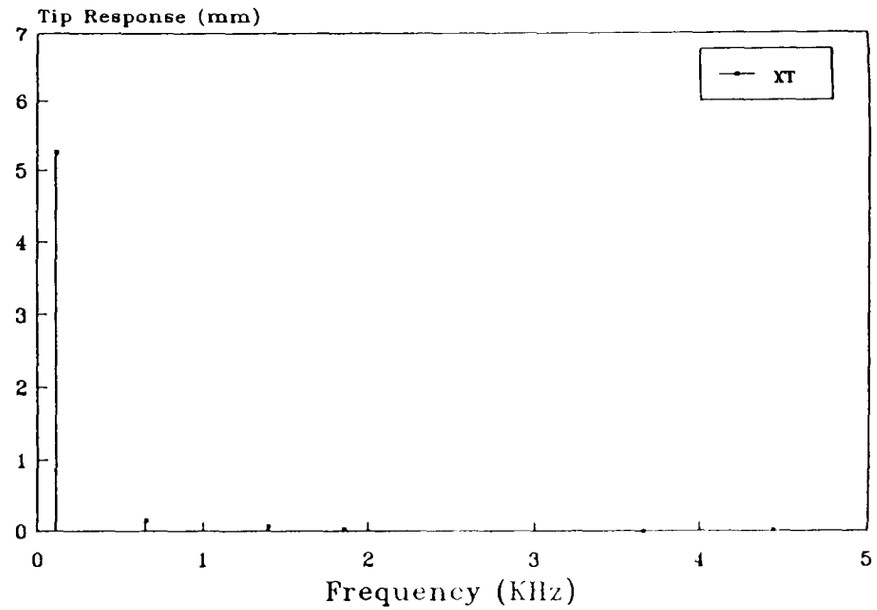

Figure 8.10–Tip Response at various Damping levels –Inserted

Figure 8.10.c–Tip Response at 3% Dampin

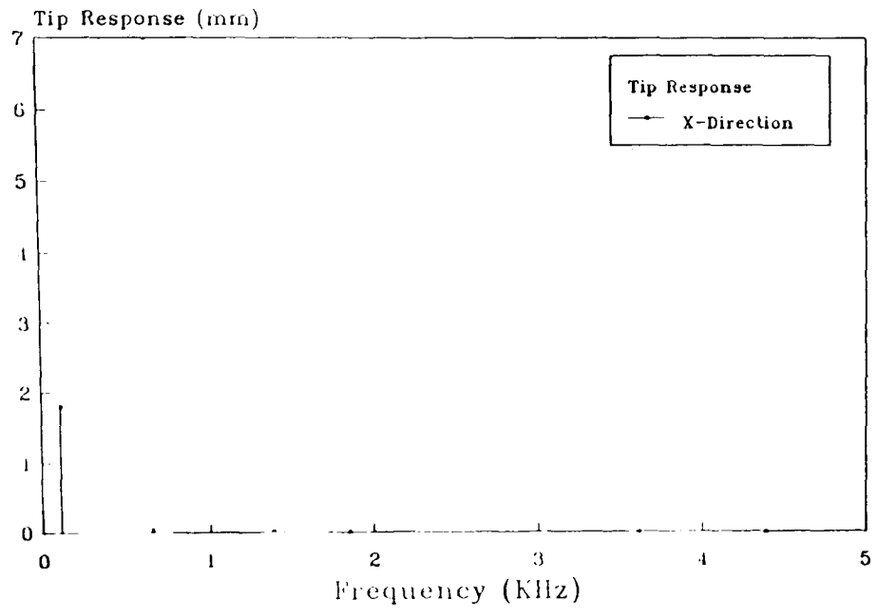

Figure 8.10.d–Tip Response at 5% Damping

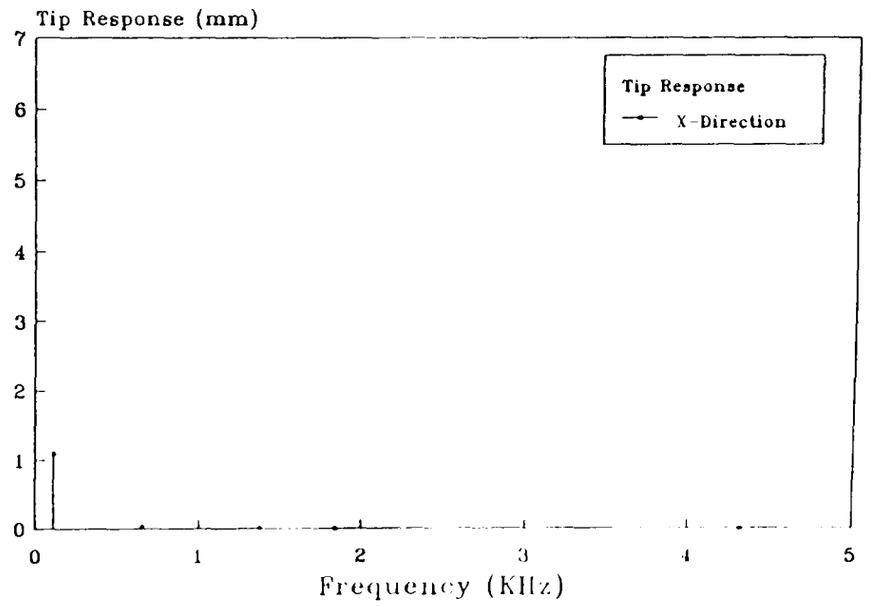

Figure 8.11 – Inserted Tool
Tip Amplitude Response
5% Damping – 1st frequency

Figure 8.11.a–Overhang Variation

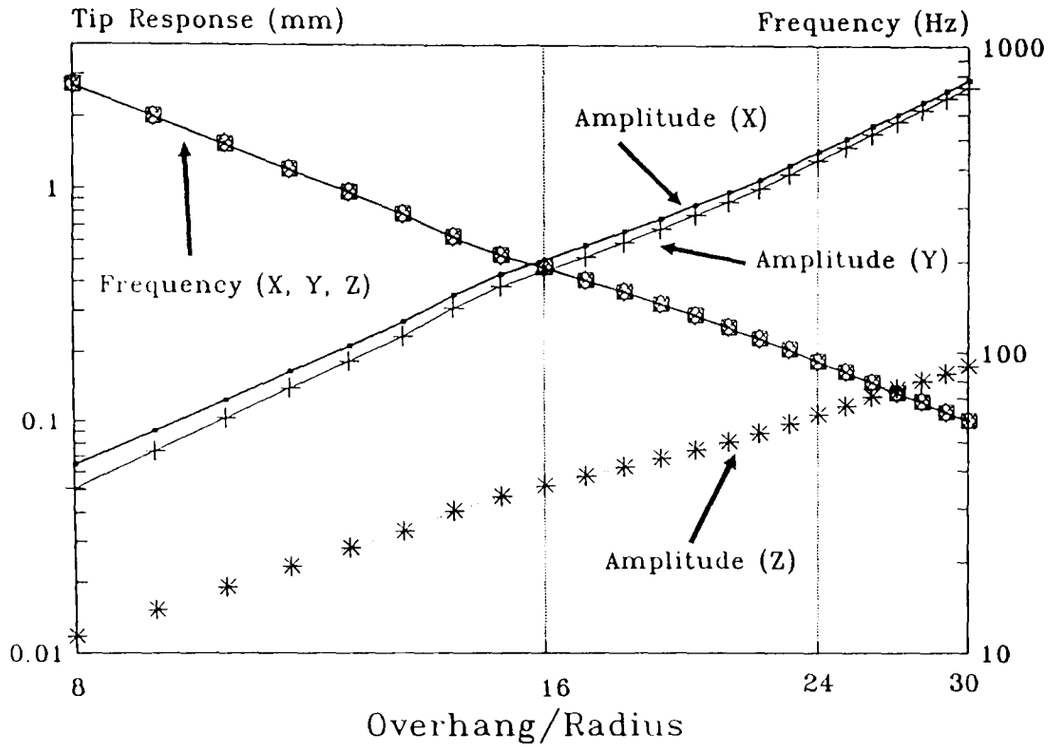

Figure 8.11.b – Force Variation

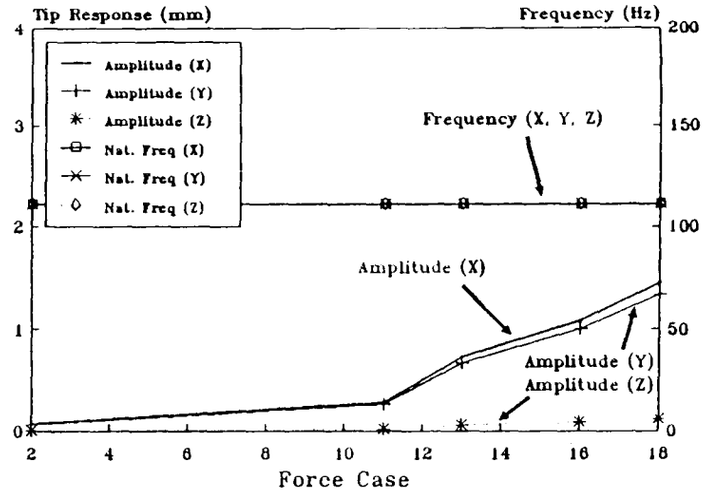

Figure 8.11.c – Shank Material Variatio

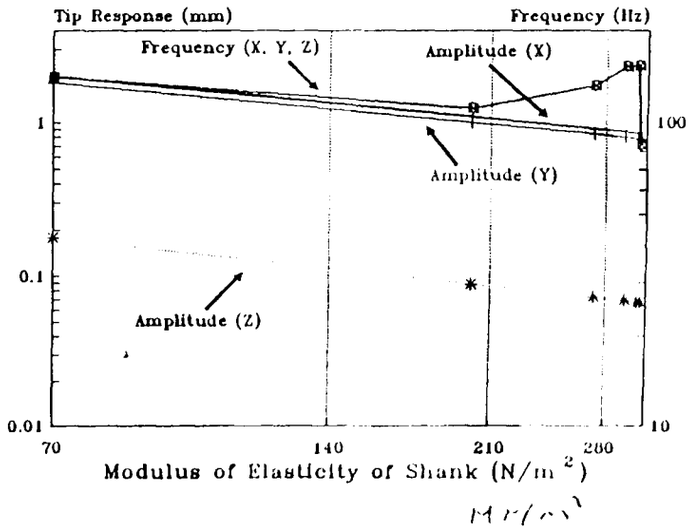

Figure 8.11.d – Length of Core Variatio
(Steel Shank)

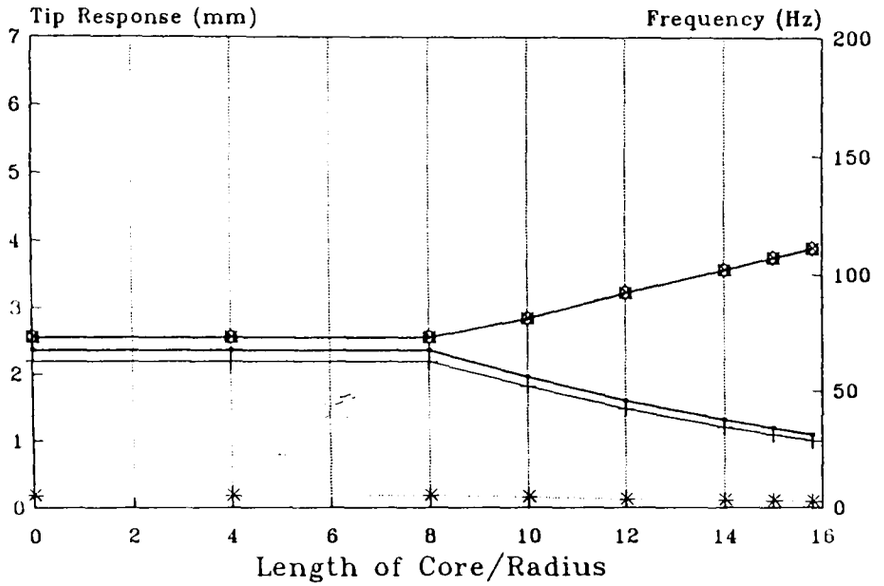

Figure 8.11.e – Core Length Variation
ALAL Shank

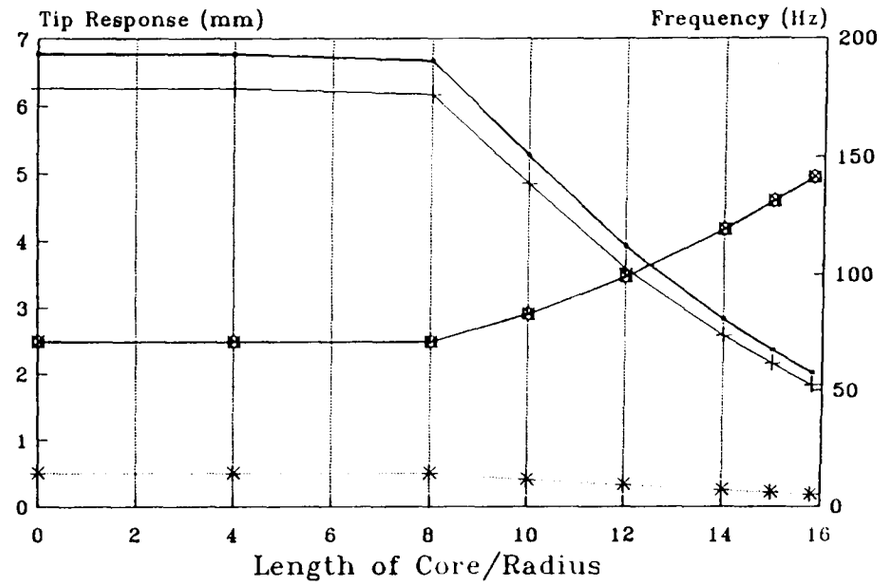

Figure 8.12.a – Comparative Frequency Performance Variation of Design Tools.

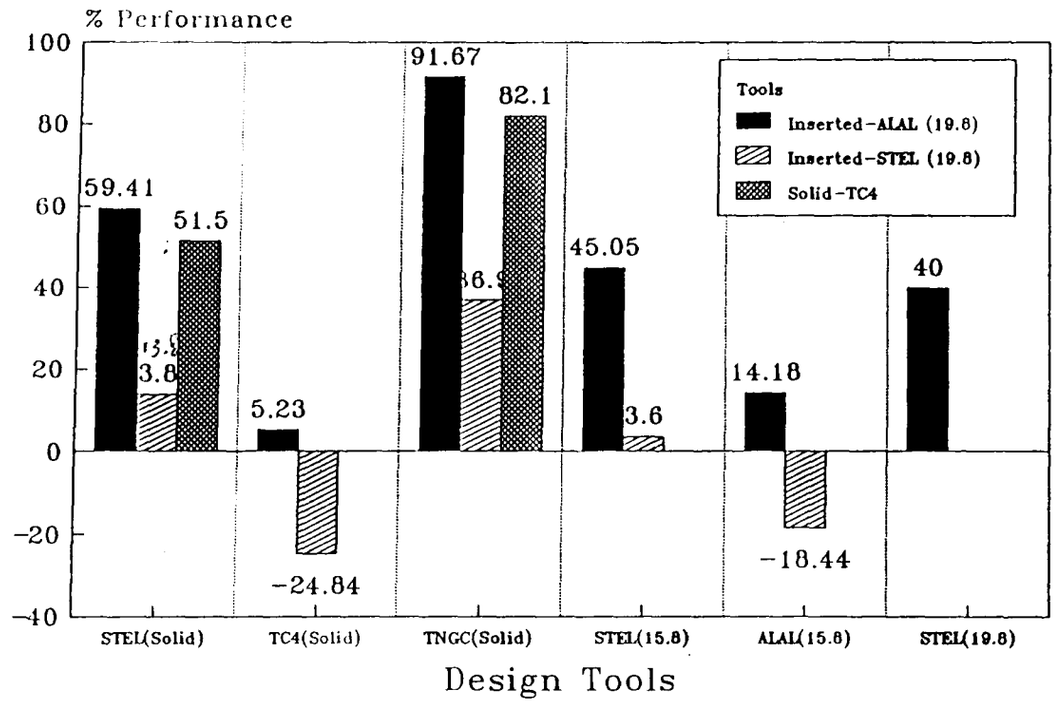

Figure 8.12.b – Fundemental Frequency Variation of Design Tools.

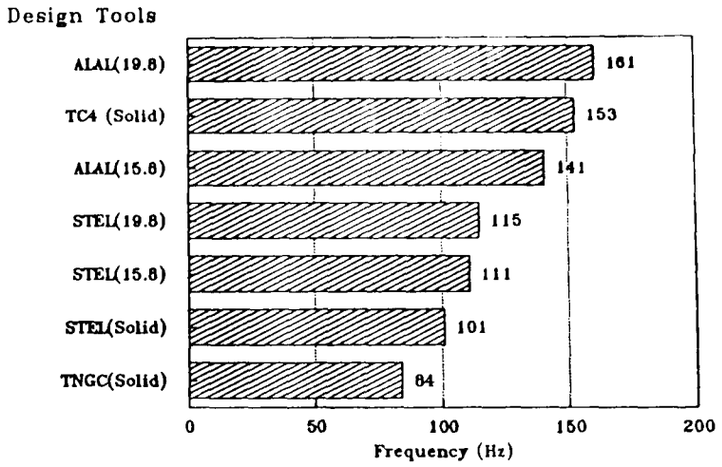

Figure 8.12.c – Amplitude Variation of Design Tools.

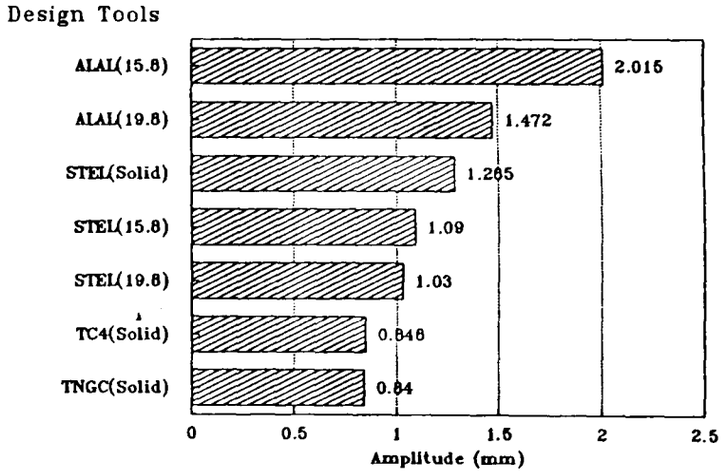

CHAPTER 9

CONCLUSIONS AND RECOMMENDATIONS FOR FUTURE RESEARCH

9.00 GENERAL

This study has described a detailed analysis of an enhanced design using a new materials and structural optimisation to improve the limit of stability associated with extended length tool holders.

Because of the need to maintain tighter tolerances at large length to diameter ratios, attention has been directed to four areas of interest.

a) Examination of the important characteristic chatter vibrations with respect to both structural response and determination of cutting process parameters in dynamic metal cutting.

b) Efforts have been directed towards improving mechanical properties of the cutting tool through structural design and material development. The practical aspects of material development were confined to improving equivalent stiffness through alloying elements and processing techniques.

c) Experimental verification of the stability performance of tool holders with respect to the variation of related fundamental determinants.

d) Computational simulation of the dynamic properties of the tool by Finite element analysis. Also, an analysis of the dynamic characteristics have been presented which substantiate the comparative magnitudes of frequency, response and mode shape performance of the combination tool holders.

9.1 CONCLUSIONS ON THE DESIGN PRACTICE

The principle factors influencing the cutting stability have been analyzed and confirmed by practical experimentation. They have revealed that smaller deviations in the R_a values are attainable with optimisation of the cutting conditions combined with the use of material of high stiffness. Application of passive constraint layer damping provides an added advantage with limited effect on quality of the finished workpiece. The basic considerations in design to minimise chatter are illustrated in Figure (9.1).

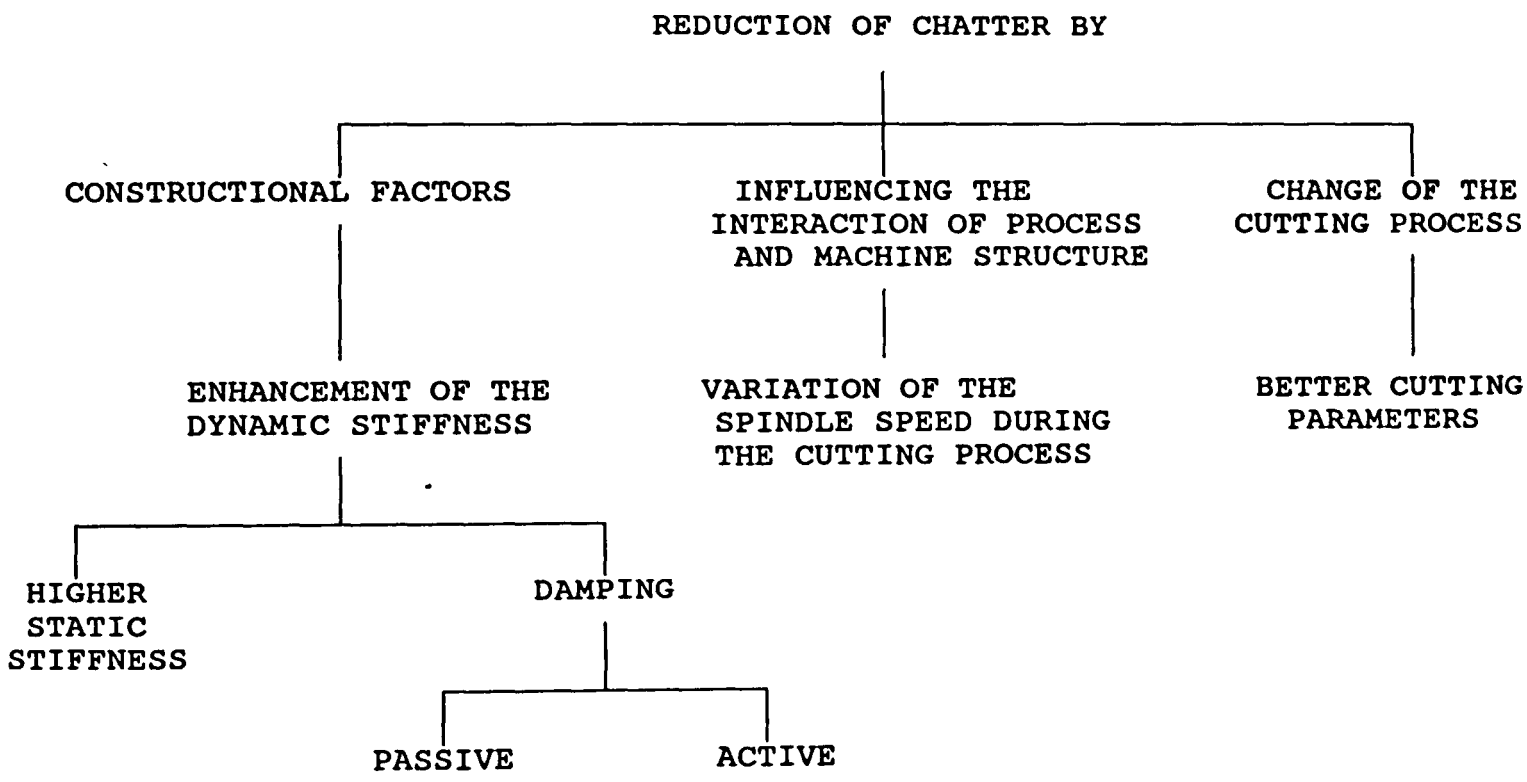

Figure 9.1 : Factors Influencing Cutting Stability.

The solutions to the problem have been based on passive system treatment. This has resulted in consideration of equivalent stiffness and mechanical energy dissipation from a systems approach.

From the manufacturing point of view it is important for the tool to be versatile and modular to lend itself to a broad variation of

process variables and cutting conditions. A modular construction was adopted to establish the enhancing effect of coinciding frequencies.

9.2 CONCLUSIONS ON CUTTING TOOL VIBRATION

In this study, an assumption has been made that the random components of the surface profile could come from tool vibratory motion caused by random excitation. It has been demonstrated that the optimal dynamic rigidity of the composite tool holder can be attained under the definite coupling specifications of high-stiffness and high damping materials.

Since any material disturbance would carry its maximum strain energy on the surface of the body, application of surface damping treatment as a design option for the vibration control was practical.

The results from the finite element model on the mode shapes of vibration were used to determine the positions of high strain concentrations. The application of surface damping materials on the boring bar was based on the modal shape so that the cyclic tension and compression of the damper would yield a maximum loss factor.

The integrated construction of the boring bar design benefits from three fold characteristics of mass, stiffness and damping through;

- Material development
- Optimisation through structural design.
- Visco-elastic constraint layer damping.
- Friction damping

In order to obtain the best specific configuration, the proposed design was formulated in a general way. Numerical procedure from the mathematics of the operation in the computational model was used to adjust the independent variables for an optimum design .

9.3 CONCLUSIONS ON MATERIAL DEVELOPMENT AND DESIGN

Additions of Titanium carbide (TiC) to the steel forming matrix were experimentally demonstrated to produce a dense composite product with increased elastic modulus. The amount of increase in stiffness was not a linear function of the ceramic content but rather the majority of the stiffening effect was achieved by the initial addition of ceramic. It was further shown that the important dynamic quantities E/ρ and the damping capacity of the composite are higher than that of conventional or sintered carbide materials used for boring bar applications.

The composite material developed, designated herewith TC4, consisted of ceramic particles namely titanium carbide dispersed within a steel particulate matrix. The ceramic Titanium carbide (TiC) imparts strength, stiffness and the metal matrix provided toughness.

Powder compacts of TiC and steel matrix of the two groups were fabricated using Vacuum sintering and Hot Isostatic Pressing (HIP) techniques. The effectiveness of these materials as a candidate for the proposed application was investigated by measurement of the mechanical properties of the product.

The dense materials fabricated by the HIPing process have been shown to have mechanical properties that are better than the properties published in the literature (U.S patent 2,752,666 (4.3)).

In terms of practical achievement due to material development it was shown that the static and dynamic quantities that could influence the increase in fundamental natural frequency and reduce the high amplitude of vibrations (ie, Equivalent Stiffness (E/ρ) and Damping) have been improved by respective factors of 110% and 447% , compared to the conventional steel tool.

From the analytical consideration of the vibration control parameters and functional specification of the tool a feasible approach

was adapted for the design.

In order for the boring bar to possess maximum stiffness the compliance of the joint between the Titanium carbide composite insert and the steel tube had to be minimised. The influence of interference pressure between the bar and the insert under dynamic loading was analyzed through computational simulation. This was estimated to have reached saturation (520 Mpa) practically eliminating joining influence.

The amount of energy dissipated in each component of a composite system is equal to the damping coefficient multiplied by the maximum strain energy stored in that component. Further increase in system damping was attained by composite construction. The level of increase in strain energy of the system through composite construction was substantiated through Finite Element Simulation.

The result indicates that the composite boring bar with aluminium front section and constraint layer damping exhibits the widest stable zone with respect to fundamental natural frequency.

9.4 CONCLUSIVE REVIEW ON ANALYSES OF RESULTS

The comparative analyses of experimental results indicated that the fabricated design without auxillary damping could operate with a stability criterion equal or better to that of the Sandvic TNS bars. The high modulus and damping associated with the TC4 material developed in this thesis resulted in an improved dimensional accuracy and reduced eccentricity at high length to diameter ratios. These advantages are accompanied by elimination of the requirement for in-process damping variation which is pre-set with TNS bars.

Stability charts with respect to metal removal rate have been obtained in which "unstable" indicates the zone free from characteristic vibration marks. The proposed design is theoretically

examined and experimentally verified to operate within acceptable levels of vibration, in the length to diameter ratio up to 11.

9.5 CONCLUSIVE REVIEW ON THE FINITE ELEMENT MODEL

The computational simulation of the model generated for the estimation of frequency and response have been analyzed for variation of the fundamental determinants.

The results presented analyzed the tool with respect to ;

- Overhang variation subjected to the same cutting force.
- Cutting force variation for a given overhang.
- Shank material variation for tools of equal overhang subjected to the same cutting force.

The results indicate that the tip deflections grow disproportionately with increasing tool overhang, emphasizing the importance of minimizing the overhang.

The computed strain energy from the obtained force-deflections revealed, that force/deflection characteristics along x and y are the major contributory components to the total strain energy. The shanks strain energy distribution depends upon the direction of forces and varies disproportionately across the shank where the maximum is located on the surface and the minimum at its centre. The results verify the operative applications of constraint layer damping on the surface of the tool holder.

The dynamic (modal and harmonic) behaviour of the cutting tools for various design options have been analyzed with respect to modal shapes and harmonic tip response. Knowledge of the natural frequencies and mode shapes was essential to prevent the designed bar from vibrating at or near its fundamental frequencies.

The general trend of the results verifies that the rise in strain level either due to Length to Diameter ratio or machining variables would result in higher damping capacity of the overall system. Moreover, it was shown that increasing the rate of damping will significantly reduce the tip responses.

Analysis of the variation of the damping level demonstrated the significance of damping on the response of the tool and the necessity of selecting tool materials which can offer high levels of damping.

Tip amplitude responses of the fundamental frequency in the solid tool showed that the TC4 solid tool exhibits the lowest amplitude response and that the ALAL shank inserted tool with core length of 19.8 times the radius exhabits the highest frequency.

It was demonstrated that as the TC4 core protrudes into the overhang region it increases both the static and dynamic stiffness of the boring bar. This effect is maximum when the TC4 core is extended to its full designed length (52.3% of the overhang).

9.6 RECOMMENDATIONS FOR FUTURE RESEARCH

The thesis examines the optimum design of boring bars. This is only the small part of the manufacturing scene. It seems plausible to suggest that the same philosophy could be applied to tool shank design. Although the cantilever effect is much smaller the basic problem is the same. It is anticipated that such design may be useful in the new technology of ultra precision machining where stiffness and damping are critical factors for maintaining the accuracy of finish (9.1).

The metal composite TC4 developed in this thesis for the improvement of the static and dynamic stiffness of boring bars is considered to have much use beyond its original scope of application. The full potential of this material may be realised through further investigation into the mechanical properties such as thermo-elastic

modulus, thermal expansion coefficient, thermal and electrical conductivity, interface damping characteristics and the application of precision machining.

It should also be mentioned that at the time of developing this material concern was for a solution in improving the equivalent stiffness. Therefore, the study of a metallurgical approach is perceived to be more effective and requires further attention, especially with respect to the damping capacity at the bonding interface for various material combinations. This was considered to be separate from the scope of the research.

It is therefore suggested that for further investigation of methods to optimize the mechanisms responsible for damping characteristics, the metallurgical effects should be dealt with. This would require careful analysis with regards to the study of internal friction resulting from thermal expansion mismatch of particulate elements and thermoplastic damping. The prospective investigator could make reference to the work of Vikram et all (4.8) and Z.Xing et al (4.9) for direction in to the design, for an increase in damping without a substantial reduction of stiffness.

REFERENCES

CHAPTER 1

1.1 P.Landberg, (1956) " Vibrations caused by chip formation ". Int. J. Prod. Eng. Res.

1.2 Donaldson, (1971) Lecain and Goold, " Tool Design Handbook " McGRAWHILL TMH Edition.

1.3 J.S.Lin and C.I.Weng, (1979) " A Non-Linear Dynamic Model of Cutting " Int. J. Mach Tools Manufact, Vol 30, No 1 pp. 53 - 64.

1.4 D.B.Welbourn, (1969) " Machine Tool Dynamics " John Wiley & Sons,.

1.5 S.Kato and E.Marui, (1974) "On The Cause Of Regenerative Chatter Due To Workpiece Deflection " ASME, J. of. Eng. For Indty. pp. 179 - 186.

1.6 S.A.Tobias, (1965) " Machine Tool Vibration Phenomena " John Wiley & Sons, Inc Newyork, .

1.7 R.G.Klein and C.L.Nachtigal, (1975) " A Theoretical Basis For The Active Control Of Boring Bar Operation ", Trans. Of A.S.M.E, pp. 172-175

CHAPTER 2

2.1 Donaldson, Lecain, Goold. (1969) Tool Design Handbook. 3rd Edittion, Macgraw hill PP.211.

2.2 G.T. Smith. (1989) Advanced Machining, The Handbook Of Cutting Technology. Springer-Verleg .

2.3 N.H.Cook, (1980) Tool wear sensors, Jurl of Wear Vol.62, pp 49-55

2.4 J.Tlusty and G.C.Andrews, (1983) A critical review of sensors for unmanned machining, Annls of CRIP, Vol. 32, pp563-572.

2.5 H.K.Tönshoff et al, (1988) Development and trends in monitoring and control of machining process, Annls of CRIP, Vol 37,No.2, pp. 611-622.

2.6 D.Li and J.Mathew, (1990) Tool wear and failure monitoring techniques for turning - Int. J. of Mach. Tools & manufact. Vol. 30, No.30, pp 579 - 598.

2.7 Y.Koren, (1986) Tool wear and breakage detection using a process model. Annls of CRIP, Vol.35, pp 283 - 288.

2.8 K.Danai and A.G.Ulsoy. (1987) A dynamic state model for on-line tool estimation in turning, Trans. ASME, J. of Eng. for Indsty. Vol. 1 pp 1 - 26.

2.9 R.Mackinnon, G.E.Wilson and A.J.Wilkinson, (1986) Tool condition monitoring using multi-component force measurements, Proc. of 26th Mach. tool Design & Res. Conf. Vol 10, pp 317 - 324.

2.10 P.Martin, B.Mutel and J.P.Drapier, (1974) Influence of lathe tool wear on the vibrations sustained in cutting, Proc. of 15 th. Int. Mach. Tool. dsgn. & Res. Conf. Vol. 16, No.3 pp 251 - 257.

2.11 S.M.Pandit and S.Kashou, (1982) A data dependent system of online tool wear sensing. Trans. ASME, J. of Eng. for indsty. Vol. 104 pp.212-223.

2.12 D.J.Whitehouse, (1978) Surfaces, A link between manufacture and function., Proc. of the Inst. of Mech. Eng. Vol. 192, pp. 179,

2.13 R.N. Arnold. (1946) The Mechanism Of Tool Vibration In Cutting Steel. Proc. Int. Mech. Eng. 154, PP.261.

2.14 R. Komanduri. (1981) On The Mechanics Of Chip Segmentation In Machining. Trans. ASME. Vol. 103, PP.33-50.

2.15 R. Komanduri. (1980) New Observations On The Mechanism Of Chip Formation When Machining Titanium Alloy. Trans. ASME.

2.16 H. Ernst and M.E. Merchant. (1941) "Chip Formation, Friction and High Quality Machined Surfaces" Surface Treatment Of Metals. Trans. ASME. Vol 29.

2.17 M.E. Merchant, (1945) Mechanics Of Metal Cutting Process. Joul. Of Applied Physics Vol. 16, PP. 268-318.

2.18 E.H. Lee and W.B. Shaffer. (1951) The Theory Of Plasticity Applied To The Problem Of Machining. Joul. Of Applied Mechanics. Vol. 18, Trans. ASME Vol. 82 PP. 405-413.

2.19 S. Kobayashi, R.P. Herzog, D.M. Eggleston and E.G. Thomsen. (1960) A Critical Comparison Of Metal Cutting Theories With New Experimental Data. Trans. ASME. Vol. 82 PP. 333-347.

2.20 N.N. Zorev. (1963) Inter-Relation Between Shear Process Occurring Along Tool Face and On Shear Plane In Metal Cutting. Proc. Int. Prod. Eng. Res. Conf. Pittsburg, PP.42.

2.21 M. C. Show, N.H. Cook and I. Finnie. (1953) The Shear Angle Relation Ship In Metal Cutting. Trans. ASME Vol. 75, PP. 273-288.

2.22 S. Kobayashi and E.G. Thomsen. (1959) Some Observation On The Shearing Process In Metal Cutting. Trans ASME Vol 81 PP. 251-262.

2.23 S. Kobayashi and E.G. Thomsen. (1960) The Role Of Friction In Metal Cutting. Trans. ASME Vol. 82 PP 324.

2.24 D.M. Eggleston, D. Herzog and E.G. Thomsen. Observations On The Angle Relation Ship In Metal Cutting.

2.25 P.W. Wallace and G. Boothroyd. (1966) Tool Forces and Tool-Chip Friction In Orthogonal Machining. Jol. Mech. Eng. Sci. Vol. 8 No3, PP. 264-675.

2.26 M.C. Shaw. (1963) Resumg and Critique Of Papers In Part One. Int. Prod. Eng. Res. Conf. Pittsburg, PP.3.

2.27 M.K. Das and S.A. Tobias. (1965) The Basis Of The Universal Machinability Index, Advances In Machine Tool Design and Research. Proc. Of 5th M.T.D.R Conf. PP. 183-198.

2.28 P. Albecht. (1965) Dynamics Of Metal Cutting Process. Trans. ASME. Vol. 87, PP.429-441.

2.29 N.H. Cook. (1959) Self Excited Vibrations In Metal Cutting. Trans.ASME. Vol. 81, PP.183.

2.30 A.J. Chisholm. (1949) The Cause Of Chatter Vibrations. Machinery Vol. 75 PP.51.

2.31 R.S. Hahn. (1953) Metal Cutting Chatter and Its Elimination. Trans. ASME. Vol. 75 PP.1073

2.32 S.A. Tobias and W. Fishwick. (1958) Theory Of Regenerative Machine Tool Chatter. The Engineer Vol. 205, PP.199.

2.33 J.D. Smith and S.A. Tobias. (1961) The Dynamic Cutting Of Metals. Int. Mach. Tool Des. Res. Vol. 1 No4, PP.283.

2.34 C. Andkew and S.A. Tobias. (1961) A Critical Comparison Of Two Current Therories Of Machine Tool Chatter. Int. J. Mach. Tool. Des. Res. PP.325.

2.35 A.A Shumsheruddin. (1965) PhD Thesis University Of Birmingham .

2.36 P.W. Wallace and C. Andrew. (1965) Machining Forces: Some Effects Of Tool Vibration Jour. Mech. Eng. Soci. Vol. 7, No2 PP.152- 16.

2.37 P.W. Wallace and C. Andrew. (1966) Machining Forces: Some Effects Of Removing A Wavy Surface. Jour. Mech. Eng. Soci. Vol. 8 No2 PP. 129-140.

2.38 M.K. Dos and S.A. Tobias. (1967) The Relation Between The Static and The Dynamic Cutting Of Metal. Int. Jour. Mach. Tool Des. Res. Vol.7 PP.63.

2.39 G.S. Kainth. (1969) Investigation In To The Dynamics Of The Metal Cutting Process. PhD thesis, Birmingham University.

2.40 W.A. Knight. (1970) Some Observations Of The Vibratory Metal Cutting Process Employing High Speed Photography. Int. Jour. Of Mach. Tool Des. Res. Vol. 10.

2.41 W.A. Knight. (1972) Chatter In Turning, Some Effects Of Tool Geometry and Cutting Conditions. Int. Jour. Of Mach. Tool. Des. Res. Vol.12 PP.201.

2.42 F.Koenigsberger and J.Tlusty, (1970) Machine tools structures, Pergamon press, Oxford England.

2.43 I.N.Tansel, A.Wagiman and A.Tziranis, (1991) Recognition of chatter with neural networks, Int. J. Mach. Tools. Manufact. Vol, 31. No. 4, PP. 539 - 552.

2.44 C.R.Liu and T.M.Liu., (1985) Automated chatter suppression by tool geometry control., Trans. of ASME., J. of Eng for Indust. Vol. 107, PP. 95 - 98.

2.45 I.N.Tansel, (1990) Machine tool structures. Int. J. Mach. tools & Manufact, Vol.30, PP.535 - 547.

2.46 P.N.Rao, U.R.K.Rao and J.S.Rao, (1988) Towards improved design of boring bars part 1 & 2, Int. J. Mach. Tools Manufact. Vol. 28, No. 1, pp. 33 - 44.

2.47 J.Tlusty, (1978) Analysis of the state of research in cutting dynamics, CRIP Annals, Vol. 27, No. 2, PP. 403 - 412

2.48 F.Ismail., (1982) Identification, Modelling and modification of mechanical structures from modal analysis testing, Ph.D. Thesis, McMaster University, Dec.

CHAPTER 3

3.1 S.A. Tobias, (1965) Machine-Tool Vibration. Blackie Glasgow.

3.2 R.G White and J.G.Walker, (1982) Noise and Vibration, Pub. Ellis horwood Book Co.

3.3 J.P.Den Hartlog, (1956) Mechanical vibrations, Pub. McGraw-Hill Book Co.

3.4 A.D.Nashif, D.I.G.Jones, and J.P.Henderson ; (1985) Vibration damping, Pub. by John wiley & sons, PP. 27.

3.5 V.K.Kinra and A.Wolfenden, (1992) M³ D:Mechanics and mechanisms of material damping, Pub, ASTM.

3.6 D.J.mead, (1979) Damping effects in aerospace structures, AGARD Conf. Proc. Paper 2, No.277.

3.7 R.M.Phelan, (1967) Dynamics of machinery, Pub. by. MacGraw Hill, Newyork, PP. 178 - 190.

3.8 A.Donaldson et al, (1969) Tool design Hand book, 3rd edition Pub. McGraw-Hill Book Co. pp.211.

3.9 D.J.Lee, (1988) Manufacturing and testing of chatter free Boring bars, Annls of CRIP, PP.365 - 368.

3.10 M.D.Tomas, (1970) W.A.Night and M.M.Sadek, Comparative dynamic performance of boring bars, 11th Int. M.T.D.R Conf., Birmingham, pp.159.

3.11 J.Tlusty, (1981) Criterion for static and dynamic stiffness of structures, Report. of. (MTTF) Vol. 3.

3.12 R.S.Hahn, (1951) Design of lanchaster damper for elimination of metal cutting vibration, Trans. of ASME. Vol. 73, pp.331 - 335.

3.13 E.I.Rivin, (1974) Cantilever tool mandrels, U.S. Patent, No: 3,820,442,

3.14 E.I.Rivin and H.Kang, (1989) Improvement of machining conditions for slender parts by tuned dynamic stiffness of tool., Int. J. mach. Tools Manufact. Vol. 29, No, 3, pp 361 - 376.

3.15 E.I.Rivin and H.Kang, (1989) Optimal tuning conditions for boring bar with damped vibration absorber., Trans. NAMRI. Inst. of SME, pp. 123 - 129.

3.16 Y.H.J.Au, K.W.Ng, and R.W.New, (1979) The lanchaster damper, A design procedure for optimizing the damping ratio for a cylindrical slug damper fitted to a machine element., Trans. of ASME, Vol, 109, pp. 291 - 297.

3.17 R.W.New and Y.H.J.Au, (1980) Chatter proof over hang boring bars, Stability criteria and design procedure for a new type of damped boring bar., Trans. of. ASME., Vol, 102, pp. 611 - 618.

3.18 R.G.Ni and R.D.Adams, (1984) The damping and dynamic moduli of symmetric laminated composite beams - theoretical and experimental results. J. of Compst. Materials. Vol.18, pp. 104-121.

3.19 P.Cawley and R.D.Adams., (1978) The predicted and experimental natural modes of free-free plates., J. of Compst. Materials., Vol. 12 . pp 336 - 347.

3.20 D.A.Saravanos and C.C.Chamis., (1991) Computational simulation of damping in composite structures,. J. of Rnforcd. Plasts. and compst., Vol. 10, pp. 256 - 278.

CHAPTER 4

4.1 D.G.Lee, (1985) Manufacturing and testing of composite machine tool structures., Ph.D. Thesis, Dept. of Mech. Eng. M.I.T, pp. 179 - 182.

4.2 U.Vandeurzen et all., (1981) Additive damping treatment for mechanical structures., annls of CRIP, Vol. 30, No.1.

4.3 G.Claus et all., (1956) Heat resistant titanium carbide containing body and method of making same., U.S. Patent 2,752,666.

4.4 H.V.Atkinson and B.A.Rickinson., (1991) Hot Isostatic Pressing. Adam Hilger.,

4.5 G.G.Weran and V.K.Kinra , (1990) An experimental study of the complex dynamic modulus, ASTM STP 1045, A. PP.58-74.

4.6 ASTM Designation: c 623 - 71, (1974) Standard method of test for young modules, shear modules, and passions ratio by resonance,

4.7 R.Plunkett, (1992) Damping analyses : An Historical perspective, M^3D: Mechanics and mechanism of material damping, pp. 563 , ASTM PP. 1169.

4.8 Z.Xing, R.Fougeres, and A.Vincent, (1992) Internal friction resulting from a thermal expansion missmatch between Aluminium and Silicon in Al 11.8Si Alloy., M^3D: Mechanics and mechanism of material Damping, pp. 548 - 561, ASTM- Stp1169.

4.9 V.K.Kinra and K.B.Milligan, (1992) Irreversible heat transfer as a source of thermoelastic damping, M^3D : Mechanics and mechanism of material damping, pp. 94 - 123, ASTM- Stp1169.

CHAPTER 5

5.1 M.E. Merchant, (1945) Mechanics of metal cutting process(II) Journal of applied physics, Vol. 16, No.6, pp 318-324

5.2 A.K. Rakhit, M.O.M. Osman and T.S. Sankar, (1973) Proc. 4th Appl. Mech. Montreal, pp. 463 - 464.

5.3 G.M.Zhang and S.G.Kapoor, (1991) Dynamic generation of machined surfaces, Part 1: Description of random excitation system., Journal of Eng. for Indust, Vol. 113, pp. 137-153.

CHAPTER 6

6.1 ANSYS Manuals: Swanson Analysis Systems Inc.

6.2 R. Courant , (1943) Variational methods for the solutions of the problems of equilibrium and vibrations, Bulletin of the american mathematical society.

6.3 M.J.turner et al , (1956) Stiffness and analysis of complex structures. J.aeronautical society, Vol. 23. No 9.

6.4 N.P. Suh and N.Saka, (1978) " Fundamentals of Tribology", Proc. of Int. Conf. on the Fundamentals of Tribology, pp 142.

CHAPTER 7

7.1) E.I.Rivin and H.L.Kang, (1989) "Improvement of machining conditions for slender parts by tuned dynamic stiffness of tool", Int. J. Mach. Tools Manufact. Vol. 29, No. 3, pp 361-376.

CHAPTER 8

8.1) S.A.Petrusewics and D.K.Longmore (1967) "Noise and Vibration Control for Industrialists", pp 58-116.

8.2) E.Marui, S.Ema, and S.Kato, (1987) " Contact Rigidity at Tool Shank of Turning Tools", Transactions of the ASME, Journal of Engineering for Industry, Vol. 109, pp 169-172

CHAPTER 9

9.1) Professor D.J.Whitehouse; (November 1994) Discussion on the future scope for current practice in design out lined in this thesis

APPENDIX "A"

SUMMARY OF SONIC-VELOCITY METHOD OF TEST FOR MECHANICAL CHARACTERISTICS OF THE PRODUCED SAMPLES.

THEORETICAL CONSIDERATION

Whenever a material is subjected to a time-harmonic stress, some mechanical energy is converted to heat; this is called damping. A measure of damping is the specific damping capacity, $\psi = \Delta W / W$, where ΔW is the mechanical energy dissipated during one cycle, and W is the maximum elastic stored energy.

One of the classical methods of measuring elastic modules and ψ is to study resonance frequency in flexure, for the free decay of first mode of vibration.

A common damping apparatus uses the free-free beam where the beam is suspended at its nodal points by two elastic strings and vibrates in the plain of the support strings.

This method was used to measures the resonance frequencies of test specimens of a given geometry by exciting them at continuously variable frequencies. Mechanical excitation of the specimen is provided through use of transducer that transforms an initial electrical signal to mechanical vibration. Another transducer senses the resulting mechanical vibrations of the specimen and transforms them into an electrical signal that can be displayed on the screen of an oscilloscope to detect resonance. The resonance frequencies, the dimensions and the density of the specimen may be used to calculate Young's modulus, specific damping and poison ratio.

Although in practice it may not be impossible to achieve exact nodal position, through trial and error the effective resultant error may be minimised to less than 0.1%.

Due to a relatively small dimensions of the specimens and low amplitude of the exciting frequency, the effect of air damping was ignored.

This testing system has advantages in certain respects over the use of static loading system;

I) Only minute stresses are required with non destructive approach to the testing of specimen .

II) The period of time during which stress is applied and removed is of order of microseconds making it feasible to perform number of tests.

III) Small geometry of test specimens may be used which has an advantage of time and cost savings.

The best existing theory for flexural vibration of rectangular prisms is that, for the fundamental mode of vibration, equation is equivalent to;

$$E = 0.94642 \left(\frac{L}{t}\right)^3 \left(\frac{M}{B}\right) f^2 T$$

Where

L = Length mm., t = Thickness mm., B = Width mm., M = Mass Kg.,

F^2= Resonant Frequency Hz. (Variable for each sample)

T = Correction Factor ≈ 1.

T may be approximated to unity for specimens of small geometrical configuration.

The poison ratio may be estimated by;

$$\mu = \left(\frac{E}{2G}\right) - 1$$

When a metallic specimen is subjected to flexural vibrations, the tensile side cools whereas the compressional side heats up. This temperature gradient set up transverse thermal current that result in

the production of entropy.

The thermoelastic damping may be approximated by the expression;

$$\psi = \psi_0 \frac{\omega\tau}{1+(\omega\tau)^2}$$

where ;

ψ_0 = Thermoelastic Damping Parameter

ω = Natural Frequency.

τ = Relaxation Time.

For experimental measurements, the decay of amplitudes would reveal the decay factor. As an illustration , let A_1 and A_2 be the amplitude of two successive cycles separated by one period of oscillation, T.

Then specific damping $\psi = 2 \ln (A_1/A_2)$

In order to obtain any reasonable degree of accuracy, an acreage over a large number of cycles were obtained.

APPARATUS

The test apparatus consists of a variable audio frequency audio oscillator, used to generate a sinusoidal voltage, and a power amplifier and transducer to convert the electrical signal to a mechanical driving vibration. A frequency meter monitors the audio oscillator output to provide an accurate frequency determination. A silk tread suspension-coupling system cradles the test specimen, and another transducer acts to detect mechanical resonance in the specimen and to convert it into an electrical signal which is passed through an amplifier and displayed in the vertical plates of an oscilloscope.

Figure B1 illustrates the schematic diagram of free-free apparatus and Figure B2 shows the experimental test rig set up used for

the measurements of the mechanical properties.

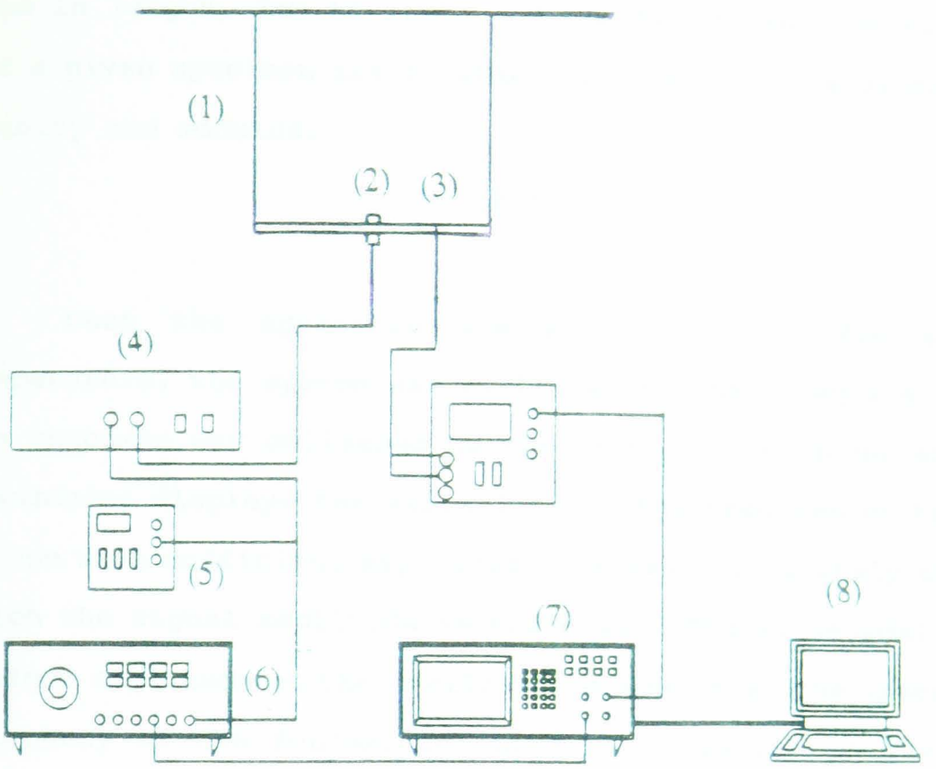

(1) Silk Strings
(2) Magnetic driving transducer
(3) Detector transducer
(4) NAD2200 amplifier
(5) DC504 frequency counter
(6) Wavetek Model 164 wave form generator.
(7) Digital oscilloscope
(8) Hewlett Packard 9000/217 computer

Figure B1 : The schematic diagram of free-free apparatus

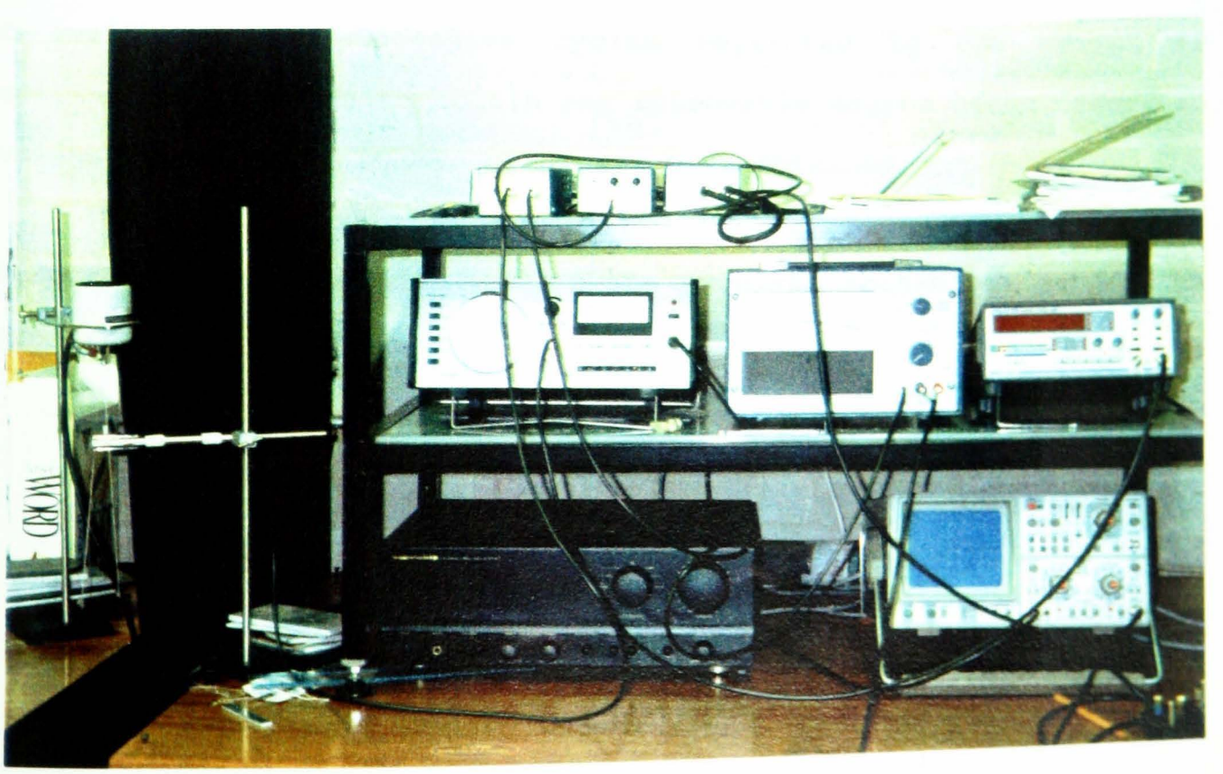

Figure B2 : The experimental test rig for the measurements of the mechanical properties.

TEST SPECIMENS

Test specimens were prepared with rectangular cross section of 60mm in length, 2mm in width and 1mm thickness. Resonance frequencies for a given specimen are functions of the bar dimensions as well as its density and modulus.

PROCEDURE

Once the apparatus was set up as in Figure B1, at room temperature, the system was activated so that adequate power to excite the specimen was delivered to the driving transducer and the detector transducer displays the vibrations in the specimen on the oscilloscope screen with sufficient amplitude to measure accurately the frequency at which the signal amplitude is maximized. The sinusoidal pattern of the maximum amplitude on the oscilloscope indicates the specimens resonance frequency of the fundamental mode of vibration in flexure. Then the first overtone of the fundamental flexure mode was established by positioning the detector at the appropriate nodal position of the specimen. At this point the amplitude of the resonance signal will decrease to zero and the strings will be motionless.

The damping quantities were estimated as a measure of the decay of amplitudes in successive cycles separated by one period of oscillation. In order to obtain any reasonable degree of accuracy, an average over a large number of cycles were obtained.

The measured data were analyzed through the on line computer where the numerical quantities of the required mechanical properties were extracted.